CHAPTER 8: Stellar Atmospheres

In previous chapters we examined the nature of radiation and its interactions with matter. In this chapter we will use our knowledge of how radiation flows through matter to develop a plan to establish the structure of a stellar atmosphere. Our first step is to understand how the matter in a gas interacts with itself and what parameters we can use to characterize the gas.

Gas Properties

A gas is composed of particles of matter that move independently. The gas particles do interact with each other through collisions, exchanging momentum and energy, and normally reach a steady state in which the bulk gas properties obey a few basic relations, as shown below.

Particle Velocities

In Chapter 6 it was noted that broadened line profiles may result from gas particles moving along the observer's line of sight; the distribution of velocities along this single direction was given by Boltzmann's equation. We now wish to expand this discussion to include motions in all three directions, which will allow us to determine the pressure exerted by the gas.

To begin, let v_x be the velocity of a particle along the x axis, either positive or negative; the kinetic energy of this particle will be $E = {}^1/_2\, m v_x^{\,2}$. Now let $N(v_x)\, dv_x$ be the number density of particles with an x velocity in the range $v_x \rightarrow v_x + dv_x$, and let N be the total number density of particles (for which the average value of v_x is 0). Assuming an ideal gas – for which sufficient states are available that particles are not limited by statistical weights – then the *fraction* of particles $N(v_x)\, dv_x / N$ with an x-velocity component v_x is given by a Boltzmann equation:

Eq. 8.1
$$\frac{N(v_x)dv_x}{N} = Ce^{-E/kT}dv_x = Ce^{-mv_x^2/2kT}dv_x$$

The quantity C is a normalization constant, found by requiring that a sum over all the possible x velocities yields the total number density N.

Eq. 8.2
$$\int N(v_x)dv_x = N \cdot C\int_{-\infty}^{\infty} e^{-mv_x^2/2kT}dv_x = N \quad \Rightarrow \quad \frac{1}{C} = 2\int_0^{\infty} e^{-mv_x^2/2kT}dv_x$$

Using $\int_0^{\infty} e^{-ax^2} = \frac{1}{2}\sqrt{\frac{\pi}{a}}$, where $a = m/2kT$, we can solve for C :

Eq. 8.3 $$\frac{1}{C} = 2\frac{\sqrt{\pi}}{2\sqrt{\frac{m}{2kT}}} = \sqrt{\frac{2\pi kT}{m}} \quad \Rightarrow \quad C = \sqrt{\frac{m}{2\pi kT}}$$

This provides the distribution function for the *x* velocity:

Eq. 8.4 $$\frac{N(\mathrm{v}_x)d\mathrm{v}_x}{N} = \sqrt{\frac{m}{2\pi kT}}\, e^{-m\mathrm{v}_x^2/2kT} d\mathrm{v}_x$$

Similar equations can be written for velocities in the *y* and *z* directions. Multiplying these all together gives the fraction of particles with v_x, v_y, and v_z all in the given ranges:

Eq. 8.5 $$\frac{N(\mathrm{v}_x)d\mathrm{v}_x}{N}\frac{N(\mathrm{v}_y)d\mathrm{v}_y}{N}\frac{N(\mathrm{v}_z)d\mathrm{v}_z}{N} = \left(\frac{m}{2\pi kT}\right)^{3/2} e^{-\frac{m}{2kT}\left(\mathrm{v}_x^2+\mathrm{v}_y^2+\mathrm{v}_z^2\right)} d\mathrm{v}_x d\mathrm{v}_y d\mathrm{v}_z$$
$$= \frac{N(\mathrm{v}_x,\mathrm{v}_y,\mathrm{v}_z)d\mathrm{v}_x d\mathrm{v}_y d\mathrm{v}_z}{N}$$

We can simplify our notation by substituting $d\mathrm{v}_x d\mathrm{v}_y d\mathrm{v}_z = d\vec{\mathrm{v}} = \mathrm{v}^2 d\mathrm{v}\, d\Omega$ and $\mathrm{v}_x^2 + \mathrm{v}_y^2 + \mathrm{v}_z^2 = \mathrm{v}^2$ to yield the following:

Eq. 8.6 $$\frac{N(\vec{\mathrm{v}})d\vec{\mathrm{v}}}{N} = \left(\frac{m}{2\pi kT}\right)^{3/2} e^{-\frac{m\mathrm{v}^2}{2kT}} \mathrm{v}^2 d\mathrm{v}\, d\Omega$$

In most of our applications, the *direction* of particle travel is not of particular interest, but the *speed* of the particles is. Thus, we may integrate this equation over all angles to give the **Maxwellian velocity distribution**:

Eq. 8.7 $$\frac{N(\mathrm{v})d\mathrm{v}}{N} = \left(\frac{m}{2\pi kT}\right)^{3/2} e^{-\frac{m\mathrm{v}^2}{2kT}} 4\pi\, \mathrm{v}^2 d\mathrm{v}$$

Figure 8.1: The Maxwellian velocity distribution

This gives the fraction of particles with speeds in the range $\mathrm{v} \rightarrow \mathrm{v} + d\mathrm{v}$. Figure 8.1 shows a plot of this distribution function. This graph shows that relatively few particles will have speeds

that are either extremely high or extremely low (near zero). Most of the particles will have intermediate speeds, with the most probable speed being found at the location of the peak in the distribution function. This speed can be determined using calculus:

Eq. 8.8 $$\frac{d}{d\mathrm{v}}\frac{N(\mathrm{v})}{N}=\left(\frac{m}{2\pi kT}\right)^{3/2}e^{-\frac{m\mathrm{v}^2}{2kT}}4\pi\left(2\mathrm{v}-\frac{m\mathrm{v}^3}{kT}\right)\quad\Rightarrow 0$$

The solution is $2kT = m\mathrm{v}^2$, which gives the **most probable speed** (or peak speed), v' as follows:

Eq. 8.9 $$\mathrm{v}'=\sqrt{\frac{2kT}{m}}$$

We might also inquire as to the *average* speed ($\bar{\mathrm{v}}$) of a particle in the gas. This can be found by weighting each speed with its probability, adding them up, and dividing by the total:

Eq. 8.10 $$\bar{\mathrm{v}}=\frac{\int_0^\infty \mathrm{v}N(\mathrm{v})d\mathrm{v}}{N}=\left(\frac{m}{2\pi kT}\right)^{3/2}4\pi\int_0^\infty \mathrm{v}^3 e^{-\frac{m\mathrm{v}^2}{2kT}}d\mathrm{v}$$

The definite integral is easily found: $\int_0^\infty x^3e^{-ax^2}dx=\frac{\Gamma(2)}{2a^2}=\frac{1}{2a^2}$, where $a = m/2kT$. The integral is then $\frac{1}{2}\left(\frac{2kT}{m}\right)^2=2\left(\frac{kT}{m}\right)^2$, giving the following value for the **average speed**:

Eq. 8.11 $$\bar{\mathrm{v}}=\left(\frac{m}{2\pi kT}\right)^{3/2}4\pi\cdot 2\left(\frac{kT}{m}\right)^2=\sqrt{\frac{kT}{m}}\frac{8\pi}{(2\pi)^{3/2}}=\frac{2^{3/2}}{\sqrt{\pi}}\sqrt{\frac{kT}{m}}\quad=\sqrt{\frac{8kT}{\pi m}}$$

Note that this value is slightly greater than the most probable speed: $\bar{\mathrm{v}}=\frac{2}{\sqrt{\pi}}\mathrm{v}'\approx 1.128\,\mathrm{v}'$.

Gas Pressure

Moving particles collide with each other, exchanging momentum and creating gas pressure. In Chapter 2, we noted that pressure can be expressed as a momentum flux:

Eq. 2.12 $$\text{pressure}=\frac{\perp\text{ force}}{\text{area}}=\frac{\frac{\mathrm{d}}{\mathrm{dt}}\perp\text{ momentum}}{\text{area}}=\text{momentum flux}\left[\frac{\text{momentum}}{\text{cm}^2\text{-s}}\right]$$

To determine this flux, we consider a gas of number density N with a uniform distribution of particle velocities, defined as follows: one third of the particles in each unit volume ($^1/_3\,N$) move parallel to the x axis, with speed $\mathrm{v}_x = \bar{\mathrm{v}}$; similarly, another third have only y velocities, with $\mathrm{v}_y = \bar{\mathrm{v}}$, and the remainder have only z velocities, with $\mathrm{v}_z = \bar{\mathrm{v}}$.

We now establish an area (A) that is perpendicular to the x axis and use it to construct a cylinder of length $2\bar{\mathrm{v}}\Delta t$ and volume $V = 2A\bar{\mathrm{v}}\Delta t$, as shown in Figure 8.2. The number of

particles in the cylinder is then $NV = 2NA\bar{\mathrm{v}}\Delta t$, with one third of these ($\frac{1}{3}NV = \frac{2}{3}NA\bar{\mathrm{v}}\Delta t$) having non-zero *x* velocities.

Figure 8.2: Volume for deriving gas pressure

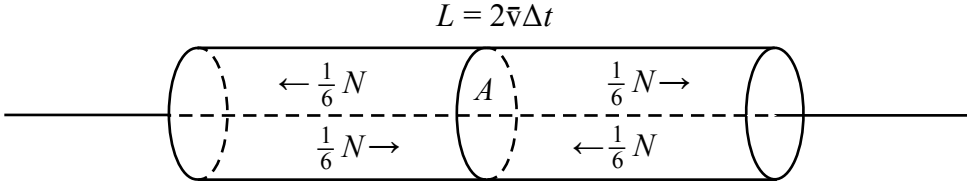

Of these *x*-moving particles, half of them ($\frac{1}{2}(\frac{1}{3}NV) = \frac{1}{6}NV = \frac{1}{3}NA\bar{\mathrm{v}}\Delta t$) will move in the +*x* direction and the other half will move in the –*x* direction. Thus, within the cylinder, half of the *x*-moving particles are moving *toward* area *A* while the other half are moving *away from* it. The particles moving toward area A (from either side) will all pass through it in time Δt – a total of $\frac{1}{3}NA\bar{\mathrm{v}}\Delta t$ particles. The rate of particle flow through A is then $\frac{1}{3}NA\bar{\mathrm{v}}$ particles per second, and the rate per unit area (the particle flux) is $\frac{1}{3}N\bar{\mathrm{v}}$. The momentum carried by each particle is $p = m\bar{\mathrm{v}}$, and the momentum flux – which is equal to the pressure *P* – is then $\frac{1}{3}N\bar{\mathrm{v}}p = \frac{1}{3}Nm\bar{\mathrm{v}}^2$.

Now if the velocity distribution is Maxwellian, rather than the special uniform distribution utilized above, then we substitute v for $\bar{\mathrm{v}}$ and *N*(v) for *N* and integrate over all velocities. The pressure will then be as follows:

Eq. 8.12 $$P = \tfrac{1}{3}\int_0^\infty N(\mathrm{v})p\,\mathrm{v}\,d\mathrm{v} = \tfrac{1}{3}m\int_0^\infty N(\mathrm{v})\mathrm{v}^2\,d\mathrm{v}$$

We now insert the Maxwellian distribution $\left(N(\mathrm{v}) = 4\pi\left(\frac{m}{2\pi kT}\right)^{3/2} N\mathrm{v}^2 e^{-\frac{m\mathrm{v}^2}{2kT}} \right)$ and solve for the pressure:

Eq. 8.13 $$P = \frac{1}{3}m\cdot 4\pi\left(\frac{m}{2\pi kT}\right)^{3/2} N\int_0^\infty \mathrm{v}^4 e^{-\frac{m\mathrm{v}^2}{2kT}}d\mathrm{v}$$

The definite integral is $\int_0^\infty x^4 e^{-ax^2}dx = \frac{\Gamma(5/2)}{2a^{5/2}} = \frac{3\sqrt{\pi}}{8a^{5/2}}$, where $a = m/2kT$; this yields the following simple result:

Eq. 8.14 $$P = \frac{4\pi}{3}m\left(\frac{m}{2\pi kT}\right)^{3/2} N\frac{3\sqrt{\pi}}{8}\left(\frac{2kT}{m}\right)^{5/2} = NkT = P_g$$

The **gas pressure** is just the product of number density and temperature – a statement of the **ideal gas law**.

Mean Kinetic Energy

We may also use the distribution function to determine the **mean kinetic energy** of a particle in the gas.

Eq. 8.15 $$\overline{KE} = \overline{\tfrac{1}{2} m \mathrm{v}^2} = \tfrac{1}{2} m \overline{\mathrm{v}^2} = \tfrac{1}{2} m \frac{\int_0^\infty N(\mathrm{v}) \mathrm{v}^2 \, d\mathrm{v}}{N}$$

But this is the same integral used in Equation 8.12 to determine the pressure; thus, we can substitute from that equation to obtain the following:

Eq. 8.16 $$\tfrac{1}{2} m \overline{\mathrm{v}^2} = \frac{1}{2} \frac{m}{N} \cdot \frac{P_g}{\frac{1}{3} m} = \frac{3}{2} \frac{P_g}{N} = \underline{\underline{\tfrac{3}{2} kT}}$$

This is the average kinetic energy of a particle in the gas at temperature T. We can use this expression to define another speed: v_{rms} or the **root mean square speed**.

Eq. 8.17 $$\mathrm{v}_{rms} \equiv \sqrt{\overline{\mathrm{v}^2}} = \sqrt{\frac{3kT}{m}}$$

Note that this speed is slightly greater than the two previously defined speeds: $\mathrm{v}_{rms} \approx 1.085\,\bar{\mathrm{v}} \approx 1.225\mathrm{v}'$. Also note while the particle speeds all relate to temperature, there are several different ways to define the temperature of a star.

Temperature

(1) We could use spectra to determine the relative populations of atomic energy levels in the atmosphere and then apply the Boltzmann equation $\left(\frac{N_n}{N_m} = \frac{g_n}{g_m} e^{-\Delta E_{nm}/kT} \right)$ to find T. The temperature calculated in this manner would be an **excitation temperature**.

(2) We could use spectra to determine the relative populations of different ionization stages and then apply the Saha equation $\left(\frac{N_{i+1} N_e}{N_i} = \frac{2U_{i+1}(T)}{U_i(T)} \left(\frac{2\pi m_e kT}{h^2} \right)^{3/2} e^{-\chi_i/kT} \right)$ to find T. The temperature calculated in this manner would be an **ionization temperature**.

Alternatively, we could relate the star's radiation to the Planck function $\left(B_\nu(T) = \frac{2h\nu^3}{c^2} \frac{1}{e^{h\nu/kT} - 1} \right)$:

(3) We could equate the intensity (or flux) of the star's radiation at some frequency (I_ν) to that of a blackbody at the same frequency ($B_\nu(T)$) and solve for T ; this would give us a **brightness temperature** – often used in radio astronomy.

(4) We could measure the intensities (or fluxes) of the star at two different frequencies and find the ratio of these two; we could calculate the corresponding ratio for a blackbody, adjusting its temperature to match the ratio measured for the star; this would give us a **color temperature**.

(5) We could measure the stellar intensity (or flux), integrated over all frequencies (or wavelengths), and equate this result to the corresponding value for a blackbody at some temperature T:

Eq. 8.18 $$B(T) = \int_0^\infty B_\lambda(T)\,d\lambda = 2hc^2 \int_0^\infty \frac{1}{\lambda^5} \frac{1}{e^{hc/\lambda kT} - 1} d\lambda$$

Letting $x = \dfrac{hc}{\lambda kT}$ we have $d\lambda = -\dfrac{hc}{kT}\dfrac{dx}{x^2}$, and the equation is transformed:

Eq. 8.19 $$B(T) = 2hc^2 \frac{k^4T^4}{h^4c^4} \cdot \int_0^\infty \frac{x^3}{e^x - 1} dx = \frac{2k^4T^4}{h^3c^2} \cdot \frac{\pi^4}{15} = \frac{2\pi^4k^4}{15h^3c^2} T^4$$

The temperature identified in this manner is the **effective temperature**.

Two constants have been defined in connection with this result: the **Stefan-Boltzmann constant (σ)** and the **radiation pressure constant (a)**[*].

Eq. 8.20 $$\sigma \equiv \frac{2\pi^5k^4}{15c^2h^3} \approx 5.67 \times 10^{-5} \quad \left(\frac{\text{erg}}{\text{cm}^2\text{-K}^4\text{-s}}\right)$$

Eq. 8.21 $$a \equiv \frac{8\pi^5k^4}{15c^3h^3} \approx 7.56 \times 10^{-15} \quad \left(\frac{\text{erg}}{\text{cm}^3\text{-K}^4}\right)$$

Clearly $\sigma = ac/4$. The integrated Planck function is then as follows:

Eq. 8.22 $$B(T) = \frac{\sigma T^4}{\pi}$$

(6) As a final temperature determination method, we could return to the gas and examine the particle velocity distribution to find the average kinetic energy of the gas particles $\overline{\frac{1}{2}m\text{v}^2} = \frac{1}{2}m\dfrac{\int_0^\infty N(\text{v})\text{v}^2\,d\text{v}}{N}$. This would be equated to $^3/_2\,kT$; the resulting temperature is the **kinetic temperature**.

As can be seen, we may define three different temperatures in terms of the state of the matter in the atmosphere, and another three different temperatures based on the radiation field in the atmosphere; ideally, in equilibrium, these values will all be the same. In normal usage, when we talk about the 'temperature' of a *star*, we usually mean the effective temperature; when we talk about the 'temperature' of a *gas*, we usually mean the kinetic temperature.

Model Atmospheres

Now that we understand temperature, we are ready to investigate the structure of a stellar atmosphere. How do the various gas properties change with position within the atmosphere? How does the flow of radiation through the atmosphere affect the gas properties at each level? These and other questions can be answered by constructing a **model atmosphere** – a numerical

[*] See Appendix: Constants

tabulation of gas and radiation properties as a function of altitude, generated by a series of equations linking all the variables. If we assume an atmosphere in radiative equilibrium – one with no energy sources or sinks – what equations can we apply to determine the atmospheric structure?

Hydrostatic Equilibrium

Figure 8.3: Force diagram for an atmospheric mass element

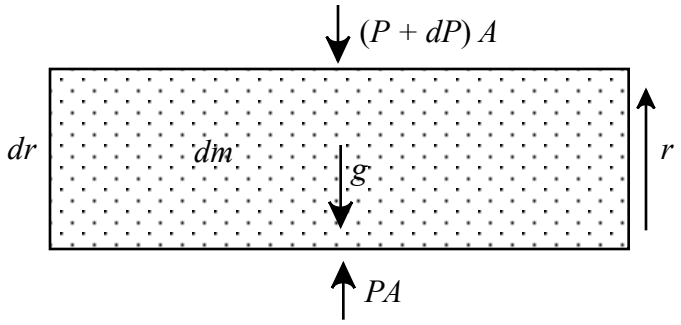

Consider a differential mass element *dm*, of vertical thickness *dr* and horizontal area *A*, as shown in Figure 8.3. The vertical forces on this mass element are produced by gravity (*g*) and also pressure forces acting on the bottom (*P*) and the top (*P* + *dP*) of the element. If the atmosphere is in **hydrostatic equilibrium**, there will be no vertical acceleration, and we can formulate an equation by requiring that the upward forces balance the downward forces.

The vertical force balance requires that $PA = (P + dP)A + g\,dm$; the mass can be expressed in terms of the density ρ as $dm = \rho A\,dr$. Combining these two gives $P = (P + dP) + \rho\, g\, dr$, which then yields the **equation of hydrostatic equilibrium**:

Eq. 8.23 $$\frac{dP}{dr} = -\rho\, g$$

Note that for a thin atmosphere ($r \approx R$), gravity is essentially constant, with $g = GM/R^2$, while the density is a function of radius ($\rho = \rho(r)$).

Ideal Gas Law

In Equation 8.14 we generated the **ideal gas law**, which relates the gas pressure to the number density of particles in the gas: $P_g = NkT$. However, because the equation of hydrostatic equilibrium relates gas pressure to *mass* density, we will need a connection between these two densities. This can be provided by dimensional analysis: to convert grams/cc into particles/cc we multiply the former by moles/gram and then by particles per mole (Avogadro's number):

Eq. 8.24 $$N\left(\frac{\#}{\text{cc}}\right) = \rho\left(\frac{\text{g}}{\text{cc}}\right)\cdot\frac{1}{\mu}\left(\frac{\text{mole}}{\text{g}}\right)\cdot N_A\left(\frac{\#}{\text{mole}}\right) \quad\Rightarrow\quad N = \frac{\rho N_A}{\mu}$$

Alternatively, we could write this expression in terms of the amu relation: $H \equiv N_A^{-1} = 1.66 \times 10^{-24}$ g/amu.

Eq. 8.25 $$N\left(\frac{\#}{\text{cc}}\right)=\rho\left(\frac{\text{g}}{\text{cc}}\right)\cdot\frac{1}{\mu}\left(\frac{\text{atoms}}{\text{amu}}\right)\cdot\frac{1}{H}\left(\frac{\text{amu}}{\text{g}}\right)\quad\Rightarrow\quad N=\frac{\rho}{\mu H}$$

Note that in place of H, some authors use $m_H = 1.67\ \times 10^{-24}$ g/hydrogen atom; this gives the approximate relation $N \approx \rho/\mu m_H$.

Using these relations we may now write the ideal gas law in several different ways:

Eq. 8.26 $$P_g = NkT \qquad P_g = \frac{\rho kT}{\mu H} \qquad P_g \approx \frac{\rho kT}{\mu m_H} \qquad P_g = \frac{\rho N_A kT}{\mu} \qquad P_g = \frac{\rho \Re T}{\mu}$$

In the last of these we use the **gas constant** $\Re \equiv N_A k$. In this book we will normally utilize either the first or last of these forms.

Mean Molecular Weight

In most of these expressions of the ideal gas law we find the **mean molecular weight** μ, with units of either grams per mole or, equivalently, amu's per particle. The name is misleading as μ is actually an *average particle mass*. It is found by dividing the total mass of all particles (in amu) by the total number of particles – a relatively simple concept. But the number of particles will depend on the degree of ionization, which must be known in order to determine the value of μ.

Consider an atom of helium, which has a mass (m) of 4.0026 amu. A gas of pure neutral helium (He I) would have one particle per atom and a mean molecular weight of 4.0026 amu per particle. A gas of singly ionized helium (He II) would produce two particles per atom – one electron and one ion – and thus have a mean molecular weight of 4.0026 ÷ 2 = 2.0013 amu per particle. Similarly, a gas of doubly ionized helium (He III) would have a mean molecular weight of 1.3342.

The concept can easily be expanded to include gases that are mixtures of different elements. In general, if N_i is the number density of species i (including free electrons) and m_i is the mass of species i (in amu), then the mean molecular weight is calculated as follows:

Eq. 8.27 $$\mu = \frac{\sum N_i m_i}{\sum N_i} = \frac{\sum N_i m_i}{N_T}$$ where N_T is the total number density (of all particles)

The degree of ionization is usually high in stellar interiors but may be either high or low in stellar atmospheres, depending on temperature and pressure. If all atomic species are assumed to be neutral, with no free electrons, then the sum is simply performed over the atomic numbers Z.

Eq. 8.28 $$\mu = \frac{\sum_Z N_Z m_Z}{N_T} = \overline{m}$$ where $\overline{m}$ is the mean atomic mass (in amu)

Naturally μ is composition dependent. In modeling, one normally assumes an appropriate composition for the stellar type in question. Composition is often given in terms of **mass fractions**: X, Y, and Z.

Mass Fractions

X is the mass fraction of hydrogen – the mass of hydrogen divided by the total mass of the star. Y is the mass fraction of helium, and Z (not to be confused with the atomic number Z) is the mass fraction of **metals**: all the elements other than hydrogen and helium. As these three quantities should add up to 1, only two of them need be specified. Explicit calculation of each would be done as follows:

Eq. 8.29 $$X = \frac{N_H m_H}{\sum_z N_z m_z} = \frac{N_H m_H}{N_T \mu} = \frac{N_H m_H}{\rho N_A}$$

Eq. 8.30 $$Y = \frac{N_{He} m_{He}}{\sum_z N_z m_z} = \frac{N_{He} m_{He}}{N_T \mu} = \frac{N_{He} m_{He}}{\rho N_A}$$

Eq. 8.31 $$Z = \frac{\sum_M N_M m_M}{\sum_z N_z m_z} = \frac{\sum_M N_M m_M}{N_T \mu} = \frac{\sum_M N_M m_M}{\rho N_A}$$

Here the subscript M indicates *metals*, and the sum is over the metals. Also, N_H indicates the number density of hydrogen *nuclei*, no matter what their ionization state; similarly for N_{He} and N_M. All masses m_i are in amu's.

A fair uncertainty exists for the abundance of helium in stellar atmospheres; this is because helium lines do not appear in the spectra of cooler stars. The range of estimates for the number ratio N_{He}/N_H is approximately 0.03 to 0.14. This yields the following ranges for the values of the mass fractions:

$X \approx 0.86 \rightarrow 0.63$ $Y \approx 0.13 \rightarrow 0.35$ $Z \approx 0.018 \rightarrow 0.013$

Not all stars have the same composition; some are *metal poor* while others are *metal rich*. It is a good idea to always note the composition used to generate a particular model or graph. One should also note that sometimes compositions are given as **number fractions** rather than mass fractions.

Total Pressure

We have seen how pressure is produced by both particles and photons. Gas pressure was given by Equation 8.26 as $P_g = \rho \Re T/\mu$; radiation pressure was given in Equation 2.18 as $P_\nu = (4\pi/3c)\, I_\nu$ for isotropic radiation. Integrating the latter over frequency (we do not care about the spectral distribution of pressure) yields $P = (4\pi/3c)\, I$. Now if the radiation field is that of a blackbody, then $I = B(T) = \sigma T^4/\pi$, and the radiation pressure P_r is as follows:

Eq. 8.32 $$P_r = \frac{4\pi}{3c}\left(\frac{\sigma T^4}{\pi}\right) = \frac{4\sigma T^4}{3c} = \tfrac{1}{3} a T^4$$

The total pressure can then be written as the sum of the gas pressure and the radiation pressure:

Eq. 8.33 $$P = P_g + P_r = \frac{\rho \Re T}{\mu} + \tfrac{1}{3} a T^4$$

In general, the total pressure should be used in making a model atmosphere, although there are some occasions when the contribution from the gas or the radiation may be negligible. We may get some idea of where this might occur by inquiring when the gas and radiation pressures will be equal to each other. For this we set $P_g = P_r$:

Eq. 8.34 $$\frac{\rho \Re T}{\mu} = \tfrac{1}{3} a T^4 \quad \Rightarrow \quad T^3 = \frac{3\Re \rho}{a\mu} = \frac{3\Re N}{a N_A} = \frac{3kN}{a}$$ (using Equation 8.24: $\rho N_A = N\mu$)

Eq. 8.35 $$T = \left(\frac{3kN}{a} \right)^{1/3} \approx 0.3797 N^{1/3}$$

So the equivalency depends on the density and the temperature: for N = 10^{15}, the two pressures are equal at T = 37,970 K; for N = 10^{12}, the two pressures are equal at T = 3797 K. Thus, radiation pressure will be important at relatively high temperatures and/or low densities.

Equilibrium Calculations

In order to calculate a model atmosphere, we need to be able to determine the pressure at any given point; this value will depend on the various gas properties such as temperature, density, composition, etc. In particular, we will need to know the degree of ionization of each element, as this affects the values of N and μ. In Chapter 4 we learned how to use the Saha equation to calculate ionization, and we learned the basic principles to use if there are multiple elements or multiple ionization stages. For our model atmosphere, we will likely use all of these options in order to make the model as realistic as possible. How do we proceed in order to determine the state of a gas in equilibrium?

In theory, we should be able to determine the equilibrium state by knowing the composition (*X, Y, Z*) and any two gas properties (*T, P, N, ρ*, etc.). For this method, we will choose the temperature and the electron pressure as our independent variables – for reasons that will soon become clear.

Our chosen composition will consist of hydrogen (*H*), helium (*He*), and a number of metals (M_j). From these we will identify the species to be included in the model:

- Hydrogen: H, H^+, H^- (and in cool stars, we would add H_2 and H_2^+)
- Helium: He, He^+, He^{++}
- Metals: M_j, M_j^+, M_j^{++}
- Electrons: e^-

We will assume that all the ionization reactions are in equilibrium, with **equilibrium constants** (*K*) defined as follows:

Reaction	Equilibrium Constant	Ionization Potential
$H \rightleftharpoons H^+ + e^-$	$K_H \equiv \frac{N_{H^+} P_e}{N_H}$	$\chi_H = 13.598$ eV
$H^- \rightleftharpoons H + e^-$	$K_{H^-} \equiv \frac{N_H P_e}{N_{H^-}}$	$\chi_{H^-} = 0.754$ eV
$He \rightleftharpoons He^+ + e^-$	$K_{He} \equiv \frac{N_{He^+} P_e}{N_{He}}$	$\chi_{He} = 24.587$ eV
$He^+ \rightleftharpoons He^{++} + e^-$	$K_{He^+} \equiv \frac{N_{He^{++}} P_e}{N_{He^+}}$	$\chi_{He^+} = 54.416$ eV
$M_j \rightleftharpoons M_j^+ + e^-$	$K_{M_j} \equiv \frac{N_{M_j^+} P_e}{N_{M_j}}$	
$M_j^+ \rightleftharpoons M_j^{++} + e^-$	$K_{M_j^+} \equiv \frac{N_{M_j^{++}} P_e}{N_{M_j^+}}$	

It will be immediately recognized that the equilibrium constants can be calculated using Saha equations:

Eq. 8.36 $$K_i = \frac{N_{i+1} P_e}{N_i} = \frac{2U_{i+1}(T)}{U_i(T)} \left(\frac{2\pi m_e}{h^2} \right)^{3/2} (kT)^{5/2} e^{-\chi_i / kT}$$

Note that these are *pressure* equilibrium constants (K_P) as they have units of pressure.

Given our independent variables (T and P_e) and the atomic properties for each element, we may calculate all of the equilibrium constants. The unknowns are the various partial pressures: P_H, P_{H^+}, P_{H^-}, P_{He}, P_{He^+}, $P_{He^{++}}$, P_{Mj}, P_{Mj^+}, $P_{Mj^{++}}$.

We then express all the partial pressures in terms of the partial pressures of the neutral species:

Eq. 8.37 $$P_{H^+} = P_H \frac{K_H}{P_e}$$ Eq. 8.38 $$P_{H^-} = P_H \frac{P_e}{K_{H^-}}$$

Eq. 8.39 $$P_{He^+} = P_{He} \frac{K_{He}}{P_e}$$ Eq. 8.40 $$P_{He^{++}} = P_{He^+} \frac{K_{He^+}}{P_e} = P_{He} \frac{K_{He} K_{He^+}}{P_e^2}$$

Eq. 8.41 $$P_{M_j^+} = P_{M_j} \frac{K_{M_j}}{P_e}$$ Eq. 8.42 $$P_{M_j^{++}} = P_{M_j^+} \frac{K_{M_j^+}}{P_e} = P_{M_j} \frac{K_{M_j} K_{M_j^+}}{P_e^2}$$

We can now use composition information to link the **elemental number abundances** A_i; we will need A_H, A_{He}, and A_{Mj}. (These are given in Allen (1973) and Cox (2000) as $\log A_H = 12.00$,

log A_{He} = 10.99, etc.) We can then write the total number density of helium nuclei and metal nuclei in terms of the total number density of hydrogen nuclei and their relative abundances:

Eq. 8.43 $$N_{He\,tot} = \frac{A_{He}}{A_H} N_{H\,tot} = f_{He} N_{H\,tot} \qquad \text{where } f_{He} \equiv \frac{A_{He}}{A_H}$$

Eq. 8.44 $$N_{M_j\,tot} = \frac{A_{M_j}}{A_H} N_{H\,tot} = f_j N_{H\,tot} \qquad \text{where } f_j \equiv \frac{A_{M_j}}{A_H}$$

The total number densities of the elements are simply sums of the number densities of the relative species (at least as long as molecules are not considered):

Eq. 8.45
$$N_{H\,tot} = N_H + N_{H^+} + N_{H^-} = \left(P_H + P_{H^+} + P_{H^-}\right)/kT$$
$$= \left(1 + \frac{K_H}{P_e} + \frac{P_e}{K_{H^-}}\right)\frac{P_H}{kT} \equiv W_H \frac{P_H}{kT}$$

Eq. 8.46
$$N_{He\,tot} = N_{He} + N_{He^+} + N_{He^{++}} = \left(P_{He} + P_{He^+} + P_{He^{++}}\right)/kT$$
$$= \left(1 + \frac{K_{He}}{P_e}\left(1 + \frac{K_{He^+}}{P_e}\right)\right)\frac{P_{He}}{kT} \equiv W_{He} \frac{P_{He}}{kT}$$

Eq. 8.47
$$N_{M_j\,tot} = N_{M_j} + N_{M_j^+} + N_{M_j^{++}} = \left(P_{M_j} + P_{M_j^+} + P_{M_j^{++}}\right)/kT$$
$$= \left(1 + \frac{K_{M_j}}{P_e}\left(1 + \frac{K_{M_j^+}}{P_e}\right)\right)\frac{P_{M_j}}{kT} \equiv W_j \frac{P_{M_j}}{kT}$$

Now all species' partial pressures can be expressed in terms of $K_i(T)$, P_e, P_H, and f_i:

Eq. 8.48 $$P_{He} = f_{He} P_H \frac{W_H}{W_{He}}$$

Eq. 8.49 $$P_{M_j} = f_j P_H \frac{W_H}{W_j}$$

We now introduce the **equation of charge conservation**, which asserts that the number of negative charges should equal the number of positive charges:

Eq. 8.50 $$P_e + P_{H^-} = P_{H^+} + P_{He^+} + 2P_{He^{++}} + P_{M^+} + 2P_{M^{++}}$$

The metal pressures are sums over all the metals in the model:

Eq. 8.51 $$P_{M^+} = \sum_j P_{M_j^+} = \sum_j P_{M_j} \frac{K_{M_j}}{P_e} = P_H \frac{W_H}{P_e} \sum_j \frac{f_j K_{M_j}}{W_j}$$

Eq. 8.52 $$P_{M^{++}} = \sum_j P_{M_j^{++}} = \sum_j P_{M_j} \frac{K_{M_j} K_{M_j^+}}{P_e^2} = P_H \frac{W_H}{P_e^2} \sum_j \frac{f_j K_{M_j} K_{M_j^+}}{W_j}$$ and

Eq. 8.53 $$P_{M^+} + 2P_{M^{++}} = P_H \frac{W_H}{P_e} \sum_j \frac{f_j K_{M_j}}{W_j} \left(1 + 2 \frac{K_{M_j^+}}{P_e} \right)$$

A similar expression can be written for the helium pressures:

Eq. 8.54 $$P_{He^+} + 2P_{He^{++}} = P_H \frac{W_H}{P_e} \frac{f_{He} K_{He}}{W_{He}} \left(1 + 2 \frac{K_{He^+}}{P_e} \right)$$

All of these can be substituted into the charge conservation equation:

Eq. 8.55 $$P_e = P_H \left[\frac{K_H}{P_e} - \frac{P_e}{K_{H^-}} + \frac{W_H}{W_{He}} \frac{f_{He} K_{He}}{P_e} \left(1 + 2 \frac{K_{He^+}}{P_e} \right) + \frac{W_H}{P_e} \sum_j \frac{f_j K_{M_j}}{W_j} \left(1 + 2 \frac{K_{M_j^+}}{P_e} \right) \right]$$

This is a linear equation in P_H that can easily be solved. (If diatomic hydrogen molecules are included in the model, this equation becomes quadratic.) From this solution, all the other partial pressures can be calculated, and from these, the total gas pressure can be determined:

Eq. 8.56 $$P_g = \sum_i P_i$$

The mean molecular weight can be found from a weighted average of the particle masses. (Electrons need not be explicitly listed in the numerator as their masses are already included in the atomic masses; electrons *are* included in the denominator.)

Eq. 8.57 $$\mu = \frac{\sum N_i m_i}{\sum N_i} = \frac{\sum P_i m_i}{P_g} = \frac{P_H W_H}{P_g} \left(m_H + m_{He} f_{He} + \sum_j m_{M_j} f_j \right)$$

And finally the density can be calculated:

Eq. 8.58 $$\rho = \frac{\mu P_g}{\Re T}$$

Thus, given the composition, the temperature, and the electron pressure, the concentrations (or partial pressures) of all species and the bulk gas properties can be determined – assuming local thermodynamic equilibrium. This is the type of information needed to determine opacities.

As noted above, we can use the composition and any two gas properties to find the equilibrium configuration. We chose temperature and electron pressure because they input directly into the Saha equations, allowing us to determine equilibrium constants. But this is somewhat inconvenient, as the electron pressure depends on temperature, and in itself does not tell us much about the state of the gas.

It would seem far more reasonable to choose the temperature and *density* of the gas as independent variables; both of these affect the rate at which particles collide with each other, and collisions are the primary mechanisms by which the gas attains equilibrium. But density does

not enter directly into the Saha equation; in fact, it was the *last* property calculated in our procedure above. How can we modify our process to make it work with density?

We have species concentrations (x_i) as functions of temperature and electron pressure ($x_i = f(T, P_e)$), but would prefer to know them as functions of temperature and density ($x_i = f(T, \rho)$). We can get $\rho(T, P_e)$, and we want $x_i(T_o, \rho_o)$ – the equilibrium configurations at some particular temperature T_o and density ρ_o. All we have to do is solve the following equation for P_e:

Eq. 8.59 $$\rho(T_o, P_e) = \rho_o$$

As we cannot isolate P_e, we must instead *guess* its value, calculate ρ, compare this with ρ_o, and use this result to guess a new value of P_e. It is hoped that our sequence of guesses will ultimately converge on the correct value of P_e, allowing us to determine the other equilibrium values. One procedure to employ in this problem is the **secant method**.

The Secant Method

In applying the secant method to this problem, we first write logarithmic forms of our variables. (These particular variables may range over several orders of magnitude, and log forms provide a more efficient means of covering the necessary range.) Let $x = \log P_e$, $y_o = \log \rho_o$, and $f(x) = \log[\rho(T_o, P_e)]$. Then solve $f(x) - y_o = 0$ for x by iteration using the secant method, where successive approximations are given by the following:

Eq. 8.60 $$x_{n+1} = x_n + (x_n - x_{n-1})\frac{y_o - f(x_n)}{f(x_n) - f(x_{n-1})}$$

Figure 8.4 demonstrates the basic procedures of the secant method. We seek the x value at which the curve $f(x)$ crosses the y_o line. We choose the first two x values, and the rest are generated by Equation 8.60.

Figure 8.4: Illustration of the secant method

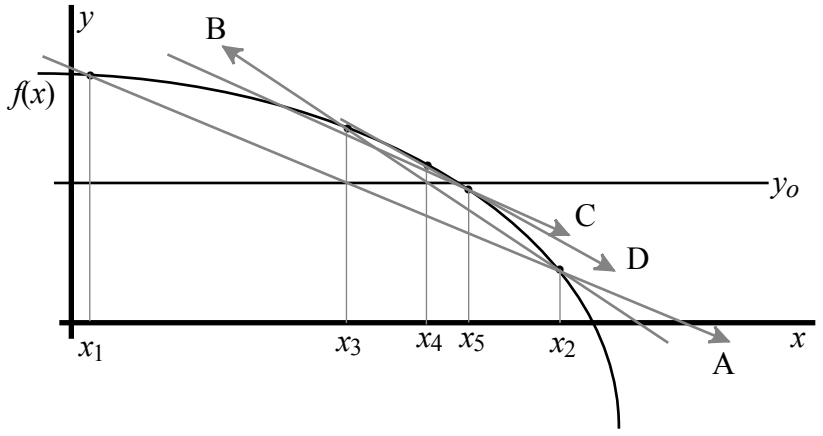

- Secant A passes through $[x_1, f(x_1)]$ and $[x_2, f(x_2)]$.
- Secant B passes through $[x_2, f(x_2)]$ and $[x_3, f(x_3)]$.

- Secant C passes through $[x_3, f(x_3)]$ and $[x_4, f(x_4)]$.
- Secant D, passes through $[x_4, f(x_4)]$ and $[x_5, f(x_5)]$.

Secant D appears to pass very close to the intersection of $f(x)$ and y_o. That is, because $f(x_6) \approx y_o$; the next value (x_6) will be very close to the solution we seek.

Altitude Variations

We have seen how the gas properties can be determined as functions of density and temperature; but these quantities will vary with position in the atmosphere. We now need to determine how temperature and density (and all the other gas properties) vary with altitude in the photosphere.

We may begin by assuming hydrostatic equilibrium in the atmosphere, as derived above:

Eq. 8.23 $$\frac{dP}{dr} = -\rho g$$

If we neglect radiation pressure for the moment, we have pressure as a function of density and temperature:

Eq. 8.61 $$P \approx P_g = \frac{\rho \Re T}{\mu} \qquad \text{where } \mu = \mu(\rho, T)$$

If we could derive $\rho(r)$ and $T(r)$, we could solve the problem.

Toward the end of Chapter 2 we used radiative transfer to obtain a relation between temperature and optical depth, assuming the gray case, the Eddington approximation, and radiative equilibrium:

Eq. 8.62 $$T(\tau) = T_e(^1/_2 + ^3/_4 \tau)^{1/4}$$

As τ is related to r, this equation might prove useful. However, because optical depth is also frequency dependent, we must be careful, as we do not want temperature to be frequency dependent as well. Instead, we will use a mean optical depth $\bar{\tau}$, rather than τ_ν.

From our definition of τ_ν ($d\tau_\nu \equiv -\kappa_\nu \rho\, dr$) we will define a **mean optical depth** $\bar{\tau}$:

Eq. 8.63 $$d\bar{\tau} \equiv -\bar{\kappa}\rho\, dr$$

Here $\bar{\kappa}$ is a mean absorption coefficient (to be defined later).

We may then combine this equation with hydrostatic equilibrium to eliminate r and ρ:

Eq. 8.64 $$\frac{dP}{d\bar{\tau}} = \frac{g}{\bar{\kappa}}$$

Thus, given the model parameters T_e and g ($=GM/R^2$), and using a $T(\bar{\tau})$ relationship such as Equation 8.62, we can arrive at $P(\bar{\tau})$, assuming that $\bar{\kappa}$ can be found.

And if $P \approx P_g$, then $P \approx \rho \Re T/\mu$ and $\rho \approx P\mu / \Re T$. Hydrostatic equilibrium then can be written in terms of temperature:

Eq. 8.65 $$-\frac{dP}{dr} = \rho g = \frac{\mu g}{\Re}\frac{P}{T} \quad \Rightarrow \quad -\frac{d\ln P}{dr} = \frac{\mu g}{\Re}\frac{1}{T}$$

This allows calculation of the altitude coordinate:

Eq. 8.66 $$dr = -\frac{\Re T}{\mu g} d\ln P$$

Thus, the goal – obtaining $T(r)$ and $P(r)$ – is not really attained; rather, we determine $r(T,P)$, which provides us with the same information in the end.

Effective Gravity

Note that in the above proceedings, we assumed that radiation pressure was negligible, but this will not be valid for every stellar atmosphere. For higher temperature models, we may include radiation pressure by the following method. Begin with the expression for total pressure:

Eq. 8.67 $$P = P_g + P_r$$

Differentiate both sides with respect to $\bar{\tau}$ to obtain an equation similar to Equation 8.64:

Eq. 8.68 $$\frac{dP}{d\bar{\tau}} = \frac{dP_g}{d\bar{\tau}} + \frac{dP_r}{d\bar{\tau}} = \frac{g}{\bar{\kappa}} \quad \Rightarrow \quad \frac{dP_g}{d\bar{\tau}} = \frac{g}{\bar{\kappa}} - \frac{dP_r}{d\bar{\tau}}$$

From Chapter 2 we have the following for the gray case and radiative equilibrium:

Eq. 2.124 $$\frac{dK}{d\bar{\tau}} = \frac{F_0}{4\pi}$$

Eq. 8.69 $$P_r = \frac{4\pi}{c}K \quad \Rightarrow \quad dK = \frac{c}{4\pi}dP_r$$

These combine to form the following:

Eq. 8.70 $$\frac{dP_r}{d\bar{\tau}} = \frac{F_0}{c} = \frac{\sigma T_e^4}{c}$$

Inserting this result into Equation 8.68 produces an expression not unlike Equation 8.64:

Eq. 8.71 $$\frac{dP_g}{d\bar{\tau}} = \frac{g}{\bar{\kappa}} - \frac{\sigma T_e^4}{c}$$

We then define an **effective gravity**:

Eq. 8.72 $$g_{eff} \equiv g - \frac{\bar{\kappa}\sigma T_e^4}{c}$$

This transforms Equation 8.71 and allows us to proceed as before:

Eq. 8.73 $$\frac{dP_g}{d\bar{\tau}} = \frac{g_{eff}}{\bar{\kappa}}$$

Note that construction of model atmospheres involves simultaneous solution of radiative equations and gas equations. In practice, the two sets are solved alternately until they converge on a particular solution.

Scale Height

Suppose that a portion of the atmosphere is essentially isothermal, meaning that T (and μ) are constant (in addition to g). Then the altitude equation can easily be integrated:

Eq. 8.74 $$\frac{d\ln P}{dr} = -\frac{\mu g}{\Re T} = \text{constant} \quad \Rightarrow \quad P = P_o e^{-\frac{\mu g}{\Re T} r} = P_o e^{-\frac{r}{H}}$$

Here $H \equiv \Re T/\mu g$ is the (pressure) **scale height**; this is the distance over which the pressure changes by a factor of e. (Density scale heights are used as well.) Although the scale height concept is defined for an essentially constant temperature, it is sometimes used even if this condition is not met.

The scale height can be thought of as the ratio of two competing quantities – the ratio of thermal energy ($\Re T$) to gravitational force (μg). The former is trying to hold the atmosphere up while the latter is trying to pull it down. For relatively low values of g (as found in atmospheres of giants and supergiants), the scale height will be large and the atmosphere will be extended. For the higher g values found in main sequence dwarfs, the scale height will be small and the atmosphere will be compacted.

Non-equilibrium atmospheres

The above discussion is applicable to atmospheres in hydrostatic equilibrium, which can be found in most normal stars; for such stars the atmospheric structure is essentially constant over time. But this is not the case for certain types of variable stars. As an example, we will consider the case of the long-period variable stars (LPVs). The atmospheres of these stars are periodically traversed by shock waves that impart upward momentum to the gas particles, rendering hydrostatic equilibrium inapplicable. We begin by considering the basics of shock waves.

Shock Waves

In a gas, information is transmitted by particle collisions at the speed of sound (c_s), which depends on the local gas properties.

Eq. 8.75 $$c_s^2 = \left.\frac{\partial P}{\partial \rho}\right|_S \quad \text{(at constant entropy)}$$

If a disturbance moves through the gas at speed v < c_s, information about the disturbance is transmitted ahead of it, preparing the gas in advance. If the disturbance is a compression wave, the gas ahead becomes slightly compressed *before* the wave arrives, making changes to the gas properties fairly gradual. Figure 8.5 shows a plot of density vs. position for the leading edge of a subsonic compression wave.

Figure 8.5: Density variation across the leading edge of a subsonic wave

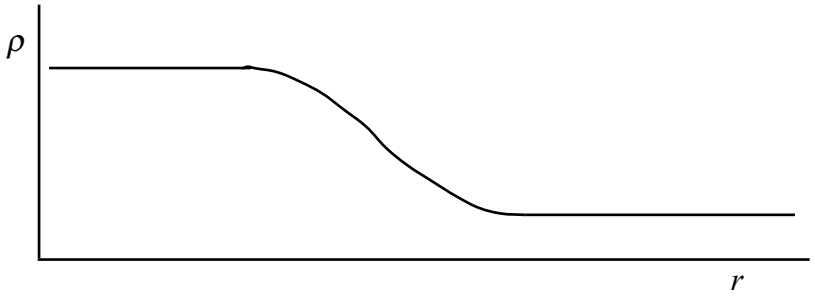

However, if the disturbance moves at $v > c_s$, then no advance warning is given and the compression comes as a complete surprise to the gas. In this case, the compression is essentially instantaneous and a shock wave results, as depicted by the vertical segment in Figure 8.6.

Figure 8.6: Density variation across the leading edge of a supersonic wave

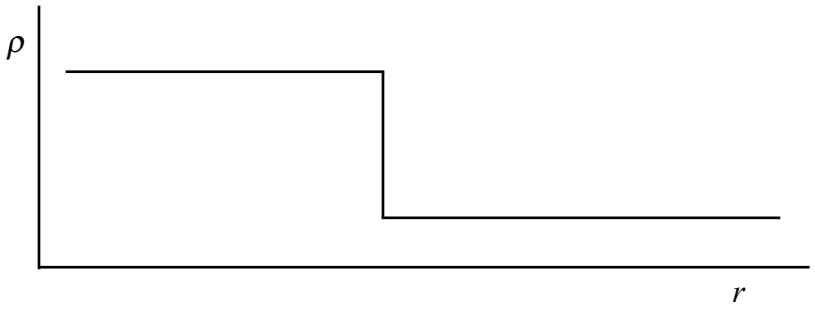

Description of a stellar shock wave involves velocities and densities in the atmosphere. Generally two reference frames are employed: the star, and the shock. Figure 8.7 identifies the relevant densities ahead of and behind the shock, and the velocities as measured in each reference frame.

Figure 8.7: Shock velocities, as defined in the reference frames of the star and the shock

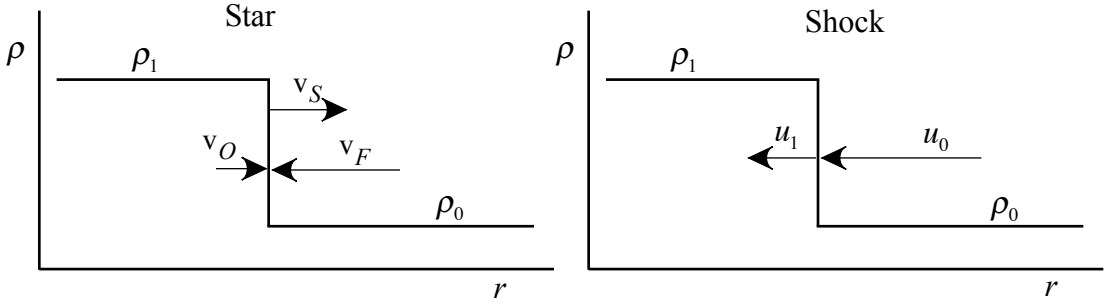

ρ_0 = pre-shock density

ρ_1 = post-shock density

v_S = shock velocity, relative to star ($v_S > 0$)

v_O = outward velocity of post-shock material, relative to star ($v_O > 0$)

v_F = infall velocity of pre-shock material, relative to star ($v_F < 0$)

u_1 = post-shock velocity, relative to shock ($u_1 = v_O - v_S$) ($u_1 < 0$)

u_0 = pre-shock velocity, relative to shock ($u_0 = v_F - v_S$) ($u_0 < 0$)

The shock reference frame is moving at v_S with respect to the star. Thus, the gas velocities are related by a simple transformation. Also of interest is the **velocity discontinuity** across the shock:

Eq. 8.76 $\Delta v = v_O - v_F = u_1 - u_0$ (Note that three of these velocities are negative.)

We may employ conservation of mass across the shock; the mass flow rate into the shock is equal to the mass flow rate out of it:

Eq. 8.77 $\rho_1 u_1 = \rho_0 u_0$

The **compression ratio** (or **shock strength**) S is the ratio of the densities:

Eq. 8.78 $$S = \frac{\rho_1}{\rho_0} = \frac{u_0}{u_1}$$

As the shock progresses through the atmosphere, it has several effects on the gas:

- It imparts an outward velocity (v_O) to previously in-falling material.
- It adds internal energy to the gas, obtained from the bulk kinetic energy difference: the increase in enthalpy per gram is $\Delta H = (u_0^2 - u_1^2)/2$ (where $H = U + PV$ and $\Delta H = \Delta U + \Delta(PV)$).
- It compresses the gas, increasing the density (and also the pressure and temperature).

The influx of energy from the passing shock disrupts the ionization equilibrium of the gas. The kinetic temperature and density both increase significantly across the shock, and this causes atomic collisions to be more frequent and more violent, blasting atoms and molecules apart. Radiation from the gas behind the shock and the work done in expanding this gas both serve to cool the atmosphere and drive it back towards equilibrium at a more normal lower temperature. The time scale of this **relaxation** process depends on the local temperature and density, both of which are continually changing.

Meanwhile, each layer in the atmosphere rises and falls in response to the passing shock, as shown in Figure 8.8. Here the diagonal features mark the location of the shock, which moves outward at a constant velocity, while the solid curve at the bottom marks the location of the photosphere. (One stellar radius = 262.3 $R_\odot$; period = 332 days; phase = 0 at maximum light.)

These variations make the atmosphere quite different from a normal static atmosphere; in particular, the scale height in such a dynamic atmosphere is much greater, as the gas is periodically levitated by the shocks. Clearly, LPVs cannot be accurately modeled by static atmospheres but will require considerable modifications.

Figure 8.8: Trajectories of individual layers in an LPV atmosphere, shown over three periods

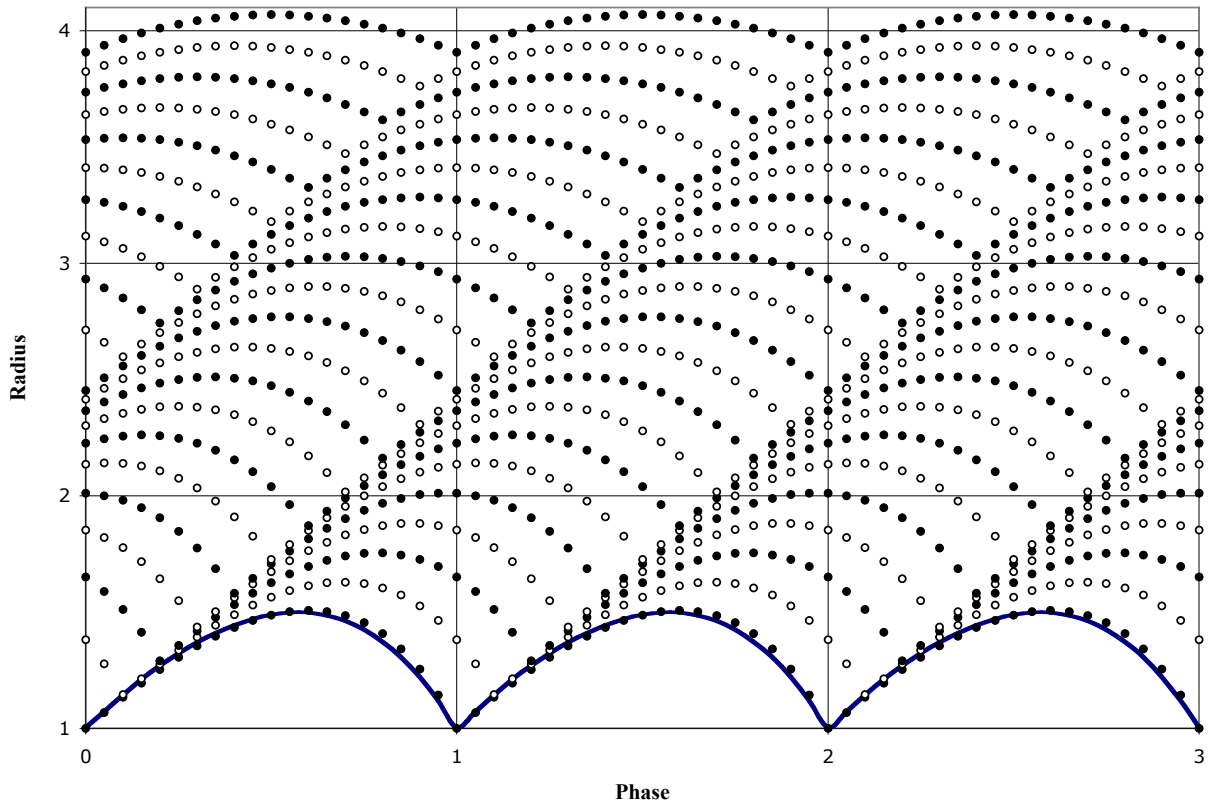

Dynamic Scale Height

To get the pre-shock density distribution for an LPV atmosphere we must somehow estimate the scale height, a concept introduced earlier in this chapter. We first define the **static scale height**:

Eq. 8.79 $$H_S = \frac{\Re T}{\mu g} = \frac{kT}{mg} = \frac{\text{thermal energy}}{\text{gravitational force}}$$

To modify this to obtain a **dynamic scale height**, we add the bulk kinetic energy of the gas to the thermal energy:

Eq. 8.80 $$H_D = \frac{kT + \frac{1}{2} m \left\langle \mathrm{v}^2 \right\rangle}{mg}$$

We can approximate $\langle \mathrm{v}^2 \rangle$ by $\mathrm{v}_O^{\,2}$ and should recall that $g = g(r) = GM/r^2$ must be used for extended atmospheres. This gives the following expression for the dynamic scale height – a quantity that will always be greater than the static scale height.

Eq. 8.81 $$H_D = \frac{kT + \frac{1}{2} m \mathrm{v}_O^2}{GMm/r^2}$$

The resulting pulsating atmosphere is considerably more chaotic and less well-behaved than a normal static one – and thus is more difficult to model. This is in part because the usual assumption of thermodynamic equilibrium is often not appropriate in such atmospheres.

In the next chapter we will turn our attention to the stellar interior, examining the basic physical laws that apply there and determining what assumptions can be made that will allow us to form reasonable models of this fundamental region of a star.

CHAPTER 9: Stellar Interior Models

As noted in Chapter 1, astrophysicists have found it convenient to divide a star into two regions: the atmosphere and the interior. This is because there are significant differences in many of the equations that govern the matter and radiation in these regions. Table 9.1 lists the major differences between these two regions.

Table 9.1: Atmosphere vs. interior

atmosphere – outside	interior – inside
optically thin	optically thick
g is constant	g varies $\approx 1/r^2$
atoms may be neutral and/or ionized	atoms are usually ionized
relatively low temperature, pressure, density	relatively high temperature, pressure, density
no energy sources or sinks	energy generation
low fraction of star's mass	high fraction of star's mass
visible to us	invisible to us

The last point is an important difference in our effort to understand the structure of the star. Unlike the stellar atmosphere, the interior is hidden from our direct view; we do not receive visible photons directly from the stellar interior, making it difficult to gather observational data about this region. Instead we will have to examine the applicable equations of physics that relate the various stellar properties. If we are lucky, we may find an appropriate function that describes the variation of these properties inside the star; alternatively, we may use these equations to construct a numerical model of the stellar interior.

Before we begin, we will make a few simplifying assumptions about the star we choose to study. Real stars are extremely complex, and we do not expect to be able to model or predict *each* of their characteristics. Our task will be difficult enough, even *with* the following simplifications:

Assumptions

- No rotation.
- No magnetic field.
- Spherical symmetry (no θ or ϕ dependence – just r).
- Equilibrium (only *very* slow changes with time will be allowed).

The first two assumptions are obviously not true in all cases, but we would rather not deal with the complexities they would introduce – at least not right now. They can always be added after a basic model is established.

We will now proceed with the basic physical equations that govern the structure of a star.

Continuity of Mass

The most fundamental parameter of a star is its mass, as it determines not only the structure of the star but also the course of its evolution. The mass of a star is constant throughout most of its lifetime, but at this point we are interested in the manner in which the mass is distributed within the star. The mass variable we need is the *mass interior to a given radius*, denoted M_r; as we move outward from the center of the star, this quantity increases as more and more of the star becomes interior to the specified radius. Upon reaching the surface, r becomes R and M_r becomes M – the total mass of the star.

We need M_r because it is this quantity that determines the gravity at a particular radius:

Eq. 9.1 $$g(r) = \frac{GM_r}{r^2}$$

(A spherical shell of matter exerts no net gravitational force on interior mass points.)

Between the center and the surface, the change of M_r with radius is found as follows. Consider a point inside a star at a distance r from the center. The mass contained within this sphere will be M_r. If we now increase the radius by a small amount (dr), we add a spherical shell of thickness dr and surface area $4\pi r^2$ to the sphere of matter interior to the point at r. The mass of this shell (dM_r) will be the volume of the shell ($4\pi r^2 dr$) multiplied by the density of matter in the shell ($\rho(r)$). This gives us the **equation of mass continuity** – the first of our equations of stellar structure.

Eq. 9.2 $$dM_r = 4\pi \rho\, r^2 dr \quad \Rightarrow \quad \frac{dM_r}{dr} = 4\pi\rho r^2$$

Hydrostatic Equilibrium

In the previous chapter we introduced the equation of hydrostatic equilibrium for stellar atmospheres, noting at the time that the value of g was presumed to be constant throughout the atmosphere.

Eq. 8.23 $$\frac{dP}{dr} = -\rho g$$

While this assumption is usually good in an atmosphere, it is never applicable in the interior because interior points farther from the center will have higher values of M_r and thus higher gravity. Therefore we must modify Equation 8.23 by inserting Equation 9.1 into it, to obtain the more general **equation of hydrostatic equilibrium** for the interior:

Eq. 9.3 $$\frac{dP}{dr} = -\frac{GM_r\rho(r)}{r^2}$$

Equation of State

Neither of our first two equations involves temperature – another key variable in the stellar interior. We can introduce temperature by utilizing the **ideal gas law** as our **equation of state** (an equation that shows the functional dependence of the pressure on the other gas properties). This equation for the gas pressure was given in the previous chapter.

Eq. 9.4 $$P_g = \frac{\rho \Re T}{\mu}$$

This equation also introduces the **mean molecular weight μ**, which was difficult to determine for the atmosphere because it involved temperature- and pressure-dependent Saha equations. In the interior however, we may presume that ionization is complete, and this permits considerable simplification.

As before, the mean molecular weight is the ratio of particle mass to particle number. An atom of element z has an atomic mass m_z; when completely ionized it will produce one nucleus and z electrons for a total of $1 + z$ particles. The mean molecular weight for this element is then $m_z/(1 + z)$ and for the entire gas with elemental number densities N_z we have the following:

Eq. 9.5 $$\mu = \frac{\sum N_z m_z}{\sum N_z (1+z)}$$

This expression can be further simplified:

Eq. 9.6
$$\frac{1}{\mu} = \frac{\text{total \# particles}}{\text{total particle mass (amu)}} = \frac{\text{total \# moles}}{\text{total particle mass (gram)}} = \frac{\sum \text{moles of } z}{\text{gram}}$$
$$= \sum \frac{\text{moles } z}{\text{gram } z} \cdot \frac{\text{gram } z}{\text{gram}} = \sum \frac{\text{moles } z}{\text{gram } z} \cdot X_z = \sum \frac{\#\text{particles } z}{\text{mass } z\,(\text{amu})} \cdot X_z = \sum_z \frac{1+z}{m_z} \cdot X_z$$

Now for most heavy elements, $m_z \approx 2z \approx 2(z + 1)$; this means that $(1 + z)/m_z \approx 1/2$ for $z > 2$. We will now employ our *XYZ* notation for mass fractions and write $X = X_1$, $Y = X_2$, and $Z \equiv \sum_{z>2} X_z$. Inserting these expressions into the previous equation we find the following:

Eq. 9.7 $$\frac{1}{\mu} = \sum \frac{1+z}{m_z} X_z = \frac{2}{m_H} X + \frac{3}{m_{He}} Y + \frac{1}{2} Z$$

We now note that m_H =1.008 ≈ 1 amu, and m_{He} = 4.003 ≈ 4 amu, which produces our final approximation of the **mean molecular weight** in the case of **complete ionization**:

Eq. 9.8 $$\frac{1}{\mu} = 2X + \frac{3}{4}Y + \frac{1}{2}Z$$

The range of values for μ is fairly small. A gas of pure hydrogen (X =1) would have $\mu = {}^1/_2$; pure helium (Y =1) would have $\mu = {}^4/_3$; and for pure metals (Z =1), μ = 2.

A related quantity that will eventually be needed is the mean molecular weight per (free) electron (μ_e):

Eq. 9.9 $$\mu_e = \frac{\#\text{amu}}{\text{free electron}} \cdot \frac{N_A}{N_A} = \frac{\text{grams}}{\text{mole } electrons} = \frac{\text{g}}{\text{cc}} \cdot \frac{\text{cc}}{electron} \cdot \frac{electrons}{\text{mole } electrons} = \frac{\rho N_A}{N_e}$$

We can obtain an expression for the number density of electrons in the case of complete ionization:

Eq. 9.10
$$N_e = \frac{\text{elec}}{\text{cc}} = \sum \frac{\text{elec}}{\text{gram } z} \cdot \frac{\text{gram } z}{\text{gram}} \cdot \frac{\text{gram}}{\text{cc}} = \sum \frac{\text{elec}}{\text{atom } z} \cdot \frac{\text{atom } z}{\text{gram } z} \cdot \frac{\text{gram } z}{\text{gram}} \cdot \frac{\text{gram}}{\text{cc}}$$
$$= \sum z \frac{\text{atom } z}{\text{mole } z} \cdot \frac{\text{mole } z}{\text{gram } z} X_z \rho \quad = \sum z N_A \frac{1}{m_z} X_z \rho \quad = \rho N_A \sum \frac{z X_z}{m_z}$$

We now insert this into the expression for μ_e :

Eq. 9.11 $$\mu_e = \frac{\rho N_A}{N_e} = \frac{1}{\sum \frac{z X_z}{m_z}} \quad \text{or} \quad \frac{1}{\mu_e} = \sum \frac{z X_z}{m_z}$$

This equation applies to the case of complete ionization, for which $z/m_z \approx {}^1/_2$ for $z > 2$. Then we write the sum explicitly:

Eq. 9.12 $$\frac{1}{\mu_e} = \sum \frac{z X_z}{m_z} = \frac{1 \cdot X}{1} + \frac{2 \cdot Y}{4} + \frac{1}{2} \sum X_z$$

We now substitute $Z = \sum X_z$ and note that $Z = 1 - X - Y$; this gives our final expression for the **mean molecular weight per free electron**:

Eq. 9.13 $$\frac{1}{\mu_e} = X + \tfrac{1}{2}Y + \tfrac{1}{2}(1 - X - Y) = \tfrac{1}{2}X + \tfrac{1}{2} \quad \Rightarrow \quad \mu_e = \frac{2}{1+X}$$

Note that we have used either $m_z = 2z$ or $m_z = 2z + 2$, as needed.

The range of values for μ_e is even smaller than it was for μ: when $X = 1$, $\mu_e = 1$, and when $Y = 1$ or $Z = 1$, $\mu_e = 2$. We now recall Equation 9.11 to write an expression for N_e – again good only for complete ionization:

Eq. 9.14 $$N_e = \frac{\rho N_A}{\mu_e} = \tfrac{1}{2}\rho N_A(1+X)$$

Just as we can use μ in the ideal gas law to calculate the total gas pressure, we can use μ_e in the same law to calculate the electron pressure:

Eq. 9.15 $$P_e = \frac{\rho \Re T}{\mu_e}$$

The Linear Model

At this point we have two differential equations that can be integrated to give the pressure in a star as a function of radius:

Eq. 9.16 $$M_r = \int_0^r 4\pi\rho(r) r^2 dr$$

Eq. 9.17 $$P(r) = -\int_0^r \frac{GM_r\rho(r)}{r^2} dr$$

Combining these with the ideal gas law allows us to determine $T(r)$ as well. All we need is an equation that gives the density as a function of radius – preferably a function that permits us to solve both integrals. We have not yet considered the form of such a function, but we might expect that it would be a decreasing function on r (from $r = 0$ to $r = R$). For starters, let us investigate a very simple function with this property:

Eq. 9.18 $$\rho = \rho_c\left(1 - r/R\right)$$ where ρ_c is the central value of the density

Figure 9.1 shows this distribution. For obvious reasons, the solution we obtain based on this density function will be known as the **Linear Model**.

Figure 9.1: Density distribution for the Linear Model

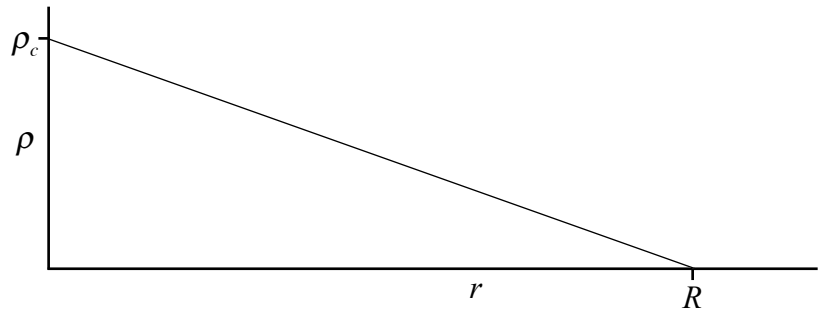

We begin by inserting this density function into the mass continuity expression:

Eq. 9.19 $$dM_r = 4\pi r^2 \rho_c\left(1 - r/R\right)dr = 4\pi\rho_c\left(r^2 - r^3/R\right)$$

The first integral is straightforward:

Eq. 9.20 $$M_r = \int dM_r = \int_0^r 4\pi\rho_c \left(r^2 - r^3/R\right) dr = 4\pi\rho_c \left(\frac{r^3}{3} - \frac{r^4}{4R}\right)$$

This gives the mass interior to radius *r*. The total mass of the star is found by evaluating this expression at *r* = *R*:

Eq. 9.21 $$\mathrm{M} = 4\pi\rho_c \left(\frac{R^3}{3} - \frac{R^4}{4R}\right) = \frac{\pi\rho_c R^3}{3}$$

From this we can determine the value of the central density:

Eq. 9.22 $$\rho_c = \frac{3M}{\pi R^3} = 4\bar{\rho} \qquad \text{where the mean density is given by } \bar{\rho} = 3M/4\pi R^3$$

Next we can use the result of the first integration to solve the pressure integral:

Eq. 9.23
$$dP = -\frac{GM_r\rho(r)}{r^2}dr = -\frac{G\cdot 4\pi\rho_c\left(\frac{r^3}{3} - \frac{r^4}{4R}\right)\cdot\rho_c\left(1 - r/R\right)}{r^2}dr$$
$$= -4\pi\rho_c^2 Gr\left(\frac{1}{3} - \frac{r}{4R}\right)\left(1 - \frac{r}{R}\right)dr = -\pi\rho_c^2 G\left[\frac{4r}{3} - \frac{7r^2}{3R} + \frac{r^3}{R^2}\right]dr$$

The pressure at radius *r* can then be found by integrating from the center outward:

Eq. 9.24 $$\int_{P_c}^{P} dP = -\pi\rho_c^2 G\int_0^r \left[\frac{4r}{3} - \frac{7r^2}{3R} + \frac{r^3}{R^2}\right]dr$$

The result is the change in pressure from the center to the radius in question:

Eq. 9.25 $$P - P_c = -\pi\rho_c^2 G\left[\frac{2r^2}{3} - \frac{7r^3}{9R} + \frac{r^4}{4R^2}\right]$$

Next we substitute our value for the central density ($\rho_c = 3M/\pi R^3$):

Eq. 9.26 $$P = P_c - \frac{9M^2G}{\pi R^6}\left[\frac{2}{3} - \frac{7r}{9R} + \frac{r^2}{4R^2}\right]r^2$$

We require that the pressure in the star should drop to essentially zero at the surface ($P(R) = 0$), and this gives a value for the central pressure:

Eq. 9.27 $$P_c = \frac{9M^2G}{\pi R^6}\left[\frac{2}{3} - \frac{7}{9} + \frac{1}{4}\right]R^2 = \frac{5GM^2}{4\pi R^4}$$

Substituting $\zeta = r/R$, our expression for the pressure is then as follows:

Eq. 9.28 $$P = \frac{GM^2}{\pi R^4}\left[\frac{5}{4} - \zeta^2\left(6 - 7\zeta + \frac{9}{4}\zeta^2\right)\right] = P_c\left[1 - \zeta^2\left(\frac{24}{5} - \frac{28}{5}\zeta + \frac{9}{5}\zeta^2\right)\right]$$

From above, we have the density function in a similar form:

Eq. 9.29 $$\rho = \frac{3M}{\pi R^3}(1-\zeta) \quad = \rho_c(1-\zeta)$$

If we now assume that radiation pressure is negligible ($P_r << P_g$), we can find the temperature from the ideal gas law: $P \approx P_g = \rho \Re T/\mu$.

Eq. 9.30 $$T = \frac{\mu P}{\Re \rho} = \frac{\mu}{\Re} \frac{\frac{GM^2}{\pi R^4}\left[\frac{5}{4} - 6\zeta^2 + 7\zeta^3 - \frac{9}{4}\zeta^4\right]}{\frac{3M}{\pi R^3}(1-\zeta)} = \frac{\mu}{\Re}\frac{G}{3}\frac{M}{R}\frac{1}{4}\left[5 + 5\zeta - 19\zeta^2 + 9\zeta^3\right]$$

Eq. 9.31 $$T = \frac{GM\mu}{12\Re R}\left[5 + 5\zeta - 19\zeta^2 + 9\zeta^3\right] = T_c\left[1 + \zeta - \frac{19}{5}\zeta^2 + \frac{9}{5}\zeta^3\right] \text{ where } T_c = \frac{5}{12}\frac{GM}{R}\frac{\mu}{\Re}$$

This all assumes a constant value of μ, which is not unreasonable, given the small range of values for this quantity.

To summarize, the linear model predicts the following properties:

$$\rho_c = \frac{3M}{\pi R^3} \qquad \rho = \rho_c(1-\zeta)$$

$$P_c = \frac{5GM^2}{4\pi R^4} \qquad P = P_c\left[1 - \frac{24}{5}\zeta^2 + \frac{28}{5}\zeta^3 - \frac{9}{5}\zeta^4\right]$$

$$T_c = \frac{5GM\mu}{12R\Re} \qquad T = T_c\left[1 + \zeta - \frac{19}{5}\zeta^2 + \frac{9}{5}\zeta^3\right]$$

How well does this model work? Let us insert values for the Sun and calculate its central values. We will need the following:

$M = 1\ M_\odot = 1.99 \times 10^{33}$ $R = 1\ R_\odot = 6.96 \times 10^{10}$ $G = 6.67 \times 10^{-8}$ $\Re = 8.314 \times 10^7$

$X = 0.73$ $Y = 0.25$ $Z = 0.02$ $\Rightarrow$ $\mu = [2X + {}^3\!/_4\, Y + {}^1\!/_2\, Z]^{-1} \approx 0.6$

Then the central values are as follows:

Eq. 9.32 $$\rho_c = \frac{3M}{\pi R^3} = \frac{3(1.99e33)}{\pi(6.96e10)} = 5.64$$

Eq. 9.33 $$P_c = \frac{5GM^2}{4\pi R^4} = \frac{5(6.67e-8)(1.99e33)^2}{4\pi(6.96e10)^4} = 4.48 \times 10^{15}$$

Eq. 9.34 $$T_c = \frac{5GM\mu}{12R\Re} = \frac{5(6.67e-8)(1.99e33)(0.6)}{12(6.96e10)(8.314e7)} = 5.73 \times 10^6$$

We now compare these results with the same central values calculated by numerical models of the Sun: Model 7-14 in Novotny (1973) and Model 13.2 in Bohm-Vitense (1992).

Table 9.2: Linear Model comparison ($T_6 = T/10^6$)

	ρ_c	P_c	T_{6c}
Linear Model	5.64	4.48E+15	5.73
Novotny 7-14	85.15	1.62E+17	13.9
Bohm-Vitense 13.2	148	2.29E+17	15.6

Each of the central values for the linear model is considerably lower than the corresponding values from the numerical models; this would seem to imply that the density distribution in the Sun is not very close to linear. We will need to look for a better model.

Polytropes

So far we have three stellar structure equations:

1. Mass Continuity $\frac{dM_r}{dr} = 4\pi\rho r^2$ with variables M_r, ρ, r

2. Hydrostatic Equilibrium $\frac{dP}{dr} = -\frac{GM_r\rho}{r^2}$ with variables P, M_r, ρ, r

3. Equation of State $P_g = \frac{\rho\Re T}{\mu}$ with variables P_g, ρ, T

The equation of state added another equation to the list but also introduced another variable (T); thus, we still require another equation to solve the problem. What other limitation can be placed on stellar structure?

In the early days of astrophysics there were no computers with which to construct numerical models of stars. Instead, considerable effort was expended in finding combinations of functions and differential equations that could then be solved to produce reasonable stellar models. One of the next equations to be considered was the **polytropic law**:

Eq. 9.35 $P = K\rho^{n+1/n}$ where K is a constant and n is the **polytropic index**

If this law does indeed apply, then a solution can be found (in conjunction with the existing stellar structure equations). A gaseous sphere in hydrostatic equilibrium that obeys the polytropic law is called a **polytrope of index *n***.

Of course, *any* relation between pressure and density could be used to find a solution; why should we use *this* one? The answer is that if we can argue that there are real stars that can be described by a polytropic law, then this could be a useful path to follow.

Relevant Polytropes

Consider a 'boiling' star – a star in adiabatic convective equilibrium. Such a star is completely convective, with mass elements rising and falling without exchanging heat with their

surroundings as they transport energy from the inside of the star to the surface. If we assume that radiation pressure is negligible ($P \approx P_g$), then the **adiabatic law** applies:

Eq. 9.36 $P = K\rho^{\gamma}$ where $\gamma = C_P/C_V$, the **ratio of specific heats**

The **first law of thermodynamics** says that the *heat added* to a system (dQ) is equal to the *change in the internal energy* of the system (dU) plus the *work done by* the system ($dW = PdV$):

Eq. 9.37 $dQ = dU + dW = dU + PdV$

Any system has some capacity to absorb energy from its surroundings, but this capacity will depend on whether or not the system is capable of doing any work. Because a gas must change its volume in order to do work, a gas that is constrained at a constant volume will be unable to do work and thus will absorb less energy than a gas that is not so constrained. In such a case, any heat absorbed by the gas must be stored as internal energy, producing a rise in temperature. The amount of heat required to raise the temperature of a mole of gas *at constant volume* by one degree is the **specific heat capacity C_V**. On the other hand, a gas held at a constant pressure will be able to expand and do work as heat is added to it, permitting a greater amount of energy to be absorbed. The amount of heat required to raise the temperature of a mole of gas *at constant pressure* by one degree is the **specific heat capacity C_P**.

For one mole of gas, we have the following relations:

Eq. 9.38 $PV = \Re T$ (the ideal gas law)

Eq. 9.39 $U = {}^3/_2\, kT$ (per particle) $\Rightarrow$ $U = {}^3/_2\, \Re T$ (per mole) for a monatomic gas

Then we may define the specific heat capacities and determine values for them:

Eq. 9.40 $$C_V \equiv \left.\frac{\partial Q}{\partial T}\right|_V = \frac{\partial U}{\partial T} = \tfrac{3}{2}\Re$$

Eq. 9.41 $$C_P \equiv \left.\frac{\partial Q}{\partial T}\right|_P = \frac{\partial U}{\partial T} + P\frac{\partial V}{\partial T} = C_V + P\frac{\partial}{\partial T}\left(\frac{\Re T}{P}\right) = \tfrac{3}{2}\Re + \Re = \tfrac{5}{2}\Re$$

So for a monatomic gas, $C_V = {}^3/_2\Re$, $C_P = {}^5/_2\Re$, and the ratio of specific heats is then as follows:

Eq. 9.42 $$\gamma = {}^{C_P}\!/_{C_V} = {}^5\!/_3$$

Noting that the adiabatic law is also a polytropic law, we can solve for the polytropic index:

Eq. 9.43 $$\frac{n+1}{n} = \gamma = {}^5\!/_3 \quad \Rightarrow \quad n = {}^3\!/_2$$

Thus, a fully convective star in hydrostatic equilibrium, with negligible radiation pressure is a **polytrope of index 1.5**.

We may obtain another possible polytrope by considering a star *with* radiation pressure:

Eq. 9.44 $P = P_g + P_r$

If we let $P_g = \beta P$ and $P_r = (1-\beta)P$, we can then combine these to eliminate P :

Eq. 9.45 $$\beta P_r = (1-\beta)P_g$$

Then, inserting the standard expressions for the two pressures we obtain an equation in T :

Eq. 9.46 $$\frac{\beta}{3}aT^4 = (1-\beta)\frac{\rho\Re T}{\mu}$$

This can be solved for T :

Eq. 9.47 $$T = \left[\frac{3}{a}\frac{\Re}{\mu}\frac{1-\beta}{\beta}\rho\right]^{1/3}$$

The total pressure is then given by the following:

Eq. 9.48 $$P = \frac{P_g}{\beta} = \frac{\rho\Re T}{\beta\mu} = \left[\frac{3}{a}\left(\frac{\Re}{\mu}\right)^4\frac{1-\beta}{\beta^4}\right]^{1/3}\rho^{4/3}$$

Now if β and μ are constant with r, this equation takes on an interesting form:

Eq. 9.49 $$P = K'\rho^{4/3} \qquad \text{where } K' = \left[\frac{3}{a}\left(\frac{\Re}{\mu}\right)^4\frac{1-\beta}{\beta^4}\right]^{1/3}$$

Once again we have a polytropic law, this time with $\gamma = {}^4/_3 = (n+1)/n \implies n = 3$. Therefore we may conclude that a star in radiative equilibrium – with no convection – is **a polytrope of index 3**. This particular polytrope is called **the Standard Model**.

Note: This expression for K' is only good for $n = 3$. K' is different from the general K. Also note that for $n = 3$, β is constant throughout the star; for $n = 1.5$, β can be calculated from $\beta = P_g/P$, but it is *not* assumed to be constant.

The Lane-Emden Equation

Although we now have better methods for generating stellar models, polytropes are still useful as first approximations to obtain $T(r)$ and $\rho(r)$. How do we obtain these functions?

We begin with the equation of hydrostatic equilibrium $\left(\frac{dP}{dr} = -\frac{GM_r\rho}{r^2}\right)$, written as follows:

Eq. 9.50 $$\frac{r^2}{\rho}\frac{dP}{dr} = -GM_r$$

We then take the derivative and substitute the mass continuity equation:

Eq. 9.51 $$\frac{d}{dr}\left(\frac{r^2}{\rho}\frac{dP}{dr}\right) = -G\frac{dM_r}{dr} = -4\pi Gr^2\rho$$

Eq. 9.52 $$\frac{1}{r^2}\frac{d}{dr}\left(\frac{r^2}{\rho}\frac{dP}{dr}\right)=-4\pi G\rho$$

Next we use the polytropic law $\left(P=K\rho^{n+1/n}\right)$ to substitute for the pressure:

Eq. 9.53 $$\frac{K}{r^2}\frac{d}{dr}\left[\frac{r^2}{\rho}\frac{d}{dr}\left(\rho^{\frac{n+1}{n}}\right)\right]=-4\pi G\rho$$

It now becomes convenient to introduce dimensionless variables, called the **Emden variables**. These are a temperature variable $\theta \equiv T/T_c$ (not to be confused with $\theta \equiv 5040/T$ – seen in previous chapters), and a radius variable $\xi \equiv r/\alpha$ (not to be confused with $\zeta \equiv r/R$ – used earlier in this chapter). As before, T_c is the central temperature; the quantity α will be named later.

We can introduce the variable θ by first writing the polytropic law as a ratio:

Eq. 9.54 $$\frac{P}{P_c}=\left(\frac{\rho}{\rho_c}\right)^{\frac{n+1}{n}}$$

Next we do the same for the ideal gas law (assuming a constant μ and $P \approx P_g$):

Eq. 9.55 $$\frac{P}{P_c}=\frac{\rho T}{\rho_c T_c}$$

Equating these two allows us to eliminate the pressure:

Eq. 9.56 $$\left(\frac{\rho}{\rho_c}\right)^{\frac{1}{n}}=\frac{T}{T_c}=\theta \quad\Rightarrow\quad \rho=\rho_c\theta^n \text{ and } P=P_c\theta^{n+1}$$

The variable θ is an as-yet-unknown function of ξ (equivalent to $T(r)$). Determination of this function would then lead directly to functions for density and pressure.

We now make substitutions into Equation 9.53, setting $r = \alpha\xi$ and $\rho = \rho_c\theta^n$:

Eq. 9.57 $$\frac{K}{(\alpha\xi)^2}\frac{d}{\alpha d\xi}\left[\frac{(\alpha\xi)^2}{\rho_c\theta^n}\frac{\rho_c^{\frac{n+1}{n}}}{\alpha}\frac{d\left(\theta^{n+1}\right)}{d\xi}\right]=-4\pi G\rho_c\theta^n$$

Eq. 9.58 $$\frac{K}{\alpha^2}\frac{\rho_c^{1/n}}{\xi^2}\frac{d}{d\xi}\left[\frac{\xi^2}{\theta^n}(n+1)\theta^n\frac{d\theta}{d\xi}\right]=-4\pi G\rho_c\theta^n$$

Next we collect the constants:

Eq. 9.59 $$\frac{(n+1)K\rho_c^{\frac{1}{n}-1}}{4\pi G\alpha^2}\cdot\frac{1}{\xi^2}\frac{d}{d\xi}\left[\xi^2\frac{d\theta}{d\xi}\right]=-\theta^n$$

We will now conveniently define α:

Eq. 9.60 $$\alpha \equiv \sqrt{\frac{(n+1)K\rho_c^{\frac{1-n}{n}}}{4\pi G}}$$

The result is the **Lane-Emden equation**:

Eq. 9.61 $$\frac{1}{\xi^2}\frac{d}{d\xi}\left[\xi^2\frac{d\theta}{d\xi}\right] = -\theta^n$$

Solution of this second-order differential equation gives $\theta(\xi) \Rightarrow T(r)$. We will need two boundary conditions – both at the center of the star ($r = 0$): $T(0) = T_c$ and $\left.\frac{dT}{dr}\right|_0 = 0$. In terms of our dimensionless variables, the boundary conditions will occur at $\xi = 0$, where $\theta(0) = 1$ and $\left.\frac{d\theta}{d\xi}\right|_0 = 0$.

We also prefer that as $r \rightarrow R$, $T \rightarrow 0$. This means that we want a function $\theta(\xi)$ that goes to 0 at some $\xi = \xi_1$, where ξ_1 is the **first zero** of θ – corresponding to $r = R$. (The behavior of $\theta(\xi)$ beyond ξ_1 is irrelevant.)

We now calculate the basic stellar properties in terms of the polytropic variables and constants.

Radius

Radius is determined from the definition of ξ:

Eq. 9.62 $$r = \alpha\xi \quad \Rightarrow \quad R = \alpha\xi_1 = \sqrt{\frac{(n+1)K}{4\pi G}}\rho_c^{\frac{1-n}{2n}}\xi_1$$

Mass

The mass interior to a point is found from the mass continuity equation:

Eq. 9.16 $$M_r = \int_0^r 4\pi\rho(r')r'^2 dr' \quad \Rightarrow \quad M(\xi) = 4\pi\alpha^3\rho_c\int_0^\xi \xi^2\theta^n d\xi$$

We then substitute the Lane-Emden equation into the integral:

Eq. 9.63 $$M(\xi) = -4\pi\alpha^3\rho_c\int_0^\xi \frac{d}{d\xi}\left(\xi^2\frac{d\theta}{d\xi}\right)d\xi = -4\pi\alpha^3\rho_c\xi^2\frac{d\theta}{d\xi}$$

Finally we insert the value of α to obtain the desired expression:

Eq. 9.64 $$M(\xi) = 4\pi\left[\frac{(n+1)K}{4\pi G}\right]^{3/2}\rho_c^{\frac{3-n}{2n}}\left(-\xi^2\frac{d\theta}{d\xi}\right)$$

Note that for $n = 3$, M_r is independent of ρ_c.

Total Mass

The total mass is found by evaluating Equation 9.64 at the first zero:

Eq. 9.65 $$M(\xi_1) = 4\pi\left[\frac{(n+1)K}{4\pi G}\right]^{3/2} \rho_c^{\frac{3-n}{2n}} \left(-\xi_1^2 \left.\frac{d\theta}{d\xi}\right|_{\xi_1}\right)$$

Mean Density

We first write a general expression for the mean density of the portion of the star interior to radius r :

Eq. 9.66 $$\bar{\rho}(\xi) = \frac{M(\xi)}{\frac{4}{3}\pi\alpha^3\xi^3} = \frac{4\pi\alpha^3\rho_c\xi^2\left(-d\theta/d\xi\right)}{\frac{4}{3}\pi\alpha^3\xi^3} = \frac{3}{\xi}\left(-\frac{d\theta}{d\xi}\right)\rho_c$$

We then evaluate this expression at the first zero:

Eq. 9.67 $$\bar{\rho}(\xi_1) = \frac{3}{\xi_1}\left(-\left.\frac{d\theta}{d\xi}\right|_{\xi_1}\right)\rho_c \quad \Rightarrow \quad \frac{\rho_c}{\bar{\rho}} = \frac{\xi_1}{3\left(-\left.\frac{d\theta}{d\xi}\right|_{\xi_1}\right)}$$

From this expression, we see that the ratio of central density to mean density depends only on the polytropic index (which determines the function θ). This ratio is tabulated for different indices n.

Mass-Radius Relation

Some groups of stars appear to exhibit correlations between their masses and their radii. Here we explore the relation between the mass and the radius of a polytrope.

We first use the definition of α to solve for the central density:

Eq. 9.68 $$\rho_c = \left[\frac{R}{\xi_1}\sqrt{\frac{4\pi G}{(n+1)K}}\right]^{\frac{2n}{1-n}}$$

This is then inserted into the expression for the total mass:

Eq. 9.69
$$\begin{aligned} M(\xi_1) &= 4\pi\left[\frac{(n+1)K}{4\pi G}\right]^{3/2} \rho_c^{\frac{3-n}{2n}} \left(-\xi_1^2 \left.\frac{d\theta}{d\xi}\right|_{\xi_1}\right) \\ &= 4\pi\left[\frac{(n+1)K}{4\pi G}\right]^{3/2} \left(\frac{R}{\xi_1}\right)^{\frac{3-n}{1-n}} \left[\frac{(n+1)K}{4\pi G}\right]^{\frac{3-n}{2(n-1)}} \left(-\xi_1^2 \left.\frac{d\theta}{d\xi}\right|_{\xi_1}\right) \end{aligned}$$

This can be rearranged to group the mass and radius together:

Eq. 9.70 $$GM^{\frac{n-1}{n}}R^{\frac{3-n}{n}} = \frac{(n+1)K}{(4\pi)^{1/n}}\left[-\xi^{\frac{n+1}{n-1}}\frac{d\theta}{d\xi}\right]^{\frac{n-1}{n}}\Bigg|_{\xi_1}$$

And this can be simplified by defining some additional constants, which are tabulated in the literature:

Eq. 9.71 $$\omega_n \equiv -\xi_1^{\frac{n+1}{n-1}}\frac{d\theta}{d\xi}\bigg|_{\xi_1} \qquad \text{and}$$

Eq. 9.72 $$N_n \equiv \frac{1}{n+1}\left[\frac{4\pi}{\omega_n^{n-1}}\right]^{1/n}$$

The result is the **mass-radius relation**:

Eq. 9.73 $$K = N_n G M^{\frac{n-1}{n}} R^{\frac{3-n}{n}}$$

Central Values

The easiest way to find the **central density** of a polytrope is to multiply the tabulated value of $\rho_c/\bar{\rho}$ by the calculated mean density:

Eq. 9.74 $$\rho_c = \left(\frac{\rho_c}{\bar{\rho}}\right)_n \frac{M}{\frac{4}{3}\pi R^3}$$

The **central pressure** can then be found from the adiabatic law (Equation 9.35) or from the following:

Eq. 9.75 $$P_c = W_n \frac{GM^2}{R^4} \qquad \text{where } W_n \equiv \left[4\pi(n+1)\left(\frac{d\theta}{d\xi}\bigg|_{\xi_1}\right)^2\right]^{-1}$$

(This relation is obtained by substituting Equations 9.67 and 9.73 into Equation 9.35. The constant W_n is tabulated.)

The **central temperature** is obtained from the central density and pressure and the equation of state:

Eq. 9.76 $$P_g = \beta_c P_c = \frac{\rho_c \Re T_c}{\mu} \quad \Rightarrow \quad T_c = \frac{\mu}{\Re}\frac{\beta_c P_c}{\rho_c}$$

Solutions of the Lane-Emden Equation

All that remains is to solve the Lane-Emden equation:

Eq. 9.61 $$\frac{1}{\xi^2}\frac{d}{d\xi}\left[\xi^2\frac{d\theta}{d\xi}\right] = -\theta^n$$

The boundary conditions are set at the center of the star (ξ =0), where θ =1 and $d\theta/d\xi$ = 0.

The n = 0 Solution

We begin by examining the case of n = 0. This simplifies our equation considerably:

Eq. 9.77 $$\frac{d}{d\xi}\left[\xi^2\frac{d\theta}{d\xi}\right]=-\xi^2$$

This integrates easily:

Eq. 9.78 $$\xi^2\frac{d\theta}{d\xi}=-\tfrac{1}{3}\xi^3-C \quad\Rightarrow\quad \frac{d\theta}{d\xi}=-\tfrac{1}{3}\xi-\frac{C}{\xi}$$

As we require that $d\theta/d\xi \to 0$ as $\xi \to 0$, the constant C must be zero:

Eq. 9.79 $$\frac{d\theta}{d\xi}=-\tfrac{1}{3}\xi$$

And this also integrates easily:

Eq. 9.80 $$\theta = D - {}^1\!/_6\,\xi^2$$

The boundary condition $\theta(0)$ =1 requires that D = 1. Thus, the solution for n = 0 is parabolic:

Eq. 9.81 $$\theta_0 = 1 - {}^1\!/_6\,\xi^2$$

The first zero occurs at $\xi_1=\sqrt{6}$. And because $d\theta/d\xi = -\,{}^1\!/_3\,\xi$, the mean density and central density are equal (see Equation 9.67). Thus, n = 0 is the uniform density case – a rather unlikely scenario for a star made from an ideal gas.

The n = 1 Solution

We now attempt a solution for n = 1. The Lane-Emden equation is then as follows:

Eq. 9.82 $$\frac{1}{\xi^2}\frac{d}{d\xi}\left[\xi^2\frac{d\theta}{d\xi}\right]=-\theta$$

This can be solved with the appropriate substitution, letting $\theta = \chi/\xi$; the derivative is then modified:

Eq. 9.83 $$\frac{d\theta}{d\xi}=\frac{1}{\xi}\frac{d\chi}{d\xi}-\frac{\chi}{\xi^2}$$

These two expressions are inserted into the Lane-Emden equation:

Eq. 9.84 $$\frac{1}{\xi^2}\frac{d}{d\xi}\left[\xi^2\left(\frac{1}{\xi}\frac{d\chi}{d\xi}-\frac{\chi}{\xi^2}\right)\right]=-\frac{\chi}{\xi} \quad\Rightarrow\quad \frac{1}{\xi}\left[\frac{d\chi}{d\xi}+\xi\frac{d^2\chi}{d\xi^2}-\frac{d\chi}{d\xi}\right]=-\chi \quad\Rightarrow\quad \frac{d^2\chi}{d\xi^2}=-\chi$$

This equation has a very well-known solution:

Eq. 9.85 $\chi = C \sin\xi + D \cos\xi \quad \Rightarrow \quad \theta = C\frac{\sin\xi}{\xi} + D\frac{\cos\xi}{\xi}$

Applying the boundary conditions, we find that as $\xi \to 0$, $\theta \to C + D/\xi = 1$. This requires that $D = 0$ and $C = 1$. Then the solution for $n = 1$ is a **sinc function**, with a first zero at $\xi_1 = \pi$.

Eq. 9.86 $\theta_1 = \frac{\sin\xi}{\xi} \equiv \mathrm{sinc}\,\xi$

The n = 5 Solution

The Lane-Emden equation can also be solved for $n = 5$, but not easily. The solution is presented here:

Eq. 9.87 $\theta_5 = \frac{1}{\sqrt{1+\frac{1}{3}\xi^2}} \quad \Rightarrow \quad \frac{d\theta}{d\xi} = \frac{-\xi}{3\left(1+\frac{1}{3}\xi^2\right)^{3/2}}$

For this solution, $\theta_5 \to 0$ only as $\xi \to \infty$: the first zero is at $\xi_1 = \infty$. The density ratio is also a bit extreme:

Eq. 9.88 $$\frac{\rho_c}{\bar{\rho}} = \frac{\xi_1}{3\left(-\left.\frac{d\theta}{d\xi}\right|_{\xi_1}\right)} = \frac{\xi_1}{3\left(\left.\frac{\xi}{3\left(1+\frac{1}{3}\xi^2\right)^{3/2}}\right|_{\xi_1}\right)} = \lim_{\xi\to\infty}\left(1+\tfrac{1}{3}\xi^2\right)^{3/2} = \infty$$

Either ρ_c is infinite, or $\bar{\rho} = 0$ – which would mean that the radius is infinite (or perhaps both may be true). Clearly, $n = 5$ marks an upper limit on polytropes.

Polytropic Models

The polytropic index ranges from 0 to 5. Only $n = 0$, 1, and 5 can be solved analytically; but the various constants have been tabulated for other values of n over this range (see Chandrasekhar (1967), Clayton (1968), Bowers & Deeming (1984), etc.).

Tables of the various polytropic functions over the range of ξ from 0 to ξ_1 are also available (see Novotny (1973) Tables 10-11 and 10-12; note that she uses ξ_0 as the first zero, in place of ξ_1). These allow us to construct profiles of the temperature, density, pressure, etc. throughout the interior of the star. Table 9.3 shows how the Lane-Emden variables relate to the corresponding physical variables.

We obtained the linear model for a star by calculating the central values of temperature, density, and pressure and using them to scale the respective functions of r (or ζ). Similarly, we can use polytropic expressions to calculate these three central values and then combine them with a solution of the Lane-Emden equation for $\theta(\xi)$ to give us temperature, density, and pressure throughout the interior (using $T = T_c\,\theta$, $\rho = \rho_c\,\theta^n$, and $P = P_c\,\theta^{n+1}$). The limited range of polytropic indices provides a small number of different solutions for $\theta(\xi)$, but we can obtain different models by starting with different central values. Because the solutions $\theta_n(\xi)$ depend

only on the polytropic index n, we may tabulate the constants (ξ_1, $(\rho_c/\bar{\rho})_n$, ω_n, N_n, W_n, etc.) for the appropriate range of indices and then apply them to specific models.

Table 9.3: Lane Emden variables

Lane-Emden variable	physical variable	relation
ξ	r	$r = \alpha\xi$
ξ/ξ_0	r/R	$r/R = \xi/\xi_0$ (use direct from the table)
θ	T	$T = T_c\,\theta$
$\frac{d\theta}{d\xi}$	$\frac{dT}{dr}$	$\frac{dT}{dr} = \frac{T_c}{\alpha}\frac{d\theta}{d\xi}$
θ^n	ρ	$\rho = \rho_c\,\theta^n$
θ^{n+1}	P	$P = P_c\,\theta^{n+1}$
$-\xi^2\frac{d\theta}{d\xi}$	M_r	$M_r = 4\pi\alpha^3\rho_c\left(-\xi^2\frac{d\theta}{d\xi}\right)$

To calculate a polytropic model, we begin with the star's mass, radius, and composition (*X, Y, Z*). From these we can calculate μ (= $[2X + {}^3/_4\,Y + {}^1/_2\,Z]^{-1}$) and $\bar{\rho}$ (= $3M/4\pi R^3$). Choosing a polytropic index n, we can look up the corresponding values of $(\rho_c/\bar{\rho})_n$ and W_n and use these to find ρ_c and P_c. Central temperature is found from the ideal gas law:

Eq. 9.89 $$T_c = \frac{\mu}{\Re}\frac{P_{gc}}{\rho_c} = \frac{\mu}{\Re}\frac{\beta_c P_c}{\rho_c} \approx \frac{\mu}{\Re}\frac{P_c}{\rho_c} \quad \text{if } \beta_c \approx 1$$

If β_c is *not* assumed to be 1, then we can estimate β_c, calculate T_c, and find a new β_c value:

Eq.9.90 $$\beta_c = 1 - \frac{P_r}{P_c} = 1 - \frac{\frac{1}{3}aT_c^4}{P_c}$$

As an example, let us use polytropes of indices 1.5 and 3 to model a star with $M = 2.25\ M_\odot$ and $R = 1.4559\ R_\odot$ (Novotny (1973) Model 7-21); these values give $\bar{\rho}$ = 1.0291 and $GM^2/R^4 = 1.271\times10^{16}$. The composition used in the model is $X = 0.708$, $Y = 0.272$, $Z = 0.020$, which yields μ =0.6135; $\beta_c = 1$ is assumed.

The necessary polytropic constants are obtained from the literature:

$W_{1.5} = 0.77014$ $W_3 = 11.05066$ $(\rho_c/\bar{\rho})_{1.5} = 5.99071$ $(\rho_c/\bar{\rho})_3 = 54.1825$

Table 9.4 compares the resulting central values for the two polytropes and the linear model with the values generated by Novotny's numerical model.

Table 9.4: Model comparisons with Novotny 7-21

	ρ_c	P_c	T_{6c}
Linear Model	4.12	5.06E+15	9.07
$n = 1.5$	6.16	9.79E+15	11.7
$n = 3$	55.8	1.41E+17	18.6
Novotny 7-21	58.9	1.77E+17	22.2

As a second example, we perform the same calculations for a star with $M = 3\ M_\odot$ and $R = 1.7381\ R_\odot$ (Novotny Model 7-22); these values give $\bar{\rho} = 0.8064$ and $GM^2/R^4 = 1.113 \times 10^{16}$. The composition is the same as above, and we will be using the same polytropic constants. Results are shown in Table 9.5.

Table 9.5: Model comparisons with Novotny 7-22

	ρ_c	P_c	T_{6c}
Linear Model	3.23	4.43E+15	10.1
$n = 1.5$	4.83	8.57E+15	13.1
$n = 3$	43.7	1.23E+17	20.8
Novotny 7-22	41.3	1.35E+17	24.1

It would seem that the standard model polytrope ($n = 3$) gives the best approximation for the central values in each case. Of course, this depends on the *type* of star being modeled – in both cases, an upper main sequence star.

Table 9.6: Density, pressure, and temperature values at $r \approx {}^1/_4 R$

Model	$\zeta = \xi/\xi_1$	$r / R_\odot$	ρ / ρ_c	ρ	P / P_c	P	T / T_c	T_6
Linear	0.2465	0.3589	0.7535	3.10	0.7856	3.97E+15	1.0426	9.45
$n = 1.5$	0.2463	0.3586	0.8155	5.03	0.7118	6.97E+15	0.8728	10.2
$n = 3$	0.2465	0.3589	0.2924	16.3	0.1941	2.73E+16	0.6638	12.3
Nov. 7-21	0.2469	0.3595	0.3282	19.3	0.1760	3.12E+16	0.5546	12.3

As a further check, in Table 9.6 we compare values of density, pressure, and temperature at a point away from the center at an approximate radius given by $\zeta = \xi / \xi_1 = 0.2465$, again using Novotny Model 7-21.

Once again, the standard model provides the best match to Novotny's 7-21, for all three properties. Polytropes can give reasonable approximations in many cases, although they lack the details used to produce the numerical models.

The Isothermal Gas Sphere

We have already noted that the practical range of polytropic indices is from $n = 0$ (the uniform density case) to $n = 5$ (the infinite central density case). Another interesting possibility is the uniform temperature case – the **isothermal gas sphere**. To investigate this we first write the ideal gas law (assuming $P \approx P_g$):

Eq. 9.91 $$P = \frac{\rho \Re T}{\mu} = K\rho$$

Comparing this to the polytropic law, we determine a polytropic index:

Eq. 9.92 $$P = K\rho^{\frac{n+1}{n}} \quad \Rightarrow \quad \frac{n+1}{n} = 1 \quad \Rightarrow \quad n = \infty$$

The previous polytropic derivation is not valid for $n = \infty$; instead we begin again by taking the derivative of the ideal gas law, assuming a constant temperature:

Eq. 9.93 $$\frac{dP}{dr} = \frac{\Re T}{\mu}\frac{d\rho}{dr}$$

This is inserted into Equation 9.52:

Eq. 9.94 $$\frac{1}{r^2}\frac{d}{dr}\left(\frac{r^2}{\rho}\frac{dP}{dr}\right) = -4\pi G\rho \quad \Rightarrow \quad \frac{1}{r^2}\frac{d}{dr}\left(\frac{r^2}{\rho}\frac{\Re T}{\mu}\frac{d\rho}{dr}\right) = -4\pi G\rho$$

We now substitute $\rho = \rho_c e^{-\psi}$ and $r = \alpha\xi$:

Eq. 9.95 $$\frac{-1}{\alpha^2\xi^2}\frac{d}{\alpha d\xi}\left(\frac{\alpha^2\xi^2}{\rho_c e^{-\psi}}\frac{\Re T}{\mu}\frac{\rho_c e^{-\psi}}{\alpha}\frac{d\psi}{d\xi}\right) = -4\pi G\rho_c e^{-\psi}$$

Eq. 9.96 $$\left(\frac{\Re T}{4\pi G\mu\rho_c}\right)\frac{1}{\alpha^2}\frac{1}{\xi^2}\frac{d}{d\xi}\left(\xi^2\frac{d\psi}{d\xi}\right) = e^{-\psi}$$

We then define the constant α :

Eq. 9.97 $$\alpha^2 \equiv \left(\frac{\Re T}{4\pi G\mu\rho_c}\right)$$

Eq. 9.98 $$\frac{1}{\xi^2}\frac{d}{d\xi}\left(\xi^2\frac{d\psi}{d\xi}\right) = e^{-\psi}$$

This must be integrated numerically, using the following boundary conditions:

At $r = 0$, $\rho = \rho_c$ $\Rightarrow$ At $\xi = 0$, $\psi = 0$ and

$$\text{At } r = 0, \frac{d\rho}{dr} = 0 \quad \Rightarrow \quad \text{At } \xi = 0, \frac{d\psi}{d\xi} = 0$$

The solution is infinite, with an infinite mass – hardly a realistic model to use. We may conclude that stars are *not* isothermal gas spheres, at least as long as the ideal gas law is their equation of state.

In the next chapter we will continue our quest for appropriate physical laws to apply in the study of stellar structure. Those that we discover will involve the generation and flow of energy in the stellar interior.

CHAPTER 10: Energy Generation and Transport

In the previous chapter we described several possible equations to be used in modeling the stellar interior. If the polytropic law is not applicable within a star, we are back to just three stellar structure equations: mass continuity, hydrostatic equilibrium, and the ideal gas law as the equation of state. We may obtain more equations by considering the manner in which energy is generated and transported inside a star.

The Radiative Temperature Gradient

We begin by making an assumption about the mode of energy transport within the star. Specifically, if we assume radiative transfer, we may use the **radiative transfer equation** – here a modified version of Equation 2.83:

Eq. 10.1 $$\cos\theta \frac{dI_\nu}{\kappa_\nu \rho\, dr} = -I_\nu + S_\nu$$

We multiply through by cos θ :

Eq. 10.2 $$\cos^2\theta \frac{dI_\nu}{\kappa_\nu \rho\, dr} = -I_\nu \cos\theta + S_\nu \cos\theta$$

Integrating over solid angle eliminates the source function term, as S_ν is presumed to be isotropic; the first term on the right becomes the flux. On the left side, we substitute $I_\nu = B_\nu(T)$, which is independent of solid angle ω:

Eq. 10.3 $$\frac{1}{\kappa_\nu \rho} \frac{dB_\nu(T)}{dr} \int_{4\pi} \cos^2\theta\, d\omega = -F_\nu \quad \Rightarrow \quad \frac{4\pi}{3\kappa_\nu \rho} \frac{dB_\nu(T)}{dr} = -F_\nu$$

We now use the chain rule to rewrite the derivative:

Eq. 10.4 $$\frac{dB_\nu(T)}{dr} = \frac{\partial B_\nu(T)}{\partial T} \frac{dT}{dr}$$

Eq. 10.5 $$\frac{4\pi}{3\kappa_\nu \rho} \frac{\partial B_\nu(T)}{\partial T} \frac{dT}{dr} = -F_\nu$$

We then integrate this expression over frequency:

Eq. 10.6 $$\frac{4\pi}{3\rho}\frac{dT}{dr}\int_0^\infty \frac{1}{\kappa_\nu}\frac{\partial B_\nu(T)}{\partial T}d\nu = -F$$

Next we define the **Rosseland mean absorption coefficient** $\bar{\kappa}$ by the following equation:

Eq. 10.7 $$\frac{1}{\bar{\kappa}}\int_0^\infty \frac{\partial B_\nu(T)}{\partial T}d\nu = \int_0^\infty \frac{1}{\kappa_\nu}\frac{\partial B_\nu(T)}{\partial T}d\nu$$

This allows us to remove the opacity from the integral, which can then be solved.

Eq. 10.8 $$\frac{4\pi}{3\bar{\kappa}\rho}\frac{dT}{dr}\int_0^\infty \frac{\partial B_\nu(T)}{\partial T}d\nu = -F$$ and

Eq. 10.9 $$\int_0^\infty \frac{\partial B_\nu(T)}{\partial T}d\nu = \frac{d}{dT}\int_0^\infty B_\nu(T)\,d\nu = \frac{dB(T)}{dT} = \frac{d}{dT}\left(\frac{\sigma T^4}{\pi}\right) = \frac{4\sigma T^3}{\pi} = \frac{acT^3}{\pi}$$

Eq. 10.10 $$\frac{4\pi}{3\bar{\kappa}\rho}\frac{dT}{dr}\frac{acT^3}{\pi} = -F$$

We now write the flux as the luminosity per unit area: $F = L_r/4\pi r^2$, where L_r is the net rate of radiant energy flowing out of a sphere of radius r. This leads to the **radiative temperature gradient** – our fourth stellar structure equation:

Eq. 10.11 $$\left.\frac{dT}{dr}\right|_{rad} = -\frac{3}{4ac}\frac{\bar{\kappa}\rho}{T^3}\frac{L_r}{4\pi r^2} \quad (=\nabla_{rad})$$

This equation provides the rate at which temperature declines with radius in a region of the star in which radiative transfer is dominant.

Opacity Sources

To evaluate $\bar{\kappa}$ we will use the principal opacity sources in the interior: **free-free absorption**, **bound-free absorption**, and **electron scattering**. Expressions for each opacity, averaged over frequency, are as follows:

Eq. 10.12 $\bar{\kappa}_{ff} = \kappa_o \rho T^{-3.5}$ where $\kappa_o = 3.68 \times 10^{22}(1+X)(1-Z)\,\bar{g}_{ff}$

This is **Kramers' opacity**; X and Z are composition variables, and $\bar{g}_{ff}$ is the **frequency-averaged Gaunt factor**, which is on the order of 1.

Eq. 10.13 $\bar{\kappa}_{bf} = \kappa_o \rho T^{-3.5}$ where $\kappa_o = 4.34 \times 10^{25} Z(1+X)\,\bar{g}_{bf}/t$

Here $\bar{g}_{bf}$ is another **frequency-averaged Gaunt factor**, and t is the **guillotine factor**, ranging from 1 to 100, which corrects for an overestimate of bound electrons. (When the last electron is lost, bound-free absorption can no longer occur (the guillotine has fallen).) Novotny (1973) Table 10-15 gives guillotine factors.

Eq. 10.14 $$\kappa_e = \frac{\sigma_T N_e}{\rho} = 0.2(1+X)$$

This is **Thomson scattering** – discussed in Chapter 7 – which is frequency independent. These sources can be added to produce a mean opacity: $\bar{\kappa} = \kappa_{ff} + \kappa_{bf} + \kappa_e$. The relative importance of each source will depend on the temperature, density, and composition at the point in question.

The Eddington Limit

We can rearrange the radiative temperature gradient as follows:

Eq. 10.15 $$\frac{\bar{\kappa}\rho L_r}{4\pi r^2 c} = -\frac{4aT^3}{3}\frac{dT}{dr} = -\frac{d}{dr}\left(\frac{1}{3}aT^4\right) = -\frac{d}{dr}\left(\frac{1}{3}u\right) = -\frac{dP}{dr} = \rho\ddot{r}$$

Here u is the radiation energy density, and $\ddot{r}$ is the acceleration of the gas due to radiation pressure.

Eq. 10.16 $$\ddot{r} = \frac{\bar{\kappa}L_r}{4\pi r^2 c}$$

The outermost layers of the star are pushed outward by radiation pressure and pulled inward by gravity. The star will be stable as long as the net acceleration is inward; for what parameters will this be true? We begin by writing the condition for stability:

Eq. 10.17 $$\frac{\bar{\kappa}L_r}{4\pi r^2 c} \le \frac{GM_r}{r^2}$$

This places an upper limit on the star's luminosity:

Eq. 10.18 $$L_r \le \frac{4\pi c G M_r}{\bar{\kappa}}$$

At the surface of the star, $L_r = L$ and $M_r = M$; then we may write $L = L_{Edd}$: the **Eddington limit**.

Eq. 10.19 $$L_{Edd} = \frac{4\pi c G M}{\bar{\kappa}}$$

We may carry this further by assuming the opacity is due primarily to Thomson scattering, for which $\kappa_e = 0.2(1+X)$:

Eq. 10.20 $$\frac{L_{Edd}}{L_\odot} = \frac{4\pi c G M_\odot}{0.2(1+X)L_\odot}\frac{M}{M_\odot} = \frac{4\pi(2.998e10)(6.674e-8)(1.989e33)}{0.2(1+X)(3.845e33)}\frac{M}{M_\odot}$$

Eq. 10.21 $$\frac{L_{Edd}}{L_\odot} = \frac{65030}{1+X}\frac{M}{M_\odot} = 38250\frac{M}{M_\odot} \quad \text{for } X \approx 0.7$$

On the main sequence, a mass-luminosity relation exists. Bowers and Deeming (1984) give this relation for upper main sequence stars:

Eq. 10.22 $$\frac{L}{L_\odot} = 10^{0.479}\left(\frac{M}{M_\odot}\right)^{2.91}$$

The previous two equations can be combined to eliminate the luminosity:

Eq. 10.23 $$38250\frac{M}{M_\odot} = 10^{0.479}\left(\frac{M}{M_\odot}\right)^{2.91} = 3.01\left(\frac{M}{M_\odot}\right)^{2.91}$$

Eq. 10.24 $$\frac{M}{M_\odot} = \left[\frac{38250}{3.01}\right]^{\frac{1}{1.91}} = 141$$

This mass marks the maximum mass a star may have without blowing itself apart by radiation pressure. Extremely massive stars will not be stable.

The Adiabatic Temperature Gradient

In some stars, energy transport is *convective*, rather than radiative. In such stars, local density fluctuations produce bubbles of gas that are hotter and less dense than their surroundings and thus rise until they eventually reach equilibrium with and mix with the surrounding gas. In this manner, rising convective cells transport energy – stored as the internal energy of the gas – toward the outside of the star. The process is assumed to be adiabatic, meaning no energy is transferred to or from the cells as they rise. The question is how the temperature varies with radius in such a convective star (or region of a star).

Because the convective process is adiabatic, we need a pressure-temperature relation that is valid for $dQ = 0$. The first law of thermodynamics becomes our starting point:

Eq. 10.25 $dQ = dU + dW$ where $dQ = C_P dT$, $dU = C_V dT$, and $dW = PdV$

With the adiabatic condition ($dQ = dU + dW = 0$), we have the following:

Eq. 10.26 $0 = C_V dT + PdV$

We then differentiate with respect to T:

Eq. 10.27 $$0 = C_V + P\frac{dV}{dT}$$

Differentiating the ideal gas law ($PV = \Re T$) with respect to T gives the following:

Eq. 10.28 $$P\frac{dV}{dT} + V\frac{dP}{dT} = \Re \quad \Rightarrow \quad P\frac{dV}{dT} = \Re - V\frac{dP}{dT}$$

This is inserted into the previous equation:

Eq. 10.29 $$0 = C_V + \Re - V\frac{dP}{dT} = C_P - V\frac{dP}{dT}$$

We now reuse the ideal gas law:

Eq. 10.30 $$V = \frac{\Re T}{P} = (C_P - C_V)\frac{T}{P}$$

Inserting this into the previous equation yields a temperature-pressure relation:

Eq. 10.31 $$0 = C_P - \left[(C_P - C_V)\frac{T}{P}\right]\frac{dP}{dT}$$

Eq. 10.32 $$\frac{dT}{T} = \frac{C_P - C_V}{C_P}\frac{dP}{P} = \frac{\gamma - 1}{\gamma}\frac{dP}{P}$$

This can also be written in log form:

Eq. 10.33 $$d\ln T = \frac{\gamma - 1}{\gamma} d\ln P \quad \Rightarrow \quad d\ln P = \frac{\gamma}{\gamma - 1} d\ln T$$

Eq. 10.34 $$P = KT^{\frac{\gamma}{\gamma - 1}}$$

Inserting another form of the ideal gas law ($T=P\mu/\rho\Re$) we obtain an expected result:

Eq. 10.35 $$P = K\left(\frac{P\mu}{\rho\Re}\right)^{\frac{\gamma}{\gamma-1}} = K\left(\frac{\mu}{\Re}\right)^{\frac{\gamma}{\gamma-1}}\left(\frac{P}{\rho}\right)^{\frac{\gamma}{\gamma-1}} = K\left(\frac{P}{\rho}\right)^{\frac{\gamma}{\gamma-1}}$$

Eq. 10.36 $$P^{\gamma-1} = K\left(\frac{P}{\rho}\right)^{\gamma} \quad \Rightarrow \quad P = K\rho^{\gamma} \qquad \text{(the adiabatic gas law)}$$

Equation 10.33 provides the required P - T relation, which can appear in several different, but equivalent forms, including the following:

Eq. 10.37 $$\frac{d\ln T}{d\ln P} = \frac{\gamma - 1}{\gamma} \qquad \text{or}$$

Eq. 10.38 $$\frac{dT}{dr} = \frac{\gamma - 1}{\gamma}\frac{T}{P}\frac{dP}{dr}$$

We now insert the ideal gas law ($T/P = \mu/\rho\Re$) and the hydrostatic equilibrium equation into Equation 10.38:

Eq. 10.39 $$\frac{dT}{dr} = \frac{\gamma - 1}{\gamma}\frac{\mu}{\rho\Re}\left(-\frac{GM_r\rho}{r^2}\right) = -\frac{\gamma - 1}{\gamma}\frac{GM_r\mu}{\Re r^2}$$

We next write the ratio of specific heats ($\gamma = C_P/C_V$) in terms of the polytropic index n:

Eq. 10.40 $$\gamma = \frac{n+1}{n} \quad \Rightarrow \quad \gamma - 1 = 1/n \quad \Rightarrow \quad \frac{\gamma - 1}{\gamma} = \frac{1}{n+1}$$

Inserting this gives us our final form for the **adiabatic temperature gradient** – our fifth stellar structure equation:

Eq. 10.41 $$\left.\frac{dT}{dr}\right|_{ad} = -\frac{GM_r\mu}{(n+1)\Re r^2} \quad \left(=\nabla_{ad}\right)$$

The appropriate value of n to use in this case would be 1.5 (from our earlier discussion of polytropes); as before, this corresponds to $\gamma = {}^5/_3$.

The adiabatic temperature gradient tells the rate at which temperature changes with radius for a star (or region of a star) in convective equilibrium. We previously derived the *radiative* temperature gradient, which tells the rate at which temperature changes with radius for a star (or region of a star) in *radiative* equilibrium. This means that we have expressions for two different temperature gradients, but it is unlikely that they can both be correct for a given region of the star. How will we know which one to use? How will the star know? As stars do not use computers, there had better be a good physical explanation that the star can understand.

Convection vs. Radiation

The star must be able to figure out when to use ∇_{rad} and when to use ∇_{ad}. These are both temperature gradients, and both of them are *negative*. T diminishes with r in each case, but in general, the rates will be different; one will be steeper, and the other will be shallower.

Consider a region of the star in radiative equilibrium, in which T vs. r is given by ∇_{rad} as shown in Figure 10.1a. The gas properties at radius r_1 are ρ, T, and P.

Figure 10.1: Conditions for convective instability

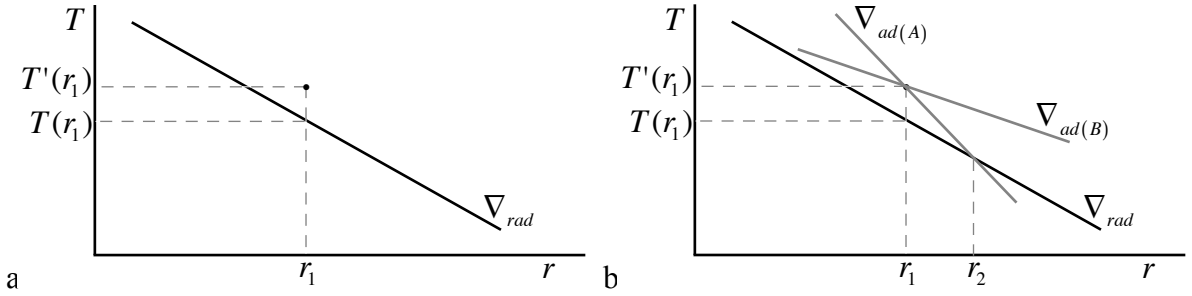

Now suppose that a local temperature fluctuation occurs at r_1 such that a bubble forms with temperature $T'(r_1) > T(r_1)$, as shown in Figure 10.1a. Then if P' (inside the bubble) equals P (outside the bubble) – as it will – then $\rho'(r_1) < \rho(r_1)$. This lower density bubble will rise adiabatically without mixing, following the local adiabatic gradient ∇_{ad}. How does this adiabatic gradient compare with the radiative gradient ∇_{rad}?

In general, there are two possibilities of interest for ∇_{ad}: it may either be *steeper* ($\nabla_{ad(A)}$) or *shallower* ($\nabla_{ad(B)}$) than ∇_{rad}. These two cases are illustrated in Figure 10.1b.

Case A ($\nabla_{ad(A)}$): As the bubble rises, it follows the steeper adiabatic curve (A) until it intersects the original radiative curve at r_2. At this point, $T'(r_2) = T(r_2)$, $\rho'(r_2) = \rho(r_2)$, and the rise stops. Further convection does not occur, and the gas continues to use radiative transfer because convection cannot be sustained.

Case B ($\nabla_{ad(B)}$): The rising bubble follows the shallower adiabatic curve (*B*), which does *not* intersect the original radiative curve. The bubble *remains* hotter – and therefore less dense – than the surroundings and continues to rise, producing convection.

Thus the gas will be stable against convection where the adiabatic gradient is steeper than the radiative gradient; convection will not occur, and the gas will rely on radiative transfer to transport energy. Convection will occur where the adiabatic gradient is shallower than the radiative gradient. In general, the star will use the energy transport process that has the *shallower* gradient.

Recalling the radiative temperature gradient $\left(\nabla_{rad} = -\frac{3}{4ac}\frac{\bar{\kappa}\rho}{T^3}\frac{L_r}{4\pi r^2}\right)$, we note that this will be relatively steep when the opacity is high, the density is high, or the temperature is low. Under such conditions, the photon flow will be impeded, and radiative transfer will not provide an efficient means of transporting energy. Instead, the energy will remain locally in the gas, creating bubbles with higher temperatures and initiating convection. Very simply, the star transports energy using the most efficient process it has available. Even computers can be taught to make this choice.

Energy Generation

The radiative temperature gradient introduced L_r – the luminosity generated within r ; therefore, we will need another equation with this quantity, perhaps one that addresses the issue of energy generation in the star.

Thermal Equilibrium

Let us begin by defining ε as the energy per gram per second produced within a shell of matter. The energy generation rate for the shell (dL_r) will then be equal to the shell mass (dM_r) multiplied by ε:

Eq. 10.42 $$dL_r = \varepsilon\, dM_r$$

Inserting the mass continuity equation ($dM_r = 4\pi\rho r^2 dr$) we arrive at the **equation of thermal equilibrium** – our sixth stellar structure equation:

Eq. 10.43 $$dL_r = \varepsilon\, 4\pi\rho r^2 dr \quad \Rightarrow \quad \frac{dL_r}{dr} = 4\pi\rho r^2 \varepsilon$$

Of course, this equation introduces still another quantity that will need to be calculated. The energy generation rate per gram is likely to be a function of density, temperature, and composition. Additionally, there may be several mechanisms by which the star may produce energy. We will consider the two principal mechanisms: gravitational contraction and nuclear reactions.

Gravitational Contraction

A star undergoing gravitational contraction will release gravitational potential energy in the process. For a shell of mass dM_r, the potential energy $d\Omega$ is as follows:

Eq. 10.44 $$d\Omega = -\frac{GM_r}{r} dM_r$$

This can be integrated to give the potential energy of the entire star:

Eq. 10.45 $$\Omega = -\int_0^M \frac{GM_r}{r} dM_r$$

The thermal energy (T) of the star is $^3/_2\, kT$ per particle = $^3/_2\, \Re T$ per mole = $^3/_2\, \Re T/\mu$ per gram = $^3/_2\, P/\rho$ per gram. Then the total thermal energy in a shell of mass $dM_r = 4\pi\rho r^2 dr$ is as follows:

Eq. 10.46 $$\frac{3}{2}\frac{P}{\rho} dM_r = \frac{3}{2} \cdot 4\pi r^2 P dr$$

And the total thermal energy in the star is found by integrating this expression:

Eq. 10.47 $$\mathrm{T} = \tfrac{3}{2}\int_0^R 4\pi r^2 P dr$$

The integration proceeds by parts, letting $u = P$ and $dv = r^2 dr$:

Eq. 10.48 $$\int_0^R P r^2 dr = \left.\frac{P r^3}{3}\right|_0^R - \int_0^R \frac{r^3}{3}\frac{dP}{dr} dr$$

The first term vanishes because $P(R) = 0$. We then utilize hydrostatic equilibrium (even though the star is contracting, for it is a very *gradual* contraction):

Eq. 10.49
$$\mathrm{T} = \tfrac{3}{2}\int_0^R 4\pi \frac{r^3}{3}\left(\frac{-dP}{dr}\right) dr = \tfrac{3}{2}\int_0^R 4\pi \frac{r^3}{3}\left(\frac{GM_r\rho}{r^2}\right) dr$$
$$= \tfrac{1}{2}\int_0^R \left(\frac{GM_r}{r}\right) 4\pi r^2 \rho\, dr = \tfrac{1}{2}\int_0^M \left(\frac{GM_r}{r}\right) dM_r = -\tfrac{1}{2}\Omega$$

The result says that the thermal energy of a star is one half of the magnitude of the star's gravitational potential energy; furthermore, reducing the potential energy through gravitational contraction will increase the thermal energy, but only by one half of the amount of potential energy released.

Eq. 10.50 $$\Delta \mathrm{T} = -\,^1/_2\, \Delta\, \Omega$$

This a statement of the **virial theorem**: only half of a star's gravitational potential energy is available to be converted into thermal energy; the remainder is radiated away and lost to the star. Thus there is a link between the rate of contraction and the luminosity of a star; knowing the luminosity, we can calculate the contraction rate, and therefore the lifetime of such a star.

Kelvin-Helmholtz Time Scale

Assuming a contraction from $R = \infty$ (where $\Omega = 0$) to the present radius, the change in potential energy should be equal to its current value:

Eq. 10.51 $$\Delta\Omega = \Omega \approx -\frac{GM^2}{R}$$

By the virial theorem, only half of this energy is available for radiation:

Eq. 10.52 $$\Delta E = -\tfrac{1}{2}\Delta\Omega = \frac{GM^2}{2R}$$

Assuming a constant luminosity over time, $L = \Delta E/\Delta t$, and from this we can estimate the lifetime of the star – the time required to reach its present state:

Eq. 10.53 $$\Delta t = \frac{\Delta E}{L} = \frac{GM^2}{2RL}$$

In studying the evolution of stars, it is important to know the approximate time scale over which a process operates. For gravitational contraction or cooling by radiation losses, the appropriate value is the **Kelvin-Helmholtz** (or **thermal**) **time scale**, which is very similar to our value above:

Eq. 10.54 $$t_{KH} = \frac{GM^2}{RL}$$

For the Sun, $t_{KH} \approx \dfrac{(6.7e-8)(2e33)^2}{(7e10)(3.8e33)} \approx 10^{15}\,\text{s} \approx 32$ million years. The Sun's age would then be estimated at about half this value, or about 16 million years. Geologists regard this as insufficient time to produce the various geological features on the Earth, meaning that gravitational contraction is not apt to be the principal energy source for the Sun.

Nuclear Reactions

Stars may also obtain energy by performing nuclear reactions. These can be divided into two types: those in which nuclei combine to form a larger nucleus (**fusion**), and those in which a nucleus splits apart into smaller nuclei (**fission**). As most stars contain relatively few large nuclei, we will ignore fission for now and concentrate on fusion reactions.

During the fusion process, energy will be released if the sum of the reactant masses is greater than the mass of the product nucleus. Such reactions are **exothermic**. If this same mass difference is negative, the reaction is **endothermic**, and it absorbs energy rather than releasing it. Stars in equilibrium require exothermic reactions in order to replace the energy that is lost through luminosity.

The link between the change in mass (Δm) and the energy released is given by Einstein's equation:

Eq. 10.55 $$E = (\Delta m)c^2$$

This can be illustrated by a simple example: consider the fusion of hydrogen into helium. By examining their approximate atomic masses (1 and 4, respectively) we see that the reaction will require four hydrogen nuclei to form one helium. Determination of Δm demands that we use more significant figures, as the difference is not large. (Note that we are using *atomic* masses –

which include the electron masses – even though the electrons do not participate in the reaction. This is easier than subtracting the same amount from both sides of the equation.)

$$m_H = 1.00783 \quad 4m_H = 4.03132 \text{ amu}$$
$$m_{He} = 4.00260 \text{ amu}$$
$$\Delta m = 0.02872 \text{ amu}$$

The conversion efficiency is rather low, as only 0.712% of the reacting mass is changed into energy. At 931.48 MeV per amu, this amounts to 26.75 MeV released per helium atom formed. At this rate of energy production, how long can a star last?

Nuclear Time Scale

As a starting point, we introduce the **nuclear time scale**, in which Mc^2 is the nuclear energy content of the star.

Eq. 10.56 $$t_{nuc} \approx \frac{Mc^2}{L}$$

For the Sun, $t_{nuc} \approx \frac{(2e33)(3e10)^2}{(3.8e33)} \approx 5\times10^{20}\text{s} \approx$ 15,000 billion years. This is obviously a much longer time scale than for gravitational contraction, but it needs some refinement before it will serve as a good estimate of the lifetime.

First, we predict that hydrogen fusion will require the very high temperatures found only in the central core of the star; therefore, we must introduce a core fraction (f_c) to reduce our available mass to the core mass. Next we recall that the star will generally not be composed *exclusively* of hydrogen, meaning that we must include the mass fraction (X) of hydrogen to further reduce the estimate of reacting mass. Finally we note that the hydrogen fusion reaction does not convert *all* of the reacting hydrogen into energy – only a small fraction of it. Thus we must include an efficiency factor (e) in the numerator. With these modifications we may now estimate the life span of a star, with reasonable estimates for the Sun included:

Eq. 10.57 $$\Delta t \approx \frac{Mf_cXec^2}{L} \approx \frac{(2e33)(0.1)(0.75)(0.007)(3e10)^2}{(3.8e33)} \approx 2.5\times10^{17}\text{s} \approx 8 \text{ billion years}$$

This estimate is in good agreement with lifetimes calculated from solar models.

The Proton-Proton Chain

So far we have seen that four hydrogen nuclei will provide sufficient mass to form one helium nucleus, but we have not yet described the process by which this fusion will occur. We might suppose that it could proceed by the simultaneous collision of the four hydrogen nuclei, resulting in synthesis of a helium nucleus. However, four-body collisions are highly improbable, even in the chaos of the stellar interior, and it turns out that the most likely scenario involves a series of two-body collisions. We now present a sequence of steps by which hydrogen fusion may proceed: **the proton-proton chain**.

Table 10.1: The proton-proton chain – pp I

		ΔE (MeV)	ν loss (MeV)		ΔE total	ν loss total
[A1]	$^1H + {}^1H \rightarrow {}^2D + e^+ + \nu$	+1.442	–0.263	×2	+2.884	–0.526
[A2]	$^2D + {}^1H \rightarrow {}^3He + \gamma$	+5.493		×2	+10.986	
[A3]	$^3He + {}^3He \rightarrow {}^4He + {}^1H + {}^1H$	+12.859			+12.859	
Net:	$4\,{}^1H \rightarrow {}^4He$				+26.729	–0.526

Step [A1] involves the collision of two protons (^1H) – the most abundant nuclei in most stars. The principal fusion product is a **deuterium** nucleus (^2H or ^2D), which consists of one proton and one neutron, rather than the two protons that collided to produce it. This is because one of the protons is transformed into a neutron, creating a **positron** (e^+) to carry the former proton's charge and a **neutrino** (ν), which conserves the **lepton number** for the reaction: –1 (for the positron) and +1 (for the neutrino) totals 0 for the reaction.

The positron is the anti-particle of the electron; when the two collide, they annihilate each other, turning themselves completely into energy (included in ΔE). The neutrino is a nearly massless particle that moves at nearly the speed of light while hardly ever interacting with matter. Its main role here is to carry away some of the energy released by the reaction – the amount shown in the neutrino loss column.

In step [A2], the deuterium reacts with a proton to produce a helium-3 nucleus and a gamma-ray photon – another form of energy. Steps [A1] and [A2] are then repeated, producing a second helium-3 and paving the way for the production of helium-4 in step [A3], where more energy is released in the form of increased kinetic energy of the particles. This reaction also generates two protons, partly replacing the six protons required to make the two helium-3 nuclei. Thus, the net reaction is as expected. This sequence of steps is known as **pp I**.

The pp I sequence requires a temperature sufficient to allow the colliding nuclei to overcome their repulsive Coulomb forces – about 10 to 15 million K. At higher temperatures, there are other options for completing the reaction:

Table 10.2: The proton-proton chain – pp II

		ΔE (MeV)	ν loss (MeV)
[A1]	$^1H + {}^1H \rightarrow {}^2D + e^+ + \nu$	+1.442	–0.263
[A2]	$^2D + {}^1H \rightarrow {}^3He + \gamma$	+5.493	
[A3']	$^3He + {}^4He \rightarrow {}^7Be + \gamma$	+1.586	
[A4]	$^7Be + e^- \rightarrow {}^7Li + \nu$	+0.861	–0.80
[A5]	$^7Li + {}^1H \rightarrow {}^4He + {}^4He$	+17.347	
Net:	$4\,{}^1H \rightarrow {}^4He$	+26.729	–1.063

The **pp II** sequence requires the presence of helium-4 nuclei and is dominant at temperatures of 14 to 23 million K. At temperatures higher than 23 million K, the **pp III** sequence can be performed efficiently:

Table 10.3: The proton-proton chain – pp III

		ΔE (MeV)	ν loss (MeV)
[A1]	${}^1H + {}^1H \rightarrow {}^2D + e^+ + \nu$	+1.442	–0.263
[A2]	${}^2D + {}^1H \rightarrow {}^3He + \gamma$	+5.493	
[A3']	${}^3He + {}^4He \rightarrow {}^7Be + \gamma$	+1.586	
[A4']	${}^7Be + {}^1H \rightarrow {}^8B + \gamma$	+0.135	
[A5']	${}^8B \rightarrow {}^8Be + e^+ + \nu$	+17.98	–7.2
[A6]	${}^8Be \rightarrow {}^4He + {}^4He$	+0.095	
Net:	$4\,{}^1H \rightarrow {}^4He$	+26.73	–7.46

Of course in a real star, these reactions all compete at the same time, with the dominant sequence determined by the conditions in the core. For example, the Standard Solar Model (Bahcall 1989) produces energy as follows: 85% pp I (26.2 MeV), 15% pp II (25.7 MeV), and 0.02% pp III (19.1 MeV) – where the energies have been adjusted for neutrino losses.

The individual reactions in the pp chain proceed at different rates, depending on the probability of the reaction, the concentration of the reactants, and the temperature. It is common to indicate these rates by giving reaction lifetimes τ, which may be considered as the average time a particle waits before participating in the reaction. The following lifetimes are found for the pp chain reactions, assuming $X = Y = 0.5$, $\rho = 100$, and $T_6 = 15$ (typical solar values):

Table 10.4: Lifetimes for individual reaction in the pp chain (Clayton 1968)

Reaction	τ	Reaction	τ	Reaction	τ
[A1]	7.9 billion years	[A3']	970,000 years	[A4']	66 years
[A2]	1.4 seconds	[A4]	140 days	[A5'] & [A6]	0.95 seconds
[A3]	240,000 years	[A5]	9.5 minutes		

Reactions with very short lifetimes will happen very quickly, given a sufficient supply of reactants; those with longer lifetimes will delay the overall process. Thus the **controlling reaction** in a sequence is the one with the *longest* lifetime, as the cycle cannot proceed any faster than this reaction can happen. For the pp chain, the controlling reaction is [A1] because this reaction has the longest lifetime, and it is included in each of the three pp cycles.

From the lifetime for reaction [A1], we see that the probability of a given proton reacting in any one year is about one in 8 billion; for a collection of 8 billion protons, on average about one of them should react each year. We may use this idea to estimate the luminosity of the Sun, based on the number of protons contained in its core and the rate at which they react.

The number of core protons n_p should be the mass of hydrogen in the core divided by the mass of one hydrogen atom:

Eq. 10.58 $$n_p = \frac{M_{sun} f_c X}{m_H}$$

The probability of a reaction is $1/\tau$, the energy released by each complete cycle is ≈ 26.7 MeV, and four protons react in each cycle. Combining these, we can write an expression for the luminosity:

Eq. 10.59 $$L \approx \frac{\#\text{protons}}{\text{protons/rxn}} \cdot \frac{\Delta E}{\text{rxn}} \cdot \text{probability} = \frac{n_p}{4} \cdot \Delta E \frac{1}{\tau} = \frac{M_\odot f_c X}{4 m_H} \cdot \frac{\Delta E}{\tau}$$

Inserting solar values and a few conversion factors, we obtain the luminosity estimate:

Eq. 10.60 $$L \approx \frac{(2e33)(0.1)(0.75)}{4(1.67e-24)} \cdot \frac{26.7e6\,(\text{eV})}{7.9e9\,(\text{yrs})} \cdot \frac{1.6e-12(\text{ergs/eV})}{3.16e7(\text{s/yr})} \approx 3.8 \times 10^{33}\,(\text{ergs/s})$$

As this is in good agreement with the observed value, it would appear that our figure for the lifetime of the controlling reaction is quite reasonable. The pp chain is the principal source of energy for the Sun and cooler main sequence stars.

The CNO Cycle

Hotter stars are capable of changing hydrogen into helium by a different route, if the appropriate catalysts are present. This collection of reactions is known as the **CNO cycle**:

Table 10.5: The CNO cycle – option 1

		ΔE (MeV)	ν loss (MeV)
[B1]	$^{12}C + {}^1H \rightarrow {}^{13}N + \gamma$	+1.944	
[B2]	$^{13}N \rightarrow {}^{13}C + e^+ + \nu$	+2.221	–0.710
[B3]	$^{13}C + {}^1H \rightarrow {}^{14}N + \gamma$	+7.550	
[B4]	$^{14}N + {}^1H \rightarrow {}^{15}O + \gamma$	+7.293	
[B5]	$^{15}O \rightarrow {}^{15}N + e^+ + \nu$	+2.761	–1.000
[B6]	$^{15}N + {}^1H \rightarrow {}^{12}C + {}^4He$	+4.965	
Net:	$4\,{}^1H \rightarrow {}^4He$	+26.734	–1.710

While the first three reactions may occur at temperatures less than 10 million K, the last three require at least 10 million K. An alternate cycle is provide by a branch at the sixth reaction, as shown in Table 10.6:

Table 10.6: The CNO cycle – option 2

		ΔE (MeV)	ν loss (MeV)
[B4]	$^{14}N + {}^1H \rightarrow {}^{15}O + \gamma$	+7.293	
[B5]	$^{15}O \rightarrow {}^{15}N + e^+ + \nu$	+2.761	–1.000
[B6']	$^{15}N + {}^1H \rightarrow {}^{16}O + \gamma$	+12.126	
[B7]	$^{16}O + {}^1H \rightarrow {}^{17}F + \gamma$	+0.601	
[B8]	$^{17}F \rightarrow {}^{17}O + e^+ + \nu$	+2.762	–0.94
[B9]	$^{17}O + {}^1H \rightarrow {}^{14}N + {}^4He$	+1.193	
Net:	$4\,{}^1H \rightarrow {}^4He$	+26.736	–1.94

Reaction [B6'] requires temperatures in excess of 17 million K; only three of these reactions occur per 1000 [B6] reactions. The **controlling reaction** for CNO is reaction [B4]; the actual lifetimes depend on conditions in the core.

CNO requires higher temperatures than pp, due to the larger, more positively charged nuclei involved in the CNO reactions. Note that carbon-12 (in option 1) and nitrogen-14 (in option 2) both serve as catalysts for the production of helium-4, as does helium-4 in pp II and pp III.

Together the pp chain and CNO cycle comprise the means by which hydrogen is converted to helium in stars. Other reactions are possible, given heavier raw materials and higher temperatures, but they do not involve hydrogen fusion.

The Triple-Alpha Process

The most abundant nuclei in the universe are ^{1}H and ^{4}He, occurring in a roughly 10:1 ratio. This abundance can be achieved from an initial universe of pure hydrogen and 13 billion years or so of hydrogen fusion, although this is not considered to be likely.

The next most abundant nuclei are ^{12}C and ^{16}O. How can fusion produce these? And what about the nuclei in between ^{4}He and ^{12}C ?

We cannot simply add protons one at a time to ^{4}He because there are no stable nuclei with five nucleons. And there are never enough ^{2}D around to bridge the gap because reaction [A2] proceeds so quickly. Similarly, adding two ^{4}He together is a problem because there are no stable nuclei with eight nucleons. No clever chains of light particles have been found that can hurdle these gaps, nor are three- or four-body collisions apt to be probable. It would seem that metals are nearly impossible to make!

But consider the reaction $^{4}He + ^{4}He \rightarrow ^{8}Be$ (the reverse of [A6]). This reaction is endothermic and requires a temperature of 100 million K; in addition, the ^{8}Be product is unstable. However, the lifetime of the ^{8}Be nucleus is about 2.6×10^{-16} seconds, but as short as this seems, it is still much longer than the time required for two ^{4}He nuclei to scatter past each other – which is on the order of 10^{-20} seconds. This means that the temporary formation of a ^{8}Be nucleus significantly increases the probability that three ^{4}He nuclei will be in sufficiently close proximity for the reaction sequence to continue.

Even though the ^{8}Be nucleus is unstable, a small, non-zero equilibrium concentration of ^{8}Be will be established in the helium gas. For example, at $T = 100$ million and $\rho = 10^{5}$, there will be about one ^{8}Be nucleus per billion ^{4}He nuclei, which is enough to allow the sequence $^{8}Be + ^{4}He \rightarrow ^{12}C^{*} \rightarrow ^{12}C + \gamma$ to proceed (where $^{12}C^{*}$ is an excited state). This relatively short sequence – shown in Table 10.7 – is known as the **triple-alpha process (3α)**:

Table 10.7: The triple-alpha process (3α)

		ΔE (MeV)
[C1]	$^4He + ^4He \rightarrow ^8Be$	–0.092
[C2]	$^8Be + ^4He \rightarrow ^{12}C^*$	–0.286
[C3]	$^{12}C^* \rightarrow ^{12}C + \gamma$	+7.656
Net:	$3\ ^4He \rightarrow ^{12}C$	+7.274

From here, **alpha capture** may continue:

[C4]	$^{12}C + ^4He \rightarrow ^{16}O + \gamma$	+7.161

These helium-burning reactions are believed to result in roughly equal amounts of ^{12}C and ^{16}O nuclei produced in stars. The combined net reaction can be expressed as follows:

Net:	$7\ ^4He \rightarrow ^{12}C + ^{16}O$	+21.709

We now calculate the energy released per reacting particle. For triple-alpha/alpha capture, we have 21.709 ÷ 7 ≈ 3.1 MeV per reacting particle. This is compared with hydrogen burning, which releases 26.73 ÷ 4 ≈ 6.7 MeV per reacting particle. Hydrogen burning is clearly more efficient than helium burning at generating energy. Essentially all visible stars derive the bulk of their energy from hydrogen burning and/or helium burning; reactions involving heavier fuels will be considered later during discussion of stellar evolution.

Binding Energy

To determine the nuclear energy released, we must examine the binding energy, which holds protons and neutrons together in the nucleus. This quantity can be defined in terms of the **mass defect** ΔM:

Eq. 10.61 $$\Delta M \equiv N m_n + Z m_p - M_{nuc} = (A - Z) m_n + Z m_p - M_{nuc}$$

Here Z is the number of protons, N is the number of neutrons, and A (= $Z + N$) is the number of nucleons; this means the mass defect is the difference between the sum of the masses of the nucleons and the mass of the nucleus (M_{nuc}). (Note: ΔM is *not* the same as the Δm used earlier for the mass conversion in a reaction, but the mass defect can be used to calculate Δm. Also note that the mass of the nucleus is *not* the same as the atomic mass – which contains electron masses.)

Given the mass defect, the **binding energy** E_B is easily calculated:

Eq. 10.62 $$E_B \equiv \Delta M\, c^2$$

The greater the binding energy, the more energy will be released when the nucleus is formed from its constituent nucleons. However, most nuclei are not formed from a collection of protons and neutrons, but rather from other nuclei; thus it will be more useful to compare binding energies of different nuclei with each other. In general it will be true that larger nuclei have greater binding energies, simply because they contain more nucleons. But we will gain the most insight by considering the binding energy per nucleon, also known as the **binding fraction** f_B.

Eq. 10.63 $$f_B = \frac{E_B}{A}$$

The binding fraction and the mass defect for a range of nuclei are tabulated in Table 10.8, along with the quantities used to calculate them. (Atomic masses from http://www.chem.ualberta.ca/~massspec/atomic_mass_abund.pdf)

Table 10.8: Mass defects and binding fractions for representative isotopes

Isotope	A	Z	M_{atom} (amu)	M_{nuc} (amu)	ΔM (MeV)	f_B (MeV)
^{1}H	1	1	1.007825	1.007276	0.0000	0.0000
^{2}D	2	1	2.014102	2.013553	2.2244	1.1122
^{3}He	3	2	3.016029	3.014932	7.7184	2.5728
^{4}He	4	2	4.002603	4.001506	28.2959	7.0740
^{7}Li	7	3	7.016004	7.014358	39.2446	5.6064
^{9}Be	9	4	9.012182	9.009988	58.1651	6.4628
^{12}C	12	6	12.000000	11.996709	92.1618	7.6801
^{14}N	14	7	14.003074	13.999234	104.6587	7.4756
^{16}O	16	8	15.994915	15.990526	127.6190	7.9762
^{18}O	18	8	17.999160	17.994771	139.8075	7.7671
^{20}Ne	20	10	19.992440	19.986954	160.6451	8.0323
^{24}Mg	24	12	23.985042	23.978459	198.2569	8.2607
^{28}Si	28	14	27.976927	27.969247	236.5366	8.4477
^{56}Fe	56	26	55.934942	55.920679	492.2542	8.7903
^{89}Y	89	39	88.905848	88.884453	775.5382	8.7139
^{107}Ag	107	47	106.905093	106.879310	915.2665	8.5539
^{138}Ba	138	56	137.905241	137.874521	1158.2985	8.3935
^{169}Tm	169	69	168.934211	168.896359	1371.3536	8.1145
^{197}Au	197	79	196.966552	196.923214	1559.4017	7.9157
^{238}U	238	92	238.050783	238.000314	1801.6947	7.5701

It is instructive to consider a plot of the binding fraction over the range of values of A, as shown in Figure 10.2. For the lighter nuclei, the binding fraction rises steeply with A to a peak at ^{56}Fe, after which it declines gradually. Fusion of these lighter elements produces heavier isotopes with higher binding fractions and releases energy. Fusion of elements heavier than iron produces still heavier isotopes, but with lower binding fractions; such reactions *absorb* energy, rather than releasing it. In general, nuclear reactions that result in products with greater binding fractions will be exothermic; those that reduce the binding fraction will be endothermic. Thus fusion is normally exothermic for isotopes up to ^{56}Fe, but it is endothermic for isotopes beyond; the reverse is true for fission. This fact plays a key role in nucleosynthesis and stellar evolution.

Figure 10.2: Binding fraction vs. nucleon number

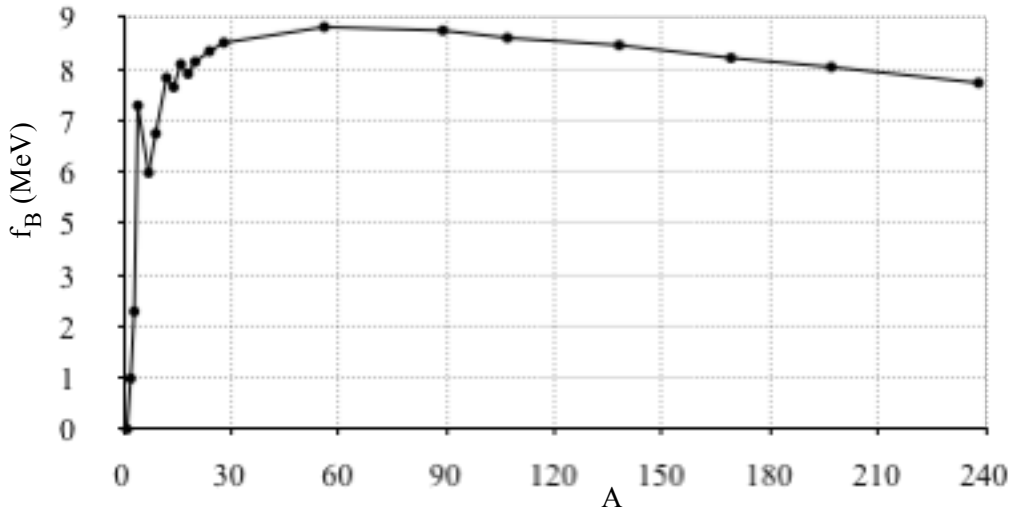

Reaction Rates

To achieve fusion, nuclei must get very close together – to within about one nuclear radius: $r_o \approx 1.1 \times 10^{-13} A^{1/3}$ cm. The nuclei are repelled by the Coulomb potential, where the potential energy of two nuclei at a distance $r > r_o$ is as follows:

Eq. 10.64 $$E = \frac{Q_1 Q_2}{r} = \frac{Z_1 Z_2 e^2}{r}$$

Within r_o the nuclei are held together by the **strong nuclear force**. The potential function is approximately as shown in Figure 10.3. The height of the potential barrier at r_o depends on the nuclei involved:

Eq. 10.65 $$E(r_o) \approx 1.3 \frac{Z_1 Z_2}{A^{1/3}} MeV$$

For the pp chain's controlling reaction, $E(r_o) \approx 1.3$ MeV $= {}^3/_2 kT \Rightarrow T \approx 10^{10}$. This would seem to imply that temperatures on the order of 10 billion K are required for hydrogen fusion; but estimates of the central temperature for the Sun amount to only about 10 million K. What could explain this difference?

The simplest solution is that only *some* of the nuclei participate in the reactions; only those in the high velocity tail of the Maxwellian distribution can have sufficient energy to overcome the Coulomb repulsion. (The above calculation equated the potential barrier height to the *average* kinetic energy of the particles.)

An additional factor is **tunneling** – a purely quantum mechanical phenomenon with no classical analog. Classically, only those nuclei with kinetic energies *greater* than the barrier height will be able to approach closely enough to react. But in quantum mechanical treatments,

there is a finite probability that an approaching particle may tunnel *through* the potential barrier, emerging in the potential well and reacting. (Note the dashed line labeled E_o in Figure 10.3.) The tunneling probability increases with the energy of the particle (because the barrier narrows at higher energies): probability $\approx e^{-b/\sqrt{E}}$, where $b = 0.99\, Z_j Z_k \sqrt{\mu}$.

Figure 10.3: Coulomb barrier for colliding nuclei

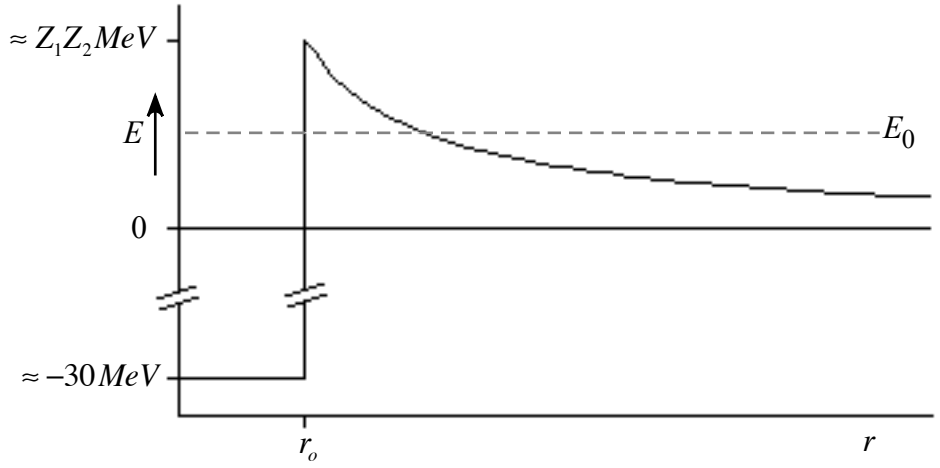

But the number of available nuclei *decreases* for higher energies: probability $\approx e^{-E/kT}$. Thus, these two factors work against each other; if either one becomes too small, the reaction will not proceed. The product of these two probabilities yields the **Gamow peak**, as shown in Figure 10.4.

Figure 10.4: The Gamow peak

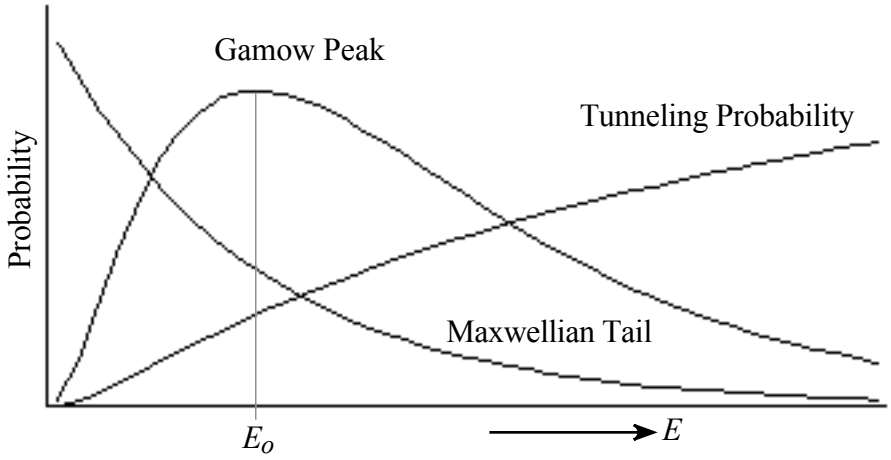

The optimal reaction energy is E_o, and the reaction rate is proportional to the area under the Gamow peak. Most of the reactions will be produced by particles with energies around E_o, which is generally several times *kT*.

Eq. 10.66 $$\frac{E_o}{kT} = 6.574\left(\frac{W}{T_7}\right)^{1/3} \qquad \text{where } W = Z_j^2 Z_k^2 \frac{A_j A_k}{A_j + A_k} \quad (A_i \text{ are nucleon numbers})$$

For the pp chain's controlling reaction, at T_7=1, $W = {}^1/_2$, and $E_o/kT = 5.22$.

We are now ready to formulate an equation for the reaction rate ε that appeared in the equation of thermal equilibrium. We may assume that it will involve the density, temperature, and composition, with factors determined as follows:

Eq. 10.67 $$\varepsilon\left(\frac{\text{ergs}}{\text{g-s}}\right) = \left(\frac{\text{ergs}}{\text{rxn}}\right)\cdot\left(\frac{\text{rxns}}{\text{cc-s}}\right)\cdot\left(\frac{\text{cc}}{\text{g}}\right)$$

The first factor is determined from the binding energy, and the third factor is the inverse of the density. The second factor is further broken down:

Eq. 10.68 $$\left(\frac{\text{rxns}}{\text{cc-s}}\right) = \left(\frac{\text{collisions}}{\text{cc-s}}\right)\cdot\left(\frac{\text{barrier penetrations}}{\text{collision}}\right)\cdot\left(\frac{\text{rxns}}{\text{penetration}}\right)$$

The collision rate is proportional to the concentrations of the colliding species (N_i), which in turn are proportional to ρX_i . So for an *i-j* collision, the collision rate is proportional to the product $(\rho X_i)(\rho X_j)$. The ${}^1/_\rho$ factor from Equation 10.67 cancels one of these densities and gives the following structure for the reaction rate:

Eq. 10.69 $$\varepsilon \propto \rho\, X_i X_j f(T)$$

The positively charged nuclei repel each other, but this repulsion is reduced by intervening electrons, which screen the nuclei from each other. Because the nuclei perceive a reduced positive charge, the reaction rate is enhanced; this increase is modeled by the **electron shielding (**or **electron screening) factor**:

Eq. 10.70 $$f_{i,j} = \exp\left(0.188 Z_i Z_j \sqrt{\rho\zeta/T_6^3}\right) \approx 1 + 0.188 Z_i Z_j \sqrt{\rho\zeta/T_6^3} \quad (\text{using } e^x \approx 1 + x + ...)$$

Here Z_i and Z_j are nuclear charges and $\zeta = \sum_Z \left(Z^2 + Z\right)\left({}^{X_Z}/_{m_Z}\right) \approx \frac{1}{2}(X+3)$ for low metal fractions. (Z is the atomic number, X_Z is the mass fraction of element Z, and X is the mass fraction of hydrogen.)

To calculate the reaction rate for a sequence, we need only consider the controlling reaction:

- pp – [A1]: ${}^1H + {}^1H \rightarrow$
- CNO – [B4]: ${}^{14}N + {}^1H \rightarrow$

The appropriate screening functions are then as follows:

- pp: $f_{1,1} \approx 1 + 0.25\sqrt{\rho/T_6^3}$
- CNO: $f_{14,1} \approx 1 + 1.75\sqrt{\rho/T_6^3}$

- 3α: $f_{3\alpha} \approx 1 + 0.0024\sqrt{\rho / T_8^3}$

A correction must also be made for approximating the Gamow peak as a gaussian function:

- pp: $g_{1,1} = 1 + 0.0123\ T_6^{1/3} + 0.0109 T_6^{2/3} + 0.0009 T_6$
- CNO: $g_{14,1} = 1 + 0.0027\ T_6^{1/3} - 0.00778 T_6^{2/3} - 0.000149 T_6$
- 3α: (no correction)

In general, $g \approx f \approx 1$.

For the pp chain, another factor is needed to account for the different endings and efficiencies in pp I, pp II, and pp III, which depend on the abundance of helium-4. This factor ψ ranges from 1 to 2 (see Novotny (1973) Figure 10-7), reflecting the number of ^4He nuclei produced per pp reaction [A1]. The reaction rates are then as follows:

Eq. 10.71 $\varepsilon_{pp} = 2.38 \times 10^6 \rho X_1^2 f_{1,1} g_{1,1} \psi_{pp} T_6^{-2/3} e^{-33.80/T_6^{1/3}}$ ergs/(g-s) (Kippenhahn & Weigert 1990)

Eq. 10.72 $\varepsilon_{CNO} = 7.94 \times 10^{27} \rho X_1 X_{CNO} f_{14,1} g_{14,1} T_6^{-2/3} e^{-152.313/T_6^{1/3}}$ ergs/(g-s) (Cox & Giuli 1968)

Here $X_{CNO} = X_C + X_N + X_O$, as these three nuclei are interconvertible by this process.

Eq. 10.73 $\varepsilon_{3\alpha} = 5.09 \times 10^{11} \rho^2 X_4^3 f_{3\alpha} T_8^{-3} e^{-44.027/T_8}$ ergs/(g-s) (Kippenhahn & Weigert 1990)

The temperature dependence is a bit obscure in these expressions; it is often useful to rewrite the rates in a different form that will show the temperature dependence better:

Eq. 10.74 $\varepsilon_{pp} = \rho X_1^2 f_{1,1} g_{1,1} \psi_{pp} \varepsilon_o(T_o) (T/T_o)^v$

Eq. 10.75 $\varepsilon_{CNO} = \rho X_1 X_{\mathrm{CNO}} f_{14,1} g_{14,1} \varepsilon_o(T_o) (T/T_o)^v$

Eq. 10.76 $\varepsilon_{3\alpha} = \rho^2 X_4^3 f_{3\alpha} \varepsilon_o(T_o) (T/T_o)^v$

The function $\varepsilon_o(T_o)$ is tabulated for each reaction at selected values of T_o. One chooses the value of T_o closest to the target temperature and adjusts $\varepsilon_o(T_o)$ using the factor $(T / T_o)^v$. The exponent v – which relates to neither neutrinos nor frequency – is calculated as follows:

Eq. 10.77 $v = \dfrac{\tau_o - 2}{3}$ where $\tau_o = \dfrac{3E_o}{kT_o} = 19.721 \left(\dfrac{W}{T_7} \right)^{1/3}$ (see Equation 10.66)

The Gamow peak energy E_o is given by the following:

Eq. 10.78 $E_o = \left[\sqrt{\dfrac{m}{2}} \dfrac{\pi Z_i Z_j e^2 kT}{\hbar} \right]^{2/3}$

Cox & Giuli (1968) provide tables of T_o, ε_o, v, and $g_{1,1}$ for the pp chain (p494), T_o, ε_o, v, and $g_{14,1}$ for the CNO cycle (p486), and T_o, ε_o, and v for the 3α process (p505). The most notable point about this data is the very steep temperature dependence for both CNO and 3α. At a T_o

value of 15 million K, $\nu \approx 4$ for pp and $\nu \approx 20$ for CNO, while at T_o = 100 million, $\nu \approx 40$ for 3α. These differences will have interesting structural results for the stars (see Chapter 12).

We now present some sample calculations of the reaction rates. To begin, we will estimate the value of ε_{pp} at $T_6 = 12$, $\rho = 80$, and $X_1 = 0.7$. First we will use Equation 10.74, evaluated around the tabulated value of $T_o = 10$, for which $\varepsilon_o(T_o) = 0.0679$, $\nu = 4.60$, and $g = 1.07$. Further assuming that $f \approx \psi \approx 1$, we arrive at our estimate:

Eq. 10.79 $$\varepsilon_{pp} = 80\,(0.7)^2\,(1)\,(1.07)\,(1)\,(0.0679)\,(12/10)^{4.60} = 6.59 \text{ ergs/(g-s)}$$

We can obtain a more exact result by calculating each of the correction factors and using Equation 10.71. $\psi_{pp} = 1$ (from Novotny (1973) Figure 10-7).

Eq. 10.80 $$f_{1,1} = 1 + 0.25\sqrt{80}\,(12)^{-3/2} = 1.054$$

Eq. 10.81 $$g_{1,1} = 1 + 0.0123 \times (12)^{1/3} + 0.0109 \times (12)^{2/3} + 0.0009 \times (12) = 1.096$$

Eq. 10.82 $$\varepsilon_{pp} = 2.38 \times 10^6\,(80)\,(0.7)^2\,(1.054)\,(1.096)\,(1)\,(12)^{-2/3}\,e^{-33.80/(12)^{1/3}} = 7.97 \text{ ergs/(g-s)}$$

The approximation gives a reasonable value compared to the more precise version.

We now compare the rates for pp and CNO at different temperatures. For simplicity, we will use the approximations (Equations. 10.74-5), along with $g = f = \psi = 1$, $X_1 = 0.7$, and $X_{CNO} \approx 0.02$:

Eq. 10.83 $$\frac{\varepsilon_{pp}}{\varepsilon_{CNO}} \approx \frac{X_1}{X_{CNO}} \cdot \frac{\varepsilon_{o_{pp}}}{\varepsilon_{o_{CNO}}} = 35\,\frac{\varepsilon_{o_{pp}}}{\varepsilon_{o_{CNO}}}$$

Results are shown in Table 10.9; from these it is clear that the pp chain is the dominant hydrogen-burning mechanism at low temperatures while the CNO cycle dominates at high temperatures. Both reaction rates increase with temperature, but the CNO cycle has a much stronger temperature dependence than the pp chain: $\nu_{pp} \approx 4$ and $\nu_{CNO} \approx 20$.

Table 10.9: Rate comparison – pp vs. CNO (data from Cox & Giuli 1968)

T_o	$\varepsilon_{o_{pp}}$	$\varepsilon_{o_{CNO}}$	$\varepsilon_{o_{pp}}/\varepsilon_{o_{CNO}}$
10	0.0679	0.000335	7094
15	0.377	1.90	6.94
20	1.09	451	0.0846
25	2.29	21600	0.00371

Neutrinos

Some of the reactions in the hydrogen-burning sequences produce **neutrinos** – nearly massless particles that efficiently carry energy away from the reaction. The reason for this efficiency lies in the extremely small cross section for neutrino interactions with matter:

Eq. 10.84 $$\sigma \approx \left(\frac{E}{m_e c^2} \right)^2 \cdot 10^{-44}\,\mathrm{cm}^2$$

Because $m_e c^2 = 0.511$ MeV, for $E \approx 1$ MeV, $\sigma \approx 10^{-44}$, which is quite small compared to the Thomson cross section ($\sigma_T \approx 10^{-25}$). We may calculate a mean free path for the neutrino:

Eq. 10.85 $$\ell = \frac{1}{N\sigma} = \frac{\mu}{\rho N_A \sigma}$$ where $N = \rho N_A / \mu$ is the number density of target nuclei

Letting $\mu \approx 1$, $\rho \approx 1$, and $N_A = 6 \times 10^{23}$, we find an extraordinary value for the mean free path:

Eq. 10.86 $$\ell \approx \frac{1}{1 \cdot 10^{-44} \cdot 6 \times 10^{23}} \approx 1.7 \times 10^{20}\,\mathrm{cm} \approx 50\mathrm{pc}\,!$$

Even at a density of 1 million g/cc – such as found in a white dwarf – the mean free path is still about 11 AUs. Neutrinos are difficult to confine, unless their energies are *much* higher, as may be found in supernovae. They are also extremely difficult to detect, and even though they emerge directly from the core of the star, bearing information about the processes occurring there, they have been rather slow to divulge the secrets of fusion they carry.

The Equations of Stellar Structure

We now have a sufficient supply of equations to construct interior models for most stars. These are generally known as the **equations of stellar structure**:

Eq. 9.2 **[1]** $$\frac{dM_r}{dr} = 4\pi\rho r^2$$ – **the equation of mass continuity**

Eq. 9.3 **[2]** $$\frac{dP}{dr} = -\frac{GM_r\rho(r)}{r^2}$$ – **the equation of hydrostatic equilibrium**

Eq. 9.4 **[3]** $$P_g = \frac{\rho \Re T}{\mu}$$ (with $P = P_g + P_r$) – **the equation of state**[*]

Eq. 10.11 **[4]** $$\left.\frac{dT}{dr}\right|_{rad} = -\frac{3}{4ac}\frac{\bar{\kappa}\rho}{T^3}\frac{L_r}{4\pi r^2}$$ – **the radiative temperature gradient**

Eq. 10.41 **[5]** $$\left.\frac{dT}{dr}\right|_{ad} = -\frac{GM_r\mu}{(n+1)\Re r^2}$$ (with $n = 1.5$) – **the adiabatic temperature gradient**

Eq. 10.43 **[6]** $$\frac{dL_r}{dr} = 4\pi\rho r^2\varepsilon$$ – **the equation of thermal equilibrium**

In addition to these six equations, we will also need relations for appropriate energy generation rates (ε) and the mean opacity ($\bar{\kappa}$); the initial composition (X_i) must also be specified.

[*] In some regions of the star, a different equation of state may be needed; this will be investigated in the next chapter.

The desired solution will be a set of equations (or tabulated values) giving the major variables as functions of radius: $M_r(r)$, $\rho(r)$, $P(r)$, $T(r)$, and $L_r(r)$.

Most of the stellar structure equations are differential equations, which of course require boundary conditions to achieve a solution. What boundaries are available in a star?

The surface of a star provides an obvious boundary. Here we find $r = R$, $M_r = M$, and $L_r = L$. In addition, we may assign surface values to the gas properties, but these values approach 0 relative to their much higher interior values: $T = T_s \rightarrow 0$, $P = P_s \rightarrow 0$, and $\rho = \rho_s \rightarrow 0$.

We may solve the stellar structure equations by choosing the star's mass (M) and radius (R) and integrating inwards from the surface to the center. The 'correct' model will have $M_r \rightarrow 0$ as $r \rightarrow 0$, which will not be true for just any combination of M and R. We must vary R until we find the best radius for a given mass.

Another boundary can be found at the *center* of the star, where $r = 0$, $M_r = 0$, and $L_r = 0$, and the gas properties take on their central values: $T = T_c$, $P = P_c$, and $\rho = \rho_c$. Then we could solve the stellar structure equations by choosing two central values (T_c and ρ_c) and integrating outwards towards the surface. The 'correct' model will then have $T \rightarrow 0$, $P \rightarrow 0$, and $\rho \rightarrow 0$ at the same radius ($= R$). We would vary one of our two central values until this condition is met.

In principle, any two parameters (e.g. T_c and P_c, or R and X_1) may be freely chosen, and then the model is uniquely determined. It does not matter whether the integration proceeds inward or outward. In practice it is normally easiest to choose the mass and the composition as the input parameters.

This leads to the **Vogt-Russell theorem**: If the pressure, opacity, and energy generation rates are functions of the local temperature and composition only, then the structure of a star is uniquely determined by the mass and chemical composition of the star (Hopkins 1980). We know that stars form over a range of different masses, and the process of nuclear fusion serves to alter the composition of stars and the matter from which they form, given sufficient time. Thus we should be able to use our models to account for the variety of stellar species that are observed.

To illustrate the basic idea of the Vogt-Russell theorem, we consider the stellar structure equations and their accompanying relations. (Only one temperature gradient is used here because only one of the two will be used at a given location.)

[1]	$M = f(\rho,r)$	(mass continuity)
[2]	$P = f(M,\rho,r)$	(hydrostatic equilibrium)
[3]	$P = f(T,\rho,X)$	(equation of state)
[4]	$T = f(\bar{\kappa},\rho,L,r)$	(radiative temperature gradient)
[6]	$L = f(\rho,r,\varepsilon)$	(thermal equilibrium)
[7]	$\varepsilon = f(T,\rho,X)$	(energy generation rate)
[8]	$\bar{\kappa} = f(T,\rho,X)$	(mean opacity)

We now combine [4] and [8] to eliminate $\bar{\kappa}$ and form [9] $T = f(X,\rho,L,r)$.
Then combine [6] and [7] to eliminate ε and form [10] $L = f(X,\rho,T,r)$.

Then combine [9] and [10] to eliminate L and form [11] $T = f(X,\rho,r)$.
Then combine [3] and [11] to eliminate T and form [12] $P = f(X,\rho,r)$.
Then combine [2] and [12] to eliminate P and form [13] $\rho = f(X,M,r)$.
Then combine [1] and [13] to eliminate ρ and form [14] $r = f(X,M)$.

Thus, for a given mass and chemical composition, the properties of a star are determined. In the final chapters of the book, we will investigate the formation of stars of different masses and compositions and determine how these parameters change over the course of stellar evolution. But first, we must discuss an alternate equation of state.

CHAPTER 11: Degeneracy

Before tackling the subject of stellar evolution, we need to load one more piece of basic physics into our bag of tricks. This is the topic of **degeneracy**, which will lead us to an alternate equation of state (in place of the ideal gas law).

Phase Space

Gas particles have both position and momentum. In general, we need three coordinates to specify the position (x, y, z) and three more to specify the momentum (p_x , p_y , p_z) of a given particle. Together the three position coordinates and the three momentum coordinates comprise a 6-dimensional **phase space**.

Each coordinate has an uncertainty associated with it, meaning that we can localize a particle's position to within a box in position space that has dimensions $\Delta x \times \Delta y \times \Delta z$, and we can identify a particle's momentum to within a 'box' in momentum space that has dimensions $\Delta p_x \times \Delta p_y \times \Delta p_z$. The 6-dimensional volume of phase space (a **phase space cell**) occupied by the particle then has a volume ΔV given by the following:

Eq. 11.1 $$\Delta V = \Delta x \Delta y \Delta z \, \Delta p_x \Delta p_y \Delta p_z$$

Now although the six coordinates of phase space are independent of each other, their uncertainties are not. Each directional pair of position and momentum coordinates is linked by the **Heisenberg uncertainty principle**:

Eq. 11.2 $$\Delta x \, \Delta p_x \geq h \quad \Delta y \, \Delta p_y \geq h \quad \Delta z \Delta p_z \geq h$$ (or $\hbar$, $h/2$, etc.)

Combining these equations, we find a lower limit (ΔV_{min}) on the volume of a phase space cell:

Eq. 11.3 $$\Delta V = \Delta x \Delta y \Delta z \, \Delta p_x \Delta p_y \Delta p_z \geq h^3 = \Delta V_{min}$$

The minimum volume of a phase space cell is on the order of h^3, and no more than two electrons may occupy one cell, as they must have opposite spins due to the **Pauli exclusion principle** (see Chapter 3). The maximum number of electrons that can fit into a given volume of phase space (V) is then double the maximum number of cells: $2V/\Delta V_{min} = 2V/h^3$.

This places a limit on how closely packed electrons may be, whether they are in atomic bound states or existing as free particles in the gas; and this in turn places limits on the density of the gas. But because *phase* space is involved, there will also be limits on the electron *momenta*, rather than just their positions. And electron momenta depend on the temperature of the gas.

The amount of physical space available to the free electrons depends on the density of the gas while the amount of momentum space available to these electrons depends on the temperature of the gas. Degeneracy refers to the degree to which the available cells are filled: the greater proportion of cells that are filled, the greater will be the degeneracy of the gas. All gases are degenerate to some degree, but those with higher densities and/or lower temperatures will be more degenerate.

A 2-Dimensional Example

As a simple example of degeneracy, consider only the x-p_x pair of coordinates for a collection of 21 electron pairs. Suppose that the 2D phase space available to these electrons is represented by an x-p_x array; the available position space is 8 cells wide, as shown in Figure 11.1, while the momentum space is determined by the energy content of the gas.

In Figure 11.1a, the electron pairs are distributed throughout the cells in the array, showing no particular preference for position, but with a decreasing abundance of higher momentum cells, as we might find in an ideal gas. The average momentum of an electron is found to be 2.67.

Figure 11.1: 2-Dimensional degeneracy

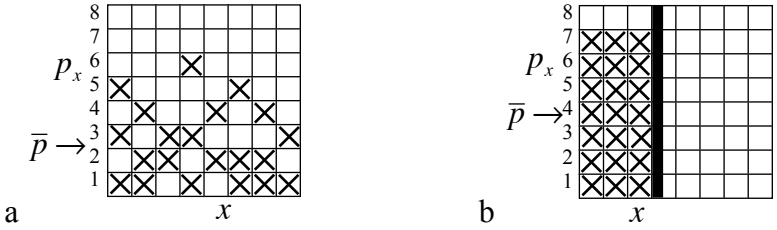

We then compress the gas, forcing the dimension of the available position space to reduce from 8 cells to 3. The electrons must still occupy cells – they cannot disappear – but with a smaller position space available to them, a greater fraction of the electrons *must* occupy higher momentum cells than they did before. By filling all the cells from the bottom momentum up, as in Figure 11.1b, we find that the average momentum is now 4.0. Increasing the density has caused the average electron momentum to increase, which in turn increases the electron pressure.

If the gas were to be further compressed, the position space cells would be reduced even more, and the electrons would be squeezed into still higher momentum states, where they would exert even greater pressure. This of course requires energy, which may or may not be supplied along with the attempted compression. That is, as a gas is compressed, it becomes more degenerate and exerts an increasingly higher pressure that counters the compression forces causing the degeneracy, possibly resulting in an equilibrium condition. The pressure of degeneracy thus can play a key role in the structure of a star – if the right conditions are met.

Ion Degeneracy

So far our discussion of degeneracy has involved only the electrons within a gas, but there will be ions present as well, and in comparable numbers. What can be said about ion degeneracy?

In a monatomic gas of temperature T the particles have an average kinetic energy given by $\overline{\frac{1}{2}m\mathrm{v}^2} = \frac{3}{2}kT$. As this relation applies to both ions and electrons, we may use it to link masses and velocities for these two types of particles. The average kinetic energy of an ion will be equal to the average kinetic energy of an electron:

Eq. 11.4 $$ {}^1\!/_2\, m_e \mathrm{v}_e^{\,2} = {}^1\!/_2\, m_i \mathrm{v}_i^{\,2} \quad \Rightarrow \quad \frac{\mathrm{v}_i}{\mathrm{v}_e} = \sqrt{\frac{m_e}{m_i}} $$

The x-momenta of the ion and electron are then related as follows:

Eq. 11.5 $$ \frac{p_{i_x}}{p_{e_x}} = \frac{m_i \mathrm{v}_{i_x}}{m_e \mathrm{v}_{e_x}} = \frac{m_i}{m_e}\sqrt{\frac{m_e}{m_i}} = \sqrt{\frac{m_i}{m_e}} $$

The ratio of the products of the momenta in all three directions is the cube of this value:

Eq. 11.6 $$ \frac{p_{i_x}}{p_{e_x}}\frac{p_{i_y}}{p_{e_y}}\frac{p_{i_z}}{p_{e_z}} = \left(\frac{m_i}{m_e}\right)^{3/2} \approx \left(1836A_i\right)^{3/2} $$ where A_i is the number of nucleons

This ratio – which represents the ratio of the momentum space of the ions relative to the electrons – is about 79,000 for hydrogen and 630,000 for helium. This means that at a given temperature and density, the ions have a *much* larger momentum space – and thus a much larger phase space – available to them than do the electrons. As the minimum size of the cells is fixed at h^3, the ions will have a much greater number of minimum cells available and thus will be far less degenerate than the electrons. Therefore we will consider only electron degeneracy.

Distribution Functions

Electrons are **fermions** – particles with half-integer spin – and they obey the Pauli exclusion principle: no two identical fermions may be in the same quantum mechanical state. Other examples of fermions include protons, neutrons, and positrons. The number of fermions in an energy state E' is given by the **Fermi-Dirac distribution law**:

Eq. 11.7 $$ N \approx \frac{1}{e^{E'/kT}+1} $$

Fermions are different from **bosons** – particles with integer spin – which do *not* obey the Pauli exclusion principle. Examples include photons, alpha particles, deuterons, etc. The number of bosons in an energy state E' is given by the **Bose-Einstein distribution law**:

Eq. 11.8 $$ N \approx \frac{1}{e^{E'/kT}-1} $$ (Note the resemblance to the Planck function.)

Both of these types of particles are indistinguishable; on the other hand, **distinguishable particles** – such as those found in an ideal gas – have a distribution given by the **Boltzmann equation**:

Eq. 11.9 $$N \approx \frac{1}{e^{E/kT} + 0} = e^{-E/kT}$$

The appropriate distribution function for electrons with momenta in the range $p \rightarrow p + dp$ is given by the following:

Eq. 11.10 $$N_e(p)dp = \frac{2}{h^3} 4\pi p^2 dp \, \mathcal{P}(p) \quad = \frac{8\pi}{h^3} p^2 dp \, \mathcal{P}(p)$$

Here $N_e(p)$ is the number density of electrons with momentum p, h^3 is the minimum cell volume, $4\pi p^2 dp$ is the volume of momentum space, 2 is for the spin, and $\mathcal{P}(p)$ is the **occupation index** for a fermi gas:

Eq. 11.11 $$\mathcal{P}(p) = \frac{1}{e^{\left(\alpha + E(p)/kT\right)} + 1}$$ Note that $E > 0$.

The parameter α – which has nothing to do with polytropes or alpha particles – will be determined later.

$\mathcal{P}(p)$ has a maximum value of 1; this is attained as the exponential term approaches zero – which reflects the Pauli exclusion principle. When $\mathcal{P}(p) = 1$, all available electron states are occupied, from $p = 0$ to $p = p_o$ (the **Fermi momentum**). The electrons are then at maximum density $N_e(p_o)_{max}$, given by the following:

Eq. 11.12 $$N_e(p_o)_{\max} = \frac{8\pi}{h^3} p_o^2$$

If more electrons are added to the volume, they must occupy higher momentum states, at $p > p_o$ because all of the lower states are filled. These higher momentum states will make a large contribution to the electron pressure. Addition of electrons to the volume (by compression) requires creation of higher momentum states to contain these electrons. But because these states will need energy in order to form, the degenerate electron gas must *absorb* energy in order to contract. If no such energy source is available, the contraction cannot occur.

The Degeneracy Parameter α

We now investigate the role played by the parameter α. (Note that the degeneracy parameter α is used in Clayton (1968), but both Novotny (1973) and Kippenhahn & Weigert (1990) use ψ (= – α) instead.) Its value is determined from normalization considerations, which require the following condition:

Eq. 11.13 $$N_e = \int_0^\infty N_e(p)dp = N_e(\alpha, T)$$

If α is large and positive, then $\mathcal{P}(p) << 1$ for all values of E, and $\mathcal{P}(p) \rightarrow e^{-E'/kT}$; that is, the electron distribution function resembles a Maxwellian distribution. This is the non-degenerate case.

As N_e increases at constant temperature, $\mathcal{P}(p)$ increases, which means that $e^{(\alpha+E)/kT}$ decreases; this in turn implies that α decreases, becoming negative. As α becomes large and negative ($\alpha \rightarrow -\infty$), the occupation index is modified as follows:

Eq. 11.14 $$\mathcal{P}(p) = \frac{1}{e^{(\alpha + E/kT)} + 1} \rightarrow \frac{1}{e^{-|\alpha|} e^{E/kT} + 1}$$

The occupation index then depends on how the energy (E) of the electron relates to this large, negative value of α:

If $\frac{E}{kT} < |\alpha|$, then $\mathcal{P}(p) \rightarrow \frac{1}{0+1} = 1.$

If $\frac{E}{kT} > |\alpha|$, then $\mathcal{P}(p) \rightarrow \frac{1}{\infty+1} = 0.$

This implies that at lower energies, the phase space cells will be filled to their maximum capacity with electrons, while at higher energies, the cells will be empty. The boundary between these two energy regions comes at $|\alpha| = E_f / kT$, where $E_f = E(p_o)$ is the **Fermi energy**, and p_o is known as the **Fermi momentum**. A plot of the occupation index for this situation is shown in Figure 11.2.

Figure 11.2: Occupation index for large, negative α

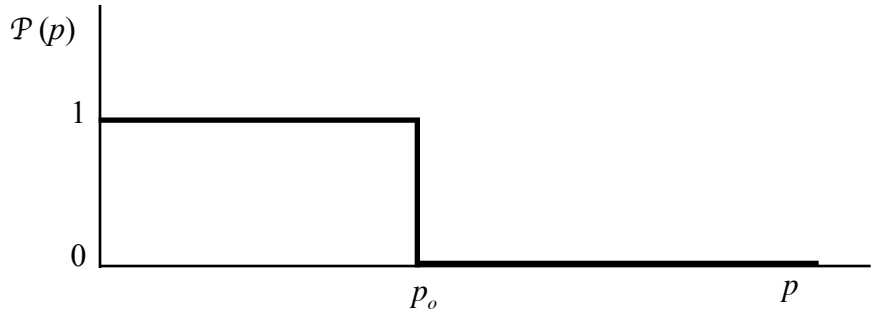

Complete Degeneracy

We have seen that $\alpha \rightarrow +\infty$ results in a Maxwellian distribution function – the case of **non-degenerate** matter. We now find that as $\alpha \rightarrow -\infty$, the electrons completely fill the available cells up to a point (the Fermi momentum), beyond which the cells are empty. This is the case of **complete degeneracy**, for which the occupation index is a step function.

In reality, complete degeneracy never occurs for finite temperatures, but it may come close. As the density of a gas increases, the electrons become more degenerate and the occupation index approaches a step function. In general, if $E(p_o) >> kT$, we may use complete degeneracy as a good approximation.

In the case of complete degeneracy, the electron distribution function depends on the momentum in a simple way. For $p < p_o$, $N_e(p)dp = \frac{8\pi}{h^3} p^2 dp$, and for $p > p_o$, $N_e(p)dp = 0$. Thus the distribution function will be parabolic up to the Fermi momentum; beyond this it will drop to zero, as shown in Figure 11.3, where the shaded region marks the filled momentum cells.

Figure 11.3: Distribution function for complete degeneracy

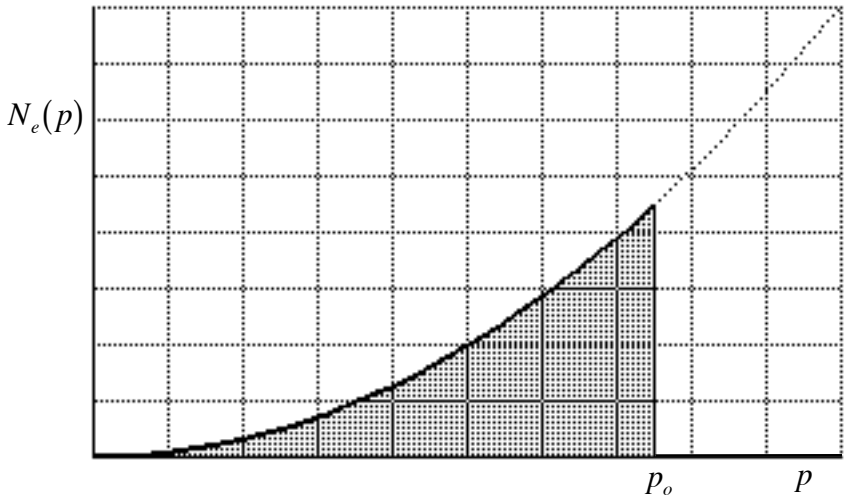

The value of the Fermi momentum depends solely on the electron density; the more closely packed the electrons are, the more high-momentum cells that will be filled, and the higher the Fermi momentum will be. The completely degenerate electron gas is a minimum kinetic energy configuration in which electrons are assigned to the lowest possible energy states. We can obtain the electron density by integrating the distribution function from $p = 0$ up to the Fermi momentum:

Eq. 11.15 $$N_e = \int_0^{p_o} N_e(p)dp = \int_0^{p_o} \frac{8\pi}{h^3} p^2 dp = \frac{8\pi}{3h^3} p_o^3 \quad \Rightarrow \quad p_o = \left(\frac{3h^3}{8\pi} N_e \right)^{1/3}$$

We may then find the partial pressure of the degenerate electrons as we did before:

Eq. 8.12 $$P_e = \tfrac{1}{3} \int_0^{\infty} N(\mathrm{v})\, p \mathrm{v}\, d\mathrm{v} = \tfrac{1}{3} \int_0^{\infty} N(p)\, p \mathrm{v}\, dp$$

Assuming the electrons are non-relativistic, we may substitute v = *p/m* and perform the integral:

Eq. 11.16 $$P_e = \tfrac{1}{3} \int_0^{\infty} N(p) \frac{p^2}{m} dp = \tfrac{1}{3} \int_0^{p_o} \left(\frac{8\pi}{h^3} p^2 \right) \frac{p^2}{m} dp$$

Eq. 11.17 $$P_e = \frac{8\pi}{3h^3 m} \int_0^{p_o} p^4\, dp = \frac{8}{15} \frac{\pi}{h^3 m} p_o^5 = P_{e,nr} \qquad \text{(non-relativistic)}$$

We may then replace the Fermi momentum with the electron density:

Eq. 11.18 $$P_{e,nr} = \frac{8}{15}\frac{\pi}{h^3 m}\left(\frac{3h^3}{8\pi}N_e\right)^{5/3} = \frac{h^2}{20m}\left(\frac{3}{\pi}\right)^{2/3} N_e^{5/3}$$

Recall the ideal gas law for the electron pressure ($P_e = N_e kT$), and note that there is no temperature in this equation (11.18) for the degenerate electron pressure!

We may continue to evolve this expression by substituting $N_e = \rho N_A / \mu_e$ (see Equation 9.14):

Eq. 11.19 $$P_{e,nr} = \frac{h^2}{20m_e}\left(\frac{3}{\pi}\right)^{2/3} N_A^{5/3}\left(\frac{\rho}{\mu_e}\right)^{5/3}$$

Inserting numerical values for the constants, we find the following:

Eq. 11.20 $$P_{e,nr} = 1.00360\times10^{13}\left(\frac{\rho}{\mu_e}\right)^{5/3} \approx 3.15771\times10^{12}\,\rho^{5/3}$$

Here we have used $\mu_e = 2.0013$ for the **mean molecular weight per electron** of a gas of pure ionized helium.

Now for a non-degenerate gas, the ideal gas law applies, for which $P \approx \rho^1$. But as the density increases, degenerate electron pressure increases to the point where it becomes much greater than the ion pressure. When the degenerate electrons dominate the gas pressure, we find the pressure equation will have changed:

Eq. 11.21 $$P \rightarrow P_{e,nr} \approx \rho^{5/3}$$ (a familiar-looking form)

Under what conditions will this occur? For what combinations of density and temperature will completely degenerate electron pressure exceed the calculated non-degenerate electron pressure?

Eq. 11.22 $$\frac{\rho\Re T}{\mu_e} < \frac{h^2}{20m_e}\left(\frac{3}{\pi}\right)^{2/3} N_A^{5/3}\left(\frac{\rho}{\mu_e}\right)^{5/3}$$

Inserting constants and solving, we find the following condition for the approximate onset of degeneracy:

Eq. 11.23 $$\frac{\rho}{\mu_e} > 23.8459\left(T_6\right)^{3/2} \simeq 24\left(T_6\right)^{3/2}$$

We may test this result using different stellar models. For the center of the Sun, we have $\rho/\mu_e \approx 100$ and $T_6 \approx 10$, giving $24(T_6)^{3/2} \approx 760$. As $100 < 760$, the Sun's core would appear to be not very degenerate. On the other hand, a typical white dwarf has $\rho/\mu_e \approx 10^6$ and $T_6 \approx 1$, making $24(T_6)^{3/2} \approx 24$. As 10^6 is considerably greater than 24, we can expect white dwarfs to be quite degenerate.

There is no sharp dividing line between degeneracy and non-degeneracy; the transition is gradual. Strictly speaking, complete degeneracy occurs only for $T = 0$, and non-degeneracy occurs only for infinite temperature. Objects in the real world exist somewhere in between these two extremes, and for this reason we should also consider partial degeneracy.

Partial Degeneracy

In the case of **partial degeneracy**, we cannot assume an extreme value for α that would simplify the electron distribution function. Instead we must use the full distribution function in our calculations:

Eq. 11.24 $$N_e(p)dp = \frac{2}{h^3}\frac{4\pi p^2 dp}{e^{(\alpha+E/kT)}+1} = \frac{8\pi}{h^3}\frac{p^2 dp}{e^{(\alpha+E/kT)}+1}$$

The electron density is found by integrating, and the pressure integral is found by inserting this distribution function into Equation 8.12:

Eq. 11.25 $$N_e = \int_0^\infty N_e(p)dp = \frac{8\pi}{h^3}\int_0^\infty \frac{p^2 dp}{e^{(\alpha+E/kT)}+1}$$

Eq. 11.26 $$P_e = \tfrac{1}{3}\int_0^\infty N_e(p)p\mathrm{v}\,dp = \frac{8\pi}{3h^3}\int_0^\infty \frac{p^3 \mathrm{v} dp}{e^{(\alpha+E/kT)}+1}$$

Before integrating, we must substitute expressions for the electron's energy E and speed v. For temperatures below one billion K, degeneracy occurs at non-relativistic electron speeds, and we may use non-relativistic expressions: $\mathrm{v} = p/m$ and $E = p^2/2m$. This yields the following:

Eq. 11.27 $$N_e = \frac{8\pi}{h^3}\int_0^\infty \frac{p^2 dp}{e^{\left(\alpha+p^2/2mkT\right)}+1}$$

Eq. 11.28 $$P_e = \frac{8\pi}{3h^3 m}\int_0^\infty \frac{p^4 dp}{e^{\left(\alpha+p^2/2mkT\right)}+1}$$

We now let $u \equiv p^2/2mkT \;\Rightarrow p = \sqrt{2mkTu} \;\Rightarrow\; dp = \frac{1}{2}\frac{2mkT}{\sqrt{2mkTu}}du$. These substitutions produce the following set of equations, which constitute an equation of state parameterized by the degeneracy parameter α:

Eq. 11.29 $$N_e = \frac{4\pi}{h^3}(2mkT)^{3/2}\int_0^\infty \frac{u^{1/2}du}{e^{(\alpha+u)}+1}$$

Eq. 11.30 $$P_e = \frac{8\pi kT}{3h^3}(2mkT)^{3/2}\int_0^\infty \frac{u^{3/2}du}{e^{(\alpha+u)}+1}$$

These equations are not integrable; therefore we will define the **Fermi-Dirac functions**:

Eq. 11.31 $$F_{1/2}(\alpha) \equiv \int_0^\infty \frac{u^{1/2}du}{e^{(\alpha+u)}+1}$$

Eq. 11.32 $$F_{3/2}(\alpha) \equiv \int_0^\infty \frac{u^{3/2} du}{e^{(\alpha+u)}+1}$$

These are tabulated in Clayton (1968) for different values of α. The electron density and pressure in the case of **non-relativistic, partial degeneracy** can then be found from these functions:

Eq. 11.33 $$N_e = \frac{4\pi}{h^3}(2mkT)^{3/2} F_{1/2}(\alpha)$$

Eq. 11.34 $$P_e = \frac{8\pi kT}{3h^3}(2mkT)^{3/2} F_{3/2}(\alpha)$$

We may modify the electron density equation by inserting the relation $N_e = \rho N_A / \mu_e$ and solving for $F_{1/2}(\alpha)$:

Eq. 11.35 $$N_e = \frac{\rho N_A}{\mu_e} = \frac{4\pi}{h^3}(2mkT)^{3/2} F_{1/2}(\alpha)$$

Eq. 11.36 $$F_{1/2}(\alpha) = \frac{\rho}{\mu_e}\frac{h^3 N_A}{4\pi}(2mkT)^{-3/2} = 1.1051087 \times 10^8 \frac{\rho}{\mu_e} T^{-3/2}$$

In calculating the pressure exerted by a non-relativistic, partially degenerate gas at a given density and temperature, we first use Equation 11.36 to determine $F_{1/2}(\alpha)$. We then use this value to find α from the tables; the tables also give the corresponding value of $F_{3/2}(\alpha)$, from which the electron pressure is calculated using Equation 11.34.

Figure 11.4: Distribution function for partial degeneracy

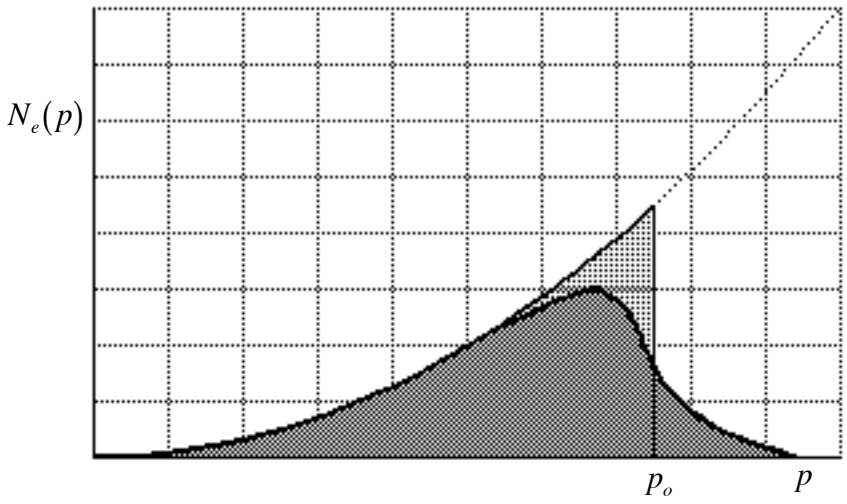

Figure 11.4 shows the momentum distribution function for a partially degenerate gas (the darker shaded region) superimposed on the distribution function for a completely degenerate gas (the lighter shaded region) from Figure 11.3. The areas under the curve in each graph – representing the electron density N_e – are the same.

If we take the ratio of electron pressure to electron density, we find the following:

Eq. 11.37 $$\frac{P_e}{N_e} = \frac{2kT}{3}\frac{F_{3/2}}{F_{1/2}} \quad \Rightarrow \quad P_e = N_e kT\left(\frac{2}{3}\frac{F_{3/2}}{F_{1/2}}\right) = \frac{\rho\Re T}{\mu_e}\left(\frac{2}{3}\frac{F_{3/2}}{F_{1/2}}\right)$$

Note the similarity of this last expression to the ideal gas law. The factor $^2/_3\,[F_{3/2}(\alpha)/F_{1/2}(\alpha)]$ is the extent to which the degenerate electron pressure differs from that of a non-degenerate gas. This factor increases without limit from 1 (for an ideal gas). The *total* gas pressure includes the ion pressure, which remains ideal as the electrons become degenerate.

Eq. 11.38 $$P_g = P_i + P_e = \frac{\rho\Re T}{\mu_i} + \frac{\rho\Re T}{\mu_e}\left(\frac{2}{3}\frac{F_{3/2}}{F_{1/2}}\right) \;=\; \rho\Re T\left[\frac{1}{\mu_i} + \frac{1}{\mu_e}\left(\frac{2}{3}\frac{F_{3/2}}{F_{1/2}}\right)\right]$$

(Here μ_e and μ_i are the mean molecular weights per electron and per *ion*, respectively.)

As an example of a partial degeneracy calculation, let us determine the electron pressure in a gas of completely ionized helium at a density of 350,000 g/cc and a temperature of 80 million K. We begin by finding the value of $F_{1/2}(\alpha)$ for these conditions:

Eq. 11.39 $$F_{1/2}(\alpha) = 1.10511\times10^8\,\frac{\rho}{\mu_e}T^{-3/2} = 1.10511\times10^8\,\frac{(350000)}{2}(80e6)^{-3/2} = 27.02764$$

In the degeneracy tables in Clayton (1968), this result is found between the α values of –11.7 and –11.8. We then interpolate to find α, and interpolate again to find the corresponding value of $^2/_3\,F_{3/2}(\alpha)$, as shown in Table 11.1:

Table 11.1: Interpolation of Fermi-Dirac functions

$F_{1/2}(\alpha)$	α	$^2/_3\,F_{3/2}(\alpha)$
26.92220	–11.7	130.47720
27.02764 $\Rightarrow$	***–11.73085*** $\Rightarrow$	***131.31315***
27.26393	–11.8	133.18650

The electron pressure can then be calculated using Equation 11.37:

Eq. 11.40 $$P_e = \frac{\rho\Re T}{\mu_e}\left(\frac{2}{3}\frac{F_{3/2}}{F_{1/2}}\right) = \frac{(350000)(8.314e7)(80e6)}{2}\frac{131.31315}{27.02764} = 5.655\times10^{21}$$

We may compare this with the pressure exerted by the nuclei (ions):

Eq. 11.41 $$P_i = \frac{\rho\Re T}{\mu_i} = \frac{(350000)(8.314e7)(80e6)}{4} = 5.820\times10^{20}$$

Thus, the degenerate electrons, which outnumber the nuclei by a factor of 2, exert nearly 10 times the pressure; the additional factor of 5 is due to degeneracy.

Relativistic Degeneracy

Suppose that the electron density is so high in a completely degenerate electron gas that the highest momentum states are relativistic. In this case, we must rework our equations because some of the relations we used are no longer valid. In particular, $p = m\text{v}$ is true only if we use the relativistic mass m, rather than the rest mass m_o, where $m = \gamma m_o = m_o \big/ \sqrt{1-\beta^2}$ and $\beta \equiv \text{v}/c$. Then the momentum is as follows:

Eq. 11.42 $$p = m\text{v} = mc^2 \cdot \frac{\text{v}}{c^2} = \frac{E\text{v}}{c^2} \qquad \text{where } E = mc^2 = \gamma m_o c^2 = \gamma E_o$$

Note: Previously, we have sometimes been using m to indicate the electron mass m_e; be very careful in using the *relativistic* equations because m now has a different meaning.

To estimate the borderline between relativistic and non-relativistic conditions, we set $\text{v} \approx c$ and $E \approx 2E_o = 2m_o c^2 \approx 1$ MeV (where $m_o = m_e = 0.511$ MeV/c^2). The Fermi momentum ($p_o = E\text{v}/c^2 \approx 2E_o c/c^2 = 2m_o c^2/c = 2m_e c$) can then be related to the density:

Eq. 11.43 $$p_o = \left(\frac{3h^3}{8\pi} N_e \right)^{1/3} = \left(\frac{3h^3}{8\pi} \frac{N_A \rho}{\mu_e} \right)^{1/3} = 2m_e c$$

Eq. 11.44 $$\frac{\rho}{\mu_e} = \left(2m_e c\right)^3 \frac{8\pi}{3h^3 N_A} = 7.744769 \times 10^6 \text{ g/cc}$$

For $\mu_e \approx 2$, $\rho > \approx 1.5 \times 10^7$ g/cc will be relativistic.

Relativistic, Complete Degeneracy

We will now find an expression for the pressure exerted by a completely degenerate gas of relativistic electrons. We will begin by writing the relativistic speed in terms of the relativistic momentum:

Eq. 11.45 $$p = m\text{v} = \frac{m_o \text{v}}{\sqrt{1-\left(\text{v}/c\right)^2}} \quad \Rightarrow \quad p^2 \left(1 - \frac{\text{v}^2}{c^2}\right) = m_o^2 \text{v}^2 \quad \Rightarrow \quad p^2 = \text{v}^2 \left(m_o^2 + \frac{p^2}{c^2} \right)$$

Eq. 11.46 $$\text{v} = \frac{p}{\sqrt{m_o^2 + \dfrac{p^2}{c^2}}} = \frac{p/m_o}{\sqrt{1 + \left(\dfrac{p}{m_o c}\right)^2}}$$

This is inserted into the pressure integral, along with our expression for the distribution function for complete degeneracy $N_e(p) = 8\pi p^2/h^3$:

Eq. 11.47 $$P_e = \tfrac{1}{3}\int_0^\infty N_e(p)\,p\mathrm{v}\,dp = \frac{8\pi}{3m_e h^3}\int_0^\infty \frac{p^4 dp}{\sqrt{1+\left(p/m_e c\right)^2}}$$

We now make a substitution, letting $p = m_e c \sinh\theta$ and $dp = m_e c \cosh\theta\, d\theta$, and recalling the identity $1 + \sinh^2\theta = \cosh^2\theta$:

Eq. 11.48 $$P_e = \frac{8\pi}{3m_e h^3}\int_0^\infty \frac{\left(m_e c\sinh\theta\right)^4 m_e c\cosh\theta\, d\theta}{\sqrt{1+\sinh^2\theta}} = \frac{8\pi m_e^4 c^5}{3h^3}\int_0^{\theta_o}\sinh^4\theta\, d\theta$$

The upper limit corresponds to the Fermi momentum: $\sinh\theta_o = p_o/m_e c \equiv x$. The integral can be found, and this leads to the general solution for the pressure.

Eq. 11.49 $$\int_0^{\theta_o}\sinh^4\theta\, d\theta = \frac{\sinh^3\theta_o}{4} - \frac{3\sinh 2\theta_o}{16} + \frac{3\theta_o}{8}$$

Eq. 11.50 $$P_e = \frac{\pi m_e^4 c^5}{3h^3}\left[2\sinh^3\theta_o - \tfrac{3}{2}\sinh 2\theta_o + 3\theta_o\right] = \frac{\pi m_e^4 c^5}{3h^3} f(x) = 5.94251\times 10^{22} f(x)$$

where

Eq. 11.51 $$f(x) = x\left(2x^2 - 3\right)\sqrt{x^2+1} + 3\sinh^{-1}x$$ and

Eq. 11.52 $$x \equiv \frac{p_o}{m_e c} = \frac{h}{2m_e c}\left(\frac{3N_e}{\pi}\right)^{1/3} = 1.197044\times 10^{-10} N_e^{1/3} = 1.010867\times 10^{-2}\left(\frac{\rho}{\mu_e}\right)^{1/3}$$

From this it can be shown that in the limit of a ***non-relativistic*, completely degenerate gas** (meaning $x \to 0$), the electron pressure is as previously derived:

Eq. 11.19 $$P_{e,nr} = \frac{h^2}{20m_e}\left(\frac{3}{\pi}\right)^{2/3} N_A^{5/3}\left(\frac{\rho}{\mu_e}\right)^{5/3} = 1.00360\times 10^{13}\left(\frac{\rho}{\mu_e}\right)^{5/3}$$

This is a polytrope with $\gamma = {}^5/_3 \Rightarrow n = 1.5$.

In the limit of a ***highly relativistic*, completely degenerate gas** (meaning $x \to \infty$), we find a different expression:

Eq. 11.53 $$P_{e,rel} = \frac{hc}{8}\left(\frac{3}{\pi}\right)^{1/3} N_A^{4/3}\left(\frac{\rho}{\mu_e}\right)^{4/3} = 1.24101\times 10^{15}\left(\frac{\rho}{\mu_e}\right)^{4/3}$$

This is a polytrope with $\gamma = {}^4/_3 \Rightarrow n = 3$.

Relativistic, Partial Degeneracy

For a **highly relativistic, partially degenerate gas** we again use the occupation index to find suitable expressions for the density and pressure. We begin with the distribution function from before:

Eq. 1154 $$N_e(p)dp = \frac{8\pi}{h^3} p^2 dp\, \mathcal{P}(p) = \frac{8\pi}{h^3} \frac{p^2 dp}{e^{(\alpha + E(p)/kT)} + 1}$$

We then insert this function into the integrals for the electron density and electron pressure:

Eq. 11.55 $$N_e = \int_0^\infty N_e(p)dp = \frac{8\pi}{h^3} \int_0^\infty \frac{p^2 dp}{e^{(\alpha + E(p)/kT)} + 1}$$

Eq. 11.56 $$P_e = \tfrac{1}{3} \int_0^\infty N_e(p)\, p\mathrm{v}\, dp = \frac{8\pi}{3h^3} \int_0^\infty \frac{p^3 \mathrm{v} dp}{e^{(\alpha + E(p)/kT)} + 1}$$

We must now insert an expression for the energy as a function of momentum. In the relativistic case, we have $p = \mathrm{v}E/c^2$ and $\mathrm{v} \rightarrow c$; combining these we have $E \approx pc$:

Eq. 11.57 $$N_e = \frac{8\pi}{h^3} \int_0^\infty \frac{p^2 dp}{e^{(\alpha + pc/kT)} + 1}$$

Eq. 11.58 $$P_e = \frac{8\pi}{3h^3} \int_0^\infty \frac{p^3 c dp}{e^{(\alpha + pc/kT)} + 1}$$

If we now define $u \equiv pc/kT$, then $p = ukT/c$ and $dp = (kT/c)du$. Making these substitutions, we arrive at more Fermi-Dirac functions:

Eq. 11.59 $$N_e = \frac{8\pi}{h^3} \left(\frac{kT}{c}\right)^3 \int_0^\infty \frac{u^2 du}{e^{(\alpha+u)} + 1} = \frac{8\pi}{h^3 c^3} (kT)^3 F_2(\alpha), \quad \text{where } F_2(\alpha) \equiv \int_0^\infty \frac{u^2 du}{e^{(\alpha+u)} + 1}$$

Eq. 11.60 $$P_e = \frac{8\pi c}{3h^3} \left(\frac{kT}{c}\right)^4 \int_0^\infty \frac{u^3 du}{e^{(\alpha+u)} + 1} = \frac{8\pi}{3h^3 c^3} (kT)^4 F_3(\alpha), \quad \text{where } F_3(\alpha) \equiv \int_0^\infty \frac{u^3 du}{e^{(\alpha+u)} + 1}$$

These Fermi-Dirac functions are tabulated in Kippenhahn & Weigert (1990).

For such a **highly relativistic, partially degenerate gas**, we find an expression similar to Equation 11.37 (which applied to a *non-relativistic*, partially degenerate gas):

Eq. 11.61 $$P_e = N_e kT \left[\frac{1}{3} \frac{F_3(\alpha)}{F_2(\alpha)}\right] = \frac{\rho \Re T}{\mu_e} \left[\frac{1}{3} \frac{F_3(\alpha)}{F_2(\alpha)}\right]$$

Fermi-Dirac Functions

We close this chapter with a few approximations of the Fermi-Dirac functions.

The general form is given as follows, in terms of both α and ψ ($= -\alpha$):

Eq. 11.62 $$F_n(\alpha) \equiv \int_0^\infty \frac{u^n du}{e^{(\alpha+u)} + 1} \quad \text{or} \quad F_n(\psi) \equiv \int_0^\infty \frac{u^n du}{e^{(u-\psi)} + 1}$$

Strong degeneracy is indicated by $\alpha \rightarrow -\infty$ or $\psi \rightarrow +\infty$.

Weak degeneracy is indicated by $\alpha \rightarrow +\infty$ or $\psi \rightarrow -\infty$.

Kippenhahn & Weigert (1990) present the following expansion for the case of **strong degeneracy**:

Eq. 11.63 $$F_n(\psi) = \frac{\psi^{n+1}}{n+1}\left\{1 + 2\left[C_2(n+1)n\psi^{-2} + C_4(n+1)n(n-1)(n-2)\psi^{-4} + ...\right]\right\}$$

The coefficients are $C_2 = \pi^2/12$ and $C_4 = 7\pi^4/720$. The strong degeneracy approximations for $F_{1/2}(\psi)$ and $F_{3/2}(\psi)$ are then as follows:

Eq. 11.64 $$F_{1/2}(\psi) = \frac{\psi^{3/2}}{3/2}\left\{1 + 2\left[\frac{\pi^2}{12}\left(\frac{3}{2}\right)\frac{1}{2}\psi^{-2} + \frac{7\pi^4}{720}\left(\frac{3}{2}\right)\frac{1}{2}\left(\frac{-1}{2}\right)\left(\frac{-3}{2}\right)\psi^{-4} + ...\right]\right\}$$

Eq. 11.65 $$F_{1/2}(\psi) = \frac{2}{3}\psi^{3/2}\left\{1 + \frac{\pi^2}{8}\psi^{-2} + \frac{7\pi^4}{960}\psi^{-4} + ...\right\} \approx \frac{2}{3}\psi^{3/2}$$

Eq. 11.66 $$F_{3/2}(\psi) = \frac{\psi^{5/2}}{5/2}\left\{1 + 2\left[\frac{\pi^2}{12}\left(\frac{5}{2}\right)\frac{3}{2}\psi^{-2} + \frac{7\pi^4}{720}\left(\frac{5}{2}\right)\frac{3}{2}\left(\frac{1}{2}\right)\left(\frac{-1}{2}\right)\psi^{-4} + ...\right]\right\}$$

Eq. 11.67 $$F_{3/2}(\psi) = \frac{2}{5}\psi^{5/2}\left\{1 + \frac{5\pi^2}{8}\psi^{-2} - \frac{7\pi^4}{384}\psi^{-4} + ...\right\} \approx \frac{2}{5}\psi^{5/2}$$

In the case of **weak degeneracy**, Equation 11.62 can be modified because the argument of the exponent will always be a large, positive number, making the exponential much greater than 1:

Eq. 11.68 $$F_n(\alpha) \equiv \int_0^\infty \frac{u^n du}{e^{(\alpha+u)}+1} = \int_0^\infty \frac{u^n du}{e^\alpha e^u + 1} \xrightarrow{\alpha \to \infty} \int_0^\infty \frac{u^n du}{e^\alpha e^u} = e^{-\alpha}\int_0^\infty u^n e^{-u} du$$

The integral is a gamma function:

Eq. 11.69 $$F_n(\alpha) \approx \Gamma(n+1)e^{-\alpha} = n\,\Gamma(n)\,e^{-\alpha}$$

This leads directly to approximations for $F_{1/2}(\alpha)$ and $F_{3/2}(\alpha)$ (in the case of weak degeneracy):

Eq. 11.70 $$F_{1/2}(\alpha) \approx \tfrac{1}{2}\Gamma(1/2)e^{-\alpha} = \tfrac{1}{2}\sqrt{\pi}e^{-\alpha}$$

Eq. 11.71 $$F_{3/2}(\alpha) \approx \tfrac{3}{2}\Gamma(3/2)e^{-\alpha} = \tfrac{3}{2}\left[\tfrac{1}{2}\Gamma(1/2)\right]e^{-\alpha} = \tfrac{3}{4}\sqrt{\pi}e^{-\alpha}$$

We may illustrate the reliability of these approximations by computing the Fermi-Dirac functions at each extreme and comparing with tabulated values. For **strong degeneracy**, we choose the *most degenerate* condition listed in Clayton's (1968) Table 2-3. We then use Equations 11.65 and 11.67 to approximate the Fermi-Dirac functions for this same α, as shown in Table 11.2:

Table 11.2: Comparison of strong degeneracy approximations with tabulated values

		$F_{1/2}(\alpha)$	$^2/_3\,F_{3/2}(\alpha)$
Clayton (1968)	$\alpha = -15.9$	42.47429	275.37153
Approximations	$\Rightarrow\ ^2/_3\,(-\alpha)^{3/2}$	=42.26729	$\Rightarrow\ ^2/_3[^2/_5(-\alpha)^{5/2}]$ =268.81998

Although not perfect matches, these approximate values are certainly in the ballpark.

We now repeat the process for the case of **weak degeneracy**, using the *least degenerate* condition in Clayton's (1968) Table 2-3 and Equations 11.70 and 11.71:

Table 11.3: Comparison of weak degeneracy approximations with tabulated values

		$F_{1/2}(\alpha)$	$^2/_3\, F_{3/2}(\alpha)$
Clayton (1968)	$\alpha = 4.0$	0.016128	0.016179
Approximations	$\Rightarrow \quad \frac{1}{2}\sqrt{\pi}e^{-\alpha} = 0.016232$		$\Rightarrow \quad \frac{2}{3}\left(\frac{3}{4}\sqrt{\pi}e^{-\alpha}\right) = 0.016232$

These values are identical, as the approximations for the two functions differ only by a factor of $^2/_3$. Again, the approximations provide values that are comparable to the tabulated quantities.

In the last few chapters of the book, we will be examining the evolution of stars, all the while keeping our eyes open for situations in which degeneracy might flourish. The general role played by degeneracy is to increase the pressure exerted by a gas undergoing compression – over and above the pressure predicted by the ideal gas law. Degeneracy will become significant where the gas density becomes extremely high, a condition met frequently in the realm of giant gas spheres constrained by gravitational forces.

CHAPTER 12: Stellar Synthesis

In previous chapters we examined some of the physical laws that govern the structure of stars, in hopes of building numerical stellar models that will help us understand the life cycles of stars. It is now time to apply our results to stellar evolution, to determine whether we can explain the various pathways this process can take. We begin by considering the stages in which stars are synthesized into stable, self-luminous spheres.

Star Formation

The details of star formation are not particularly well understood as yet, but it is generally believed that stars are created from clouds of interstellar gas and dust. Young stars are often found in association with such regions. Compositions of the various stellar populations can be explained in terms of the recycling of heavy elements from massive stars, through supernovae, to the interstellar medium, and back into stars. Gas and dust clouds provide concentrations of interstellar matter that appear to be logical starting points for the gravitational forces that assemble atoms into stars.

But the process of manufacturing stars is not exactly straightforward. Random thermal motions in the interstellar cloud make it difficult for gravity to force the matter to converge on any particular point. Unless these thermal motions can be reduced (by keeping the temperature low) or gravity can be enhanced (by increasing the density), the gas will remain in equilibrium and star formation will not proceed.

Further problems arise due to the immense cloud sizes involved. Transforming *clouds* with radii measured in *parsecs* into *stars* with radii measured in *solar radii* requires a radial reduction of approximately 7 orders of magnitude, which implies a spin rate increase of 14 orders of magnitude or more, if angular momentum is indeed conserved. This means that an initial rotation period on the order of the Galactic rotation period (200 million years or so) would translate into a stellar rotation period measured in seconds – which is physically impossible for normal stars to achieve. Magnetic fields may provide a solution by transferring angular momentum from the forming star to its surrounding nebula, but including such fields in our calculations is not a trivial matter. For now we will bypass these difficulties and examine a few basic principles in hopes of gaining some insight into the process of star formation.

The Jeans Criterion

For an interstellar cloud in equilibrium – neither expanding nor contracting – we should expect that the magnitudes of the kinetic and potential energies will be equal: $KE = |PE|$. We can write an appropriate expression for each, in terms of the cloud mass (M), radius (R) and temperature (T):

Eq. 12.1 $$PE = -\frac{GM}{R}\left(\frac{\text{ergs}}{\text{g}}\right)$$

Eq. 12.2 $$KE = \tfrac{1}{2}mv^2 = \tfrac{3}{2}kT\left(\frac{\text{ergs}}{\text{part}}\right) = \tfrac{3}{2}\Re T\left(\frac{\text{ergs}}{\text{mole}}\right) = \frac{3}{2}\frac{\Re T}{\mu}\left(\frac{\text{ergs}}{\text{g}}\right)$$

Equating these expressions gives us an equilibrium condition:

Eq. 12.3 $$\frac{3}{2}\frac{\Re T}{\mu} = \frac{GM}{R}$$

We may eliminate the mass by writing it in terms of the cloud density ($M = {}^4/_3\,\pi R^3\rho$) and substituting into the above expression:

Eq. 12.4 $$\frac{3}{2}\frac{\Re T}{\mu} = \frac{4}{3}\pi R^2 G\rho$$

This represents an equilibrium condition, for which the kinetic and potential energy terms are in balance. In order for the cloud to collapse, the potential term (on the right) must become dominant over the kinetic term (on the left); this can be achieved by reducing the temperature, increasing the density, and/or increasing the radius of the cloud. Solving this expression for the radius, we find the size of the cloud at equilibrium:

Eq. 12.5 $$R = \sqrt{\frac{9}{8\pi}\frac{\Re T}{\mu G\rho}}$$

For a cloud of a given density and temperature, R indicates the maximum size the cloud may have and still be stable against collapse. Sir James Jeans performed a similar analysis using a 'cloud' surrounded by interstellar gas, rather than isolated as we have presumed. His result is known as the **Jeans length** or the **Jeans criterion**:

Eq. 12.6 $$R_J = \sqrt{\frac{\pi\Re T}{\mu G\rho}}$$

We can evaluate this radius, using several different units for convenience:

Eq. 12.7
$$R_J = \sqrt{\frac{\pi(8.314e7)T}{\mu(6.674e-8)\rho}} = 6.26e7\sqrt{\frac{T}{\mu\rho}}\,(\text{cm})$$
$$= 4.18e-6\sqrt{\frac{T}{\mu\rho}}\,(\text{AU}) \qquad = 2.03e-11\sqrt{\frac{T}{\mu\rho}}\,(\text{pc})$$

The value of μ to be used depends on the type of cloud being considered. For a diffuse interstellar cloud, the hydrogen is primarily atomic (H I), giving a mean molecular weight of about 1; in a molecular cloud, the hydrogen is molecular (H_2) and $\mu \approx 2$. If we assume each cloud also contains 25% helium by mass, these values become $^{16}/_{13} \approx 1.23$ and $^{16}/_{7} \approx 2.29$, respectively.

The Jeans criterion gives an upper limit on the radius of a stable cloud; if a cloud of density ρ has a radius greater than R_J, the cloud will be bound and collapse will occur. Using this criterion, a cloud with a mean molecular weight of 2.3, a density of 1e–22 (or about 26 particles/cc), and a temperature of 10 K, would have a Jeans length of about 4.2 pc, with a mass of 470 $M_\odot$ – enough to make a small open cluster.

The mass obtained here is known as the **Jeans mass**:

Eq. 12.8 $$M_J = \tfrac{4}{3}\pi\rho\left(R_J\right)^3 = \tfrac{4}{3}\pi\rho\left(\frac{\pi\Re T}{\mu G\rho}\right)^{3/2} = 1.03\times10^{24}\sqrt{\frac{T^3}{\mu^3\rho}} \text{ (grams)}$$

A cloud of a given density that has $M > M_J$ will have sufficient gravity to be bound and thus will collapse. Clouds with $M < M_J$ will be stable against collapse. Figure 12.1 shows the variation of the Jeans mass with density and temperature, for atomic and molecular clouds.

Figure 12.1: Jeans mass vs. density, for molecular (m) and atomic (a) clouds, at temperatures of 10K and 50K

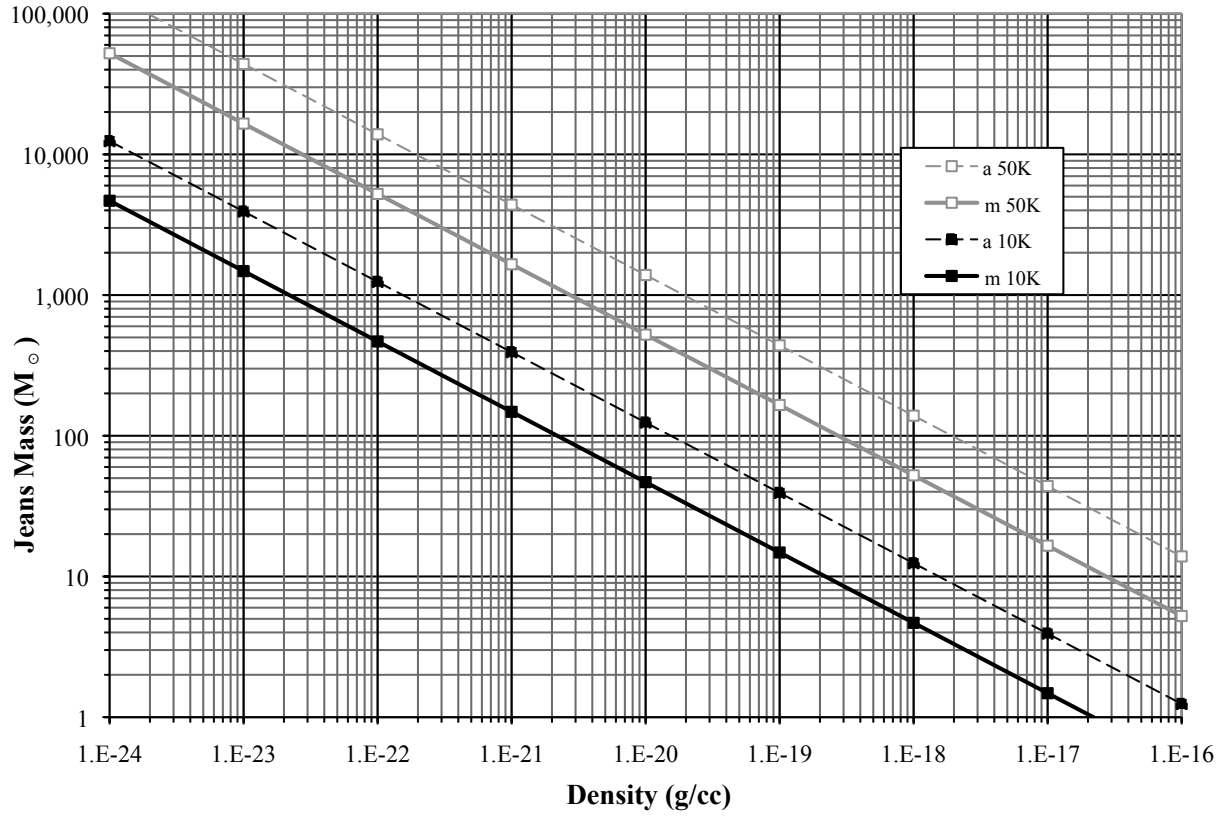

The Jeans mass criterion says that clouds with small masses are stable against collapse while larger ones are not. This implies that low mass objects such as planets, and perhaps small stars, are unlikely to form directly from the interstellar medium; instead, clouds with large masses will collapse and fragment into smaller, denser clouds, which can then form objects of lower mass. (R_J and M_J both decrease with increasing density if the collapse is essentially isothermal.)

Free-Fall Time Scale

Interstellar clouds will be comprised primarily of atomic or molecular hydrogen, helium, and dust grains, with the main opacity source being the dust grains. During collapse of the cloud, gravitational energy is released, but most of this energy is radiated away and thus lost. This is because the initial density of the cloud is so low that the optical depth $\left(\tau = \int_0^R \kappa \rho \, dr\right)$ is insignificant, and the radiation suffers little attenuation as it escapes.

Because of these initial radiation losses, the cloud temperature does not increase significantly and the pressure remains relatively low. Therefore, the collapse is nearly unhindered, and the particles in the cloud are in free fall. The time scale over which this process occurs can be estimated using Kepler's third law.

Consider a small particle dropped onto a large mass M from a distance R. The trajectory is essentially an orbit of semi-major axis $a \approx {}^1\!/_2 R$, and the time required for the particle to impact is $t \approx {}^1\!/_2 P$, where P is the orbital period, given by $P^2 = 4\pi^2 a^3/GM$. Combining these, we arrive at the **free-fall time scale** (or the **dynamic time scale**):

Eq. 12.9 $$t_{ff} \approx \tfrac{1}{2} P = \frac{1}{2} \cdot 2\pi \sqrt{\frac{a^3}{GM}} = \pi \sqrt{\frac{(R/2)^3}{GM}} = \pi \sqrt{\frac{R^3}{8GM}} \approx \sqrt{\frac{R^3}{GM}}$$

For the example given above, with $M_J = 470\ M_\odot$ and $R_J = 4.2$ pc, we find the free-fall time scale to be about 6 million years. For a smaller molecular cloud with a density of 1e–18, and a temperature of 10 K, we find a Jeans length of about 8700 AU, a Jeans mass of 4.7 $M_\odot$, and a free-fall time scale of 60,000 years. By comparison, the free-fall time scale for a particle at the Sun's surface is only about 27 minutes. All of these time scales are relatively short, considering that stellar lifetimes are typically measured in billions of years. The free-fall collapse of an interstellar cloud proceeds fairly quickly compared to most other phases of stellar evolution.

Energy Sinks

During the initial free-fall period, the density increases throughout the cloud, with the greatest increase occurring in the central regions. This causes the optical depth to increase; as the cloud collapses, the integrated path length decreases as r, but the density *increases* as $1/r^3$, making the optical depth *increase* as $1/r^2$; the cloud does not remain optically thin forever. The result is that more of the photon energy is retained within the cloud, where it raises the temperature, and with it, the pressure. The increased pressure in the center of the cloud tends to slow the collapse in that region. The increased temperature soon evaporates the dust in the central regions, eliminating it as the major source of opacity and leaving molecular hydrogen to fill that role.

As the temperature rises to near 1300 K, the H_2 begins to dissociate. This process serves as an energy sink; energy that would have gone into increasing the temperature and pressure is instead used for dissociation. The resulting pressure is insufficient to slow the in-falling gas, and a free-fall collapse again takes place. As the atomic hydrogen accumulates in the center, the pressure resumes its buildup, and a shock wave develops where the free-falling hydrogen atoms meet the growing central core of atomic hydrogen.

Inside this central region, the temperature and pressure of the atomic hydrogen continue to rise; at around 10,000 K, the neutral hydrogen ionizes, creating another energy sink. Use of gravitational potential energy to ionize the hydrogen results in insufficient energy being available to maintain the gas pressure, and the ionized hydrogen begins another free fall. As before, where these ions accumulate in the center, a shock wave develops and moves outward through the cloud. The sequence of events at a given point inside the cloud is shown in Figure 12.2; arrows show the varying infall rates of the gas, with longer arrows indicating free fall.

Figure 12.2: Sequence of ionization-dissociation events in the collapsing cloud

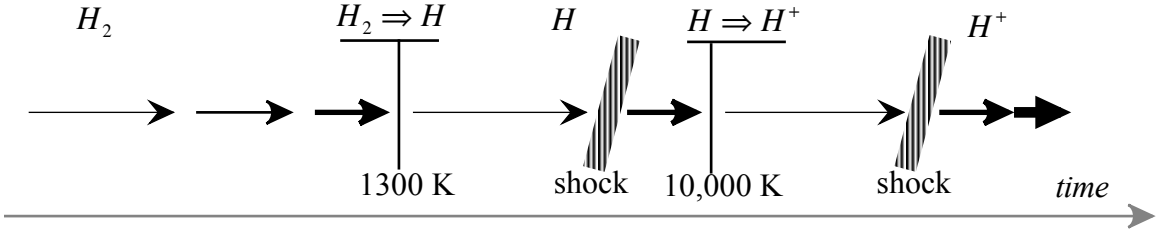

Only when the inner (star-forming) region of the cloud has been dissociated and completely ionized can the collapsing cloud enter the more gradual contraction phase of a **protostar**, which can be characterized by a quasi-hydrostatic equilibrium. We may estimate when this protostar stage will be reached by comparing the energy needed for dissociation and ionization with the gravitational potential energy liberated by collapse and contraction.

The dissociation energy of molecular hydrogen (E_D) is 4.5 eV, the ionization energy of hydrogen (χ_H) is 13.6 eV, and the ionization energy of helium (χ_{He}) is 24.6 + 54.4 = 79.0 eV for complete ionization. The total energy per gram needed to ionize and dissociate the gas mixture is then as follows:

$$E_{ID}\left(\frac{\text{eV}}{\text{g}}\right) = E_D\left(\frac{\text{eV}}{H_2\,\text{molec}}\right)\cdot N_A\left(\frac{\text{molec}}{\text{mole}}\right)\cdot\frac{1}{m_{H_2}}\left(\frac{\text{mole}}{\text{g}\,H_2}\right)\cdot X\left(\frac{\text{g}\,H_2}{\text{g}}\right)$$
$$+\chi_H\left(\frac{\text{eV}}{H\,\text{atom}}\right)\cdot N_A\left(\frac{\text{atoms}}{\text{mole}}\right)\cdot\frac{1}{m_H}\left(\frac{\text{mole}}{\text{g}\,H}\right)\cdot X\left(\frac{\text{g}\,H}{\text{g}}\right) \qquad \text{Eq. 12.10}$$
$$+\chi_{He}\left(\frac{\text{eV}}{He\,\text{atom}}\right)\cdot N_A\left(\frac{\text{atoms}}{\text{mole}}\right)\cdot\frac{1}{m_{He}}\left(\frac{\text{mole}}{\text{g}\,He}\right)\cdot Y\left(\frac{\text{g}\,He}{\text{g}}\right)$$

Ignoring the contribution of metals, we let $Y = 1 - X$. Inserting appropriate values we find a simple expression for the energy needed to dissociate and ionize each gram of the gas:

Eq. 12.11
$$E_{ID} = \left\{\left[\frac{4.5}{2}+13.6\right]X+\left[\frac{79.0}{4}\right](1-X)\right\}N_A \approx 19.75(1-0.2X)N_A$$
$$= 19.75(1-0.2X)6.02e23\left(1.6e-12\left({}^{\text{erg}}\!/\!_{\text{eV}}\right)\right) = 1.9\times10^{13}(1-0.2X)\,{}^{\text{ergs}}\!/\!_{\text{g}}$$

The source of this energy is the gravitational collapse of the cloud. From the virial theorem, the energy available from this gravitational collapse is half the change in potential energy:

Eq. 12.12
$$\frac{1}{2}\Delta\Omega \approx \frac{1}{2}\frac{GM}{R}\alpha$$

Here α is a dimensionless constant on the order of 1 that depends on the density distribution in the cloud. We now set this energy equal to the ionization-dissociation energy and solve for R:

Eq. 12.13
$$R = \frac{GM\alpha}{2E_{ID}} \quad or \quad \frac{R}{R_\odot} = \frac{G\,M_\odot\alpha}{2R_\odot E_{ID}}\left(\frac{M}{M_\odot}\right)$$

Inserting constants, and letting $\alpha = 6/7$ (suitable for a polytrope of index 1.5), we find a mass-radius relation:

Eq. 12.14
$$\frac{R}{R_\odot} = \frac{(6.67e-8)(1.99e33)(6/7)}{2(6.96e10)(1.9e13)(1-0.2X)}\left(\frac{M}{M_\odot}\right) = \frac{43}{(1-0.2X)}\left(\frac{M}{M_\odot}\right)$$

Assuming $X \approx 0.75$, we find the following:

Eq. 12.15
$$\frac{R}{R_\odot} \approx 50\frac{M}{M_\odot}$$

This represents the maximum radius for a stable protostar in quasi-hydrostatic equilibrium; this protostar is dissociated, ionized, and *contracting*. Prior to this point, the cloud *collapses* because most of the gravitational potential energy that is being released is not available to increase its temperature and pressure.

Equation 12.15 applies at the *start* of the contraction phase for all protostars. We may also write this equation as a mass-*density* relation:

Eq. 12.16
$$\frac{\rho}{\rho_\odot} = \frac{M/M_\odot}{\left(R/R_\odot\right)^3} = \frac{1}{50^3\left(M/M_\odot\right)^2}$$

From this, it is evident that higher mass protostars have lower densities when they begin their contraction phase; this trend will be maintained throughout the contraction to the main sequence.

We can model such a protostar as a polytrope of index 1.5, using equations from Chapter 9:

Eq. 9.74
$$\rho_c = \left(\frac{\rho_c}{\overline{\rho}}\right)_n \frac{M}{\frac{4}{3}\pi R^3}$$

Eq. 9.75 $$P_c = W_n \frac{GM^2}{R^4}$$

Ignoring radiation pressure, we may then find the central temperature from the ideal gas law and Equation 12.13:

Eq. 12.17 $$T_c = \frac{P_c \mu}{\rho_c \Re} = \frac{W_n}{(\rho_c/\overline{\rho})_n} \frac{4\pi\mu}{3\Re} \frac{GM}{R} = \frac{W_n}{(\rho_c/\overline{\rho})_n} \frac{4\pi\mu}{3\Re} \frac{2E_{ID}}{\alpha}$$

Inserting values, we obtain the following:

Eq. 12.18 $$T_c = \left(\frac{0.77014}{5.9907}\right)\left(\frac{8\pi}{3}\right)\left(\frac{7}{6}\right)\frac{1.9e13(1-0.2X)}{8.314e7}\mu = 290{,}000\,(1-0.2X)\mu$$

Using $X = 0.75$ (and $Y = 0.25$) we find $\mu \approx 0.59$ (for complete ionization). This yields a value of 146,000 K for the central temperature of the protostar – far too low for fusion to occur. The only energy source available to the protostar is then gravitational contraction, which will proceed on the Kelvin-Helmholtz (or thermal) time scale:

Eq. 12.19 $$t_{KH} \approx \frac{GM^2}{RL} = \frac{G(M_\odot)^2}{R_\odot L_\odot}\left(\frac{M}{M_\odot}\right)^2\left(\frac{R_\odot}{R}\right)\left(\frac{L_\odot}{L}\right)$$

Inserting constants, we reach a general result:

Eq. 12.20
$$t_{KH} \approx \frac{(6.67e-8)(1.99e33)^2}{(6.96e10)(3.84e33)}\left(\frac{M}{M_\odot}\right)^2\left(\frac{R_\odot}{R}\right)\left(\frac{L_\odot}{L}\right)$$
$$= 9.87e14\left(\frac{M}{M_\odot}\right)^2\left(\frac{R_\odot}{R}\right)\left(\frac{L_\odot}{L}\right)\ \text{s} \quad = 3.13\times10^7\left(\frac{M}{M_\odot}\right)^2\left(\frac{R_\odot}{R}\right)\left(\frac{L_\odot}{L}\right)\ \text{yrs}$$

With Equation 12.15, this can be further simplified to give the initial time scale (at the start of the contraction phase):

Eq. 12.21 $$\Delta t \approx 626{,}000\,\frac{M/M_\odot}{L/L_\odot}\ \text{yrs}$$

This time will be necessarily short because protostar luminosities are high – typically 100 to 1000 $L_\odot$. (A 1 $M_\odot$ protostar with a surface temperature of ≈ 3000 K and a radius of 50 $R_\odot$ will have a luminosity of about 180 $L_\odot$ and an initial contraction time scale of about 3400 years.) As the contraction proceeds, the radius (and for some stars, the luminosity) decreases, causing the time scale to increase and thereby slowing the evolution.

We may plot the tracks of protostars on an HR diagram, even though these objects are largely invisible to us. (The surrounding dust in the outer region of the cloud absorbs visible light, reradiating the energy in the infrared.) With large radii and low surface temperatures, collapsing clouds would be located far to the right of the familiar main sequence region. But at the start of

the contraction phase, the protostars would all appear near the upper right corner of the HR diagram, from which their paths would diverge according to mass, as shown in Figure 12.3.

Figure 12.3: Pre-main sequence evolutionary tracks

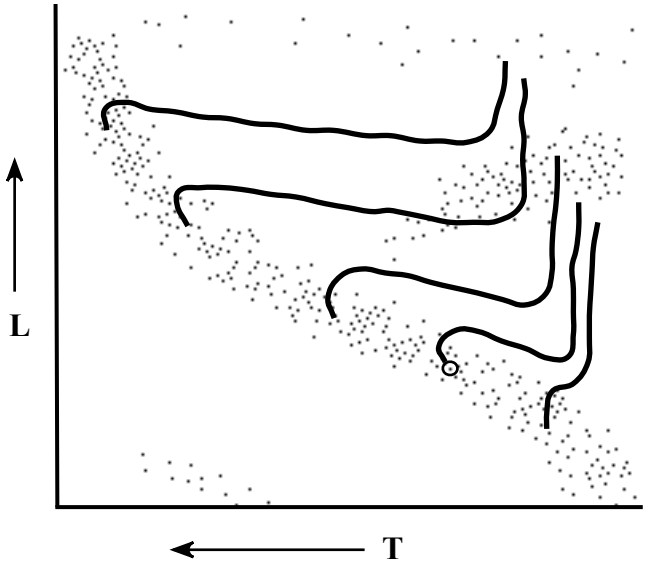

To a varying degree, each of these tracks includes a nearly vertical portion, along which the temperature remains nearly constant as the protostar contracts. This vertical portion is known as the **Hayashi track**, and it marks the high-temperature boundary of the **forbidden region**, for which hydrostatic equilibrium is unattainable for a star of a given mass and luminosity. A protostar that finds itself with a temperature that is too low – placing it in the forbidden region to the right of the Hayashi track – will collapse rapidly until it reaches this boundary, then contract and move down the Hayashi track. While on the Hayashi track, a protostar maintains the largest possible radius that is consistent with hydrostatic equilibrium. Such stars are fully convective (which is why we used an $n = 1.5$ polytrope to model our protostar).

Evolutionary tracks such as those in Figure 12.3 are *not* obtained by observing protostars as they gradually approach the main sequence; rather, they are described by numerical models of protostars in quasi-hydrostatic equilibrium as they slowly contract, heat up, and eventually begin nuclear fusion. As an example of the details of one such model, we will examine a 1 $M_\odot$ protostar as presented by Novotny (1973) Model 7-5A, B. The approximate track for this star is shown in Figure 12.4, which shows a small portion of the HR diagram.

Figure 12.4: Pre-main sequence evolution of a 1 $M_\odot$ protostar

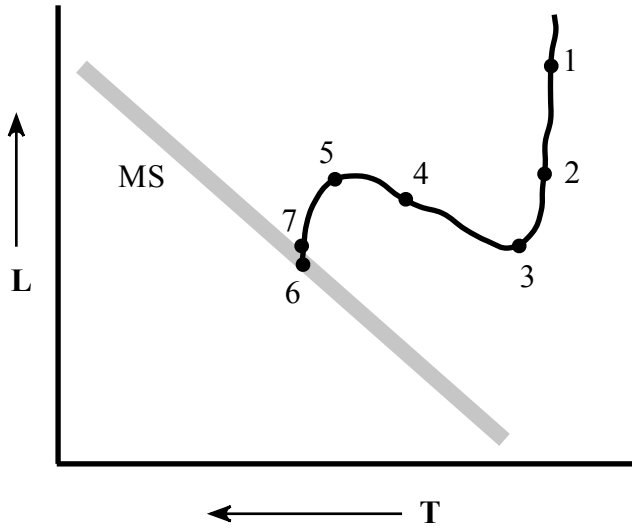

As the protostar evolves along this path, its rate of contraction gradually diminishes: point 1 is reached in 126,000 years, point 4 in 20 million years, and point 7 in 50 million years. During the descent of the Hayashi track (point 1 to 2) the star is fully convective. As it contracts, it heats up such that by point 2 the central temperature is high enough (a few million K) to ignite some of the primordial nuclei in the core. These nuclei (^2D, ^7Li, ^7Be) were part of the mixture that comprised the interstellar cloud from which the protostar formed. But these reactants are not particularly abundant, and they are not replenished by the reactions (shown in Table 12.1); therefore the energy that is released serves only to slow the contraction temporarily.

Table 12.1: Fusion of primordial nuclei

		ΔE (MeV)
[A2]	$^2D + {}^1H \rightarrow {}^3He + \gamma$	+5.493
[A5]	$^7Li + {}^1H \rightarrow {}^4He + {}^4He$	+17.347
[A4']	$^7Be + {}^1H \rightarrow {}^8B + \gamma$	+0.135

Contraction of the star heats the core, and this has an effect on the mode of heat transfer. As T increases, the opacity – which varies as $\rho / T^{3.5}$ – decreases; and the magnitude of the radiative temperature gradient – which varies as κ / T^3 – also drops. This makes the radiative gradient shallower than the adiabatic gradient, and a radiative core develops and grows outward through the star (points 2 to 4).

As the radiative core grows, the star becomes less opaque overall, allowing more energy to flow outwards and *increasing* the luminosity (the upward bend at point 3). Because the star is still shrinking, the effective temperature – which varies as $(L / R^2)^{1/4}$ – must increase, as indeed it does from point 3 to 5.

By point 4, the star is radiative throughout; but then ignition of primordial ^{12}C – burning to ^{14}N in a partial CNO cycle (reactions [B1], [B2], and [B3]) – releases additional energy in the core, raises the core temperature, and causes the (radiative) temperature gradient to become

steeper. This results in the growth of a convective core (points 4 to 6) and the return to a more vertical track. (As a general rule, convective transport produces vertical tracks while radiative transport produces nearly horizontal tracks.)

From point 3 to 6, nuclear reactions gradually take over the job of supplying energy for the luminosity, and contraction slows to a halt. From point 6 to 7 the star makes a transition from primordial ^{12}C burning to the proton-proton chain, which will serve as the principal energy source throughout the star's main sequence lifetime. Point 7 marks the **Zero Age Main Sequence** (ZAMS), which is the start of core hydrogen burning and the beginning of the main sequence phase.

Similar events can be described for protostars of other masses as they approach the main sequence. Higher mass protostars spend less time in this pre-main sequence phase, with a 15 $M_\odot$ protostar reaching the main sequence in only 60,000 years, compared to the Sun's 50 million years; protostars less massive than the Sun evolve even more slowly.

The basic reason for this disparity in evolution rates is gravity; with greater mass comes a stronger gravitational acceleration, which speeds up the contraction process and hurries the protostar on to the next phase. Stronger gravitational forces require greater pressure forces to maintain the quasi-hydrostatic equilibrium state; because higher mass protostars have lower densities (Equation 12.16), their higher pressures must be produced by greater kinetic temperatures, with the result that the more massive protostars tend to be hotter, both inside and on the surface. This is seen in the evolutionary tracks of Figure 12.3. The higher mass protostars contract to the main sequence at a nearly constant luminosity; this requires that $R^2 T_e^{\,4} \approx$ constant, which in turn means that the effective temperature varies as $1/\sqrt{R}$. In contrast, the vertical tracks of the low mass protostars produce a more constant effective temperature and presumably a more subdued rise in the core temperature.

The contraction of a protostar is ultimately halted by hydrogen fusion reactions in the core, which begin at a temperature of about 10 million K. The more massive protostars – with their higher temperatures – will reach this value fairly quickly and begin their main sequence lifetimes in short order. With their more gradual contraction rates and lower temperatures, the less massive protostars will begin fusion only after the forces of gravity have slowly squeezed the core temperature up to the threshold value. But for some protostars, this effort will be in vain. Protostars less massive than about 0.08 $M_\odot$ lack the gravity to ever attain hydrogen fusion temperatures and thus are unable to achieve stardom; such spheres are destined to become **brown dwarfs** – essentially, failed stars.

The Main Sequence

We now focus our attention on the **main sequence stars**, which emerge from the dust cocoons that enveloped the contracting protostars. The start of the main sequence phase – the ZAMS (described above) – is marked by the ignition of hydrogen fusion reactions that release sufficient nuclear energy to not only maintain the luminosity but also heat the star, producing adequate pressure to halt the gravitational collapse. Because a newly formed star has hydrogen in great abundance, this phase of stellar evolution has the potential to last for a very long time.

In fact, about 90% of the stars we observe are main sequence stars, indicating that this is an extremely stable portion of the star's life. Why is this so?

The Stellar Thermostat

When we describe a star as being stable, we do not mean to imply that the star's properties are constant. Stars change continually, and the changes range anywhere from the rapid and obvious to the gradual and subtle. Main sequence stars obtain energy by the fusion of hydrogen into helium in their cores, causing their properties to vary on the nuclear time scale. As this time scale is relatively long, the changes that result from hydrogen burning will be very gradual – so gradual that they will be unnoticeable over a few centuries of human observation. In this sense, the main sequence stars can be regarded as being quite stable.

The star needs some help to assure this stability. In order to produce nuclear energy at the same rate as the star's luminosity is releasing energy into space, the star needs some sort of feedback mechanism to control the reaction rate. And this feedback mechanism must operate on a timescale that is shorter than the nuclear time scale. The **stellar thermostat** satisfies this need.

In the core of a main sequence star, nuclear energy is produced at a rate given by ε. This energy heats the core, maintaining sufficient pressure to balance the omnipresent gravitational forces. Now suppose that for whatever reason, the energy generation rate increases slightly; the increase in available energy will raise the temperature of the core, causing the gases in the core to exert a slightly greater pressure. This pressure increase destroys the balance of hydrostatic equilibrium, and the core expands. However, the expanding gas does work on the overlying layers, which cools the core. This lower temperature, coupled with the reduced density caused by the expansion, results in a lower energy generation rate. We may express this stellar thermostat as follows:

$$\varepsilon\uparrow \Rightarrow T\uparrow \Rightarrow P\uparrow \Rightarrow R\uparrow \Rightarrow \rho\downarrow,\ T\downarrow \Rightarrow \varepsilon\downarrow$$

Similarly, a small *reduction* in ε lowers the core temperature (as energy continues to flow outward) and reduces the pressure exerted by the core. The resulting gravitational contraction of the core increases both its density and temperature and therefore raises ε :

$$\varepsilon\downarrow \Rightarrow T\downarrow \Rightarrow P\downarrow \Rightarrow R\downarrow \Rightarrow \rho\uparrow,\ T\uparrow \Rightarrow \varepsilon\uparrow$$

These adjustments occur on the thermal time scale and thus are rapid enough to keep the energy generation rate from straying too far from its equilibrium value.

Main Sequence Properties

As noted, the protostars distribute themselves along the main sequence according to their masses. Their properties vary along the main sequence as shown in Table 12.2 and illustrated in Figures 12.5 to 12.8.

Table 12.2: Main sequence properties (adapted from Cox 2000)

Sp	$M/M_\odot$	$R/R_\odot$	$\bar{\rho}/\bar{\rho}_\odot$	T_{eff}	$L/L_\odot$
O3	120	15	0.036		
O5	60	12	0.035	42000	399000
O6	37	10	0.037		
O8	23	8.5	0.037		
B0	17.5	7.4	0.043	30000	39500
B3	7.6	4.8	0.069		
B5	5.9	3.9	0.099	15200	722
B8	3.8	3	0.141	11400	135
A0	2.9	2.4	0.210	9790	47.1
A5	2	1.7	0.407	8180	11.5
F0	1.6	1.5	0.474	7300	5.69
F5	1.4	1.3	0.637	6650	2.94
G0	1.05	1.1	0.789	5940	1.34
G2	1	1	1	5790	1
G5	0.92	0.92	1.18	5560	0.720
K0	0.79	0.85	1.29	5150	0.452
K5	0.67	0.72	1.80	4410	0.174
M0	0.51	0.6	2.36	3840	0.0696
M2	0.4	0.5	3.20	3520	0.0342
M5	0.21	0.27	10.7	3170	0.00655
M8	0.06	0.1	60		

Figure 12.5: Main sequence radius vs. mass (both in solar units)

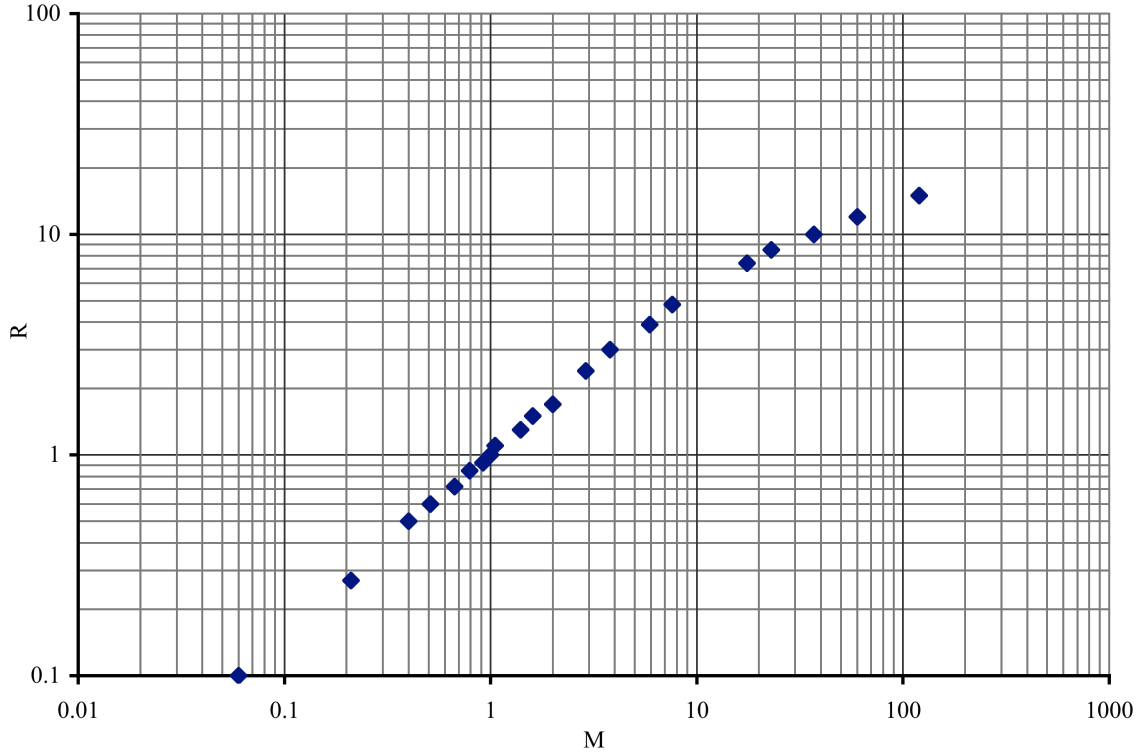

Figure 12.6: Main sequence mean density vs. mass (both in solar units)

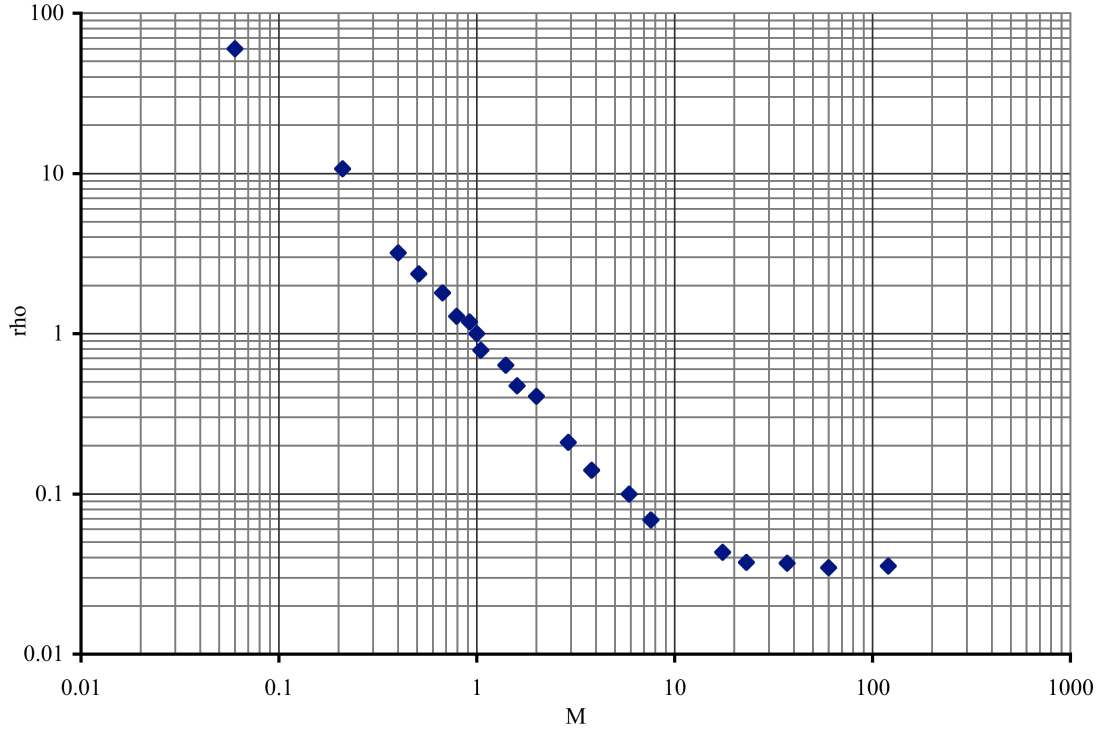

Figure 12.7: Main sequence effective temperature vs. mass (in solar units)

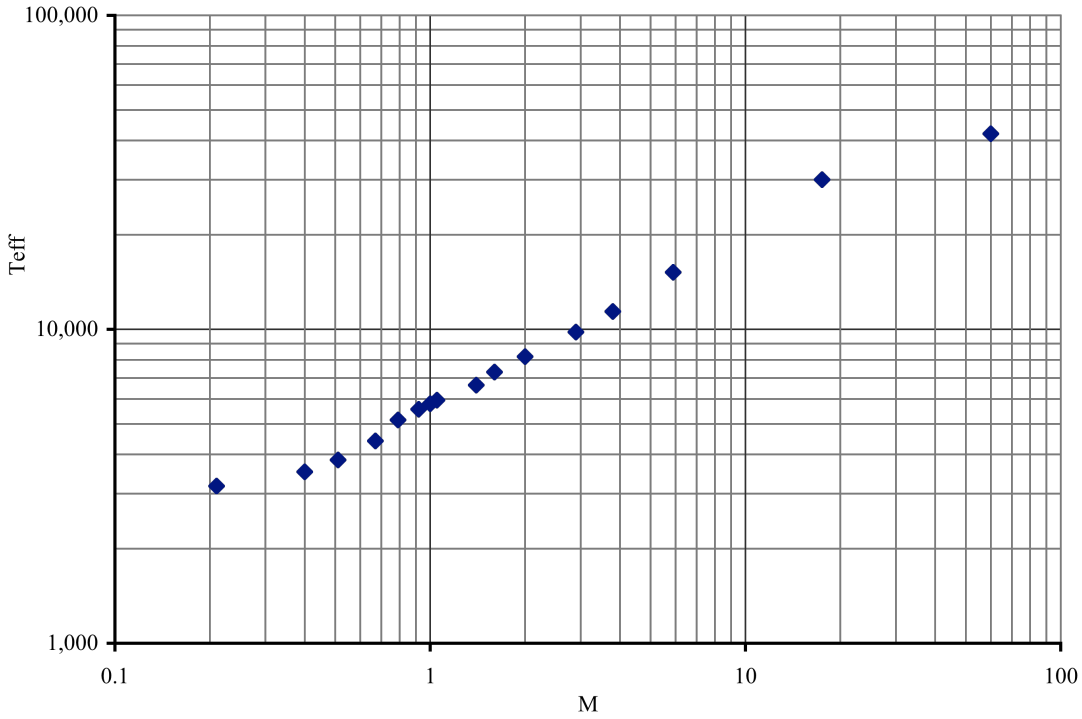

Figure 12.8: Main sequence luminosity vs. mass (both in solar units)

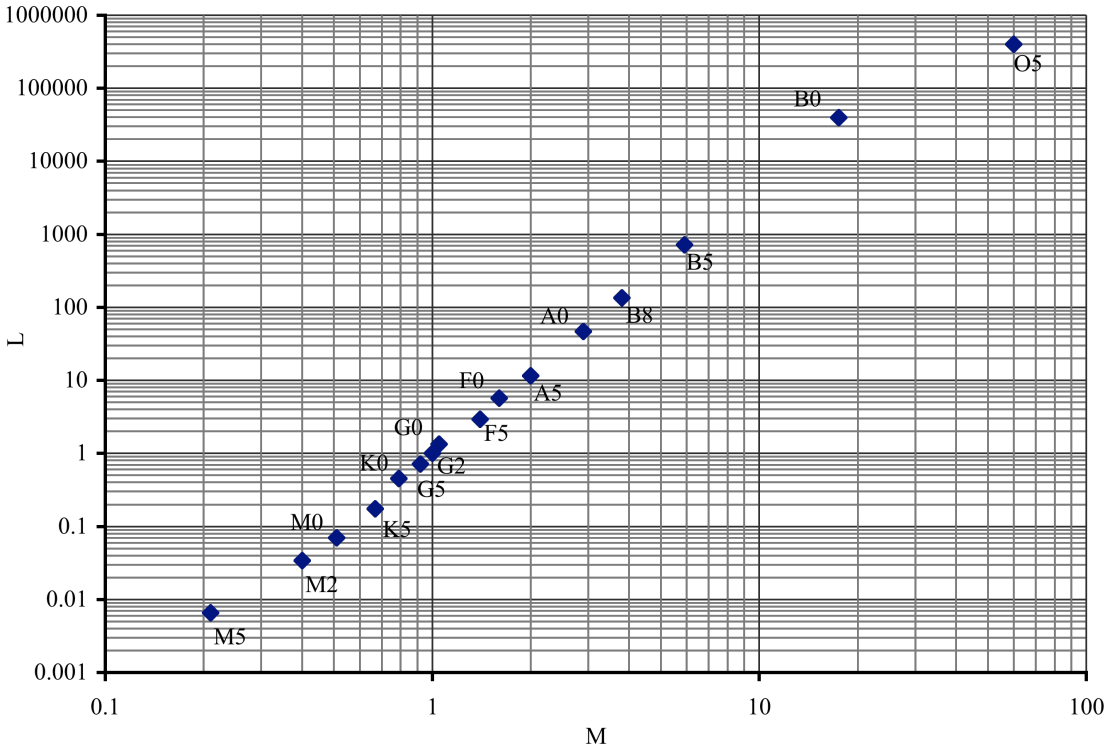

In general, the graphs are fairly linear and show clear trends. As mass increases up the main sequence, radius, luminosity, and effective temperature all increase while the mean density decreases. High mass stars are bigger, hotter, more luminous, and less dense than low mass stars, and these properties affect their energy generation, their structure, and their future evolution.

In examining the structure of main sequence stars, we will find it convenient to divide them into two groups, according to the manner in which they generate energy: the lower main sequence stars, which use the pp chain, and the upper main sequence stars, which use the CNO cycle. The boundary between these two groups is around 1.5 $M_{\odot}$.

The lower main sequence stars have less mass and consequently weaker gravitational forces holding them together. Less pressure is needed for equilibrium, and lower kinetic temperatures are sufficient to supply this pressure, in part due to the higher densities of these stars. With lower core temperatures, these stars generate energy slowly by the proton-proton chain, but this rate is enough to maintain the stars' luminosities, which are also relatively low due to their small radii and low effective temperatures.

The upper main sequence stars have greater mass and consequently stronger gravitational forces holding them together. More pressure is needed for equilibrium, and higher kinetic temperatures are needed to supply this pressure, in part due to these stars' lower densities. With higher core temperatures, these stars generate energy rapidly by the CNO cycle, but this rate is necessary to support the stars' high luminosities, which are produced by their large radii and high effective temperatures.

We saw in Chapter 10 that the temperature dependence of the hydrogen-burning reaction rates can be written as $\varepsilon \approx T^{\nu}$, where $\nu \approx 4$ for the pp chain and $\nu \approx 20$ for the CNO cycle. This means that the CNO cycle is more sensitive to temperature than the pp chain, and therefore most of the CNO energy will be generated at the highest range of temperatures found in the innermost radii at the center of the core. With the reaction rate and the temperature both peaking sharply at the center of the star, the temperature gradient will be fairly steep, and convection will develop easily. We may expect the upper main sequence stars to have convective cores, which will provide thorough mixing of the hydrogen fuel with the helium ash.

In contrast, energy generation by the pp chain will be much less centralized, with reactions spread over a comparatively broader range of temperatures and radii; the temperature gradient will then be much shallower, and convection will be more difficult to establish. Thus, a lower mass main sequence star will have a radiative core. As helium is produced by fusion, it will be deposited in the center of the star to form an isothermal helium core, which will grow throughout the main sequence lifetime.

In the outer regions of the lower main sequence stars, decreasing temperatures and less complete ionization tend to increase the opacity ($\kappa \approx \rho/T^{3.5}$), and this produces a convection zone in the outer layers. The depth of this convection zone varies with the temperature of the star; in the Sun, the outermost 20% of the radius is convective, and this fraction increases for cooler stars, such that below about 0.4 $M_{\odot}$, the star is entirely convective.

As can be seen in Figure 12.5, for stars below 10 $M_{\odot}$, $R \propto M^{3/4}$. Recalling from Chapter 9 that the central temperature scales as M/R, we may easily find that $T_c \propto M^{1/4}$. Thus, central temperature should increase slowly up the main sequence, as we had anticipated, and this gradually changes the dominant core reactions over from the pp chain to the CNO cycle.

Applying this mass-radius relation to the mean density, we find that $\bar{\rho} \approx M/R^3 \approx M/M^{9/4} \approx 1/M^{5/4}$, as our density graph seems to indicate. The combination of higher temperatures and lower densities moves the ionization zones for hydrogen and helium out beyond the surface of the upper main sequence stars, reducing the opacity of the matter just below the surface. The reduced product $\kappa\rho$ lowers the radiative temperature gradient and causes the envelopes of these stars to become radiative. Thus, upper main sequence stars have convective cores and radiative envelopes, while lower main sequence stars such as the Sun have radiative cores and convective envelopes (except for the extremely low mass stars mentioned above). It would appear that in moving up the main sequence, the convective core appears at about the same mass where the convective envelope disappears – just above 1 $M_{\odot}$.

Main Sequence Lifetimes

We may estimate the lifetimes (τ) of main sequence stars much as we did for the Sun in Chapter 10, using a modified nuclear time scale (note: τ is *not* an optical depth):

Eq. 12.22 $$\tau \approx \frac{Mef_c c^2}{L}$$ where f_c is the core fraction and e is the reaction efficiency

With solar values this gives a lifetime of about 10 billion years.

From Figure 12.8, we note a strong correlation between mass and main sequence luminosity, of the form $L \approx M^{\alpha}$. For most of the main sequence, the exponent has a value of $\alpha \approx {}^{9}/_{2.5} = 3.6$. Then the mass dependence of the lifetime can be written as follows:

Eq. 12.23 $$\tau \approx {}^{1}\!\diagup\!_{M^{2.6}}$$

We illustrate the procedure by using this relation to estimate the lifetime of an 11 $M_{\odot}$ star:

Eq. 12.24 $$\tau \approx {}^{1}\!\diagup\!_{11^{2.6}} \cdot 10 \text{ billion years } \approx 20 \text{ million years}$$

Stellar main sequence lifetimes decrease strongly with mass, which is consistent with our earlier remarks about the mass dependence of the overall evolutionary rates of stars. In the next chapter we shall see that this trend continues, as we explore the behavior of stars beyond the main sequence.

CHAPTER 13: Sequels to the Main Sequence

Stars spend the majority of their lifetimes as main sequence stars, where they convert hydrogen into helium in their cores. Because most stars are composed primarily of hydrogen, this phase of stellar evolution is relatively lengthy, but it does not last forever. Eventually the star's core nuclear fuel must be exhausted, causing a readjustment in the structure of the star. This process can be repeated, with different fuels consumed by stars of different masses, producing an interesting mix of structures that are still externally identifiable as stars. However, in many cases these stars are only temporary, and the ultimate structure resulting from stellar evolution will turn out to be quite distinct from the stars we have been discussing. It is the variety of pathways that stars follow after leaving the main sequence that is the focus of this chapter.

Each star is unique, with a different mass and composition, and thus a different evolution; even so, we should find that stars with similar masses and compositions should evolve in a similar manner. Thus, we will find it convenient to group stars according to their masses. This is commonly done, although there is not a strong consensus on how many groups to use, where to draw the boundaries of the groups, or how to label them. We will choose to form five mass groups along the main sequence, as shown in Figure 13.1, which also correlates these groups with their main sequence spectral types. The selected boundaries are approximate, and will vary from author to author; as we shall see, they are chosen to match naturally occurring changes in the structure and behavior of stars.

Figure 13.1: Main sequence mass ranges

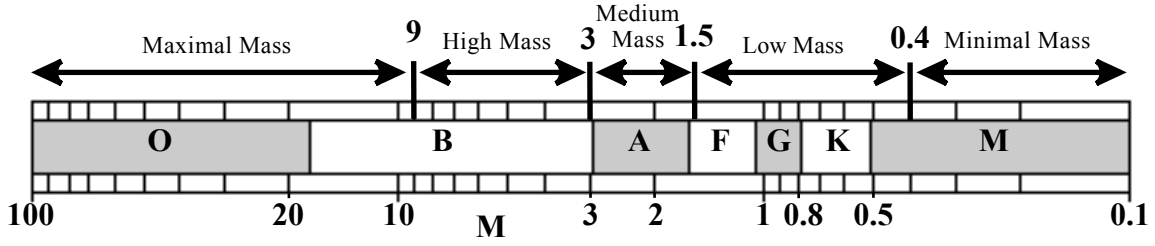

The End of the Main Sequence

We begin by recalling that main sequence stars all perform core hydrogen fusion to obtain their energy, using two competing mechanisms to do so. While the proton-proton chain is

dominant in the cooler stars, the CNO cycle is dominant in the hotter stars, with the transition occurring around 1.5 $M_\odot$ (early F stars), as shown in Figure 13.2. In our initial discussion we will examine the different characteristics of the upper and lower main sequence stars.

Figure 13.2: Core hydrogen-burning mechanisms along the main sequence

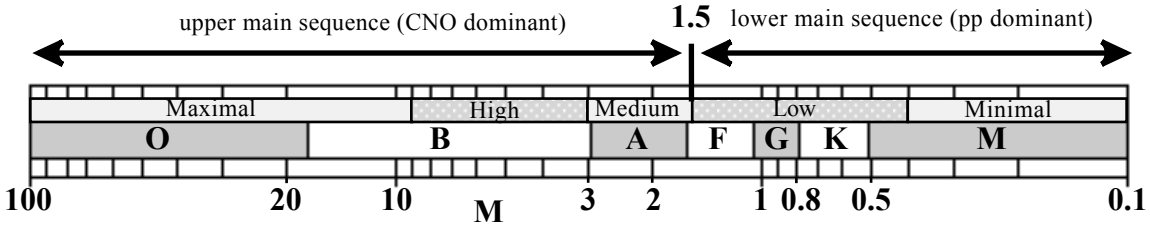

Lower Main Sequence (Minimal and Low Mass Stars)

Compared to stars higher up the main sequence, the lower main sequence stars are less massive and have lower temperatures, both on the surface and in the core. Because of this, their core energy production is dominated by the proton-proton chain. Due to the relatively weak temperature dependence of the pp reaction rate, such stars will generate nuclear energy over a broad range of radii in the core, preventing steep temperature gradients and resulting in radiative cores. With their lower surface temperatures and consequently greater opacities outside the core, they will develop convective envelopes, which deepen with decreasing mass. In the minimal mass stars, the convection zone extends all the way to the core, making these stars completely convective; around 1.5 $M_\odot$ the convective envelope is pushed to the stellar surface and disappears as ionization of the outer layers becomes complete. These boundaries are indicated in the next figure.

Figure 13.3: Convection vs. radiation along the main sequence

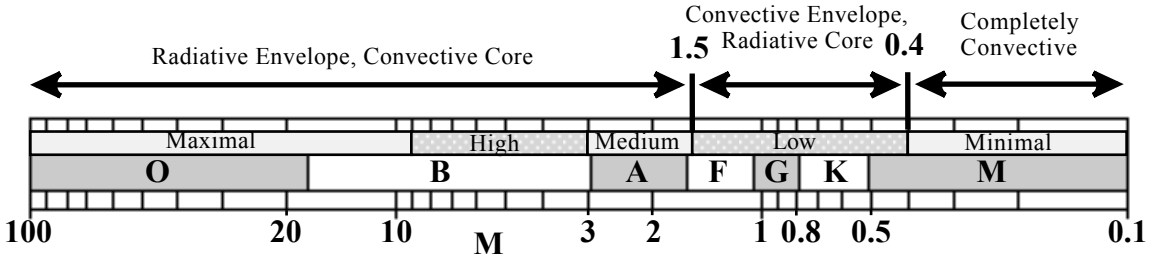

The minimal mass main sequence stars (mid to late M stars) are special cases – for two reasons. First, with the star being completely convective, *all* of the hydrogen is available to be circulated down into the center of the star where the nuclear reactions take place; at the same time, the helium ash is redistributed throughout the star. Thus, by the end of the main sequence, the star will have converted nearly all of its hydrogen into helium, leaving a homogeneous star of essentially pure helium. Second, the main sequence lifetimes of such stars exceed the estimated age of the universe by factors of 4 or more; therefore, *none* of these stars should have left the main sequence as yet or produced interesting stellar creatures for us to attempt to explain. The projected fates of these stars will be discussed later.

The rest of the lower main sequence stars (F, G, K, and early M stars) have quite different futures in store for them. These stars have *radiative* cores, which means that the helium ash that forms does *not* circulate but remains essentially in the place where it was created. Throughout the main sequence phase, the helium mass fraction increases steadily throughout the core, but not uniformly. Because the temperature is highest in the center of the core, the pp reaction rate is greatest there, and the helium builds up most rapidly there. Eventually the helium mass fraction rises to 1 at the center of the core, marking the end of the main sequence phase.

While on the main sequence, the star's properties are not exactly constant. As hydrogen is converted to helium, the mean molecular weight in the core gradually increases from about 0.6 to 1.3 (with the central core regions leading the way); the effect of this action alone would be to lower the pressure by a factor of 2 (as $P \approx \rho T/\mu$). The star responds to this trend by slowly contracting the core, increasing the density and temperature in order to maintain sufficient pressure to balance gravity. The increased temperature and density make the nuclear reactions run faster, causing the star's luminosity to increase gradually during the main sequence phase.

Once hydrogen is finally exhausted in the center of the core, nuclear reactions there cease. But nuclear energy is still being generated by the pp chain in a **thick shell** around the inert helium ash, in the portion of the core where hydrogen has not yet been eliminated. Because the helium ash core supports no reactions at this time, it cools as energy flows outward from it, but it does not contract. However, the loss of this energy source does produce gravitational contraction in the hydrogen layers above the helium core, and energy released by this contraction heats the thick hydrogen-burning shell, increasing the reaction rate at its base. The resulting increase in shell luminosity expands the outer core layers, cooling them and extinguishing the reactions there. During this **shell-narrowing phase**, the star's luminosity continues to rise; ash from the shell burning increases the core mass, which strengthens the gravity acting on the shell, which compresses and heats the shell, which drives the reaction rate even higher in a spiraling process.

The increasing flow of energy powered by the rising shell luminosity produces a steeper temperature gradient and makes convection a more viable alternative in the region above the shell. Accordingly, the existing convective envelope gradually dips deeper into the star. Convection expands the outer layers of the star, cooling them and increasing the opacity, which drives the convection even more. Thus the star becomes both larger and cooler, as viewed from the outside.

On the inside, the core of the star contracts and heats as the hydrogen shell source deposits more helium ash onto it. Due to the relatively high densities of low mass stars, their helium cores are partially degenerate at this stage, becoming increasingly degenerate as time goes on. Although not a big factor at this point, degeneracy will become rather important for these stars before very much longer.

In summary, at the end of the main sequence phase a typical low mass star exhausts its core hydrogen supply, transitions smoothly to hydrogen **shell burning**, and begins to expand and cool as it moves off the main sequence toward the giant region of the HR diagram. Meanwhile, the minimal mass stars spend an eternity on the main sequence converting themselves entirely into helium. What about the upper main sequence stars?

Upper Main Sequence (Medium, High, and Maximal Mass Stars)

The upper main sequence stars have greater masses and higher temperatures, both on the surface and in the core. Because of their higher temperatures, their core energy production is dominated by the CNO cycle. Due to the strong temperature dependence of the CNO reaction rate, such stars will have developed convective cores, and with their higher surface temperatures and consequently lower opacities outside the core, they will have radiative envelopes, as indicated in Figure 13.3.

As hydrogen burns in the convective core of such a star, the helium ashes are mixed throughout the core, and fresh hydrogen is constantly pumped to the center of the core where the reactions proceed most rapidly. As in the case of the lower main sequence stars, the steady increase in the mean molecular weight must be offset by a gradual contraction of the core, raising the core density and temperature while increasing the core reaction rate, and hence, the main sequence luminosity.

Core hydrogen burning continues in this manner until the hydrogen nuclei are so diluted by helium nuclei that the reactions can no longer proceed – a limit that is reached when the hydrogen mass fraction in the core drops to about 5%. The core then transitions from convective to isothermal as the final fraction of hydrogen is processed. At this point, the star is a helium core surrounded by a hydrogen envelope, with no nuclear reactions taking place to generate energy. Energy still flows toward the surface, cooling the central regions, reducing the pressure there, and initiating gravitational contraction.

Contraction of the star releases gravitational energy, which raises the temperature of the hydrogen envelope just above the core – enough to ignite hydrogen burning in a thick shell around the core. The helium ash produced by this shell is deposited onto the core, gradually increasing its mass, strengthening gravity in the shell, increasing the shell density and temperature and hence, the shell luminosity. The energy released is used to expand the star, cooling the outer layers and moving the star to the right of the main sequence.

Figure 13.4: Main sequence evolutionary tracks for 1, 1.5, 3, 6, and 15 $M_\odot$ stars

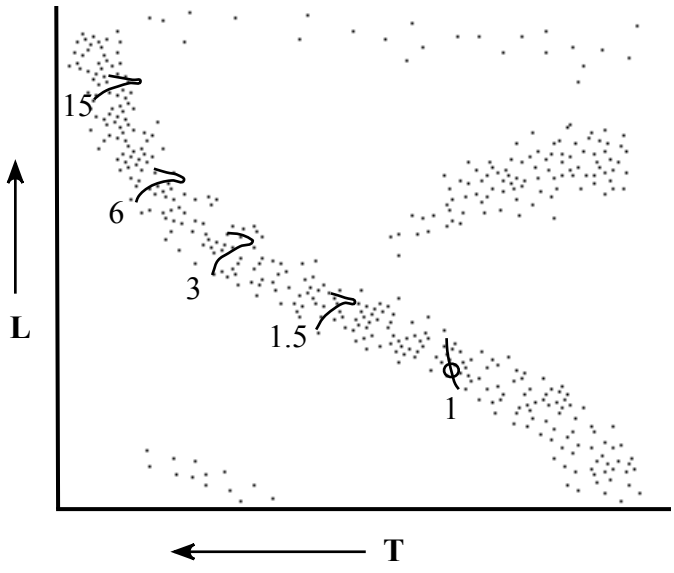

Figure 13.4 illustrates the evolutionary tracks of stars while they are on the main sequence. The lowest point in each track marks the **Zero Age Main Sequence** (**ZAMS**); from there, the stars with convective cores migrate up to the right across the main sequence during the core hydrogen burning phase. The subsequent jog to the left marks the core's adjustment from convective transfer to being essentially isothermal. With its radiative core the 1 $M_\odot$ star avoids this adjustment and makes a smooth transition from core burning to shell burning.

Toward Helium Ignition

The next set of nuclear reactions available to the star involve helium burning, via the triple-alpha process. As we learned in Chapter 10, this sequence requires a temperature of about 100 million K, a condition that is not met inside main sequence stars. But as these stars evolve off the main sequence, their cores generally contract and heat, providing the potential for triple-alpha ignition. As we might expect, stars of different masses approach helium ignition in different ways.

The Minimal Mass Stars

The minimal mass main sequence stars (mid to late M types, with $M < 0.4\ M_\odot$) manage to convert themselves entirely into helium, but they are ill-equipped to do very much with it. With their very low masses, these stars have insufficient gravity to ever raise their temperatures to the helium ignition point. Instead, they will only contract as best they can, gradually becoming smaller, hotter, denser, and more degenerate. We will ignore them for now and pick up their story again when we discuss stellar endpoints.

The Maximal and High Mass Stars

The O and early to mid B stars (with $M > 6\ M_\odot$) have no real problem with helium ignition. As they evolve off the main sequence, their helium cores contract and heat on the relatively rapid thermal time scale. Because these stars are quite hot to begin with, their cores reach 100 million K with little effort. And because the more massive stars are less dense as well, they reach the helium ignition temperature without becoming significantly degenerate. The helium core ignites smoothly, and the ensuing triple-alpha process is controlled by the stellar thermostat, much as core hydrogen burning was regulated on the main sequence. The star makes a smooth transition to core helium burning, retaining its hydrogen burning shell in the process. The maximal mass stars ignite helium as they move horizontally across the supergiant region; the mid B stars reach the right edge of the HR diagram before ignition occurs.

In the late B stars (with $6\ M_\odot > M > 3\ M_\odot$), the helium core that is present at the end of the main sequence is isothermal, and it does not begin an immediate contraction, being initially capable of supporting itself against the pressure exerted by the envelope. However, contraction of the *envelope* does occur, causing ignition of a hydrogen shell at its base, and the subsequent addition of its helium ash gradually increases the core mass, eventually triggering core contraction. This relatively rapid contraction then leads to the smooth ignition of helium as described above.

The Medium and Low Mass Stars

The medium and low mass stars comprise the middle of the main sequence, from type A through early M (with $3\ M_\odot > M > 0.4\ M_\odot$). As they evolve off the main sequence, these stars follow the basic plan, with a helium core, a hydrogen-burning shell, and an expanding hydrogen envelope. Core density increases down the main sequence, and this results in increasingly degenerate cores for the low mass stars. Additionally, as the stars move off the main sequence and their cores begin to contract, their rising densities further increase the degree of degeneracy such that helium ignition will ultimately occur in a significantly degenerate core. Details of this event will be presented shortly, but first we must set the stage.

For each of these stars, evolution off the main sequence involves expansion and cooling of the envelope. For the A and F stars this expansion occurs at a nearly constant luminosity (as we saw above with the O and B stars), with the stars evolving to the right across the HR diagram, but for types G to early M the track is more vertical, with the stars expanding at a nearly constant temperature. As can be seen in Figure 13.5, these post-main sequence tracks resemble the pre-main sequence tracks of Figure 12.3, except of course that the direction is reversed. While the pre-main sequence tracks involved contraction, with the gravitational energy released being stored as thermal energy in the star and also radiating away, the post-main sequence tracks involve expansion, with nuclear energy (from the shell source), gravitational energy (from the contracting core) and thermal energy (from the outer layers) being stored in the expanding envelope as gravitational potential energy and also supplying the luminosity.

Figure 13.5: Post-main sequence evolution to helium ignition

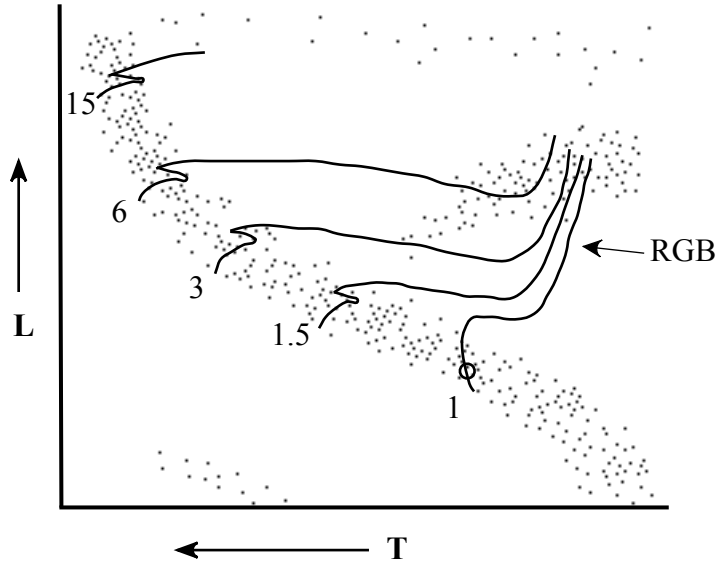

The envelope expansion is powered by the hydrogen shell source in each star, and the rate of energy generation in the shell is controlled by the gravitational contraction of the helium core, which in turn is fueled by helium ash from the shell. The more massive the core, the stronger the gravitational forces acting on the shell, causing greater compression, higher shell temperatures, and increased shell luminosity, which increases the core mass even more. As the envelope is

expanded by the increasing shell luminosity, the outer layers cool and become more opaque, making the envelope more susceptible to convection, which also contributes to the expansion.

Degeneracy also factors into the expansion. Degenerate matter is denser than non-degenerate matter, and the less massive stars in this group have denser cores while on the main sequence, giving them a head start on degeneracy. All of these stellar cores become increasingly degenerate as the core contraction proceeds, and this leads to an even more compact core and even more rapid acceleration of the expansion process.

The effects of degeneracy are most notable in the low mass stars, where the expanding star soon confronts the forbidden region (introduced in the previous chapter) where stable stellar structures do not exist. Because the star is prevented from using its increasing shell luminosity to expand and *cool* the outer layers by moving to the right on the HR diagram (the default expansion process), it is forced to turn *upwards* along the Hayashi track, becoming fully convective and increasing the luminosity of the star while maintaining a constant surface temperature. This requires more energy than simple expansion and cooling would need, but with their more degenerate cores, the low mass stars are up to the challenge. Of course with their nuclear fires burning at a lower rate than those of higher mass stars, the expansion of the low mass stars must proceed more slowly, but this is perfectly consistent with our previous ideas about the effect of mass on the evolutionary rate.

We now follow the medium and low mass stars as they move off the main sequence, expanding and cooling at nearly constant luminosities until they reach the Hayashi track. (For the low mass stars, this horizontal track will be relatively short on the HR diagram, but it will require a considerably longer time to traverse.) At the Hayashi track, the horizontal track bends upward as the convective zone reaches deeper into the envelope and the continuing expansion begins to increase the stellar luminosity. The star swells up to several dozen times its main sequence radius, becoming the large, cool, luminous star known as a **red giant**; the nearly vertical track it follows on the HR diagram is known as the **red giant branch** (**RGB**).

The Helium Flash

The helium core of the red giant continues to accumulate mass from the hydrogen shell source, becoming hotter, more compact, and more degenerate with time. When the core temperature rises to 100 million K, the helium will ignite, once again giving the star a source of nuclear energy in the core. However, for these stars, helium ignition occurs in a core that is degenerate – more so for the low mass stars. As we saw in Chapter 11, a degenerate gas plays the game by different rules, particularly in terms of the pressure it exerts. While ideal gas pressure is proportional to density and temperature, the pressure in a completely degenerate electron gas is determined solely by density and is essentially independent of temperature: small changes in temperature are not accompanied by corresponding changes in pressure.

Ignition of helium releases energy in the core, which is immediately used to increase the core temperature. If the core were operating under ideal gas conditions, this increase in temperature would produce an increase in gas pressure in the core, which would expand the core, cooling the helium, and slowing the reactions; in short, the stellar thermostat would act to control the rate at which helium burning proceeds ($\varepsilon\uparrow \Rightarrow T\uparrow \Rightarrow P\uparrow \Rightarrow R\uparrow \Rightarrow \rho\downarrow$, $T\downarrow \Rightarrow \varepsilon\downarrow$).

However, in a degenerate core, an increase in temperature does *not* result in a significant pressure increase. This is because energy added to the gas by nuclear reactions can easily be absorbed by the ion gas – which is not degenerate; but because the pressure exerted by the ions is small compared to the pressure exerted by the degenerate electrons, the release of nuclear energy has no immediate effect on the pressure in the core. The core does not expand, the temperature does not drop, and the reactions continue unchecked. In fact, the extra energy absorbed by the ion gas makes the reactions run that much faster; rather than being slowed and controlled, the nuclear reactions are accelerated and unrestricted, producing a thermal runaway ($\varepsilon\uparrow \rightleftarrows T\uparrow$).

One might suppose that this scenario could continue without bound, eventually destroying the star, but such is not the case. This is because there are two sides to degeneracy – density and temperature. Degeneracy involves combinations of high density and/or low temperature. As a gas at a certain temperature becomes denser, it will become more degenerate; but if a gas at a certain density is *heated*, it will become *less* degenerate. It is this latter situation in which the newly ignited, degenerate helium core of a red giant star now finds itself. As its nuclear reactions proceed at top speed, the energy they release serves to raise the core temperature rather dramatically, such that in short order, more high-momentum states are made available to the electrons, and the degeneracy is lifted. The core returns to an ideal gas state, the stellar thermostat is fixed, the crisis is over, and the star settles down to controlled burning of helium in its core.

Figure 13.6: Transformation of the helium flash core luminosity spike into a surface luminosity change

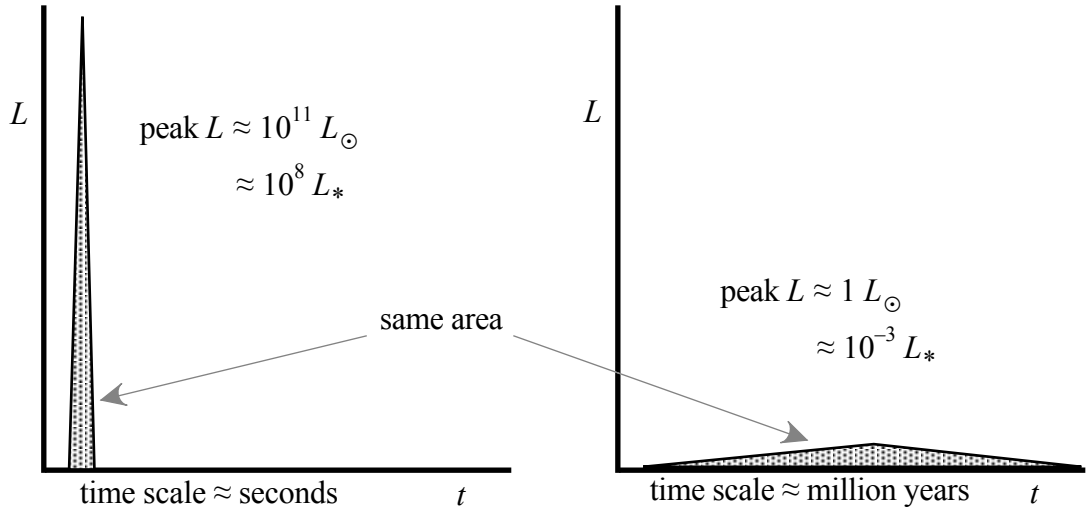

This event is brief, taking place on a time scale measured in *minutes* or *seconds*; it is referred to as the **helium flash** – the explosive ignition of helium in a degenerate stellar core. At its peak rate, the core luminosity is of the same order of magnitude as the luminosity of an entire galaxy (about $10^{11}\ L_\odot$). We do not observe this spectacle in stars because they hide it from our view, buried under a few tenths of an AU of stellar matter. Even though the core may produce an extremely high luminosity pulse, it will be of very short duration. And the descendants of the photons that result from this pulse will arrive at the surface some millions of years later, with

arrival times distributed over an interval so broad that we are unlikely to be able to detect any significant change in the star's luminosity (see Figure 13.6).

As for evolutionary tracks, we left our medium and low mass stars all ascending their respective red giant branches and bound for helium ignition. When the helium flash finally occurs – at a helium core mass of 0.45 $M_\odot$ – each star has several adjustments to make as a result of the new core energy source.

First, some of the energy released during the helium flash must be used to make the core non-degenerate again, which means that it must expand back to a much lower density, storing some of its newly released nuclear energy as gravitational energy. With a less dense core, the helium burning reactions will not proceed as fast as they did during the helium flash. Similarly, expansion of the core also expands and cools the hydrogen-burning shell, slowing those reactions as well. The result is an overall *lowering* of the star's luminosity, causing the evolutionary track to reverse direction, moving back down the Hayashi track from the **red giant tip**, the peak in the luminosity where the helium flash occurred ($L \approx 1000\ L_\odot$).

The return path down the Hayashi track is not quite the same as the ascent. The star now has a non-degenerate core with its own nuclear energy source, and this causes the descending track to veer toward higher temperatures on the HR diagram as the envelope contraction heats the visible surface. Stars with low metallicities tend to continue moving to the left across the HR diagram, halting at points determined by their individual metal contents and the masses of their envelopes. These stars trace out the **horizontal branch**, which is characterized by core helium burning and hydrogen shell burning. Stars with high metallicities tend to avoid this journey, instead forming a clump of stars at the right end of the horizontal branch that is appropriately labeled the **red clump**. These core-helium-burning red clump stars are giants with $L \approx 100\ L_\odot$ – larger than main sequence stars of the same temperature, but not as large as stars near the red giant tip. Figure 13.7 illustrates this sequence of events.

Figure 13.7: Post-main sequence evolution for 1 $M_\odot$ stars

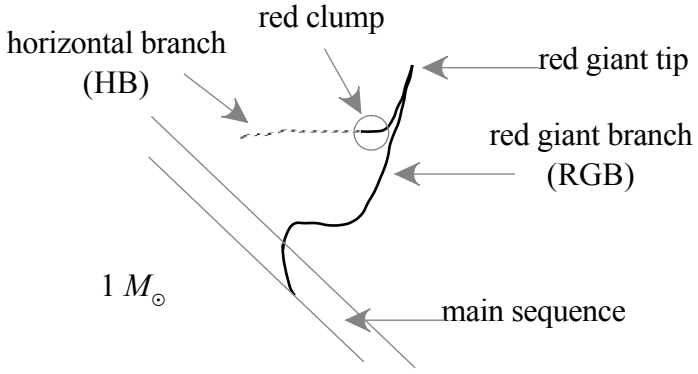

Higher mass stars also loop toward the blue after igniting helium in their cores, with the blueward extent of the loop increasing with greater mass, as shown in Figure 13.8. (The maximal mass stars do not perform such loops.)

Figure 13.8: Loops in the tracks of core helium-burning giants

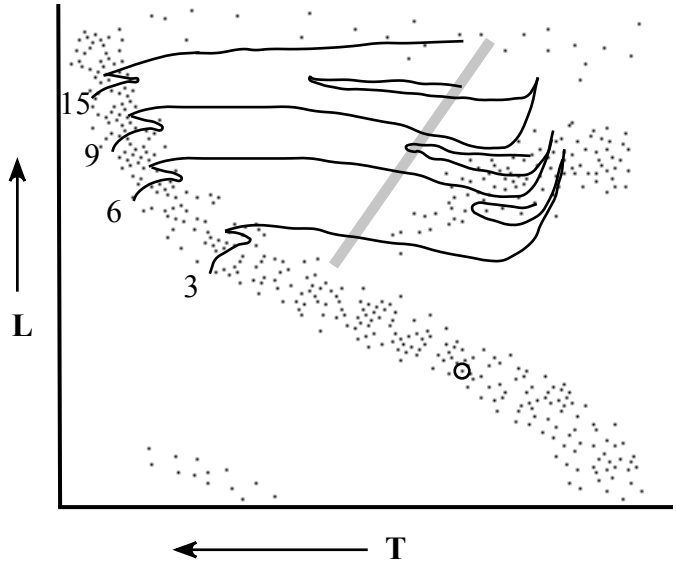

In stars of greater than 5 $M_\odot$, these loops cross the **instability strip** on the HR diagram (the diagonal gray band in Figure 13.8). In this region, the particular combination of stellar parameters makes stars unstable to radial pulsations, and they become **Cepheid variables**. but the *first* trip across the instability strip (from the main sequence to the red giant branch) does *not* produce Cepheids, for reasons that will become clear below.

The Schönberg-Chandrasekhar Limit

At the end of the main sequence phase, each star will have a helium core that has just terminated its hydrogen fusion reactions. The nature of this core and its subsequent behavior will vary with the mass of the star, as shown in Figure 13.9.

Figure 13.9: Nature of the helium core at the end of the main sequence

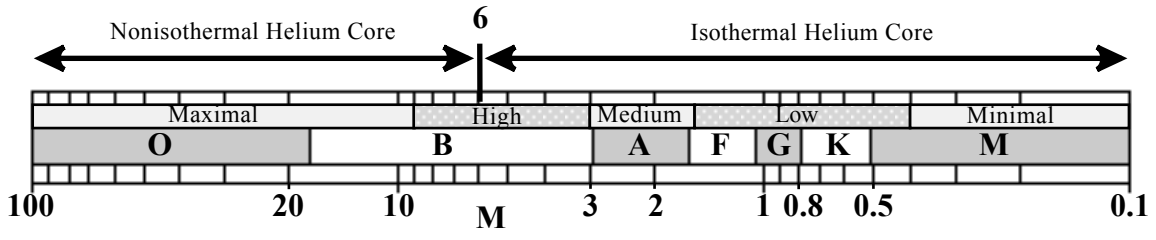

Due to the lack of a nuclear energy source inside it, the core will be unable to maintain a temperature gradient, and it will tend to become isothermal. Such an isothermal core can support itself without contracting as long as it contains a relatively small fraction of the star's mass. The upper limit on the mass of an isothermal core is known as the **Schönberg-Chandrasekhar limit**, which is given in terms of the mean molecular weights of the core and the envelope:

Eq. 13.1 $$M_{S-C} = 0.37\left(\frac{\mu_{env}}{\mu_{core}}\right)^2 M_*$$ (where M_* is the mass of the *entire* star)

Using $\mu_{env} \approx 0.6$ and $\mu_{core} \approx 1.3$, we find $M_{S\text{-}C} \approx 0.08\ M_*$. An isothermal helium core with a mass less than about 8% of the mass of the star should be stable against contraction. This condition is met by stars up to about 6 $M_\odot$; stars more massive than this (the O and early to mid B stars) will end the main sequence with cores that exceed the Schönberg-Chandrasekhar limit, resulting in immediate contraction and heating (on a relatively rapid thermal time scale) until helium ignition temperature is reached.

For stars less than about 6 $M_\odot$, the termination of core hydrogen burning does not result in immediate contraction of the core, but it does initiate contraction of the envelope. Heating of the base of the envelope establishes the hydrogen shell source around the isothermal helium core, and this shell begins to deposit its helium ash onto the core, increasing its mass. When the core mass rises to exceed the Schönberg-Chandrasekhar limit, the core will contract and heat, again on the relatively rapid thermal time scale. For late B stars, this contraction will be halted by the ignition of helium – which will occur far across the HR diagram in the red giant region.

For medium mass stars, the rapid contraction will be slowed before ignition by increasing degeneracy, with the onset of degeneracy occurring earlier in the contraction phase for lower masses. Once degeneracy sets in, contraction will still continue, but it will proceed at the much slower nuclear time scale as reactions in the hydrogen shell source slowly increase the core mass. When helium ignition finally occurs, it will do so in a degenerate core, producing the helium flash, as previously discussed.

In low mass stars, the isothermal helium core will be partially degenerate when it forms at the end of the main sequence, and this degeneracy will prevent any sort of rapid contraction. Instead, the hydrogen shell source forms by contraction of the envelope (as above), and the core then contracts on its nuclear time scale as the shell burning gradually increases the core mass.

Figures 13.10 and 13.11 summarize these variations.

Figure 13.10: Helium core contraction following the main sequence

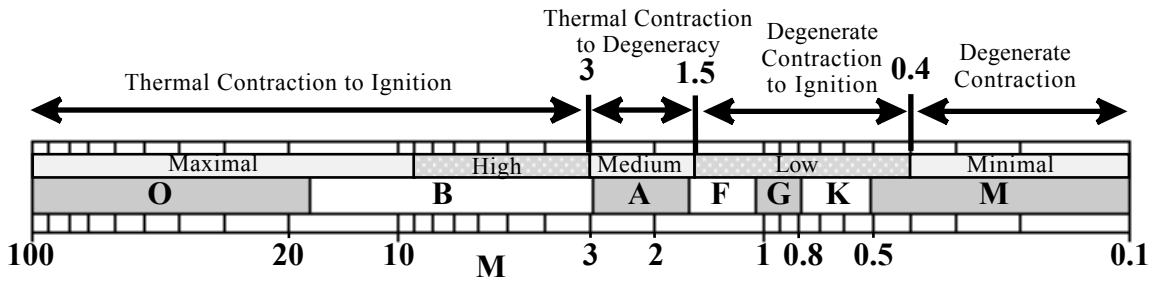

Figure 13.11: Core helium ignition in post-main sequence stars

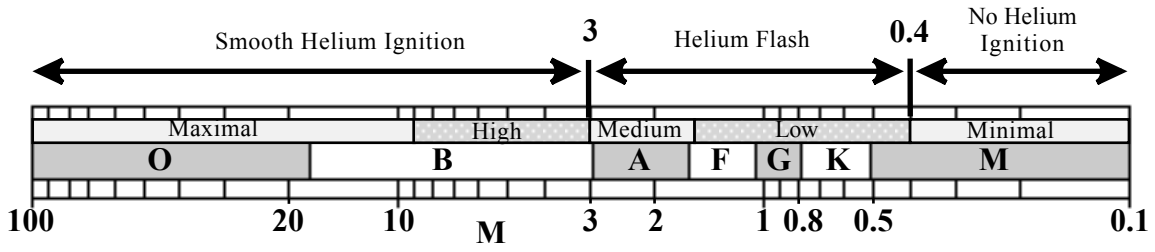

The Hertzsprung Gap

Most of the effects of the Schönberg-Chandrasekhar limit are hidden from our view, buried deep inside the star where only our computer models can detect them. However, there is one effect that can be observed, in a manner of speaking. The rapid contraction of the isothermal core that occurs in stars around 5 or 6 $M_\odot$ produces a correspondingly rapid evolution of these stars across the HR diagram from the main sequence to the red giant region. Because this movement is comparatively swift, these stars spend very little time in the intermediate stages, and the probability of observing a star in this middle portion of the HR diagram will be very small.

Such an underabundance of stars is actually noticed. On an HR diagram with a sufficient number of field stars that cover a wide range of masses and ages, the main sequence will be apparent, as will the red giant branch and the red clump. But between the upper main sequence and the red giant branch there will be a relative void, with hardly any stars, a region designated as the **Hertzsprung gap** (see Figure 13.12). This gap is bounded on the bottom by low mass stars, which evolve more slowly toward the red giant branch (due to their partially degenerate cores), thus making them more likely to be observed.

Figure 13.12: The Hertzsprung gap

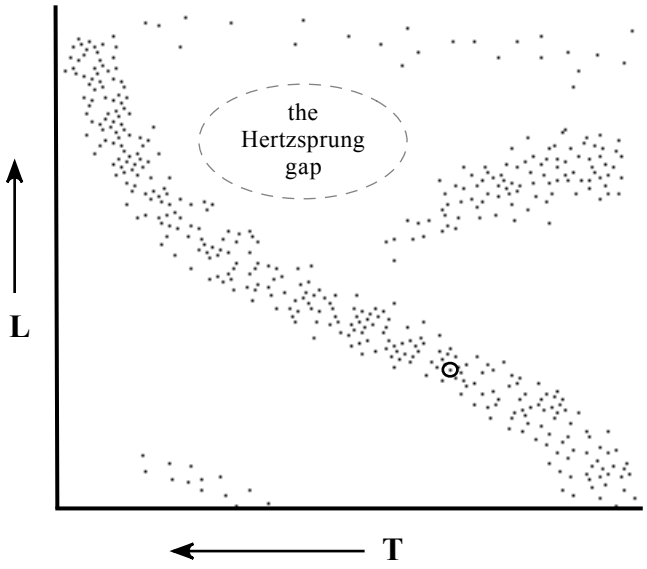

As noted above, stars of 5 $M_\odot$ or greater do *not* become Cepheids as they cross the instability strip for the first time on their way to the red giant branch; this is because of their rapid evolution across the Hertzsprung gap. Their later ventures across the instability strip are more gradual because the core helium-burning loop proceeds on a *nuclear* time scale, giving us a much higher probability of observing stars in this unstable condition.

Evolutionary Time Scales

The Hertzsprung gap is due to relatively rapid evolution by stars through a particular structural phase. This in turn is caused by evolution proceeding along different time scales, depending on the process involved. For stars of a given mass, the nuclear time scale is generally

longest, with the Kelvin-Helmholtz (or thermal) time scale next; and for a given time scale, more massive stars evolve more rapidly.

So far, we can describe the evolution of most stars as a sequence of phases leading up to helium ignition. These include pre-main sequence evolution of the protostar; main sequence; core adjustment (at the end of the main sequence); hydrogen burning in a thick shell; shell-narrowing; and the red giant branch. Most of these are illustrated in Figure 13.13.

Figure 13.13: Typical post-main sequence evolutionary stages leading to helium ignition

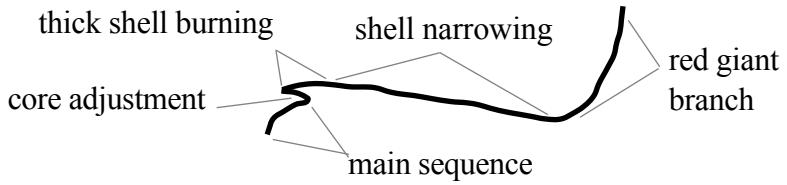

Figure 13.14 compares the length of time required for these different stages in stars of different masses.

Figure 13.14: Stellar evolution time intervals (prior to helium ignition) for stars of 1 to 15 $M_\odot$ (data from Iben (1967))

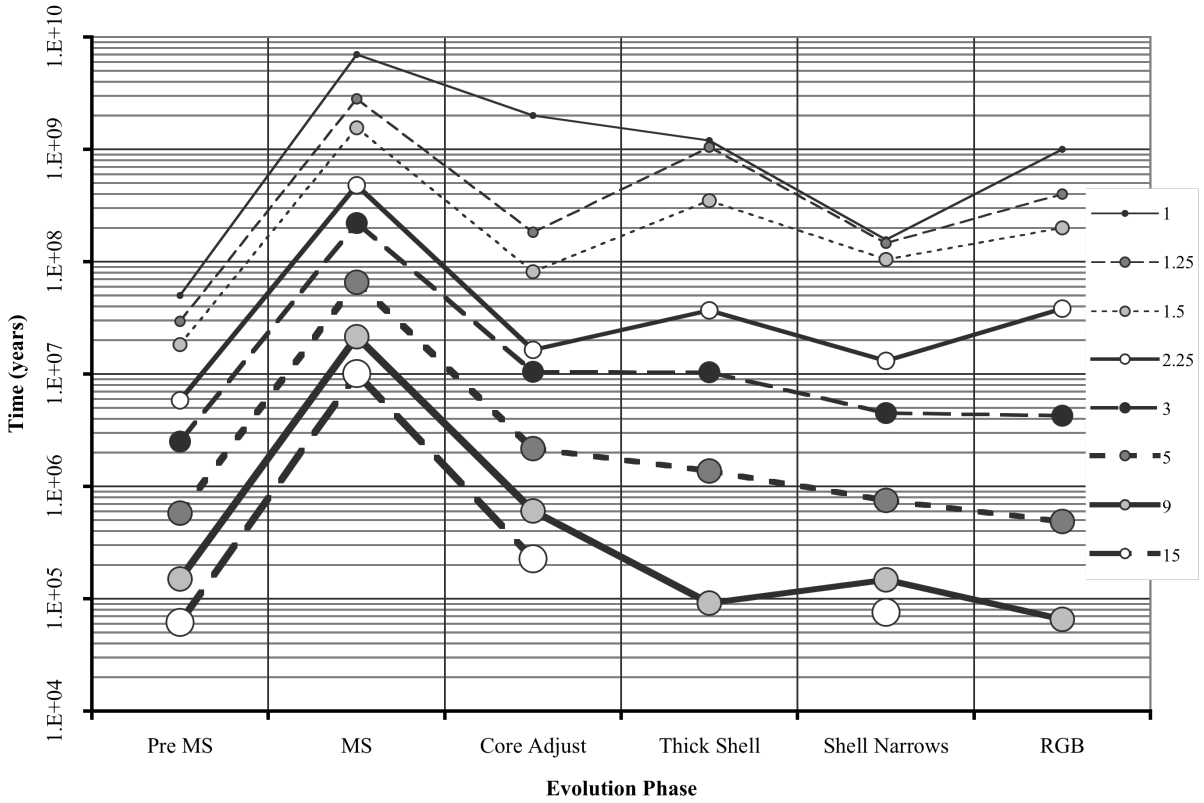

It is immediately obvious that for any given mass the longest time interval is the main sequence, by an order of magnitude or more. The shortest is generally the pre-main sequence phase, which is about two orders of magnitude less than the main sequence. Post-main sequence

phases are also considerably shorter than the main sequence, which explains why the main sequence is the most populous group of stars.

The Approach to Carbon Burning

So far we have seen that mass sets limits on the nuclear reactions that a star may perform. Below 0.08 $M_\odot$, hydrogen burning cannot be sustained, while below 0.4 $M_\odot$, helium burning does not happen. Those stars that can ignite helium (all except the minimal mass stars) will manage to produce a carbon core; whether a given star can successfully ignite this next nuclear fuel will depend, of course, on its mass.

The Medium and Low Mass Stars

We left the medium or low mass star on the horizontal branch (or in the red clump) where it was burning helium in its core and hydrogen in a shell. This it can do for a reasonable length of time – on the order of 10% of its main sequence lifetime. However, when the helium runs out, the star will again have to adjust its structure, causing another relocation on the HR diagram. In some ways, the readjustment is similar to that performed at the end of the main sequence.

Termination of core helium burning leaves a core comprised of carbon and oxygen nuclei – the result of the triple-alpha process and alpha capture. The ensuing gravitational contraction creates a helium-burning shell source just outside the carbon-oxygen core, and this shell, together with the hydrogen-burning shell above it, powers another expansion of the star. As the star expands and cools, it again moves up and to the right on the HR diagram – in a manner reminiscent of the red giant branch – past the red giant tip and beyond, along a track designated as the **asymptotic giant branch** (**AGB**). Figure 13.15 illustrates this feature.

Figure 13.15: The asymptotic giant branch for 1 $M_\odot$ stars

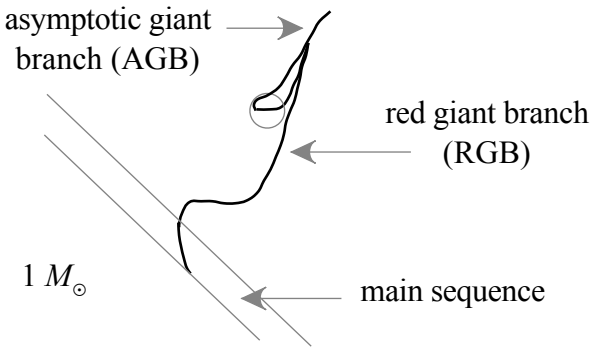

Along the AGB the core contracts and heats, in preparation for the next core fusion phase; however, just as some stars were unable to achieve core helium fusion, not all stars are destined to ignite the carbon-oxygen fuel now filling their cores. The medium and low mass stars have insufficient gravity to heat their cores to carbon fusion temperature – around 600 million K. Their cores will contract and heat, becoming increasingly degenerate in the process, while their envelopes expand and cool, swelling the stars to several hundred times their main sequence radii.

Both the RGB and the AGB involve stars swelling up as their envelopes become more convective; both of these situations provide opportunities for the star to change its outward appearance, using a process known as **dredge-up**.

Dredge-up

For the most part, the compositions that stars exhibit in their atmospheres are essentially the compositions they had when they formed. This is true even though stars are continually performing nuclear fusion in their central regions, turning light elements into heavier ones, for these reaction products are normally contained within the stellar interior, hidden from our view. However, there is a mechanism that sometimes operates to distribute fusion products throughout the star; given the right circumstances, convection can stir the stellar interior, lifting heavy elements to the surface and changing the surface abundances we observe.

We have already seen that the minimal mass stars are completely convective, and thus are able to mix helium throughout the star while gradually exhausting all the hydrogen. In other main sequence stars, this does not happen, because the convective envelopes of low mass stars do not dip into their hydrogen-burning cores, and the convective zones of upper main sequence stars do not extend into their envelopes; their surface abundances are uncontaminated by the products of their core nuclear processes. But the story is different for post-main sequence stars.

As stars evolve toward the red giant branch, their convective envelopes deepen. Around the base of the RGB, the convective envelope extends far enough into the star that it reaches material that was processed by the star's main sequence nuclear reactions. The circulation of this material can measurably alter the observed surface abundances of helium, carbon, and nitrogen in low mass stars, in a process known as **first dredge-up**. In particular, the abundance of helium is increased (by both pp and CNO), the ratio of carbon-12 to carbon-13 is decreased (by the depletion of carbon-12 in the initial reaction of CNO), and the C/N ratio is reduced (by the conversion of carbon to nitrogen in the first portion of CNO). In more massive stars, with a more extensive history of CNO processing, the O/N ratio may also be reduced.

A **second dredge-up** occurs for medium and high mass stars on the asymptotic giant branch, which have a carbon-oxygen core, a helium-burning shell at the base of a helium-rich zone, and a hydrogen-burning shell at the base of the hydrogen-rich envelope. Ignition of the helium shell source results in an increased luminosity that expands and extinguishes the hydrogen-burning shell above it. As the star expands up the AGB, the convective envelope deepens and reaches the inactive hydrogen shell, again dredging the products of hydrogen burning up to the surface. (Low mass stars do not participate in this process because the hydrogen shell is not extinguished at this point.)

The Maximal and High Mass Stars

The maximal and high mass stars will have sufficient gravity to heat their carbon cores to the ignition point. However, just as degeneracy affected the ignition of helium in the lower mass stars, it will again be a factor in the less massive stars in this group.

The boundary occurs at about 9 $M_\odot$; in the high mass stars, the core will be degenerate when carbon ignition temperature is reached. This will result in the **carbon detonation** (also called the **carbon flash**) – the explosive ignition of a degenerate carbon core – an event that is analogous to the helium flash. This explosion may tear the star apart, producing a **supernova** (see Chapter 14); alternatively, the star may be able to suppress the violence occurring in its core, repair its thermostat (by lifting the degeneracy), and move on to controlled core carbon burning.

But there is a third option, to be discussed in later sections, in which the high mass star manages to eject enough of its envelope mass that it becomes incapable of achieving carbon ignition; such a star may then produce a **planetary nebula** (see Chapter 14). As a result, carbon ignition in the high mass stars is a bit uncertain, as indicated by the dual gray arrows in Figure 13.16.

Figure 13.16: Carbon ignition options for post-main sequence stars

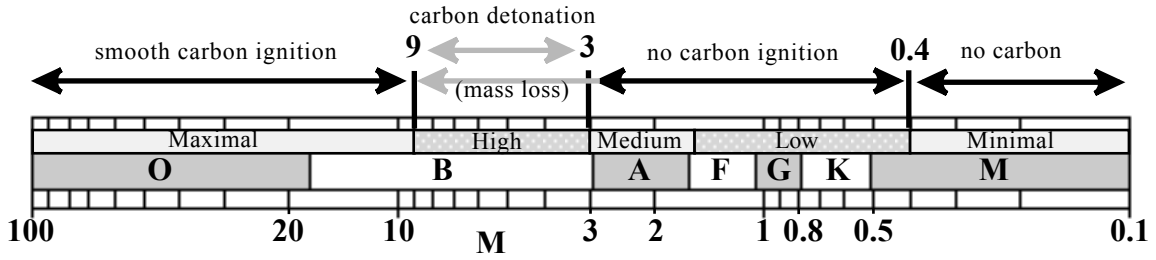

The maximal mass stars will perform smooth ignition of their carbon cores, avoiding the potential perils of the carbon detonation. Core carbon burning will temporarily slow their drift across the supergiant region toward the red, but it will not halt it. For the time being, these stars will manage to continue the basic pattern of core contraction followed by ignition of the next nuclear fuel, making increasingly heavier elements in the process. The next section will discuss the general direction these reactions will take.

Advanced Nucleosynthesis

Before continuing our tale of stellar evolution, we must pause to consider additional nuclear reactions. The pp chain and the CNO cycle covered the main sequence reactions, and the triple-alpha process and alpha capture were added for the giant branches, but now we are faced with carbon burning (and probably more). By what routes does further nucleosynthesis proceed? Lang (1980) provides the following sequences.

Alpha Capture

There are additional alpha capture reactions that can be run once oxygen nuclei have been produced:

$$^{16}O + ^{4}He \rightarrow ^{20}Ne + \gamma + 4.730 \text{ MeV}$$
$$^{20}Ne + ^{4}He \rightarrow ^{24}Mg + \gamma + 9.317 \text{ MeV}$$
$$^{24}Mg + ^{4}He \rightarrow ^{28}Si + \gamma + 9.981 \text{ MeV}$$
$$^{28}Si + ^{4}He \rightarrow ^{32}S + \gamma + 6.948 \text{ MeV}$$
$$^{32}S + ^{4}He \rightarrow ^{36}Ar + \gamma + 6.645 \text{ MeV}$$

Alpha capture reactions with some of the CNO products can produce neutrons:

$$^{13}C + ^{4}He \rightarrow ^{16}O + n + 2.214 \text{ MeV}$$

and

$$^{14}N + ^{4}He \rightarrow ^{18}F + \gamma + 4.416 \text{ MeV}$$
$$^{18}F \rightarrow ^{18}O + e^{+} + \nu_e$$
$$^{18}O + ^{4}He \rightarrow ^{21}Ne + n - 0.699 \text{ MeV}$$

and

$$^{18}O + ^{4}He \rightarrow ^{22}Ne + \gamma + 9.667 \text{ MeV}$$
$$^{22}Ne + ^{4}He \rightarrow ^{25}Mg + n - 0.481 \text{ MeV}$$

Such reactions can occur in AGB stars, and the neutrons produced in these reactions can be used to form other nuclides by the process of **neutron capture**.

Neutron Capture and Beta Decay

Neutron capture involves the capture of neutrons by a nucleus, increasing the nucleon number ($A \rightarrow A+1$) while keeping the atomic number (Z) constant:

Eq. 13.2 $${}^{A}_{Z}X + n \rightarrow {}^{A+1}_{Z}X + \gamma$$

This process creates heavier isotopes of a given element through successive neutron captures. However, some isotopes are unstable to **beta decay**, in which a neutron decays into a proton, creating an electron and a neutrino in the process:

Eq. 13.3 $${}^{A}_{Z}X \rightarrow {}^{A}_{Z+1}X + e^{-} + \bar{\nu}$$

Under conditions of a weak neutron flux (such as found in AGB stars), neutron capture proceeds gradually until it produces an unstable isotope, which then decays. Unstable isotopes will have sufficient *time* to decay before the next neutron encounter if the neutron capture rate is *slower* than the beta decay rate; therefore this is known as the **s process**.

We may illustrate the s process using an iron-56 seed nucleus to capture neutrons, eventually producing cobalt-59:

Eq. 13.4 $${}^{56}Fe \rightarrow {}^{57}Fe \rightarrow {}^{58}Fe \rightarrow {}^{59}Fe \rightarrow {}^{59}Co + \beta$$

This works up to ${}^{208}Pb$ and ${}^{209}Bi$, beyond which no nuclei are sufficiently stable for neutron capture to operate. Thus, no actinides are formed by the s process.

For certain neutron numbers (N = 28, 50, 82, 126), the neutron capture cross sections are relatively small; such nuclei are less likely to capture neutrons and are more likely to *accumulate* under s process conditions, producing local abundance peaks for certain isotopes such as ${}^{88}Sr$, ${}^{138}Ba$, and ${}^{208}Pb$ (which are observed in the solar system). The dredge-up process may bring these isotopes to the surface in AGB stars, where they can be observed, resulting in such groups as the **barium stars**.

Under conditions of *high* neutron flux, the neutron capture rate will be more *rapid* than the beta decay rate, giving rise to the **r process**. These two processes are depicted in Figure 13.17.

Figure 13.17: Nucleosynthesis with the r and s processes; n = neutron capture and β = beta decay

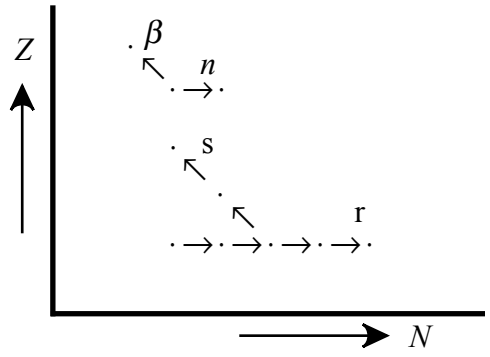

The r process conditions are not normally found inside stars; but such high neutron fluxes *can* be achieved in supernova explosions, which use endothermic reactions to produce the bulk of the elements beyond the iron peak: selenium, bromine, krypton, rubidium, tellurium, iodine, xenon, europium, gadolinium, terbium, dysprosium, holmium, erbium, thulium, ytterbium, lutecium, rhenium, osmium, iridium, platinum, gold, and uranium.

Also occurring in supernovae is the less prevalent **p process** – the capture of protons by various nuclei. This is of course more difficult, due to the Coulomb repulsion.

Carbon Burning and Beyond

As already noted, helium burning and alpha capture produce primarily ^{12}C and ^{16}O. These can be burned as follows.

For $T_6 \approx 600 \rightarrow 800$, **carbon burning** occurs:

$$^{12}C + {}^{12}C \rightarrow {}^{24}Mg + \gamma + 13.930 \text{ MeV}$$
$$^{12}C + {}^{12}C \rightarrow {}^{23}Na + p + 2.238 \text{ MeV}$$
$$^{12}C + {}^{12}C \rightarrow {}^{20}Ne + {}^{4}He + 4.616 \text{ MeV}$$
$$^{12}C + {}^{12}C \rightarrow {}^{23}Mg + n - 2.605 \text{ MeV}$$
$$^{12}C + {}^{12}C \rightarrow {}^{16}O + 2{}^{4}He - 0.114 \text{ MeV}$$

Then for $T_6 \approx 2000$, **oxygen burning** occurs:

$$^{16}O + {}^{16}O \rightarrow {}^{32}S + \gamma + 16.539 \text{ MeV}$$
$$^{16}O + {}^{16}O \rightarrow {}^{31}P + p + 7.676 \text{ MeV}$$
$$^{16}O + {}^{16}O \rightarrow {}^{31}S + n + 1.459 \text{ MeV}$$
$$^{16}O + {}^{16}O \rightarrow {}^{28}Si + {}^{4}He + 9.593 \text{ MeV}$$
$$^{16}O + {}^{16}O \rightarrow {}^{24}Mg + 2{}^{4}He - 0.393 \text{ MeV}$$

Products from the above reactions interact to form nuclides with mass numbers in the range from 16 to 28.

After carbon and oxygen burning, the most abundant nuclei are ^{32}S, ^{28}Si, and some ^{24}Mg. Then **photodisintegration** occurs, leaving mostly ^{28}Si:

$$^{32}S + \gamma \rightarrow {}^{31}P + p - 8.864 \text{ MeV}$$
$$^{31}P + \gamma \rightarrow {}^{30}Si + p - 7.287 \text{ MeV}$$
$$^{30}Si + \gamma \rightarrow {}^{29}Si + n$$
$$^{29}Si + \gamma \rightarrow {}^{28}Si + n$$

For $T_6 \approx 3000$, photodisintegration of ^{28}Si occurs:

$$^{28}Si + \gamma \rightarrow {}^{27}Al + p - 11.583 \text{ MeV}$$

At sufficiently high temperatures, many of the previous photon-producing reactions can run in reverse as endothermic photodisintegrations. At $T_6 \approx 2000$, the nuclei are approximately in equilibrium, and individual reaction rates become unimportant. These equilibrium processes result in nuclei with mass numbers in the range of 28 to 60.

Obviously, the whole sequence of nucleosynthesis becomes rather complex for the most massive stars. We present here a few summaries, to assist in grasping the overall picture. Table 13.1 gives the typical nuclear fuels and products associated with the principal burning stages.

Table 13.1: Nuclear burning stages (adapted from Avrett (1976))

Process	Fuel	Products	T_6
H burning	H	He	10 to 30
He burning	He	C, O	100 to 200
C burning	C	O, Ne, Na, Mg	600 to 800
Ne burning	Ne	O, Mg	1500
O burning	O	Mg to S	2000
Si burning	Mg to S	≈ Fe	3000

We recall from our discussion of the binding energy per nucleon that nuclear fusion is generally less efficient for heavier fuels. Each new core fuel provides a diminishing amount of energy to supply the star's luminosity; this is demonstrated by the calculated lifetimes of the different nuclear burning stages for a 25 $M_\odot$ star, as shown in Table 13.2.

Table 13.2: Lifetimes of core burning stages for a 25 $M_\odot$ star (Seeds 2008, 214)

Core Fuel	Phase	Lifetime
H	main sequence	7 million years
He	supergiant	500,000 years
C	supergiant	600 years
O	supergiant	6 months
Si	supergiant	1 day

The structure of such a star becomes rather complex. In the maximal mass stars – the only ones capable of such advanced reactions – a composition gradient will be maintained, with progressively heavier elements being found deeper inside the star. A shell source will be established at the base of each layer, to transform fuel from above into ash in the next layer below. Figure 13.18 provides a schematic diagram of the stellar interior at this point, with the radial coordinate not drawn to scale.

Figure 13.18: Onion-skin diagram of a 25 $M_\odot$ star (Kippenhahn & Weigert 1990)

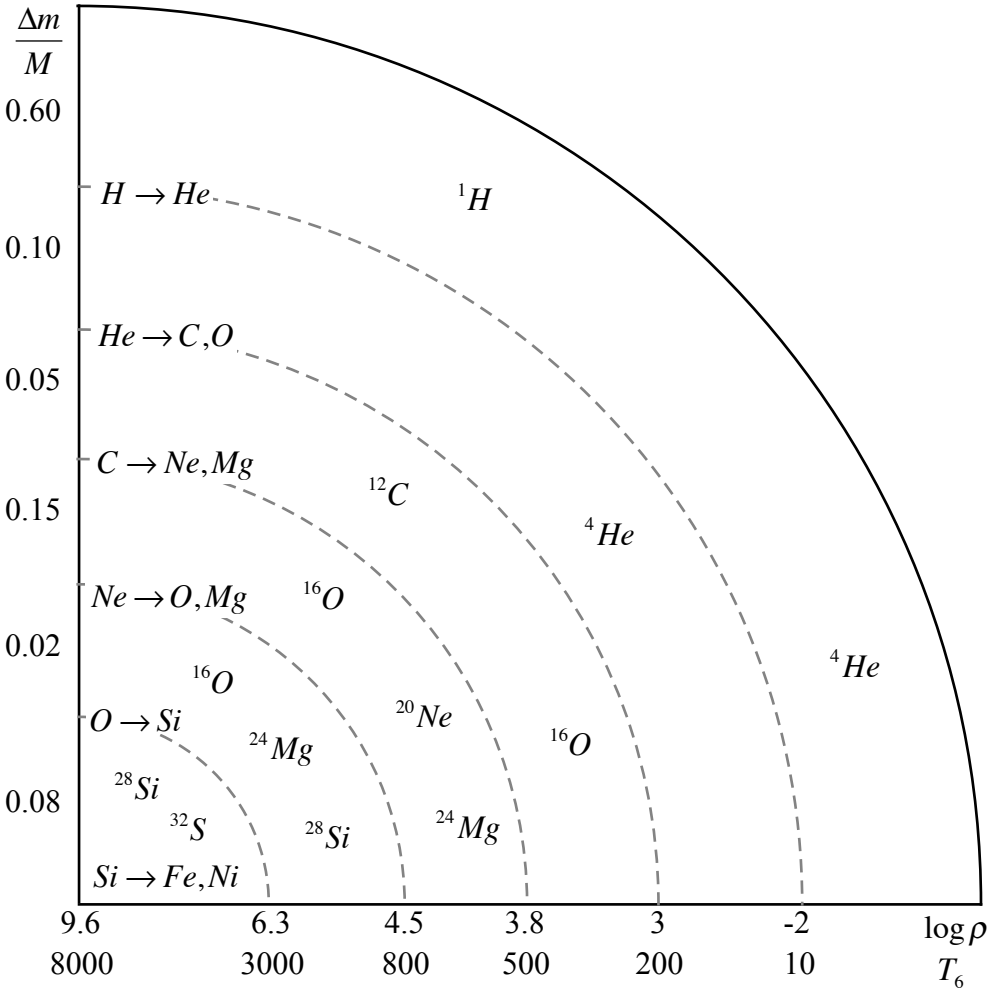

As its core turns into iron, a crisis looms for the star, for iron marks an extreme value of the binding energy per nucleon. Once iron-56 nuclei are formed, neither fusion nor fission can squeeze any more nuclear energy out of them; the ensuing core contraction will result in a supernova. We are now ready to consider this – and other terminal phases of stellar evolution – in the next chapter.

CHAPTER 14: Evolutionary Endpoints

Stars are not permanent objects; although they may exist relatively unchanged for billions of years, they do not last forever. As expected, we will find that stars of different masses will have different ultimate fates. We begin this chapter by reconnecting with the stars in our various mass groups.

Minimal Mass Stars

We left the minimal mass stars on the main sequence, where they were using their completely convective interiors to process their entire hydrogen supply into helium. Once this has been accomplished, the star will be a naked helium core, with no hydrogen envelope surrounding it. The star must then contract, but there will be no hydrogen shell to ignite, no hydrogen envelope to expand, and no insulating blanket of hydrogen to retain the core's heat. Furthermore, the star's contraction will not provide enough gravitational energy to produce helium ignition temperatures, and thus no nuclear reactions will ensue. Instead the star will slowly contract and heat, becoming denser and increasingly degenerate.

Such a small, hot, dense, degenerate star will be a helium **white dwarf** – but its formation is still far in the future, due to the extreme length of its progenitor's main sequence phase. Because we observe white dwarfs in the Galaxy today, we may conclude that there must be another, faster way to produce them. We will postpone further discussion of these objects until we find this pathway.

Medium and Low Mass Stars

When we left the medium and low mass stars, they were ascending the AGB in a futile attempt to ignite their carbon cores. Their expansion at this stage is powered by a helium-burning shell just outside the core and a hydrogen-burning shell farther out.

As the star expands up the AGB, the helium shell narrows and becomes unstable, resulting in **helium shell flashes** (or **thermal pulses**). These occur when the shell temperature rises, increasing the shell luminosity, which expands and cools the shell. (Recall that the reaction rate for the triple-alpha process is highly sensitive to temperature: $\varepsilon_{3\alpha} \approx T^{40}$.) Repeated shell flashes encourage mass loss, and the envelope mass is further reduced by the shell nuclear reactions. At high luminosities, the envelope becomes unstable to radial pulsations, producing a long-period variable star – an LPV, or Mira variable. During this phase, even more of the envelope mass is

lost as the pulsations elevate the atmosphere, increasing the density at large radii and enhancing the formation of dust grains. Radiation pressure accelerates the dust grains outward, and drag forces carry the gas particles along too, resulting in relatively high mass loss rates.

While the solar wind produces mass loss rates of $\approx 10^{-14}$ to $10^{-13} M_\odot$/year, LPV mass loss rates are estimated at about $10^{-6} M_\odot$/year. In some cases a **superwind** develops, with mass loss rates on the order of $10^{-4} M_\odot$/year. These higher rates result in a rapid thinning of the envelope.

Eventually the envelope mass becomes so low – about 1% of the star's mass – that it no longer hides the central regions of the star from view. As these deeper, hotter layers of the star are gradually revealed, the radius of the radiating surface decreases and the effective temperature increases. The luminosity remains essentially constant during this phase as it is produced by the helium-burning shell, which lies just above the core. The star thus evolves horizontally to the left across the HR diagram. When the effective temperature reaches about 30,000 K, sufficient ultraviolet radiation is emitted to ionize and excite atoms in the previously ejected envelope material, which in turn radiates visible light that we observe as a **planetary nebula**.

The **central star (CS)** in a planetary nebula – also known as a **planetary nebula nucleus (PNN)** – consists of the carbon-oxygen core of the former AGB star, surrounded by its helium-burning shell. As the envelope expands away from the core, it reduces the pressure on the core. The core then expands slightly, causing the remaining envelope just above the shell to contract and producing a separation between the envelope and the central star. The helium burning shell supplies the central star's luminosity; when the shell's helium supply is finally exhausted, the luminosity drops as the star cools, contracts, and becomes increasingly degenerate, gradually becoming a **white dwarf**. This provides an alternative method for producing white dwarfs that is considerably faster than waiting for minimal mass stars to move off the main sequence.

Figure 14.1: Evolution from AGB to white dwarf

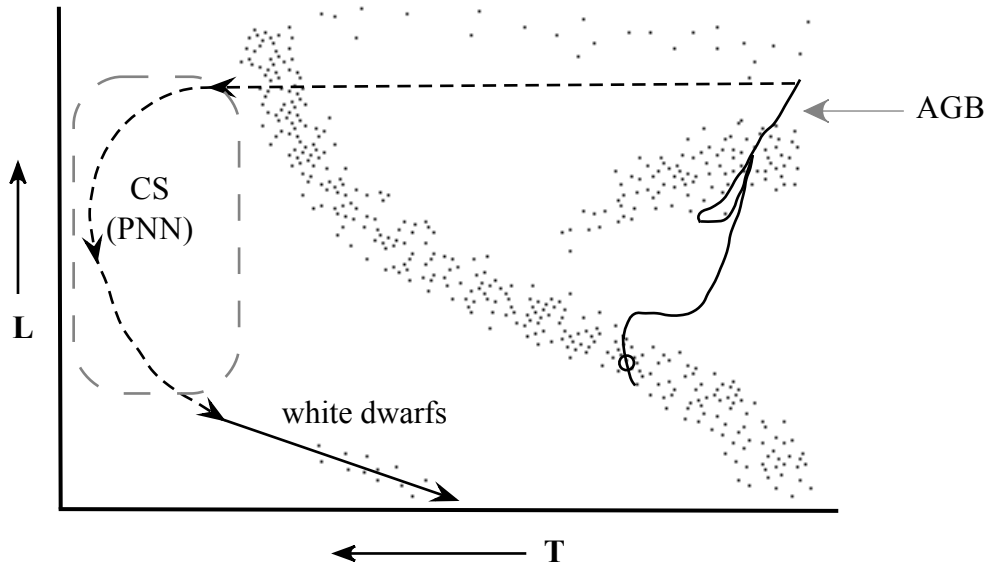

Figure 14.1 depicts the evolutionary track of a star as it transforms itself from a huge, red, pulsating AGB star to a small, hot, white dwarf. The downward turn just past the main sequence

occurs when the central star loses its helium-burning shell. Much of the pathway is dashed to indicate that we do not observe many stars in the intervening stages along this track; when we view an AGB star, we are looking at its envelope, but then we transition rapidly to direct observation of its core as the envelope becomes optically thin.

Planetary Nebulae

Figure 14.2: The Ring Nebula – a planetary nebula

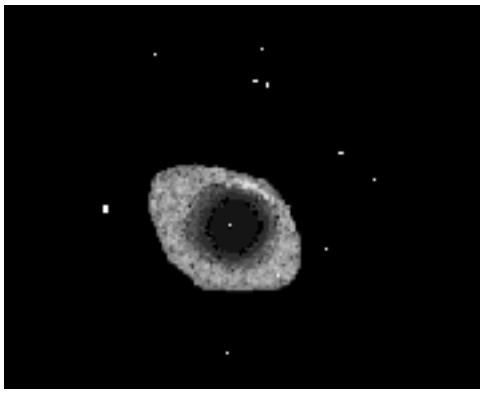

Planetary nebulae result from the ejection of envelope matter by an AGB star and the subsequent illumination of this matter by the hot central star that remains. The spectrum of a planetary nebula consists of emission lines from atoms that have been excited and/or ionized by ultraviolet radiation from the central star. In most of the better known objects, the nebulae are fairly circular in profile, resembling planets (hence the name). But the majority of planetary nebulae (≈ 80%) do *not* exhibit the spherical symmetry implied by the more circular nebulae, such as the Ring Nebula, shown in Figure 14.2. The cause of the variation in shapes of planetary nebulae is still being investigated; it may very well involve binary stars, magnetic fields, planetary disks, etc.

Planetary nebulae are reasonably common; there are about 1500 known, with an estimated 15,000 to 30,000 in the Galaxy. As judged by their kinematics and distribution in the Galaxy, planetary nebulae are old Population I objects. They are found mostly near the Galactic plane and concentrated toward the Galactic center; they are usually *not* found in star clusters, but they have have been found in a few globular clusters.

Planetary nebulae are transient objects, with the envelope gradually expanding and merging with the ISM on a time scale of ten thousand years or so; expansion velocities are typically about 20 km/s. The illumination of the nebula is produced by fluorescence, powered by ultraviolet radiation from the central star. Initial radii are about 0.1 pc, but when the radius of the nebula exceeds about 0.7 pc, the low density of the gas renders it essentially invisible. Alternatively, once the central star has cooled sufficiently, its radiation will be unable to keep the nebula ionized, and the recombined gas will cease its emissions. In any event, the planetary nebula phase is relatively brief.

About 25 planetary nebulae are estimated to by formed each year in the Galaxy. They are produced by stars covering a range of about 1 to 9 $M_\odot$; these produce central stars ranging from 0.6 to 1.1 $M_\odot$, with lower mass stars producing less massive central stars. (The break between

nebula and central star comes at the composition discontinuity at the bottom of the hydrogen-rich envelope.) Because core helium burning results in carbon-oxygen cores of about 0.5 $M_\odot$, it would appear that the less massive AGB stars in this range have their envelopes ejected by thermal pulses and/or a superwind before the helium-burning shell can add much mass onto the core. The high mass stars in this range must either eject a substantial fraction of their mass *before* the carbon core ignites *or* survive the carbon detonation and *then* eject the envelope, leaving an oxygen-neon-magnesium core to form the central star.

Central stars of planetary nebulae are among the hottest stars known, with effective temperatures up to about 200,000 K. Their luminosities range up to 100,000 $L_\odot$, and their radii extend down to 0.01 $R_\odot$. Central stars are the contracting, degenerate cores of former AGB stars, on their way to becoming white dwarfs.

White Dwarfs

White dwarfs occupy the lower left corner of the HR diagram. They are hot stars, with typical effective temperatures of 10,000 K or more, but they have very low luminosities, on the order of $10^{-3} \rightarrow 10^{-4}\ L_\odot$. These values imply that white dwarfs are very small – only about 0.01 $R_\odot$, or about the size of the Earth. Masses – obtained through spectroscopic determination of surface gravities – average around 0.6 $M_\odot$; white dwarfs in binary systems range up to about 1 $M_\odot$. Inserting a solar mass or so into a volume the size of the Earth produces a density of about a million g/cc – far denser than normal matter. We may conclude that white dwarfs must be degenerate.

The white dwarf is made up of a degenerate electron gas and a normal ion gas, the latter usually comprised of carbon and oxygen nuclei. A small gaseous fringe exists on the the surface, where the gravitational field is extremely intense – on the order of 300,000 *g*'s. An estimate of the atmospheric scale height seems to indicate that a plane-parallel atmosphere would be a suitable approximation in this case:

Eq. 14.1 $$H = \frac{\Re T}{\mu g} = \frac{(8.3e7)(10000)}{2(300000)(980)} = 1400\,\text{cm} = 14\ \text{meters} \quad \approx 2\times10^{-6} R_*$$

The degeneracy in a white dwarf is essentially complete, meaning that, up to the Fermi momentum, all available phase space cells are filled, with no filled cells beyond. The question is whether or not *relativistic* degeneracy occurs, and this depends on the white dwarf mass. Higher mass white dwarfs have stronger gravity, and they require higher pressure in order to achieve equilibrium. In a degenerate gas, higher pressure can only be achieved by higher density, as temperature is not a factor; therefore, high mass white dwarfs must have higher densities – the reverse of main sequence stars.

From Chapter 11 we have the following relations for a completely degenerate electron gas, using relativistic formulae. Higher densities correspond to higher values of $x, f(x)$, and P_e.

Eq. 11.50 $$P_e = \frac{\pi m_e^4 c^5}{3h^3} f(x)$$

Eq. 11.51 $$f(x) = x\left(2x^2 - 3\right)\sqrt{x^2+1} + 3\sinh^{-1} x$$

Eq. 11.52 $$x \equiv \frac{p_o}{m_e c} = \frac{h}{2m_e c}\left(\frac{3N_e}{\pi}\right)^{1/3} = \frac{h}{2m_e c}\left(\frac{3\rho N_A}{\pi \mu_e}\right)^{1/3} \quad \Rightarrow \quad \rho = \mu_e \frac{8\pi m_e^3 c^3}{3N_A h^3} x^3$$

For low mass, low density white dwarfs, the Fermi momentum will be low and the electrons will be non-relativistic. The pressure they exert is given by Equation 11.19 (which can be obtained by approximating $f(x)$ for $x \to 0$: the non-relativistic limit):

Eq. 11.19 $$P_{e,nr} = \frac{h^2}{20m_e}\left(\frac{3}{\pi}\right)^{2/3} N_A^{5/3}\left(\frac{\rho}{\mu_e}\right)^{5/3} = K\rho^{5/3} \qquad \text{where } K = (1.00360e13)/\mu_e^{5/3}$$

This is a polytrope with $\gamma = {}^5/_3 \Rightarrow n = 1.5$. We may then apply the mass-radius relation for polytropes (Equation 9.73):

Eq. 14.2 $$K = N_n G M^{\frac{n-1}{n}} R^{\frac{3-n}{n}} = N_{1.5} G M^{1/3} R = N_{1.5} G M_\odot^{1/3} R_\odot \left(\frac{M}{M_\odot}\right)^{1/3}\left(\frac{R}{R_\odot}\right)$$

Eq. 14.3 $$\frac{1.00360e13}{\mu_e^{5/3}} = (0.42422)(6.6743e-8)(1.9891e33)^{1/3}(6.9551e10)\left(\frac{M}{M_\odot}\right)^{1/3}\left(\frac{R}{R_\odot}\right)$$

Eq. 14.4 $$\left(\frac{M}{M_\odot}\right)^{1/3}\left(\frac{R}{R_\odot}\right) = \frac{4.0524e-2}{\mu_e^{5/3}}$$

And for $\mu_e = 2$, we find the mass-radius relation for non-relativistic white dwarfs:

Eq. 14.5 $$\left(\frac{R}{R_\odot}\right) = \frac{1.2750e-2}{\left(M/M_\odot\right)^{1/3}}$$

We note immediately that radius decreases weakly with mass; more massive white dwarfs are smaller! (Note also that this will be true for *any* polytrope for which $1 < n < 3$.)

Now as we build white dwarfs of greater mass, they become smaller, and obviously denser. As the density increases, the Fermi momentum increases and the higher momentum states become relativistic. We should then investigate the case of relativistic complete degeneracy, which will occur in a high mass white dwarf.

For high mass, high density white dwarfs, the Fermi momentum will be high and the electrons will be relativistic. The pressure they exert is then given by Equation 11.53 (which can be obtained by approximating $f(x)$ for $x \to \infty$: the relativistic limit):

Eq. 11.53 $$P_{e,rel} = \frac{hc}{8}\left(\frac{3}{\pi}\right)^{1/3} N_A^{4/3}\left(\frac{\rho}{\mu_e}\right)^{4/3} = K\rho^{4/3} \qquad \text{where } K = (1.24101e15)/\mu_e^{4/3}$$

This is a polytrope with $\gamma = {}^4/_3 \Rightarrow n = 3$. We again apply the mass-radius relation:

Eq. 14.6 $$K = N_n G M^{\frac{n-1}{n}} R^{\frac{3-n}{n}} = N_3 G M^{2/3} = N_3 G M_\odot^{2/3} \left(\frac{M}{M_\odot} \right)^{2/3}$$

Eq. 14.7 $$\frac{1.24101e15}{\mu_e^{4/3}} = (0.36394)(6.6743e-8)(1.9891e33)^{2/3} \left(\frac{M}{M_\odot} \right)^{2/3}$$

Eq. 14.8 $$\frac{M}{M_\odot} = \frac{5.8057}{\mu_e^2}$$

For $\mu_e = 2.0013$, we find $M/M_\odot = 1.4495$ (or 1.45 or 1.4, depending on the constants and precision used). This is a bit different from the non-relativistic relation obtained above, as it says nothing about the radius. Rather, it gives an upper limit on the mass in the highly relativistic case.

As we increase the white dwarf mass, the increasing density forces the electrons into higher energy states, and they become more strongly relativistic; as a result, the mass-radius relation – as shown in Figure 14.3 – gradually changes from the non-relativistic equation (black dots) to reach the relativistic mass limit at $R = 0$. This limit is known as the **Chandrasekhar limit**; white dwarfs cannot be made any more massive than this – about 1.4 $M_\odot$.

Figure 14.3: The mass-radius relation for white dwarfs (solar units)

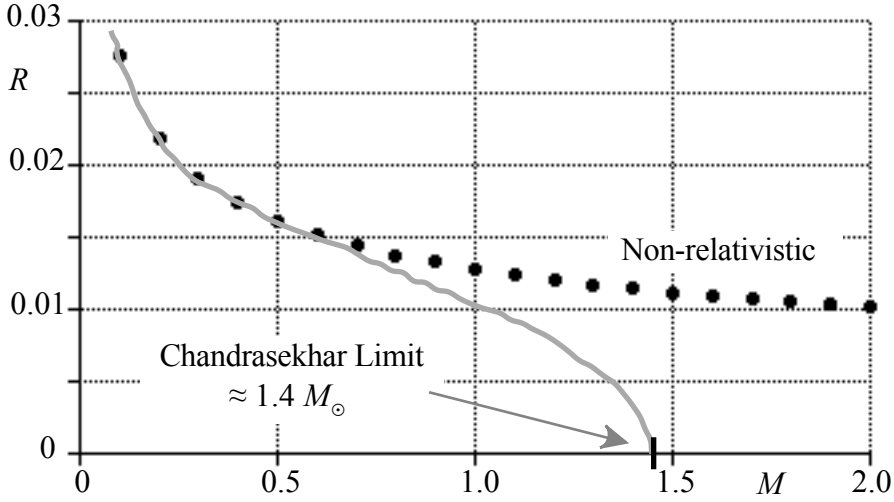

Being degenerate, a white dwarf, once formed, cannot contract further by itself. Being relatively cool inside, a white dwarf cannot do any nuclear fusion to generate energy from the fuel it has at hand. But white dwarfs do radiate and thus must draw on a source of energy to supply their luminosity; this source is the thermal energy of the nuclei, which are not degenerate. Their heat is transferred to the surface efficiently by conduction, keeping the interior of the star essentially isothermal. At the surface is a thin photosphere in which the electron gas is ideal, rather than degenerate; radiative transfer through this layer controls the heat flow and determines

the luminosity. The white dwarf cools without contracting, moving along a line of constant radius on the HR diagram. When it has cooled enough, it will no longer radiate any significant visible light; at this point it will be called a **black dwarf**.

We can estimate the white dwarf **cooling time scale** by dividing the star's thermal energy content ($E = {}^3/_2\ \Re T/\mu_i$ ergs/g) by its luminosity. (Here T is the temperature of the isothermal interior, rather than the effective temperature of the photosphere.) Inserting typical values ($T \approx 10^7$, $M \approx 0.6 M_\odot$, $L \approx 10^{-3} L_\odot$, $\mu_i \approx 12$) we find a time scale on the order of a billion years.

Eq. 14.9 $$t_{cool} = \frac{3}{2}\frac{\Re T}{\mu_i}\frac{M}{L} = \frac{3}{2}\frac{(8.3e7)(1e7)}{(12)(3.16e7(s/yr))}\frac{0.6(2e33)}{0.001(4e33)} \approx 1 \text{ billion yrs}$$

More detailed calculations that link the interior temperature to the luminosity can be utilized to give an expression for the time required for a white dwarf to cool to the luminosity indicated (from a much higher luminosity); results for typical white dwarf masses are shown in Figure 14.4.

Eq. 14.10 $$\Delta t_{cool} \approx 2.5 \times 10^6 \left(\frac{M/M_\odot}{L/L_\odot} \right)^{5/7} \text{ yrs}$$

Figure 14.4: White dwarf cooling times

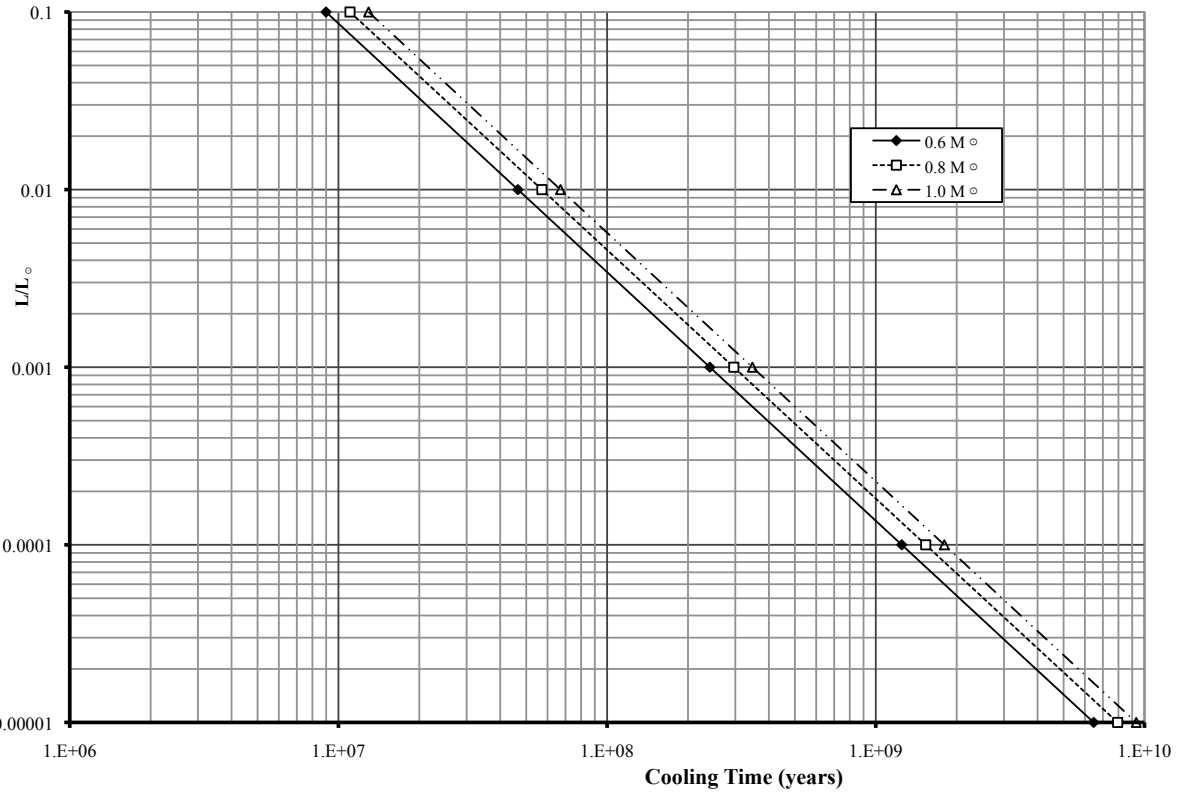

Clearly, the initial phases of cooling are quite rapid, but the process slows down as the luminosity drops. This should result in white dwarfs of a given mass collecting at lower luminosities, depending of course on the time of formation of the original star. As we have seen above, a white dwarf of 0.6 $M_\odot$ should develop from a main sequence star of about 1 $M_\odot$. Such a star would have a main sequence lifetime of about 10 billion years, followed by a giant phase of another billion years or so, leaving no more than about 1 or 2 billion years for the white dwarf cooling time. The majority of white dwarfs have cooled to effective temperatures that are somewhat greater than the Sun's; the age of the Galaxy places observable limits on the extent of cooling that has been achieved by normal white dwarf evolution.

The above discussion focuses on isolated white dwarfs; but white dwarfs do exist in binary systems, and their evolution can proceed along quite different lines, as will be discussed later.

High Mass Stars

The high mass stars have several options available at this point, as outlined here:

- A high mass AGB star may shed enough of its envelope mass that it becomes incapable of igniting carbon; in this case it should produce a planetary nebula with a carbon-oxygen central star, as described above.
- Or, the high mass star may ignite its degenerate carbon-oxygen core in a carbon detonation.
    - This may destroy the star in a supernova explosion (see **Supernovae**, below).
    - Or, the star may survive the event and perform core carbon burning.
        - It may then eject enough envelope mass to produce a planetary nebula with an oxygen-neon-magnesium central star (see **Planetary Nebulae**, above).

Obviously there is some degree of uncertainty here as to the exact pathway for a star in this mass range. Whether the stars share this same uncertainty is not clear.

Maximal Mass Stars

Stars of maximal mass manage to ignite carbon – and subsequent nuclear fuels – without their cores becoming degenerate. Once they develop the complex structure depicted in Figure 13.18, with multiple layers of different compositions and multiple shell sources in between, the next step is the production of iron nuclei by silicon burning in the core. As we have already seen, iron is incapable of yielding any nuclear energy through either fusion or fission, and this will create problems for the star.

Silicon burning creates an iron core and gradually increases its mass; when the core becomes massive enough, it contracts, and as its density increases, the core becomes more degenerate. When the degenerate core mass exceeds the Chandrasekhar limit, the contraction becomes even more rapid. The gravitational energy that is then released – which previously would have heated the core and ignited the next fuel – instead is applied to endothermic reactions.

In the first stages, **electron capture** by heavy nuclei reduces the number of electrons and hence, the degenerate electron pressure.

$$ {}_{Z}{}^{A}X + e^{-} \rightarrow {}_{Z-1}{}^{A}X + \nu_e $$

Then iron-56 nuclei are converted into alpha particles and neutrons.

$$\sim 100 \text{ MeV} + {}^{56}Fe \rightarrow 13\,{}^{4}He + 4n$$

Despite the increase in the number of particles, this does little to increase pressure in the core, and the contraction accelerates to a collapse in which the alpha particles are split apart into protons and neutrons, absorbing still more energy:

$$\sim 24 \text{ MeV} + {}^{4}He \rightarrow 2p^{+} + 2n$$

Once again, because the reactions are absorbing, rather than releasing energy, the core is not stabilized. Instead it implodes, crushing the protons and electrons together to form neutrons and neutrinos in another electron capture reaction:

$$p^{+} + e^{-} + \text{energy} \rightarrow n + \nu$$

(Note: The core does not exactly pause at each step to consider its options; rather the whole core collapse occurs on a time scale of a second or less.)

The core is not stabilized until the neutron gas thus produced becomes degenerate, at a density approaching 10^{15} g/cc and a radius of about 10 km. For stellar masses up to about 20 $M_{\odot}$, this core will become a **neutron star**; for higher mass stars, the core will be massive enough to form a **black hole**. The rest of the star – above the core – is expelled in a powerful explosion known as a **supernova**.

Supernovae

Supernovae are impressive events, with several different activities occurring in a relatively brief period of time. They are initiated by the core collapse described above, which releases sufficient energy to expel the outer layers of the star, create numerous heavy elements by endothermic reactions, light a temporary beacon to alert the local universe, send out shock waves to trigger star formation in surrounding interstellar clouds, and continue to illuminate the expelled layers for thousands of years to come, tantalizing those who missed the show.

The transformation of the core implosion into a supernova explosion appears to involve two mechanisms: in-falling material rebounds off the hard, dense core of neutrons formed in the reactions described above; and neutrinos created in the above reactions are absorbed by the overlying layers of the star, which are heated and blown off. (Recall that neutrino cross sections increase with the neutrino energy.)

To estimate the energy involved, we start with an iron core of about 1.4 $M_{\odot}$ and a radius of about 0.01 $R_{\odot}$ and then compress it to a 1.4 $M_{\odot}$ neutron star with a radius of 10 km. The potential energy released is as follows:

Eq. 14.11 $$\Delta\Omega \approx GM^2\left(\frac{1}{R_{NS}} - \frac{1}{R_c}\right) = (6.7e-8)(1.4)^2(2e33)^2\left(\frac{1}{1e6} - \frac{1}{7e8}\right) = 5.2\times10^{53}\text{ergs}$$

The nuclear energy released in converting iron into elementary particles can be estimated by multiplying the binding fraction for iron (~ 8.8 MeV) by the number of nucleons:

Eq. 14.12 $$\Delta E_{nuc} \approx f_B \frac{M_c}{m_H} = 8.8e6(eV)(1.6e-12\,ergs/eV)\frac{1.4(2e33)}{1.67e-24} \approx 2.4\times10^{52}\text{ergs}$$

The potential energy released is roughly an order of magnitude greater than the nuclear energy absorbed; thus there is considerable energy available to be used for other projects.

Supernova peak luminosities are on the order of 30 billion $L_\odot$, but they decline on a time scale of weeks to months. The radiated energy required can thus be estimated, and it appears to be easily within the energy budget:

Eq. 14.13 $$\Delta E_{rad} \approx L\,\Delta t = 3\times10^{10}\,(3.8\times10^{33})\times10^{7} \approx 1.1\times10^{51}\ \text{ergs}$$

Ejection of the envelope mass (on the order of 10 $M_\odot$) requires that it achieve escape velocity from the core's original radius:

Eq. 14.14 $$v_e = \sqrt{\frac{2GM_c}{R_c}} \approx \sqrt{\frac{2(6.7e-8)(1.4)(2e33)}{7e8}} \approx 7300\ \text{km/s}$$

We can then estimate the kinetic energy needed to launch the envelope:

Eq. 14.15 $$KE \approx {}^1\!/_2\, M v_e^{\,2} \approx {}^1\!/_2\,(10)(2e33)(7300e5) \approx 5.3\times10^{51}\ \text{ergs}$$

At this point we have created a core of neutrons, expelled the envelope, lit up the explosion, and still accounted for less than 10% of the gravitational energy made available by the collapsing core. If we further assume the production of about 1 $M_\odot$ of **r-process** elements with a net binding energy change of 1 MeV per nucleon, we may estimate this portion of the energy budget as follows:

Eq. 14.16 $$\Delta E_{heavy} \approx \Delta f_B \frac{M_{heavy}}{m_H} = 1e6(\text{eV})\left(1.6e-12\ \text{ergs/eV}\right)\frac{2e33}{1.67e-24} \approx 1.9\times10^{51}\text{ergs}$$

As this accounts for less than 1% of the total energy available, it would seem that there will be plenty of energy to make heavy elements, even if more massive stars are considered.

These conclusions may be reasonable, but only up to a point; much of the energy released in a supernova will be carried away by the huge numbers of neutrinos that are created when protons are converted to neutrons. As noted, some of these neutrinos will participate in the expulsion of the envelope, but a large fraction of them will escape directly from the dying star, carrying with them a significant amount of the collapsing core's energy. As even more massive stars are exploded, the core masses will increase and more energy-draining neutrinos will be created. At the same time, the energy needed to expel the envelope from the more massive core will rise to the point where the energy budget cannot be met. Under these conditions – perhaps found in stars above 40 $M_\odot$ – the star will no longer be able to afford a supernova, and it will produce a black hole without first blowing up.

Our opportunities to study supernovae using modern instrumentation have been somewhat limited, as there has not been a supernova visible in our Galaxy for over 400 years. The most famous of the historical supernovae occurred in the year 1054 when the Chinese observed a 'guest star' in the constellation Taurus; it is estimated to have reached an apparent magnitude of –7 and was visible to the naked eye for two years. When we point our telescopes today at the same position in the sky, we find the **Crab Nebula**. Edwin Hubble was the first to link these two

observations, allowing us to identify the Crab as a **supernova remnant** – the expelled envelope of an exploded star.

Figure 14.5: The Crab Nebula – a supernova remnant

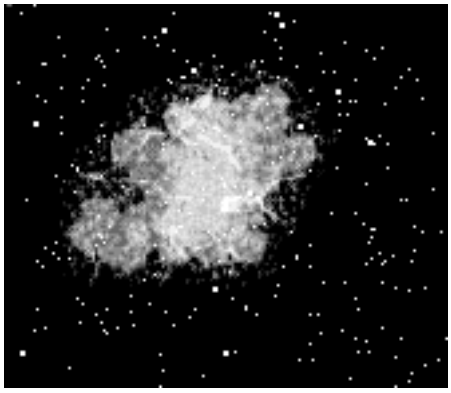

The Crab lies at a distance of about 2000 pc and has a radius of about 1.7 pc. Its expansion velocity has been measured by comparing images taken several years apart; after nearly 1000 years of expansion, this velocity has slowed to about 1500 km/s. The Crab is observed across the entire range of the spectrum, from gamma rays to radio wavelengths, and it is a source of synchrotron radiation (caused by high-energy electrons spiraling in a magnetic field). Its progenitor star is believed to have had a mass in the range of 8 to 12 $M_\odot$, based on the composition of the nebula.

Other supernova remnants can be found around the Galaxy; like the planetary nebulae, they are transient objects, and we have no observations of their progenitors. Supernovae are observed in other galaxies, but their great distances place limits on the observational data we can obtain from them. What astronomers would like is a supernova that occurs relatively nearby – but not so close that it would present a hazard to our existence!

In 1987, a supernova occurred in the Large Magellanic Cloud – safely located about 52 kpc away. SN1987A was noticed almost immediately and observations have been made continuously since then. In fact, neutrinos from the event were detected on Earth a few hours *before* the rising luminosity made the explosion visible; this is in agreement with theory, which predicts just such a delay due to the time required to expand the outer layers of the star, providing the dramatic increase in its luminosity. This event marked the first time that a supernova progenitor could be identified; its mass is estimated at about 18 $M_\odot$.

Supernovae are not all alike; they are classified according to their observational characteristics (spectra and light curves). The basic division is simple:

- **Type I** supernovae exhibit no hydrogen lines.
- **Type II** supernovae show strong hydrogen lines in emission.

Type I can be further subdivided:

- **Type Ia** has a strong Si II absorption line at 6150 Å near maximum light.
- **Type Ib** has a strong He I line at 5876 Å and no Si II absorption around 6150 Å.
- **Type Ic** has weak or no helium lines and no Si II absorption around 6150 Å.

Both Types I and II have rise times (time to reach maximum light) of several days and they remain near maximum for several days. Type Ia supernovae are about ten times more luminous than Type II. Types Ib and Ic are *less* luminous than Type II, but have light curves *similar* to Type II.

Figure 14.6: Typical light curve for Type Ia supernovae

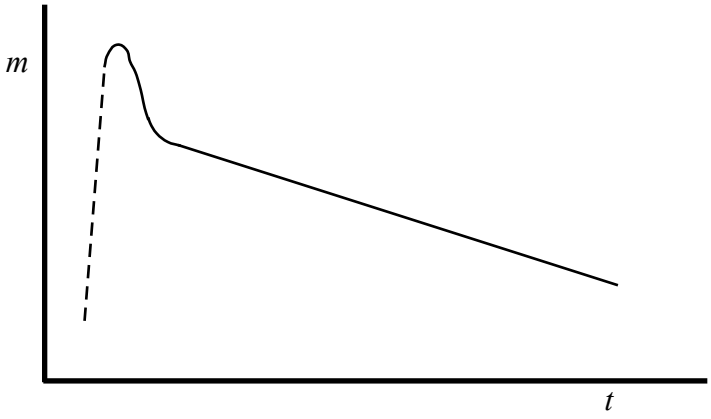

The Type Ia light curve shows a rapid decline for about 30 days, then an approximately exponential decline ($L \approx L_o e^{-t/\tau}$) with a time constant (τ) of about 70 days, as shown in Figure 14.6. This is the same for essentially all Type Ia supernovae.

Type II light curves show a decline that varies from one supernova to the next. In general there is an initial decline of about 25 days, then a level portion of 50 to 100 days, followed by a further rapid decline.

Type Ia supernovae are found in all galaxies, even those with no evidence of recent star formation. They occur at the same rate in both spiral and elliptical galaxies. Type II supernovae are found *only* in spiral galaxies, near sites of recent star formation (the spiral arms).

From these observations, we may conclude that Type II supernovae result from young, Population I stars with masses greater than about 8 to 10 $M_\odot$ (our maximal mass stars). On the other hand, Type Ia supernovae are produced by old, Population II stars of relatively low mass. Types Ib and Ic are judged to be similar to Type II. The following theoretical mechanisms have been proposed to explain the observational differences:

- A Type II supernova results from the collapse of the degenerate iron core of a massive star, as described above.
- A Type Ib supernova results from the collapse of the degenerate iron core of a massive star that has previously shed its hydrogen envelope.
- A Type Ic supernova results from the collapse of the degenerate iron core of a massive star that has previously shed its hydrogen and helium envelopes (a naked core collapse).

Core collapse requires a core mass in excess of 1.4 $M_\odot$ while production of an *iron* core requires a star larger than 8 $M_\odot$. Thus, the above supernovae mark the ends of the maximal mass stars, but they are unattainable by less massive stars.

A Type Ia supernova involves **mass transfer** onto a white dwarf in a close binary system. This situation can result when the primary – the more massive star in the original binary – evolves first and produces a white dwarf. The secondary star then evolves off the main sequence, becoming a red giant; as it expands to fill its Roche lobe, the secondary begins to transfer matter onto the white dwarf, as shown in Figure 14.7. Two different scenarios are possible, depending on the white dwarf's mass.

If the white dwarf's mass is near the **Chandrasekhar limit**, the higher pressure and temperature caused by the increasing mass ignites carbon in the center. Because the white dwarf is degenerate, this results in a thermal runaway that blows the star apart as a Type Ia supernova. Because this ignition always occurs at a mass near 1.4 $M_\odot$, the peak luminosity is fairly predictable, making these supernovae very useful as distance indicators.

Figure 14.7: Mass transfer in a close binary system

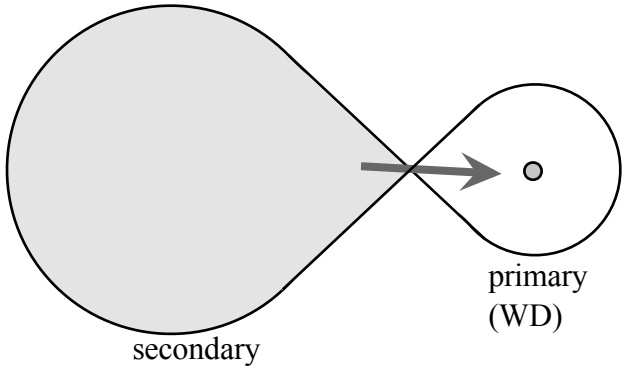

If the white dwarf mass is significantly lower than the Chandrasekhar limit, the result will be somewhat less dramatic. In this case, the accumulation of hydrogen-rich matter on the white dwarf surface will hinder radiative cooling of the star, increasing the temperature at the base of the hydrogen layer. When hydrogen fusion temperature is reached, the accumulated surface layer ignites, blowing itself off the star in an explosion known as a **nova** (more specifically, a **classical nova**). This sequence may repeat on time scales of about 10^4 years as the evolving star continues to transfer matter to the white dwarf, but we have no observational records to support this prediction. Luminosities of novae are significantly lower than those for Type Ia supernovae, by a factor of about 10^{-5}.

Related objects include the **recurrent novae**, which erupt at intervals of 10 to 100 years. These may occur on more massive white dwarfs, which have stronger surface gravity and can attain hydrogen ignition temperature after a shorter mass transfer period. Continued mass transfer may eventually increase the white dwarf mass to near the Chandrasekhar limit, when it will ignite the carbon in the core as a Type Ia supernova.

Classical novae and recurrent novae are two representatives of a group of systems called **cataclysmic variables** (CV's). All of these involve a close binary system containing a white dwarf that is the target of mass transfer from the larger companion.

Neutron Stars

As we saw above, the collapse of the iron core of a star can result in a neutron star – a sphere of degenerate neutrons at nuclear density, about 10^{14} to 10^{15} g/cc. A neutron star with a radius of 10 km and a mass of 1.4 $M_\odot$ would have a density of 6.7 $\times 10^{14}$ g/cc. In reality, the neutron star's structure is fairly complex, with an atmosphere and a solid crust that still contain nuclei and electrons, but these gradually transform into degenerate neutrons deeper in the star.

Neutron stars are theoretical beasts; they were predicted in 1934, over 30 years before they were discovered in the sky. These extremely compact objects are so tiny that their low luminosities make them quite difficult to observe: a 10-km neutron star would need to maintain an effective temperature of 1.5 million K in order to produce a luminosity equal to the Sun's – a feat that some young neutron stars may be able to accomplish. But fortunately for us, the neutron star has special properties that aid in its detection.

A neutron star should have a very strong magnetic field, due to the collapse of the core that initiates the supernova. The magnetic field lines follow the charged particles and wind up being rather densely packed together in the neutron star. (It is actually the neutrons star's small collection of protons and electrons – on the order of 10% of the neutron total – that are responsible for producing the currents that generate the magnetic field.) While the Earth's surface magnetic field strength is about 0.5 gauss, and the Sun's is around 1 gauss, the neutron star's field strength is on the order of 10^{12} gauss. This field is so strong as to constrain the radiation from the neutron star, beaming it along the axis of the magnetic field.

A neutron star should also be spinning fairly rapidly, due to conservation of angular momentum. If no external torques are applied to the core during the collapse phase, then the angular momentum of the neutron star should be equal to the angular momentum of the iron core before the collapse. The greater the reduction in the core radius, the greater the resulting spin rate.

A solid, uniform sphere has a moment of inertia $I = {}^2/_5 MR^2$; the angular momentum is then $I\omega = {}^2/_5 MR^2\omega$, where ω is the spin rate. Applying conservation of angular momentum across the collapse, we find $R^2\omega = R_o^2\omega_o$ or $P = P_o(R/R_o)^2$, where P is the period and the subscripts indicate initial values (before the collapse). Assuming initial values of $R_o = 0.01\ R_\odot = 7\times10^8$ cm and $P_o =$ 5 days $= 4.32\times10^5$ s , and a neutron star radius of 10 km $= 10^6$ cm, we calculate a spin period on the order of a second:

Eq. 14.17 $$P = P_o\left(\frac{R}{R_o}\right)^2 = (4.32e5)\left(\frac{1e6}{7e8}\right)^2 = 0.88 \text{ s}$$

Pulsars

This predicted combination of a strong magnetic field and a high spin rate is what led to the identification of neutron stars as the likely causes of **pulsars**, which were discovered in 1967. Pulsars revealed themselves by emitting pulsed radio signals with very regular periods on the order of a second. At first labeled LGM's (for Little Green Men), the pulsars were observations

in need of a good astrophysical explanation. There are only a few ways to generate such pulses: pulsation, rotation, and revolution are the principal choices, and of these, rotation seems most likely for such short periods.

Of course a rapidly rotating body will require a large centripetal acceleration at its equator, and this must be supplied by the force that holds the body together. In the case of most astrophysical objects, this force will be gravity, which depends on the mass and radius of the object. We can then estimate the minimum spin period for a spherical body of mass M and radius R by equating the gravitational acceleration at the equator to the centripetal acceleration:

Eq. 14.18 $$\frac{GM}{R^2} = \omega^2 R \quad \Rightarrow \quad P = \frac{2\pi}{\omega} = 2\pi\sqrt{\frac{R^3}{GM}}$$

We now explore some possible candidates, to see what types of objects might produce these periods. For the Sun, $R = 7 \times 10^{10}$ and $M = 2 \times 10^{33}$, giving $P = 10^4$ s = 2.8 hours. Obviously, the pulsars are not normal stars; something more compact, with stronger gravity is needed.

For a white dwarf, $R = 7 \times 10^8$ and $M = 2 \times 10^{33}$ gives $P = 10$ seconds. While this value approaches the general neighborhood of the pulsar periods, it is still too high. We need an object even more compact than a white dwarf.

For a neutron star, $R = 10^6$ and $M = 2.8 \times 10^{33}$ gives $P = 4.6 \times 10^{-4}$ seconds. This result is completely satisfactory; it is also compatible with observations of the **millisecond pulsars** (see below).

The periods of pulsars are thus covered by rapidly rotating neutron stars; shorter pulsar periods than predicted by our estimate of 0.88 seconds could be achieved by a more rapidly spinning iron core or perhaps by a stationary accretion shock instability (SASI), an acoustic wave that may develop during the collapse, depositing matter and angular momentum onto the forming neutron star.

The actual pulses are then explained by incorporating the magnetic field and its beamed radiation. If the magnetic field axis is not aligned with the rotational axis, the beams will sweep around the sky similar to a searchlight, sending pulses of radiation to observers in their paths. Thus, the only pulsars we see are the ones that point their beams at us during some time in their rotation; but each pulsar has two beams, aimed in approximately opposite directions, that can provide reasonable coverage of the sky.

The first pulsar discovered was PSR B1919+21, with a period of 1.337 seconds and a pulse width of 0.04 seconds. The best known pulsar, with a period of 0.033 seconds, resides in the Crab Nebula; it pulses at many different wavelengths, including visible light, in which the star can be seen blinking off and on 30 times each second. Pulsars are fairly common, with over 1000 known in the Galaxy; periods range from about 5 seconds down to 1/600 second.

Pulsar periods are observed to increase over time. This should occur as the spinning neutron star gradually converts some of its rotational kinetic energy into radiation. Younger pulsars – such as the Crab – should have relatively short periods.

The very shortest periods are attributed to pulsars in close binary systems in which matter and angular momentum are transferred from the companion onto the neutron star, increasing the

spin rate; these are the **millisecond pulsars**, which have periods in the 1 to 10 millisecond range. In some systems, mass transfer can coat the neutron star with a layer of hydrogen and helium, which heats and ignites, producing an **x-ray burster** – a scenario reminiscent of a nova.

Formation of a pulsar/neutron star requires the collapse of the degenerate iron core in a massive star. This occurs when the mass of the degenerate core exceeds the Chandrasekhar limit, about 1.4 $M_\odot$. However, in extremely massive stars, the iron core can grow significantly larger, with a somewhat different result.

Black Holes

In stars greater than about 20 $M_\odot$, the iron core grows to more than 3 $M_\odot$ – the estimated upper limit on the mass of a neutron star. When the core eventually contracts, it has enough gravity to overwhelm not only the degenerate electron pressure that supports white dwarfs, but also the degenerate neutron pressure that supports neutron stars. At this point there is no known structure that can successfully oppose gravitational collapse, and the core mass will compress itself into a point, producing an entity known as a **black hole**.

We will not attempt a detailed explanation of black holes as that would involve the theory of general relativity, which will not be presented here. Instead, we will note a few of the basic characteristics of black holes, to distinguish them from neutron stars and white dwarfs.

A black hole gets its name from the fact that it does not radiate light – or any other electromagnetic radiation. This is because the black hole mass has been compressed so much that its escape velocity is greater than the speed of light. The escape velocity is given by the standard formula:

Eq. 14.19 $$v_e = \sqrt{\frac{2GM}{R}}$$

Equating this velocity to the speed of light, we find the limiting value known as the **Schwarzschild radius** R_s :

Eq. 14.20 $$R_s = \frac{2GM}{c^2}$$

The Schwarzschild radius defines a spherical surface called the **event horizon**; a mass compressed to within its event horizon will be effectively invisible, as no photons will be able to escape from it. Events taking place within this surface are 'over our horizon' and thus not visible to us.

The Schwarzschild radius is proportional to the mass of the object; more massive objects have larger event horizons. For the Earth, $R_s \approx 1$ cm; for the Sun, $R_s \approx 3$ km; and at the 3 $M_\odot$ limit for neutron stars, $R_s \approx 9$ km, which is the same order of magnitude as the neutron star radius. Thus, it does not seem totally implausible that a massive core might collapse to this size.

In stars up to about 40 $M_\odot$, the core collapse to a black hole will be accompanied by a supernova explosion, but for stars greater than 40 $M_\odot$, no supernova will occur. Instead, it is believed that the remaining matter will collapse into the black hole.

Thus, the most massive stars should produce black holes of a few solar masses as they wrap up their careers, but unless these objects happen to exist in binary or multiple systems, we will have an extremely difficult time detecting them. The vast majority of stars will retire as white dwarfs.

Figure 14.8: Endpoints of stellar evolution

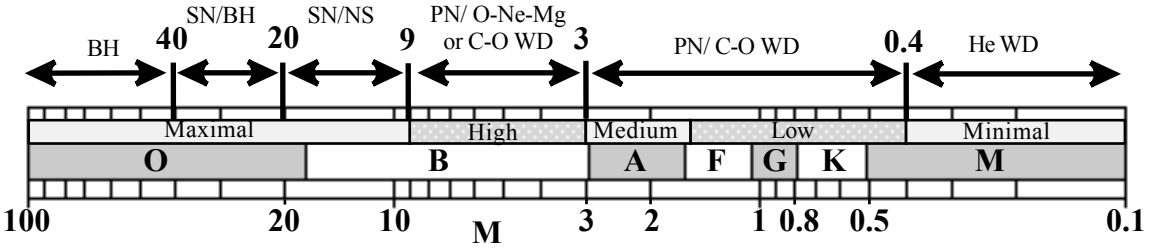

We now have a general picture of the reasons why stars evolve and the various objects they create in the process. In the next chapter we will summarize these stellar stories and compare our predictions about stellar evolution with observations of actual groups of stars.

CHAPTER 15: Evolution Conclusions

Previous chapters have focused on assembling the physics necessary to model stars and predict their behavior. In this chapter we will compare these predictions with observations of collections of real stars, to gauge whether our models are sufficiently detailed and accurate.

Stellar Stories

We begin by giving a brief summary of the evolution of stars in each of our five mass groups, to provide an unbroken story line for each.

Minimal Mass Stars: Mid to Late M Stars

Minimal mass stars ($0.4\ M_\odot > M > 0.08\ M_\odot$) evolve very slowly to the main sequence. Their low masses and gravities raise their cores to hydrogen fusion temperatures, but the stars retain relatively cool interiors. The resulting high opacities produce convective transport throughout their interiors; this insures the stars will have extremely long main sequence lifetimes (on the order of 100 billion years) as they slowly process *all* of their hydrogen to helium by the proton-proton chain. Following the main sequence their dense, degenerate cores will become even more degenerate as the stars contract to produce helium white dwarfs. But none of these stars should have reached this stage as yet because the universe has not provided sufficient time, being only about 14 billion years old.

Low Mass Stars: F, G, K, and Early M Stars

Low mass main sequence stars ($1.5\ M_\odot > M > 0.4\ M_\odot$) generate energy primarily by the pp chain, but the CNO cycle contributes equally in the earlier stars in this range. In the later stars, the pp chain results in a radiative core, which becomes larger in the earlier stars. The low interior temperatures and higher opacities produce an outer convective zone that shrinks with the higher temperatures of the earlier stars.

At the end of the main sequence lifetime – on the order of 10 billion years – these stars ignite a hydrogen-burning shell around the core; the partially degenerate helium core contracts very slowly on a nuclear time scale as ash from the shell increases its mass. As the core contracts and heats, the envelope expands and cools, pushing the star up the red giant branch. When the degenerate core reaches helium ignition temperature, it ignites in the helium flash. As the star recovers from this ignition event, its core expands, slowing the hydrogen shell reactions; this reduces the luminosity from its peak value at the red giant tip, and the star settles onto the

horizontal branch with a helium-burning core and a hydrogen-burning shell. Metal-rich stars form the red clump while metal-poor stars extend the horizontal branch farther toward the blue.

When core helium is exhausted, the star returns to the red and ascends the asymptotic giant branch, with a carbon-oxygen core, a helium-burning shell, and a hydrogen-burning shell. While on the AGB the star gradually loses envelope mass through pulsations and/or a stellar wind, eventually revealing the hot stellar core. The ejected envelope matter is bathed in ultraviolet radiation from the central star, causing it to radiate visible light as a planetary nebula; the central star gradually cools to become a carbon-oxygen white dwarf.

Medium Mass Stars: A Stars

Medium mass main sequence stars ($3\ M_\odot > M > 1.5\ M_\odot$) generate energy primarily by the CNO cycle, although the later stars have a significant pp contribution as well. The CNO reactions produce a convective core while the higher stellar temperatures and resulting lower opacities create a radiative envelope.

After about 1 billion years on the main sequence, these stars ignite a hydrogen-burning shell around the isothermal helium core. Addition of helium ash to the core initiates core contraction on the comparatively rapid thermal time scale; however, as the star evolves off the main sequence, its evolution rate slows, due to the increasingly degenerate helium core. The degeneracy continues to rise as the star ascends the RGB, igniting helium in a helium flash at the red giant tip before settling onto the horizontal branch.

The remaining story is the same as for the low mass stars, but the evolution rate is faster. Helium burning produces a carbon core, which contracts, igniting a helium-burning shell interior to the existing hydrogen-burning shell. The increased luminosity generated by these shell sources drives the star up the asymptotic giant branch, where it sheds some of its outer layers by way of an increased stellar wind and/or pulsations as a long-period variable star. When the envelope has thinned sufficiently, the core becomes visible as a hot central star; its ultraviolet emissions are absorbed by the previously ejected envelope layers, which emit visible radiation to produce a planetary nebula. The central star cools and forms a carbon-oxygen white dwarf, while the nebula expands and thins, eventually merging with the interstellar medium.

High Mass Stars: Mid to Late B Stars

The hot, high mass main sequence stars ($9\ M_\odot > M > 3\ M_\odot$) obtain energy by the CNO cycle and thus have convective cores and radiative envelopes; they evolve quickly, with main sequence lifetimes of about 100 million years. Following this, they ignite hydrogen-burning shells while their helium cores contract rapidly on a thermal time scale. This causes the stars to move swiftly across the Hertzsprung gap on the HR diagram to the giant branch, where they ignite helium smoothly in a relatively non-degenerate core.

During the core helium-burning phase, the stars follow tracks that loop toward the blue on the HR diagram, with some existing as Cepheid variables for awhile. Following the production of a carbon-oxygen core and ignition of a helium-burning shell, the high mass stars ascend the AGB, where they also lose mass from their envelopes. Although they initially have the mass necessary to compress their cores to carbon ignition temperatures, most of them probably do not

attain this goal, due to significant loss of envelope mass. These stars will produce planetary nebulae with carbon-oxygen white dwarfs.

The earlier stars in this range may lose some mass but still manage to ignite their cores in a carbon detonation. If sufficient mass loss continues during the core carbon-burning stage, these stars can produce planetary nebulae and oxygen-neon-magnesium white dwarfs.

Maximal Mass Stars: O and Early B Stars

The maximal mass stars ($M > 9\ M_\odot$) evolve very quickly, existing on the main sequence for only 100,000 to 10 million years or so. Following the main sequence, the helium core contracts immediately (on a thermal time scale) and ignites before moving very far off the main sequence. Each new nuclear fuel is ignited without interference by degeneracy as the star drifts across the HR diagram to the red. These stars are so hot that they have significant stellar winds on the main sequence and beyond, resulting in continual loss of mass from their envelopes.

The interior of the star processes increasingly heavier elements, eventually creating an iron core surrounded by multiple layers of different compositions. The ensuing gravitational collapse of the core results in a supernova in most cases, with the core forming a neutron star (and possible pulsar) in the later stars or a black hole in the more massive cases. The supernova remnant enriches the interstellar medium with heavy elements processed in the stellar interior and during the explosion itself. The most massive stars may transform directly into black holes, without any supernova phase.

Stellar Samples

Having described the evolution of stars – using primarily theoretical considerations – we would now like to determine how well these predictions correlate with actual stellar performance. What types of stars do we observe, and what fraction of all stars make up each type? The answers to these questions are complicated by several factors.

Time Scales

Stars evolve at different rates during their various stages of their existence. This occurs because the physical processes that produce the various stages proceed on different time scales. This affects our observations because we are more likely to find stars in the stages in which they spend the most time – if these stages are indeed represented in the current stellar population. Further, these time scales also depend on mass, such that more massive stars evolve more rapidly through every phase, making the lower mass stars more likely to be available for observation. The mix of stars available for us to observe is thus a function of both time and mass.

We illustrate this dependence by considering the first two stages in a star's life: the pre-main sequence and main sequence phases. In each of these phases, the most massive stars evolve most rapidly, but because they are regulated by thermal and nuclear time scales, respectively, the two phases differ in length by about two orders of magnitude. Figure 15.1 shows the variation of pre-main sequence time with mass.

Figure 15.1: Approximate pre-main sequence times (data from Iben (1967))

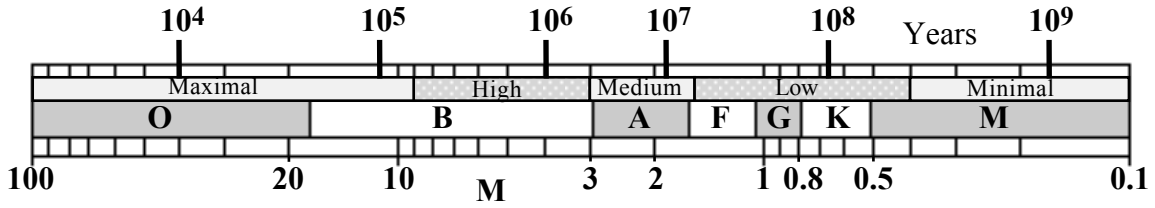

The trend shown above continues on the main sequence. Figure 15.2 shows approximate main sequence lifetimes, calculated using Equation 12.23 and an estimated lifetime of 10 billion years for a 1 $M_\odot$ star. Note again that these times are typically about two orders of magnitude greater than the pre-main sequence times.

Figure 15.2: Approximate main sequence lifetimes

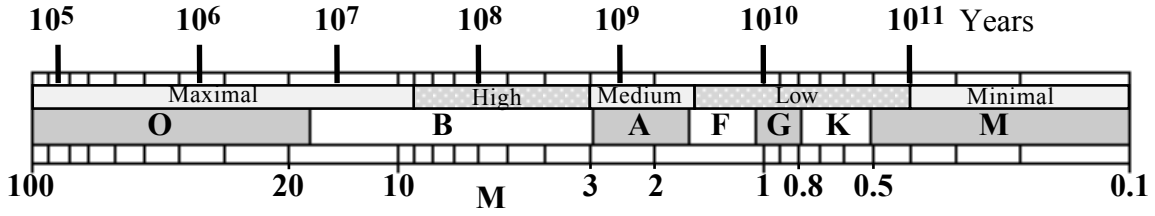

The Initial Mass Function

The next factor involves the distribution of stellar masses that are manufactured during star formation. The stellar **initial mass function** (Cox 2000) gives the relative number of stars formed per unit solar mass:

Eq. 15.1
$$\xi(M) = \begin{cases} 0.035 M^{-1.3} & \text{for } 0.08 \le M \le 0.50 \\ 0.019 M^{-2.2} & \text{for } 0.50 < M \le 1.00 \\ 0.019 M^{-2.7} & \text{for } 1.00 < M \le 100 \end{cases}$$

We illustrate this function by calculating the number of stars formed for every one star with a mass of 50 $M_\odot$, as shown in the next figure.

Figure 15.3: The initial mass function – scaled to one star of 50 $M_\odot$

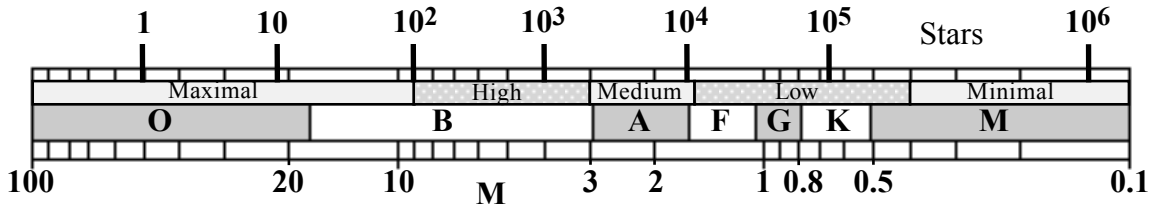

It is apparent that there are far more stars formed at the low end of the mass range; this – together with the more gradual evolution of less massive stars – should result in a greater number of these stars being observed. But there is another factor to include.

Selection Effects

We must also keep in mind the relevant selection effects; stars with high luminosities are more readily detected at large distances while those with very low luminosities will be essentially invisible, unless they are quite nearby. As lower luminosities are generally associated with lower stellar masses, selection effects tend to work *against* the previously discussed factors.

The overall combination of factors involved will generally result in stars from either the minimal or maximal main sequence mass groups being underrepresented in our observational samples, unless we make a special effort to include them. We may do this by limiting or expanding the volume of space from which we obtain our sample.

Observational Data

Our two principal variables in stellar evolution are the mass and the age of the star. We have already examined the changes that occur in stars of a particular mass range as they age, but these predictions are difficult to compare with real stars simply because stellar evolution normally progresses on extremely long time scales. Another way to obtain a comparison would be to examine stars of a particular age, over a range of stellar masses. Happily, this can be done.

To obtain our predictions, we may set up computer models of stars over the full range of masses and then run each model for the same length of time. The positions of the stars on an HR diagram will trace out an **isochrone** – the locus of stars of different masses that are all the same age; by varying the evolution time of the models, we may obtain isochrones for different ages.

From our calculated values for the pre-main sequence times and main sequence lifetimes, we can predict the approximate mass range that will populate the main sequence at any given age. These results are shown in the next figure.

Figure 15.4: Main sequence populations for different isochrones

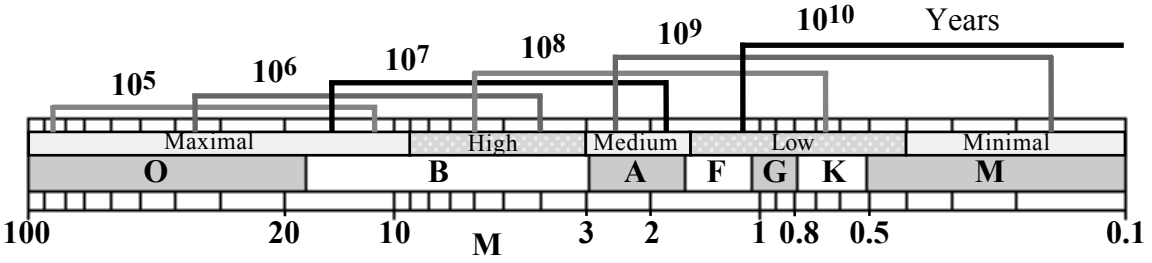

We now use this information to construct HR diagrams for a theoretical group of stars at five different ages, sketching isochrones and adding giants, supergiants, etc. as needed. Figure 15.5 displays these results.

Explanations of these predictions are as follows:

At one million years, the main sequence is populated by stars in the approximate mass range from 35 to 4 $M_{\odot}$. The less massive protostars are still approaching the main sequence while the most massive stars have already lived out their main sequence lifetimes and moved on to the supergiant region. The most massive of these will have produced black holes – which do not appear in the diagram.

Figure 15.5: HR diagrams for stars of different ages

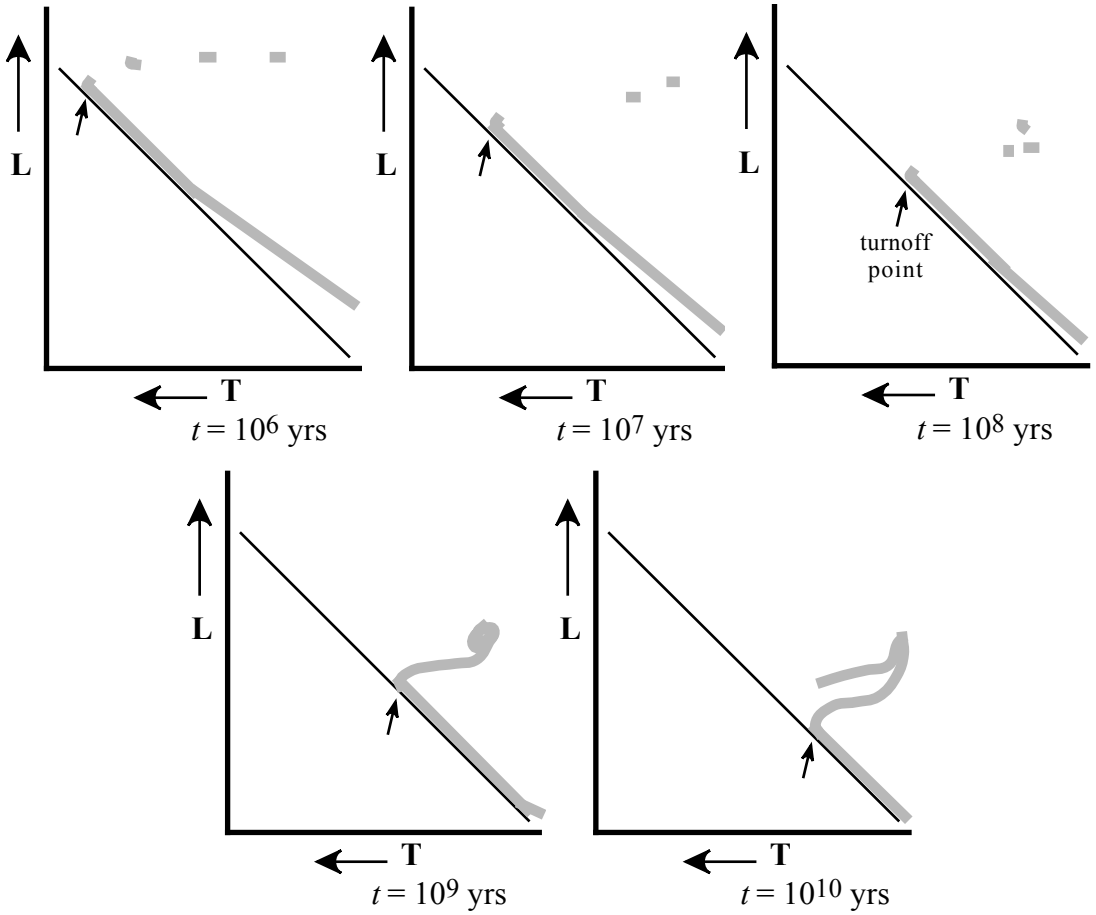

After 10 million years, the low and minimal mass protostars continue to move toward the main sequence. Most of the maximal mass stars have left the main sequence to become supergiants, with the most massive of this group destroyed by supernovae. The main sequence is populated by stars with masses from about 15 to 1.8 $M_\odot$.

By 100 million years, the lower main sequence is nearing completion, but the early to mid B stars have evolved off to the giant region; the Hertzsprung gap makes a clear distinction between the upper main sequence and the giants. The main sequence mass range is now between about 6 and 0.65 $M_\odot$.

In one billion years, the lower main sequence is essentially filled while all of the high mass stars will have disappeared. The more slowly evolving medium mass stars are seen moving off the main sequence and up the red giant branch in a nearly continuous band. The main sequence masses now range approximately from 2.5 to 0.16 $M_\odot$.

After 10 billion years of evolution even the very lowest mass stars will have arrived on the main sequence, but not many others will be left. All stars more massive than the Sun will have evolved off the main sequence. Stars around 1 $M_\odot$ will form the red giant branch and horizontal branch, with higher mass stars having moved on to their respective endpoints.

In viewing these diagrams, we observe a continuous change over time in the positions of stars that are arriving at the main sequence and leaving the main sequence. The former point is less easily identified, for it involves stars of lower luminosity and a less obvious break with the main sequence line. The upper point (small arrows), where the most massive stars are moving off the main sequence to become giants or supergiants, is known as the **turnoff point**. The farther down the main sequence we find the turnoff point, the older the group of stars will be.

All that remains is to find a group of stars that are all the same age, plot an HR diagram for them, and compare the result with the calculated isochrones.

Color-Magnitude Diagrams

Fortunately, some of the stars are organized into such groups. Because stars form in *clusters*, the stars within a given cluster should all have the same age. Additionally, because such stars all lie at about the same distance from us, we can easily obtain relative luminosities for them by measuring their apparent magnitudes; and if the distance to the cluster is known, we may obtain absolute magnitudes. Temperatures are most easily measured by the **color index** – the difference between the B and V magnitudes. Plotting the magnitude (either apparent or absolute) versus the color index produces a **color-magnitude diagram** (**CMD**) – essentially an HR diagram with observational parameters.

A color-magnitude diagram is not quite the same as an HR diagram. Absolute visual magnitude is not exactly linear with luminosity (recall the bolometric correction), and color index is not linear with effective temperature (or *log T* either). While this makes comparison of specific points on the two diagrams more difficult, it does not greatly change the overall appearance of one with respect to the other. We should be able to identify the same basic features on each diagram.

We now examine the color-magnitude diagrams of a few clusters. Astronomers recognize two basic types of clusters: globular and open (or galactic). Examples are depicted in Figure 15.6.

Figure 15.6: (a) An open star cluster; (b) a globular star cluster

a 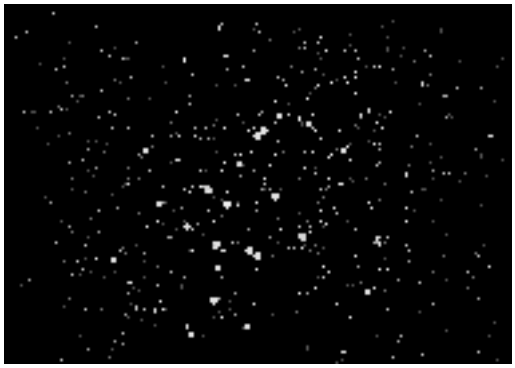 b 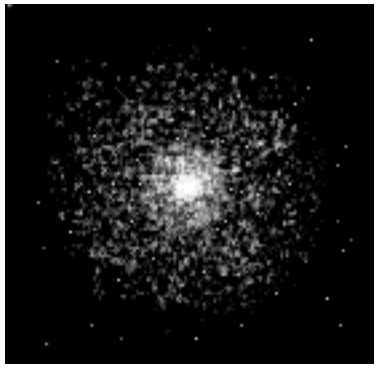

Open clusters typically contain a few hundred stars, while globular clusters may have a few hundred thousand. The latter generally appear smaller in the sky (as shown above), but this is only because they lie at much greater distances than most of the open clusters within reach of our telescopes. The next two figures present color-magnitude diagrams for two open clusters of different ages.

Figure 15.7: Color-magnitude diagram for the open cluster NGC 2264 (adapted from Payne-Gaposchkin (1979))

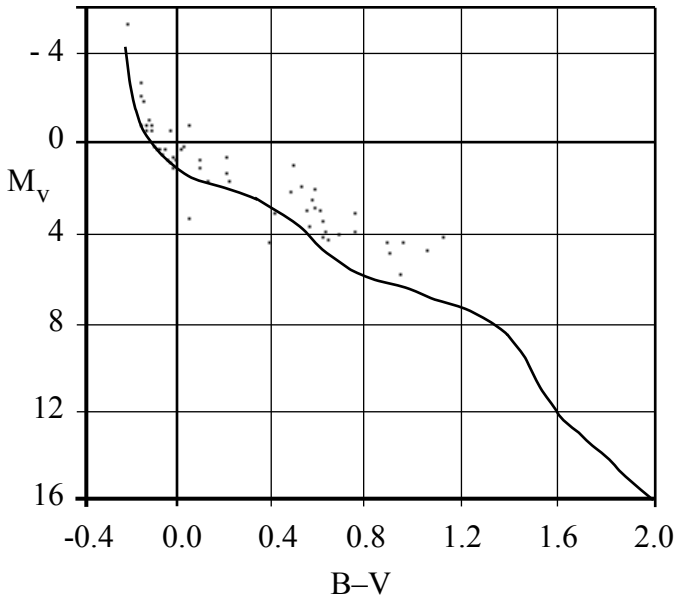

Figure 15.7 is a sketch of the color-magnitude diagram of the open cluster NGC 2264. The curve marks the main sequence – no longer a straight line as it was on the HR diagrams. NGC 2264 exhibits a main sequence populated only at the upper end; cooler stars still lie above the main sequence as they approach it in the pre-main sequence phase. NGC 2264 is thus a fairly young cluster, with a turnoff point somewhere above a magnitude of –3. (For reference, the Sun would lie at a color index of about 0.6 and an absolute magnitude of about +5. Few stars less luminous than this are plotted because only the brightest stars in the cluster were measured.)

Figure 15.8: Color-magnitude diagram for the open cluster M45 – the Pleiades (adapted from Payne-Gaposchkin (1979))

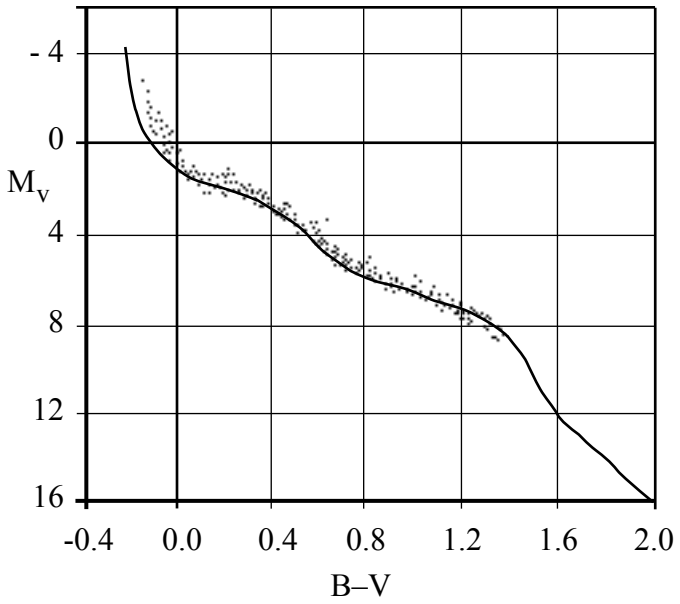

Figure 15.8 is a sketch of a color-magnitude diagram for the Pleiades, a well-known open cluster. This cluster is close enough that many less luminous stars are included, tracing out more of the main sequence. With a turnoff point around magnitude +1, the Pleiades is older than NGC 2264.

In contrast to the open clusters, we now present a sketch of the color-magnitude diagram for a metal-rich globular cluster. Figure 15.9 is actually made from a composite CMD of three such clusters: 47 Tuc, M71, and M69. The turnoff point around magnitude +3.5 implies that these clusters are considerably older than the Pleiades. New features include the subgiant and red giant branches just above the main sequence, with the short horizontal branch/red clump around $M_V = 0$. Extending upward to the right is the AGB; many of the coolest stars in this group are LPVs.

Figure 15.9: Composite color-magnitude diagram for the metal-rich globular clusters 47 Tuc, M71, and M69 (adapted from Payne-Gaposchkin (1979))

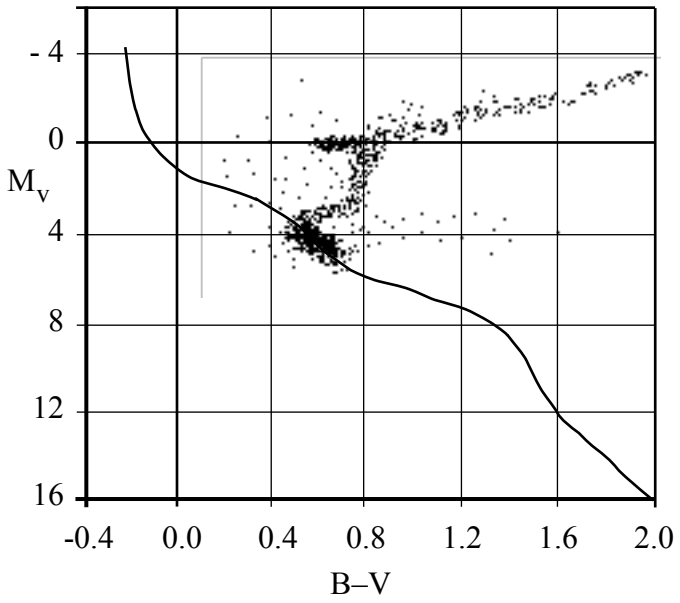

Figure 15.10 shows a sketch of the color-magnitude diagram for the globular cluster M5, which exhibits some noticeable differences from the previous diagram despite having a similar turnoff point.

First, the main sequence is displaced toward the blue; this is due to the lower metal content of this cluster. Second, there is no red clump evident; the horizontal branch extends much farther toward the blue, reaching beyond the main sequence. This is again due to the lower metal content of M5.

Third, there is a conspicuous gap in the horizontal branch around B–V = 0.3; this marks the location of the instability strip, in which stars are unstable to pulsations. The instability strip extends diagonally up to the right where it includes the two stars around $M_V = -3$; these are Cepheid variables. Horizontal branch stars found in this gap are RR Lyrae stars – short period pulsating variables.

Figure 15.10: Color-magnitude diagram for the globular cluster M5 (adapted from Payne-Gaposchkin (1979))

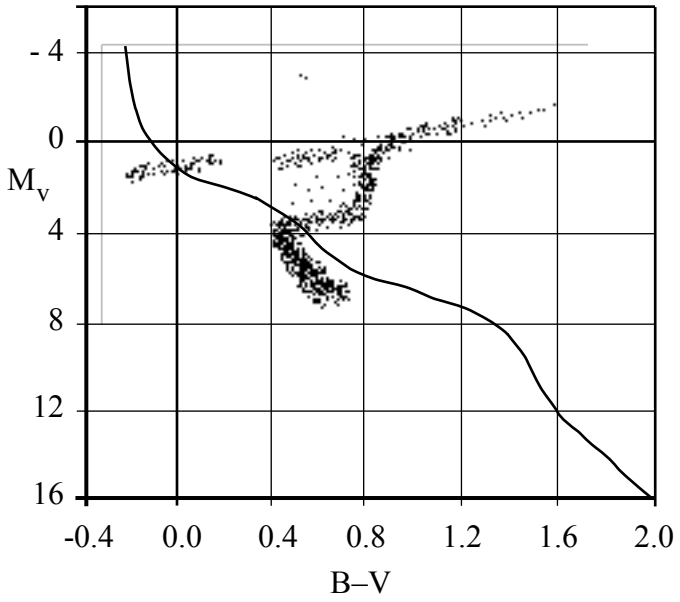

The various color-magnitude diagrams that have been obtained are in good agreement with the theoretical HR diagrams that have been generated. This evidence is fairly comforting, and indicates that our general views of stellar evolution are on the right track.

It should be noted that no star *cluster* will ever produce a *complete* main sequence, even if selection effects could be overcome. The problem is the wide range of evolution rates, which guarantees that the most massive stars will have moved off the main sequence long before the least massive stars ever arrive there. In order to obtain a color-magnitude diagram with a relatively complete main sequence, we must include stars that have a suitably wide *range* of ages.

Figure 15.11 is an example of such a diagram. It is a sketch of a color-magnitude diagram made for nearby stars, with distances (measured by the Hipparcos satellite) less than 100 parsecs. It features a nearly complete main sequence with a well-developed giant branch and red clump, plus a few white dwarfs. None of these stars are members of clusters; thus the diagram is not dominated by stars of any particular age. As expected, the uppermost and lowermost ends of the main sequence are sparsely populated, due to the various sampling factors discussed previously.

Of course there are other complicating effects that we have not covered here. For example, a large fraction of all stars exist in binary or multiple systems, where the evolution of one star can affect the evolution of its companions. Mass transfer between stars in a close binary can accelerate the evolution of the star receiving mass, while at the same time modifying the evolution of the donor star. The presence of strong magnetic fields can further modify the manner in which mass is deposited on a star. Compact objects – white dwarfs, neutron stars, black holes – in binary systems add other dimensions to stellar evolution, producing patterns of radiation not easily explained by standard stellar models. And variable stars exist with a whole assortment of amplitudes, periods, light curves, and mechanisms that do not fit our calculated image of a normal star.

Figure 15.11: Color-magnitude diagram for nearby stars (within 100 pc)

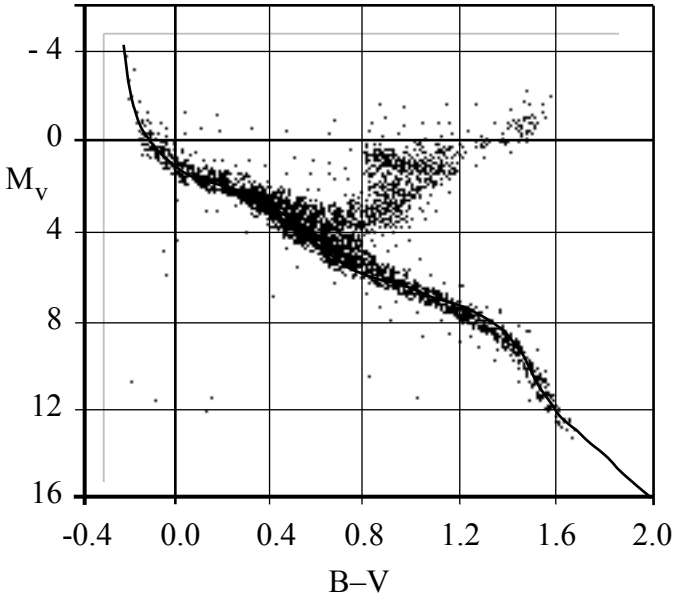

Clearly there are other paths to follow, but they must extend beyond this body of notes. By now the reader should have a reasonable grasp of the structure and evolution of normal stars; it is hoped that this background will provide pictures that can be extrapolated to more exotic species in the cosmic zoo.

APPENDIX

Constants

Values from NIST (2006): ----------

Speed of light	c	$2.99192458 \times 10^{10}$ cm/s
Gravitational constant	G	6.67428×10^{-8} dyne-cm^2/g^2
Planck's constant	h	$6.62606896 \times 10^{-27}$ erg-s
		$= 4.13566733 \times 10^{-15}$ eV-s
	$\hbar = h/2\pi$	$1.054571628 \times 10^{-27}$ erg-s
		$= 6.58211899 \times 10^{-16}$ eV-s
Boltzmann's constant	k	$1.3806504 \times 10^{-16}$ erg/K
		$= 8.617343 \times 10^{-5}$ eV/K
Stefan-Boltzmann constant	$\sigma = 2\pi^5 k^4/15h^3c^2$	5.670400×10^{-5} erg/s-cm^2-K^4
Radiation pressure constant*	$a = 4\sigma/c$	7.565767×10^{-15} erg/cm^3-K^4
Wien's law constant	λT	0.28977685 cm-K
Avogadro's number	N_A	$6.02214179 \times 10^{23}$ part/mole
Gas constant	$\Re = N_A k$	8.314472×10^7 erg/mole-K
Electron charge*	e	$4.80320427 \times 10^{-10}$ esu
Electron volt	eV	$1.602176487 \times 10^{-12}$ erg
Electron mass	m_e	$9.10938215 \times 10^{-28}$ g
Proton mass	m_p	$1.672621637 \times 10^{-24}$ g
		$= 1836.1526715\ m_e$
Neutron mass	m_n	$1.674927211 \times 10^{-24}$ g
Hydrogen atom mass*	m_H	$1.673532551 \times 10^{-24}$ g
Atomic mass unit *	amu	$1.660538782 \times 10^{-24}$ g
		$= 931.49402781$ MeV/c^2
Rydberg constant (for ∞ mass)	$R_\infty = 2\pi^2 m_e e^4/ch^3$	109737.31569 cm^{-1}
Bohr radius	$a_o = \hbar^2/e^2 m_e$	0.52917720859 Å

**Calculated values*

Values from Cox (2000): ----------

Tropical Year	yr	3.155692519×10^7 s
Astronomical unit	AU	$1.4959787066 \times 10^{13}$ cm
Parsec	pc	$3.0856775813 \times 10^{18}$ cm
Solar mass	$M_\odot$	1.9891×10^{33} g
Solar radius	$R_\odot$	6.95508×10^{10} cm
Solar luminosity	$L_\odot$	3.845×10^{33} erg/s
Solar effective temperature	$T_{e\odot}$	5779 K

Solid Angle

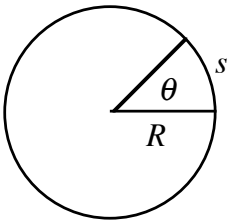

First, consider a *circle* of radius *R*:
An arc of length *s* on the circumference of the circle subtends an *angle* θ (with vertex at the center). The length *s* is as follows:
$s = R\theta$ (θ in radians) $\Rightarrow$ $\theta = s/R$ [1 radian = $180/\pi$ degrees]
In general, $s = R\int_0^{\theta} d\theta'$ and for a full circle, $s = R\int_0^{2\pi} d\theta' = 2\pi R$

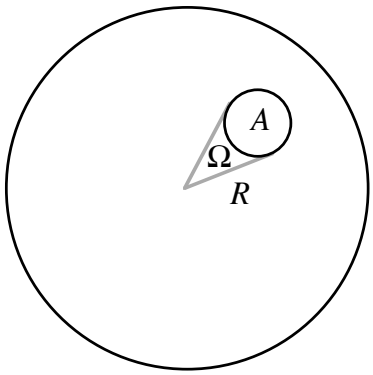

Now consider a sphere of radius R:
A closed curve – not necessarily a circle, as shown – enclosing area A on the surface of the sphere subtends a solid angle Ω (or ω) (with vertex at the center of the sphere). The area A is as follows:
$A = R^2\Omega$ (Ω in steradians = radians^2)
[1 steradian = $(180/\pi)^2$ square degrees]

$A = R^2 \int_0^{\phi}\int_0^{\theta} \sin\theta'\, d\theta'\, d\phi'$ and for the whole sphere,

$$A = R^2 \int_0^{2\pi}\int_0^{\pi} \sin\theta\, d\theta\, d\phi$$

Then $A = 2\pi R^2 \int_0^{\pi} \sin\theta\, d\theta = 2\pi R^2 \left(-\cos\theta\right|_0^{\pi} = 4\pi R^2$

The solid angle of a sphere is 4π, and the solid angle of a hemisphere is 2π.

In general, $\Omega = \dfrac{A}{R^2} = \int_0^{\phi}\int_0^{\theta} \sin\theta'\, d\theta'\, d\phi'$

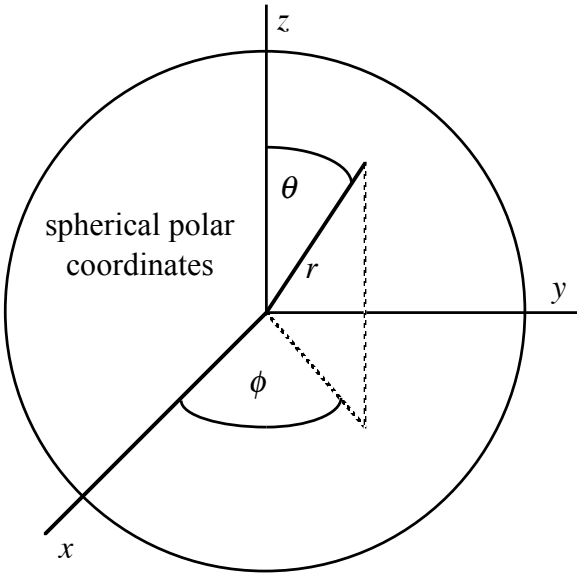

If the closed curve is a circle, we have a *disk* in the sky (such as the moon or a planet). Pointing the *z*-axis at the center of the disk gives the disk an angular radius θ.
The solid angle of this disk is then

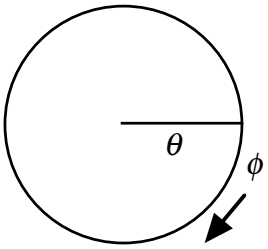

$$\Omega = \int_0^{2\pi}\int_0^{\theta} \sin\theta'\, d\theta'\, d\phi = 2\pi\int_0^{\theta} \sin\theta'\, d\theta' = 2\pi\left(1-\cos\theta\right)$$

If the disk is *small*, $\cos\theta \approx 1 - \theta^2/2!$ can be used;

then $\Omega \approx 2\pi\left[1-\left(1-\dfrac{\theta^2}{2}\right)\right] = \pi\theta^2 \approx \pi\left(\dfrac{R}{d}\right)^2$ where *R* is the disk radius and *d* is the distance to it.

Caution: The angle θ is a *general* quantity and could be used for *either* angular radius or angular diameter in different problems.

REFERENCES

Allen, C.W. 1973. *Astrophysical quantities*. 3rd ed. London: The Athlone Press.

Avrett, Eugene H. ed. 1976. *Frontiers of astrophysics*. Cambridge: Harvard University Press.

Bahcall, J. N. 1989. *Neutrino astrophysics.* Cambridge: Cambridge University Press.

Böhm-Vitense, Erika. 1989. *Introduction to stellar astrophysics, Volume 2: Stellar atmospheres*. Cambridge: Cambridge University Press.

Böhm-Vitense, Erika. 1992. *Introduction to stellar astrophysics, Volume 3: Stellar structure and evolution*. Cambridge: Cambridge University Press.

Bowers, Richard, and Terry Deeming. 1984. *Astrophysics I: Stars*. Boston: Jones and Bartlett.

Carroll, Bradley W., and Dale A. Ostlie. 1996. *An introduction to modern astrophysics*. New York: Addison-Wesley.

Chandrasekhar, S. 1967. *Stellar structure*. New York: Dover.

Clayton, Donald D. 1968. *Stellar evolution and nucleosynthesis*. New York: McGraw-Hill.

Collins, George W. 1989. *The fundamentals of stellar astrophysics*. New York: W. H. Freeman.

Cox, Arthur N. ed. 2000. *Allen's astrophysical quantities*. 4th ed. New York: Springer-Verlag.

Cox, John P. and R. Thomas Giuli. 1968. *Principles of stellar structure, Volume 1: Physical principles*. New York: Gordon and Breach.

Gray, David F. 1976. *The observation and analysis of stellar photospheres*. New York: Wiley.

Herzberg, Gerhard. 1944. *Atomic spectra and atomic structure*. 2nd ed. New York: Dover.

Herzberg, Gerhard. 1950. *Spectra of diatomic molecules*. 2nd ed. New York: Van Nostrand Reinhold.

Hopkins, Jeanne. 1980. *Glossary of astronomy and astrophysics*. 2nd ed. Chicago: University of Chicago Press.

Iben, Icko. 1967. Stellar evolution within and off the main sequence. *Annual Reviews of Astronomy and Astrophysics* 5: 571-626.

Kippenhahn, R. and A. Weigert. 1990. *Stellar structure and evolution*. New York: Springer-Verlag.

Lang, Kenneth R. 1980. *Astrophysical formulae*. 2nd ed. New York: Springer-Verlag.

Moore, Charlotte E. 1972. *A multiplet table of astrophysical interest*. Revised ed. (NSRDS-NBS 40). Washington, DC: National Bureau of Standards.

National Institute of Standards and Technology. The NIST reference on constants, units, and uncertainty: Fundamental physical constants (2006 values). http://www.nist.gov/cuu/Constants/index.html.

Novotny, Eva. 1973. *Introduction to stellar atmospheres and interiors*. New York: Oxford University Press.

Payne-Gaposchkin, Cecilia. 1979. *Stars and clusters*. Cambridge, MA: Harvard University Press.

Rybicki, George B., and Alan P. Lightman. 1979. *Radiative processes in astrophysics*. New York: Wiley.

Seeds, Michael. 2008. *Horizons: Exploring the universe*. 10th ed. Belmont, CA: Brooks/Cole.

Spiegel, Murray R. 1968. *Mathematical handbook of formulas and tables*. Schaum's Outline Series. St. Louis: McGraw-Hill.

READING LIST

Allen, C.W. 1973. *Astrophysical quantities*. 3rd ed. London: The Athlone Press.

Avrett, Eugene H. ed. 1976. *Frontiers of astrophysics*. Cambridge: Harvard University Press.

Böhm-Vitense, Erika. 1989. *Introduction to stellar astrophysics, Volume 1: Basic stellar observations and data*. Cambridge: Cambridge University Press.

Böhm-Vitense, Erika. 1989. *Introduction to stellar astrophysics, Volume 2: Stellar atmospheres*. Cambridge: Cambridge University Press.

Böhm-Vitense, Erika. 1992. *Introduction to stellar astrophysics, Volume 3: Stellar structure and evolution*. Cambridge: Cambridge University Press.

Bowers, Richard, and Terry Deeming. 1984. *Astrophysics I: Stars*. Boston: Jones and Bartlett.

Bowers, Richard, and Terry Deeming. 1984. *Astrophysics II: Interstellar matter and galaxies*. Boston: Jones and Bartlett.

Carroll, Bradley W., and Dale A. Ostlie. 1996. *An introduction to modern astrophysics*. New York: Addison-Wesley.

Chandrasekhar, S. 1967. *Stellar structure*. New York: Dover.

Clayton, Donald D. 1968. *Stellar evolution and nucleosynthesis*. New York: McGraw-Hill.

Collins, George W. 1989. *The fundamentals of stellar astrophysics*. New York: W. H. Freeman.

Cox, Arthur N. ed. 2000. *Allen's astrophysical quantities*. 4th ed. New York: Springer-Verlag.

Cox, John P. and R. Thomas Giuli. 1968. *Principles of stellar structure, Volume 1: Physical principles*. New York: Gordon and Breach.

Cox, John P. and R. Thomas Giuli. 1968. *Principles of stellar structure, Volume 2: Applications to stars*. New York: Gordon and Breach.

De Loore, Camiel W. H. and C. Doom. 1992. *Structure and evolution of single and binary stars*. Boston: Kluwer Academic Publishers.

Gray, David F. 1992. *The observation and analysis of stellar photospheres*. 2nd ed. New York: Wiley.

Hansen, C. J., and S. D. Kawaler. 1994. *Stellar interiors*. New York: Springer-Verlag.

Hearnshaw, J.B. 1986. *The analysis of starlight: one hundred and fifty years of astronomical spectroscopy*. New York: Cambridge University Press.

Hopkins, Jeanne. 1980. *Glossary of astronomy and astrophysics*. 2nd ed. Chicago: University of Chicago Press.

Jaschek, Carlos and Mercedes Jaschek. 1987. *The classification of stars.* New York: Cambridge University Press.

Kaler, James B. 1989. *Stars and their spectra: an introduction to the spectral sequence*. New York: Cambridge University Press.

Kippenhahn, R. and A. Weigert. 1990. *Stellar structure and evolution*. New York: Springer-Verlag.

Lang, Kenneth R. 1980. *Astrophysical formulae*. 2nd ed. New York: Springer-Verlag.

Novotny, Eva. 1973. *Introduction to stellar atmospheres and interiors*. New York: Oxford University Press.

Payne-Gaposchkin, Cecilia. 1979. *Stars and clusters*. Cambridge, MA: Harvard University Press.

Phillips, A. C. 1999. *The physics of stars.* 2nd ed. New York: Wiley.

Prialnik, Dina. 2000. *An introduction to the theory of stellar structure and evolution*. New York: Cambridge University Press.

Rybicki, George B., and Alan P. Lightman. 1979. *Radiative processes in astrophysics*. New York: Wiley.

Schatzman, Evry L. and F. Praderie. 1993. *The stars.* New York: Springer.

Taylor, Roger J. 1994. *The stars: their structure and evolution*. 2nd ed. New York: Cambridge University Press.

INDEX

ABOUT THE AUTHOR

Dr. James N. Pierce is emeritus professor of astronomy at Minnesota State University, Mankato, where he taught astronomy, physics, and mathematics for 32 years. His regular astronomy offerings ranged from general education courses to classes for astronomy majors. ***Notes on Stellar Astrophysics*** (2013) contains the material covered in his two-semester sequence for junior/senior astronomy majors: **AST 420** ***Stellar Astrophysics*** and **AST 421** ***Stellar Structure***.

Other books by Dr. Pierce:

Life in the Universe: The Abundance of Extraterrestrial Civilizations (2008), BrownWalker Press.

Elementary Astronomy (2013) – available online as a *free* pdf.

Dr. Pierce's web pages: Search '*pierce astronomy mankato*' for current sites.